ANNUAL REPORT 2009

NEUTRONS FOR SCIENCE®

ANNUAL REPORT 2009

Institut Laue-Langevin

ANNUAL REPORT 2009

NEUTRONS FOR SCIENCE®

Institut Laue-Langevin
6, rue Jules Horowitz - BP 156 - 38042 Grenoble Cedex 9 - France - http: // www.ill.eu

This report has been printed using FSC certified paper (http://www.fsc.org/)

FSC

SYNTHESE ECA - Tél. 04 76 90 02 73

The Institut Laue-Langevin (ILL) is an international research centre where neutrons are used to probe the microscopic structure and dynamics of a broad range of materials from the molecular, atomic and nuclear point of view. The ILL is owned and operated by three founding countries - France, Germany and United Kingdom.

The three Associate countries contributed a total of about 61 M€ to the Institute in 2009, a sum enhanced by significant contributions from the ILL's Scientific Member countries, Austria, Belgium, the Czech Republic, Denmark, Hungary, Italy, Spain, Slovakia, Sweden and Switzerland. ILL's overall budget in 2009 amounted to approximately 82 M€.

A unique flux of slow neutrons, a matching suite of experimental facilities

The ILL was founded to provide scientific communities in its member countries with a unique flux of slow neutrons and a matching suite of experimental facilities (some 40 instruments) for use in fields as varied as solid-state physics, materials science, chemistry, the life sciences and the earth sciences as well as nuclear physics and engineering.

The Institute has ever since been an exceptional centre of excellence and a fine example of successful cooperation in Europe, a prototype of the European Research Area. It operates the most intense neutron source in the world. About 2000 visiting scientists, performing a total of more than 800 experiments each year, and the output in high impact journals, bear witness to the scientific success of the facility.

PUBLISHING INFORMATION

Editors: Giovanna Cicognani, Andrew Harrison and Katja Jenkins
Production team: Giovanna Cicognani, Robert Corner,
Katja Jenkins, Susan Tinniswood and Albert Wright
Design: www.synthese-eca.com - **Printing:** Imprimerie du Pont de Claix
Photography: by ILL and Artechnique (artechnique@wanadoo.fr)

Further copies can be obtained from Institut Laue-Langevin
Scientific Coordination Office (SCO) - BP 156
F-38042 Grenoble Cedex 9 (France)
Tel: +33 (0)4 76 20 72 40 Fax: +33 (0)4 76 48 39 06
email: sco@ill.eu - web: www.ill.eu

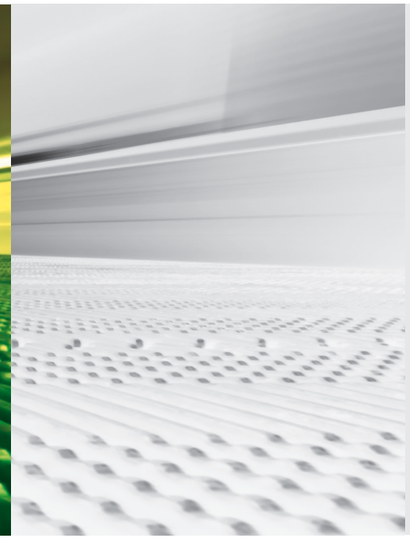

C O N T E N T S

The year 2009 was a good one for the ILL. The Institute's user community continued to benefit from the excellent reliability of our neutron source and impeccable access to instruments: the reactor delivered all 200 of the beam days asked of it, and there was no significant downtime to be noted for technical reasons on any instrument. The final three of the fourteen instruments built or upgraded under the first phase of the ILL's modernisation programme – the Millennium Programme – were successfully commissioned in 2009. All these instruments are already producing excellent science. A tribute must be paid to all our staff members who have contributed so admirably to this great achievement with their hard work and dedication!

The opportunities we offer extend beyond the privileges of access to the world's leading suite of neutron instruments

ILL's Europeanisation started back in 1986 when Spain joined the Institute as its first Scientific Member. The process has continued apace, and in 2009 we were pleased to welcome Denmark and Slovakia as new partners in science. We are convinced that users from both these countries will enjoy the unparalleled opportunities offered by the Institute, whilst contributing in their turn to our very special culture. Their endeavours will help us ensure that we continue setting the definitive benchmarks science needs through our flow of publications and innovative neutron techniques.

The opportunities we offer extend beyond the privileges of access to the world's leading suite of neutron instruments – they have been enhanced by our alliance with our sister institute the ESRF and the creation of the Partnership for Soft Condensed Matter (PSCM). This initiative follows on from the most successful Partnership for Structural Biology, founded some four years ago; it will provide the support required to fully exploit the respective and complementary advantages of neutron and synchrotron instruments. The ultimate aim is to streamline neutron- and synchrotron-based soft matter research and address the 21st-century challenges posed by the environmental and energy sciences, nanomaterials and biotechnology. The PSCM will be accommodated in the new ILL/ESRF Science Building to be constructed with a €15 million grant from national and regional sources in the framework of France's *Contrat Projets État-Région*.

Our modernisation programme is now in its second phase. In 2007 our Scientific Council and Steering Committee approved the launch of eight important new projects - new instruments and instrument upgrades. These are now well in progress and scheduled for completion in 2014. A first milestone has already been reached with the successful refurbishment of the vertical reflectometer. Projects such as this will help us lead the field, on to as yet unsuspected science beyond the next decade.

In this continuous effort to structure the future of neutron science we have already started to prepare our plans for further development beyond 2014. The inherent strength of our steady-state high-flux neutron source is obviously a major advantage. We have received strong support for a third phase of modernisation in the form of a grant from the European Commission, as part of its funding of the ESFRI Roadmap. ILL's Scientific Council has already been involved in the planning process and in defining the priorities for the future. The plans will be further refined with our users, at the ILL User Meeting to be held in September 2010 ('*ILL 2020 Vision*'). We need to be very clear on our mandate as in 2014 we enter the period of our 5th Intergovernmental Convention, which it is envisaged will take ILL's operations at least until 2023. In this context we are also prepared to collaborate with the pulsed European Spallation Source project in Lund, Sweden.

ILL's 2009 outreach activity culminated in the most successful organisation of an 'ILL Open Day' in September. For the first time in the Institute's history, public access was offered to the ILL reactor hall. Eight hundred visitors were registered over the weekend, all keen to know more about the science being produced at the ILL.

The annual report you hold in your hands offers a similar experience. Like our visitors at the Open Day, you will discover a host of remarkable results and achievements testifying to the spirit and vitality of our Institute. My warmest thanks to all those who have contributed to this success.

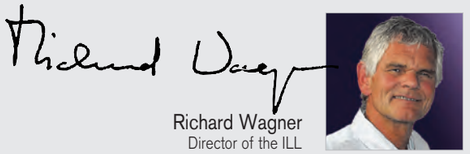

Richard Wagner
Director of the ILL

WHY NEUTRONS?

Neutron beams have the power, when used as a probe of small samples of materials, to reveal what is invisible using other radiations. Neutrons can appear to behave either as particles or as waves or as microscopic magnetic dipoles and it is these specific properties which enable them to uncover information which is often impossible to access using other techniques.

Electrically Neutral

Neutrons are non-destructive and can penetrate deep into matter making them an ideal probe for e.g. engineering components and samples under extreme conditions of pressure, temperature, magnetic field or within chemical reaction vessels.

Microscopically Magnetic

They possess a magnetic dipole moment which makes them sensitive to magnetic fields generated by unpaired electrons in materials. Precise details of the magnetic behaviour of materials at the atomic level can be investigated. In addition, the scattering power of a neutron by an atomic nucleus depends on the orientation of the spin of both the neutron and the atomic nuclei in a sample thereby providing a powerful tool to detect the nuclear spin order.

Wavelengths of Ångstroms

Their wavelengths range from 0.1 Å (10^{-2}nm) to 1000 Å making them an ideal probe of atomic and molecular structures ranging from those consisting of single atomic species to complex biopolymers.

Energies of millielectronvolts

Their energies are of the same magnitude as the diffusive motions of atoms and molecules in solids and liquids, the coherent waves in single crystals (phonons and magnons) and the vibrational modes in molecules. An energy exchange between the incoming neutron and the sample of between 1 µeV (even 1 neV with spin-echo) and 1 eV can readily be detected.

Randomly sensitive

The variation of scattering power from nucleus to nucleus in a sample varies in a quasi-random manner. This means that light atoms are visible in the presence of heavy atoms and atoms neighbouring in the periodic table may be distinguished from each other. In addition, isotopic substitution (for example D for H, or one nickel isotope for another) can allow contrast to be varied in certain samples thereby highlighting specific structural features. The neutron is particularly sensitive to hydrogen atoms and therefore is a powerful probe of hydrogen storage materials, organic molecular materials, and biomolecular samples or polymers.

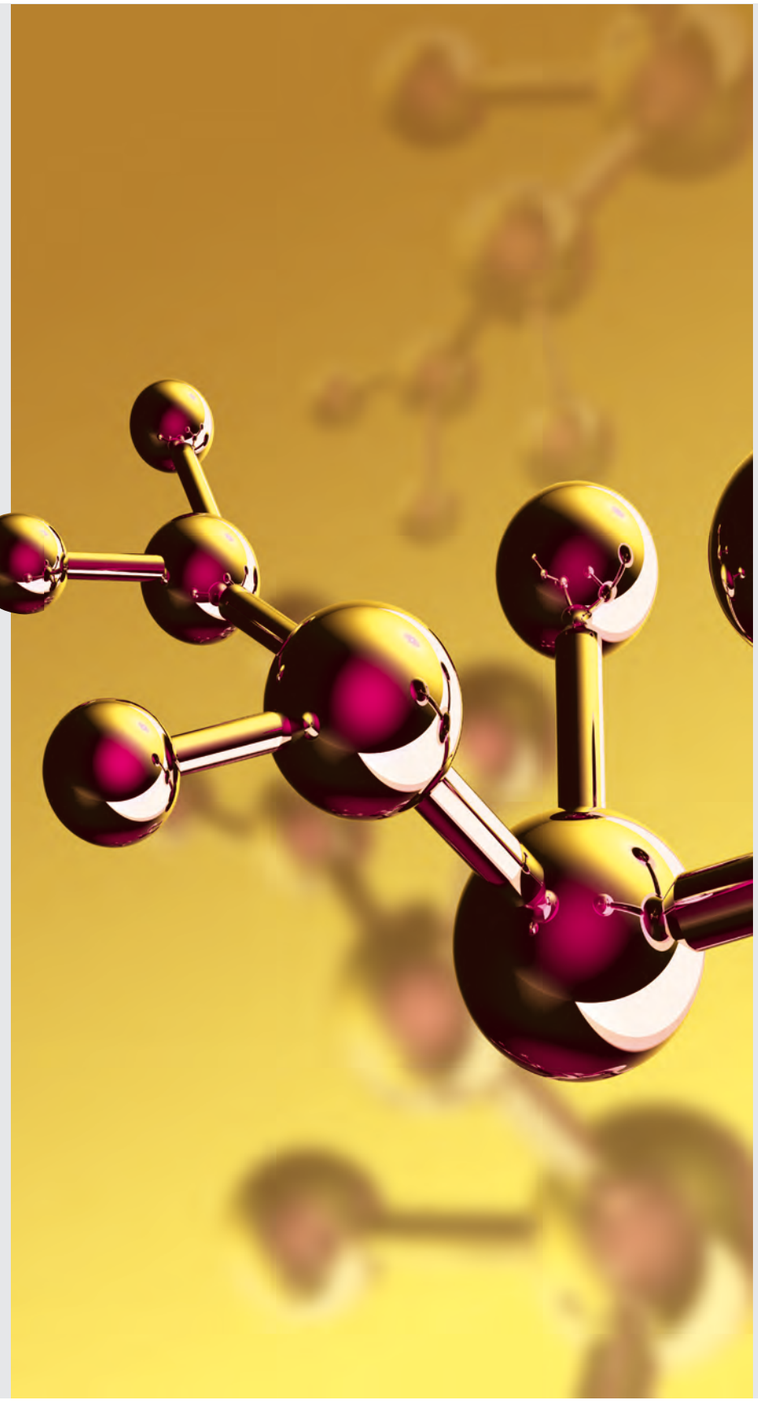

Formally, ILL is a non profit-making French company under civil law, which is governed by an International Convention, signed at Foreign Ministry level by three countries - France, Germany and the United Kingdom. Our Associates - the CNRS and the CEA representing France, the FZ Jülich representing Germany and the STFC representing the United Kingdom - own and administer the Institute. They are also responsible for all liabilities and eventual decommissioning costs.

Whilst our Associates own the facility and contribute the largest amount to the 82 M€ annual operating costs, the ILL also benefits from the scientific partnerships of ten other nations - Austria, Belgium, the Czech Republic, Denmark, Hungary, Italy, Slovakia, Spain, Sweden and Switzerland - who together contribute about 22% of the operational and investment costs of the Institute. All ten partner countries in addition can and do contribute to capital projects at the Institute, within the Institute's priorities but according to their own priorities also.

Our governing body is the Steering Committee, which meets twice-yearly and is made up of representatives of the Associates and the Scientific Partners together with Directors and Staff Representatives. Within the framework of the International Convention, the Steering Committee has the ultimate responsibility for determining operational and investment strategies for the Institute.

The Institute has a Director and two Associate Directors, representing each of the Associate countries, appointed on short-term contracts normally of five years. The Director's role is generally taken alternately by the German and British appointee. The two Associate Directors are responsible for the Science Division and the Projects and Techniques Division respectively. The Head of the Administration Division is also appointed on a short-term contract, whereas the Head of the Reactor Division is a permanent ILL employee. These five people together constitute the Management Board of the Institute and are responsible for its day-to-day operation.

The scientific life of the Institute is guided by the Directors, with input from the ILL's ten scientific colleges. A Scientific Council, comprising external scientists from the member countries, advises the Directors on scientific directions for the Institute, on the evolution of the instrument suite and technical infrastructure to best meet the needs of the user research programme, and to assess the scientific output of the Institute. It is helped in this process by the Instrument Sub-Committee and by the Chairmen of the nine Scientific Sub-Committees who twice-yearly peer review the experiment proposals.

The ILL is composed of four Divisions, each with its distinct role and, it is true to say, its own culture. The Science Division staffs the instruments and delivers the science; the Projects and Techniques Division designs and builds new instruments, develops new concepts and maintains beamlines and instruments operational; the Reactor Division delivers the neutrons, operates and mans the reactor 24 hours during 4 cycles of 50 days each per year and has responsibility for all aspects of security; the Administration Division deals with Personnel matters with particular responsibility for interactions with staff representative bodies, with Purchasing, with Finance and with Site and Building maintenance. The Director's Services deal with Radiological safety, with conventional safety, with Health and Working Practices and with Public Relations.

The ILL's neutron source is the finest in the world, being based on a single element 58.3 MW nuclear reactor designed for high brightness. The main moderator is the ambient D_2O coolant surrounding the core which delivers intense beams of thermal neutrons to 11 beamlines and to 4 neutron guides. A graphite hot source operating at 2400 K delivers hot neutrons - energies up to 1 eV and wavelengths down to 0.3 Å - to 3 beamlines. A renewal project has resulted in the installation of a new hot source and beam tubes during 2003. Two liquid deuterium cold sources at 25 K deliver cold neutrons - energies down to 200 µeV and wavelengths up to 20 Å - to some 17 instruments. An ultra-cold neutron source fed from the top of one of the cold sources delivers neutrons vertically through the reactor pool to 5 instruments on the operational floor of the reactor.

In all there are more than 50 measuring stations, 28 of which have full public access. In addition, the ILL provides a framework in which Collaborative Research groups (CRGs) can build and manage instruments to carry out their own research programmes. There are at present 10 CRGs instruments at the ILL.

Our community of users is world-wide with scientists from non-partner nations also having a chance to apply for beamtime with outstanding research proposals. This broader community of users enriches the scientific life of the Institute.

In 2000, the ILL launched an ambitious modernisation programme of instruments and infrastructure called the ILL Millennium Programme (Phase M-0: 2000-2008; Phase M-1: 2007-2013) whose aim is to optimise the ILL's instrument suite, and thereby maintaining the Institute's world-leading position for another 20 years.

We have started to draw up plans for future upgrades to the instrument suite, aiming for the period 2013-2017. We will present the 'ILL 2020 Vision' - a plan to support the best science through neutron scattering - at our User Meeting from 15-17 September 2010 in Grenoble. Further proposals for instruments and infrastructure from our user community will also be welcomed and included in the discussion at the meeting.

The ILL monitors the papers published as a result of the use of our facilities. This gives a figure of more than 600 papers per year. We pay particular attention to papers published in high impact journals. About 80 such papers per year are published from data taken on ILL instruments which is a factor of two higher than the second most productive neutron source in the world.

Instrument days delivered for science during four reactor cycles amount to 6735 in 2009.

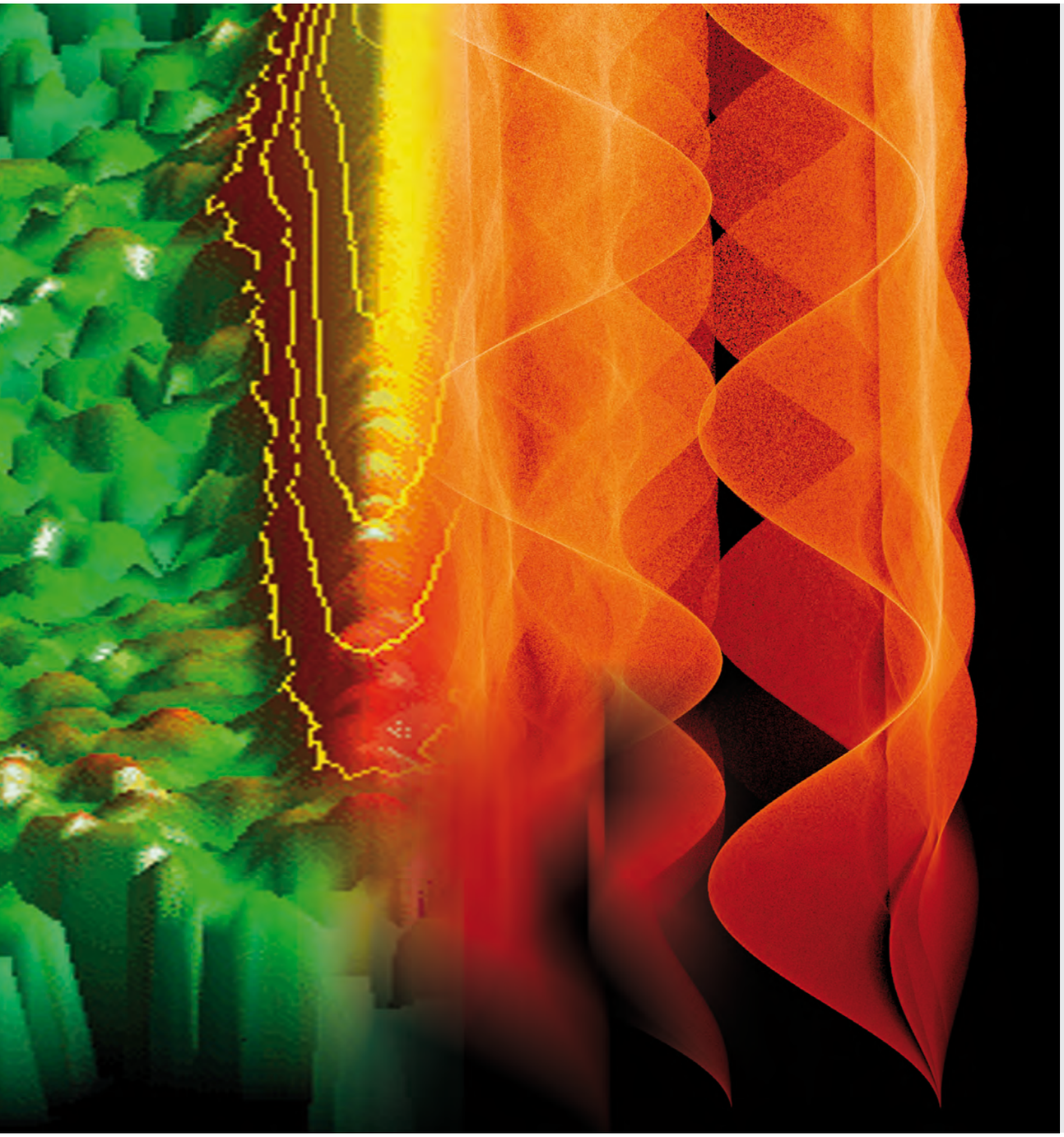

2009 has been a great year for science at ILL on all fronts: the quantity and, crucially, the quality of publications based on work here is as strong as ever, several new or extensively upgraded instruments are firmly integrated into the user programme and our reactor delivered neutrons with 100% reliability. The next few pages of this report present some of our science highlights, among which the revelation of species analogous to magnetic monopoles has created the greatest stir both in the scientific community and the popular press. This work, centred on polarised neutron scattering from defects in a spin-ice pyrochlore, was made possible by the Millennium upgrade on D7. Publications on ground-breaking experiments at ILL on the pnictide superconductors discovered last year are also filtering through, as our high flux has been brought to bear on the first, small single crystals, or samples subjected to high pressure. Such successes provide ILL's raison d'être and the strongest argument for continued funding; conversely, the continued practice of some users to fail persistently to acknowledge properly the role ILL scientists play in making their experiments possible – and in extreme cases to acknowledge ILL at all – is something we have to strive to change.

Looking further to the future, a key indicator of health is the emerging, new generation of users, as well as good, new ideas in neutron science

ILL's horizontal surface reflectometer FIGARO enjoyed its first scheduled experiments this year and is already starting to bring in users from new fields; D11 returned to the fold after an extensive upgrade, and is delivering up to three times higher detection rate. The vast increase in detection rate on the renovated cold-neutron chopper spectrometer IN5 is enabling new science, but at the same time presents new challenges: the time taken to change sample temperature may now be a much greater fraction of the experimental time, imposing greater demands on the performance of cryostats or furnaces; the sheer volume of raw data that is now created requires new methods to visualise and analyse data.

Clearly, it's not enough to build the best instruments – the best science requires a more holistic approach. Here, our interface laboratories also play a crucial role. Formal agreement was reached this year with the ESRF over joint future support for the Partnership for Soft Condensed Matter (PSCM), opening the door to investment in equipment and personnel that should greatly enhance the effectiveness of both neutrons and synchrotron X-rays in this field. The Partnership for Structural Biology (PSB) enjoyed a glowing report from the international panel that reviewed it in the summer. A recent development in the PSB has been the establishment of a joint platform for small-angle X-ray and neutron scattering, and this in turn should play a central role in a trial for a more joined-up proposal system for problems that require access to both the ILL and ESRF. Further partnerships are also under consideration: after strong representations from the community, we are considering plans for a new Partnership for Extreme Conditions Science, focused primarily on high pressure and temperature. This, together with the PSCM, and the shared chemistry laboratories, library and theory group should be housed in a new 'Science Building' a couple of years from now, funded through the Rhone-Alpes region and the city of Grenoble.

Looking further to the future, a key indicator of health is the emerging, new generation of users, as well as good, new ideas in neutron science. Both of these came together most emphatically in the last set of proposals for ILL PhD studentships, providing us with the task of choosing half a dozen projects from forty. Our student body now numbers thirty, wholly or partly supported by ILL. This, together with a steadily rising demand for beamtime from our users makes us very confident that there is a strong case for supporting the best facilities for neutron science for years to come.

Andrew Harrison
Associate Director

AUTHORS

Magnetism: Paul Steffens, College 4 Secretary, **Clemens Ritter,** College 5b Secretary
Chemistry and Structure: Thomas Hansen, College 5a Secretary
Materials Science and Engineering: Philip Bentley, College 1 Secretary
Soft Matter: Ralf Schweins, College 9 Secretary

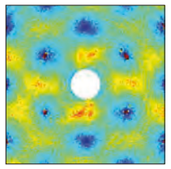

Magnetism:
cf. article 'Coulomb phase in the spin ice $Ho_2Ti_2O_7$' p.24

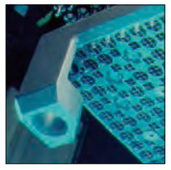

Chemistry:
cf. article 'Oxidation mechanisms of nuclear fuels elucidated by neutron diffraction' p.30

MAGNETISM

The demand to study the static and dynamic magnetic properties of materials at ILL continues to be very strong indeed, comprising a third of all applications for beamtime. A significant fraction of these requests relate to superconductivity, from studies of flux-line lattices to the implication of magnetism in the pairing mechanism for the charge carriers in high-temperature superconductors. Much the same could have been written fifteen years ago, but now the focus has broadened from cuprates alone to include an expanding family based on iron pnictides. In 2009, larger crystals of various pnictides, suitable for detailed inelastic neutron work, have become available and we anticipate that they will feature prominently in next year's Annual Report.

Another key area of study, often also entwined with superconductivity, is that of quantum critical behaviour. In particular systems, a phase transition may be tuned by a parameter such as pressure or magnetic field to occur at zero Kelvin. The behaviour of the system in the region of this 'quantum critical point', and up to significantly higher temperatures, may be strongly influenced by quantum fluctuations in a manner that is hotly debated. Knafo *et al.* describe work on the heavy-fermion material Lanthanum-doped $CeRu_2Si_2$, revealing that the quantum phase transition is driven by antiferromagnetic rather than local fluctuations.

There is also considerable interest in the study of materials in which some combination of low spin, low dimensionality and frustration produce unconventional magnetic order or correlations. Tsyrulin *et al.* describe inelastic neutron scattering studies of the two dimensional, S=1/2 square antiferromagnet $Cu(pz)_2(ClO4)_2$ that reveal how quantum fluctuations in such materials may be tuned through further-neighbour interactions and applied magnetic fields, bringing us closer to an understanding of resonating valence bond systems.

Frustration also plays a key role in the formation of new magnetic states or species in the itinerant magnet MnSi and the insulating pyrochlore holmium titanate. Pappas *et al.* report neutron spin-echo and spherical polarimetry measurements on warming MnSi revealed the formation of a novel 'skymionic spin liquid' which is dynamically disordered but possesses a unique chirality – a magnetic analogue of a liquid crystal. Holmium titanate is a spin ice, in which thermally-created defects have been predicted to interact in a Coulombic rather than a dipolar fashion, behaving as classical analogues of the magnetic monopoles predicted by Dirac over 60 years ago. Fennell *et al.* took advantage of the greatly enhanced detection rate of the polarised neutron diffractometer D7, together with IN12, to provide the first experimental signature of these elusive entities.

A key feature of many of the magnetic measurements at ILL is that the energy scale of the phenomena studied is often very low, allowing them to be manipulated by magnetic fields. The scope of such work would be greatly enhanced by an increase in the current ILL limit of 15T for dc fields, and indeed an ESFRI-funded feasibility study has just been completed to share with the ESRF infrastructure for electrical power and cooling for magnets reaching to 30T. A different approach is the use of pulsed magnetic fields and 2009 saw a significant advance on this front: Noriji et al. report the first magnetic diffraction measurements at fields up to 30T using a very compact pulsed magnet. Each pulse had an effective direction of the order of 7 milliseconds and could be repeated about 10 times per hour which was sufficient to characterise the structure of the frustrated antiferromagnet TbB_4 at half-saturation.

http://www.ill.eu/science-technology/science-at-ill/magnetism/

CHEMISTRY AND STRUCTURE

Knowledge of the structure of crystalline matter is essential to understanding the chemical properties of most solid materials, and neutron diffraction provides an essential tool in this domain. The range of applications of neutron scattering in this field is very broad, extending from molecular solids to ceramics, and embracing a wide range of functionality, even if materials considered to be 'magnetic', 'biological' or 'engineering' are excluded. Such measurements represented 13% of the demand for beamtime in 2009, making particular demands on the high-flux powder diffractometer D20, and increasing too for the hot-neutron single-crystal diffractometer D9 and the determination of pair-distribution functions on D4. We have also seen a strong increase in experiments at extreme conditions, or in reactive atmospheres, in some cases taking advantage of recent improvements in detection rate to look at samples that are either relatively small, or whose structure changes with time. This is reflected in our choice of highlights.

Cheng *et al.* and Fortes *et al.* report different high-pressure experiments on D2B, both made possible through the Millennium upgrade. The former focuses on a new perovskite polytype, and provides insights into structure-property relations in this important class of functional material. The latter solved the structure of an ammonia hydrate at high pressure and reduced temperature, comparable to the conditions found on icy moons such as Ganymede, Callisto and Titan, found further out in our solar system, and providing information vital to model accurately their geophysical behaviour.

Desgranges *et al.* performed a time-resolved high-temperature experiment in situ on the oxidation of UO_2 using D2B over a period of several hours. The results elucidate the complex oxidation mechanism for this nuclear fuel material. Malavasi et al. also studied an *in situ* transformation, observing the transformation of a cathode material for solid oxide fuel cells during oxygen exchange, but this time a shorter timescale was required and D20 was used, capturing a refineable pattern in minutes. A similarly short time-scale was also required for an *in situ* study by Bahout *et al.*, who successfully followed the structural transformation of Ruddlesen-Popper phases as they were reduced under a controlled flow of hydrogen.

ILL also continues to develop the instruments that serve this field. Thus, a new instrument, Cyclops, which is a Laue diffractometer with a bank of CCD detectors, is being commissioned and it is anticipated that it will open new opportunities with respect to time resolution, offering data acquisitions down to seconds. Plans are being drawn up under the working title 'XtremeD' for a new, high-flux instrument, with highly-focusing optics that will enable the study of very small samples mounted in bulky sample environment equipment such as pressure cells. Finally we note two other experimental trends: single-crystal experiments are involving increasingly small crystals, particularly on VIVALDI; in powder diffraction there is an increasing demand to determine the position of hydrogen in samples that cannot be readily deuterated. Clearly, we will not be short of continuing experimental challenges!

http://www.ill.eu/science-technology/science-at-ill/chemistry-crystallography/

MATERIALS SCIENCE AND ENGINEERING

'Materials science' is a very broad field, much of which can be found else where in this introduction under headings such as 'magnetism', 'chemistry and structure' and 'soft matter'. However, many important areas remain, and together with engineering currently represent 6% of the demand for beamtime: metallurgy and engineering; structural materials; many aspects of mineral structure; cultural heritage. The determination of stress or strain, and the measurement of texture cuts across many of these areas.

In recent years, this section of the report has been dominated by highlights on strain-scanning, showcasing recent work on a wide range of engineering problems, from welds to surface treatments and such work continues to feature strongly. Further, the dedicated strain-scanning instrument SALSA, together its complementary support laboratory FaME (Facility for Materials Engineering) continue to be developed, enabling strain measurements in increasingly bulky engineering components. However, this year we will direct the spotlight mostly on mineral systems, some of which feature texture measurements - an activity that has strengthened recently at ILL. It is perhaps appropriate that for 2009, the year of the Copenhagen Conference on Climate Change, many of our highlights in this field have an environmental theme. However, our choice also reflects the particular strengths of neutron scattering as a highly-penetrating probe, particularly adept at locating light atoms - and thus able to locate species such as water in mineral hosts.

Rivard *et al.* have examined the microscopic structural stability of a candidate clay-based material selected for French radioactive waste storage, when it is subjected to wet conditions. The orientation of the clay particles turn out to be remarkably stable to hydration, which is crucial for long-term structural integrity in damp, underground environments.

Neutron spin-echo spectroscopy was used by Bordallo *et al.* to measure the motion of water molecules confined in cement, providing information about the pore structure. This in turn influences the macroscopic structural properties, and may point to ways in which cement quality and hence longevity may be improved.

Fernández-Martínez *et al.* report on the adsorption properties of the mineral imogolite, found principally in volcanic soils and important in the retention of organic matter and trace elements. Their work, using neutron diffraction and molecular modelling, reveals a mechanism by which the organic matter accumulates and thus becomes a carbon sink, and also a trap for elements important for health, such as selenium.

Finally, Zucali *et al.* present their recent work on the deformation and elastic properties of gypsum, which is found in evaporitic rocks, in turn an important component of particular geological faults that have been proposed as sites for nuclear waste disposal and CO_2 storage. Their quantitative texture study promises to provide a more accurate basis for the geological modelling that will be crucial to assess the wisdom of such storage.

http://www.ill.eu/science-technology/science-at-ill/materials-science-engineering/

SOFT MATTER

2009 marked an important step forward for the soft condensed matter community at the ILL - and indeed for the support it provides its users in this field - with the signing of a memorandum of understanding with ESRF to agree to support a Partnership for Soft Condensed Matter (PSCM). This agreement will put further investment in resources -equipment, personnel and a share of a dedicated building - on a firmer footing (for further details see: http://www.ill.eu/instruments-support/labs-facilities/pscm/). It will help users to prepare and validate delicate sample, from films to colloids, and encourage the development of experimental techniques and data analysis, through collaborations between users and our scientists.

The neutron instruments that serve this area have also progressed significantly in the past year, with the return of a completely rebuilt D11 and the new horizontal surface reflectometer FIGARO. The upgrade of the CRG reflectometer ADAM - to be known as SuperADAM - made good progress too and low-resolution/high-flux option dedicated for soft matter research should be available from the middle of 2010.

The range of activity in this discipline is enormous, and overlaps with biology and materials science. An increasing number of proposals were received on the mechanism and kinetics of association of soft matter, and on nano-objects and ways of controlling their dispersion or aggregation, perhaps in association with a soft matter matrix to produce a soft composite material. Our highlights can only illustrate a few aspects of this broad field, which currently encompasses 15% of demands for beamtime; they are selected to underline the particular power of neutron scattering, exploiting contrast variation to pick out just one component of a complex system.

Rosenfeldt *et al.* performed SANS experiments on the structure and interaction of dendrimers in concentrated solutions. To date, such materials have only been described well in dilute solutions, free from the complicating effects of interactions between the molecules. However, by studying mixed deuterated and hydrogenated dendrimers it was shown to be possible to study single dendrimer conformations at high concentration. Further, it was revealed that although dendrimers are flexible, they are rather shape-persistent even at such high concentrateds.

Colloidal dispersions are frequently stabilised in industrial processes through the use of surfactants and it is often assumed that the surfactant is adsorbed onto the colloidal particles as a uniform layer. Findenegg *et al.* used SANS measurements of the structure of adsorbed surfactants on silica nanoparticles in H_2O/D_2O mixtures and showed that the surfactant adsorbs on its curved surface as micelles. This is suprising because the same surfactant forms wormlike micelles in solution and bilayer films on planar surfaces.

Finally, Mutch *et al.* also used contrast variation SANS to investigate the use of large polymeric additives to trigger crystallisation of smaller protein species, a process that is often very hit-or-miss in practice. This provides clues as to the efficiency of polymers of different size in inducing crystallisation, which could significant in optimising crystallisation conditions for proteins.

http://www.ill.eu/science-technology/science-at-ill/soft-condensed-matter/

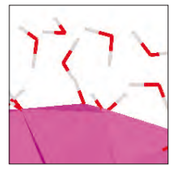

Materials:
cf. article 'Water structure on the surface of imogolite, a natural nanotube found in volcanic soils' p.38

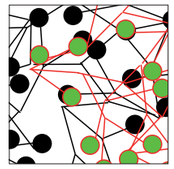

Soft Matter:
cf. article 'Structure and interaction of flexible dendrimers in concentrated solution' p.46

Liquids and Glasses: Lambert van Eijck, College 6 Secretary
Biology: Philip Callow, College 8 Secretary
Nuclear and Particle Physics: Thomas Materna, College 3 Secretary
Spectroscopy: Jacques Ollivier, College 7 Secretary
Modelling and Theory: Robert Whitney, College 2 Secretary

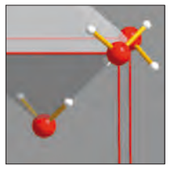

Liquids and Glasses: *cf. article 'Salty ice VII under pressure' p.50*

LIQUIDS AND GLASSES

The large penetration depth of neutrons, the use of contrast variation techniques and the energy scale of the probe in spectroscopic measurements make it an invaluable tool to investigate many of the properties of liquids and amorphous materials, and at present attracts requests for 8% of our beamtime. Particular areas of activity at present include the liquid and glassy dynamics of ionic liquids, polymers, water or biological molecules - including in nano-scale confinement where the confining media such as clays, micro-emulsions or nanoparticles can be made invisible. The incentive for such work ranges from the fundamental, to functional materials whose development depends on a better understanding of the structure and dynamics of amorphous materials over many scales of time and distance.

A trend that has been reinforced in this field in the past year has been the increasing use of extreme conditions, both with respect to temperature and pressure. One reason for this is probably stronger in-house support at ILL for high-pressure experiments with the provision of new cells. The first highlight describes the use of such a cell on D20 to explore the crystallization of ice containing large concentrations of a salt, an additive that had previous been thought to suppress ice formation. Klotz *et al.* have found that it *is* possible to form ice from such mixtures under pressure. Following a precise thermal program with a 1:6 molar concentration of LiCl in D_2O, a type-VII-like ice structure can be generated with the salt ions properly dissolved in the crystal. Further experiments on D20 seem to suggest that other forms of salty ice can exist too. In addition to improving our understanding of hydrogen bonding networks in ices, these results could also be important for modelling the geophysics of moons in the outer solar system.

Nuclear and Particle Physics: *cf. article 'Is our world really isotropic?' p.64*

A second reason for enhanced activity in extreme conditions probably arises from the new Long-Term Proposal system which supported projects to develop improved high-pressure, high-temperature sample environment for liquids and glasses, and a levitation furnace for melts. Both of these have already led to substantial improvements to techniques, which will ultimately be fed back to the wider user community. The first is already bearing scientific fruit, as illustrated by Salmon *et al.* in their work on GeO_2 an analogue of SiO_2, and an interesting model system to study polyamorphic phase transitions that occur in silicates at geological pressures in the earth's crust. Neutron diffraction experiments at corresponding pressures for GeO_2 can now be done in situ on D4 with the apparatus developed through the LTP and show that transitions occur at different length scales depending on the pressure (up to 8 GPa). The dynamics of the earth's crust and its formation are directly related to these phases and their transitions and can only be rationalised satisfactorily through understanding what happens at an atomic level.

http://www.ill.eu/science-technology/science-at-ill/liquids-and-glasses/

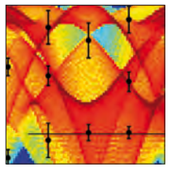

Biology: *cf. article 'Protein-protein interactions in a biological membrane' p.56*

BIOLOGY

The diversity of biological experiments performed at the ILL during 2009 has mirrored the diversity seen in nature itself. Just from the highlights presented in this report we see how biologists are turning to an ever increasing range of neutron scattering techniques and instruments to understand cellular processes; this community now demands 15% of our beamtime.

Gabel *et al.* report on how they have used small-angle neutron scattering to characterise the molecular mechanisms of protein denaturation, which is not only important for understanding protein misfolding which occurs in certain neurodegenerative diseases, but provides insights into the relationship between flexibility and function of physiologically intrinsically disordered proteins. Inelastic neutron scattering has been used by Rheinstädter *et al.* to investigate protein-protein communication and cooperativity in biological membranes, while Roosen-Runge *et al.* have used a combination of quasi-elastic, backscattering and spin-echo neutron scattering techniques to study protein diffusion within the cellular environment. A similar range of techniques were used by Ortore *et al.* when they observed a strong correlation between hydration properties and protein mobility.

It is not only in the field on neutron scattering techniques that biologists are taking a more holistic approach. During 2009 there has been an increased focus on understanding the interactions of biological macromolecules as they fulfill cellular functions, thus increasing the demand for ever more sophisticated approaches to sample preparation for neutron scattering experiments. As a result, the Partnership for Structural Biology, and particularly the Deuteration Laboratory, remains at the heart of the ILL's biology programme. This unique environment, where experts from structural biology and neutron scattering work in close collaboration, means that developments in instrumentation and sample preparation methodologies can move forward in step with the demands of the biological community.

To this end 2009 has seen the first year of operation of a new horizontal reflectometer (FIGARO), an upgraded small-angle neutron scattering diffractometer (D11) and further progress towards the installation of a third SANS instrument (D33). However, it has been recognised that biologist require more than simply world- class instrumentation. As a result, further improvements have been made to how these instruments are accessed. As is noted in the article by Gabel *et al.* complementary neutron and X-ray data collection is not only desirable but frequently vital. Building on the successes of the Block Allocation Group and Long Term Proposal systems, 2009 saw the first joint neutron and X-ray proposals for certain biological experiments.

http://www.ill.eu/science-technology/science-at-ill/biology/

NUCLEAR AND PARTICLE PHYSICS

ILL not only produces neutrons to study matter through diffraction and spectroscopy, but also as a tool to probe the four fundamental forces of Nature. Activity in the nuclear and particle physics group embraces the study of exotic neutron-rich nuclei (PN1), the exploitation of ultra-high resolution gamma spectroscopy (PN3), the use of intense cold neutron beams to study neutron decay asymmetries and neutron-induced nuclear reactions (PF1B), and ultracold beams to study the fundamental properties of the neutron itself (PF2). ILL also acts as host to the CRG instrument CryoEDM, a Rutherford-Sussex collaboration to detect or set an upper limits on the electric dipole moment of the neutron. In total, this activity corresponded to 5% of the total demand for access to ILL's facilities in 2009.

One of the most exciting challenges in particle physics is the quest for new particles beyond the standard model. Some time ago, hypothetic axion-like particles (ALPs) were introduced to explain the absence of CP-violation in strong-interactions and are viable candidates for dark matter in the Universe. A characteristic feature of these particles is that they would mediate a parity and time reversal violating interaction between a fermion and the spin of another fermion. Astronomical observations indicate that they would be light and interact only very weakly with matter, hindering discovery . The first highlight by Fomin *et al.* describes a search for the macroscopic force field these particles may induce in the vicinity of bulk matter. The observable is a neutron spin precession in the vicinity of heavy walls of a chamber for ultra-cold neutrons (UCNs). Measurements at PF2 lead to a significant improvement in the sensitivity limit of the coupling strength of ALP-induced forces.

A similar technique employed at PF2 is presented in the second highlight by Pignol *et al.* to search for a daily modulation in the Larmor frequency of free neutrons placed in a static magnetic field. Such a modulation might reflect the presence of a hypothetical constant cosmic axial field filling the whole Universe and therefore defining a privileged direction, an anisotropy forbidden by one of the most fundamental symmetries of nature, the Lorenz invariance. The study has resulted in the first limit on the coupling of a free neutron with a hypothetical cosmic field. Furthermore, the result can also be interpreted as a limit on the gravitational dipole moment of the neutron from a spin-dependent interaction with the sun.

These highlights reveal the important role of ultra-cold neutrons for research in fundamental physics. New ultra-cold neutron sources with much improved density will be very beneficial, for which a feasibility study is under way within the ESFRI project ILL-20/20. Among experiments that will profit from this source development features the second-generation gravitational neutron spectrometer GRANIT which will shortly be commissioned at the ILL. It shall be employed notably for the search of new spin-dependent and spin-independent short-range forces and for experiments concerning the foundations of quantum mechanics.

http://www.ill.eu/science-technology/science-at-ill/nuclear-and-particle-physics/

SPECTROSCOPY IN SOLID STATE PHYSICS AND CHEMISTRY

Spectroscopy in this context is concerned with structural motion and does not include magnetic excitations - though of course the two may be coupled in systems such as multiferroics. Nevertheless it has a very wide scope, ranging from lattice dynamics and phase transitions to the spectroscopy of molecules absorbed on surfaces and in confining media. It is also conducted over a wide range of instruments from inelastic scattering on the hot neutron spectrometer IN1 to the high-resolution, spin-echo instrument IN15, with a demand for beamtime sitting at 6% of the total for ILL. In many cases though it draws heavily on complementary modelling to plan how best to perform an experiment, or to rationalise what is seen, and here our Computing for Science Service goes from strength to strength with an increasing demand from users.

The cold neutron time-of-flight spectrometer IN5 was returned to the user programme in 2008, and throughout 2009 a host of users and ILL scientists tested its new capabilities, which include a huge enhancement in detected flux rate and a much larger, almost continuous coverage of (Q,ω) space. While these improvements promise much exciting new science, they present new challenges: one is the need to develop faster, more comprehensive ways to visualise and treat data, particularly for single-crystals; another is to speed up the rate at which the sample temperature is changed and equilibrated as this often becomes the rate-determining step in experiments.

The first highlight relates to studies by Horsewill *et al.* on H_2 molecules in fullerenes (C60) using IN4. They showed that all degrees of freedom of the H_2 were quantized, due to their close confinement. In particular, they observed a quantization of the translational motions, a 'quantum rattling', as revealed through additional resolution-limited lines in the spectra.This represents a textbook demonstration of the wave-like properties of a particle - the hydrogen molecule - in a box provided by the C60 cage.

The second highlight related to partial confinement, where there is still a greater degree of freedom in one or two dimensions. Malikova *et al.* used a method proposed by R. Lechner in the mid-nineties to demonstrate the two-dimensional partial confinement of water diffusing in a synthetic hectorite clay powder using IN5. The method is based on the recognition of anisotropic diffusion through the observed deviation from the behaviour expected for 3D diffusion while varying the instrumental energy resolution. This work may have important implications for the study of diffusion processes in materials ranging from hydrogen storage compounds and catalysts; it also provides a nice illustration of the versatility of IN5 in performing measurements over a very wide range of energy resolution.

http://www.ill.eu/science-technology/science-at-ill/colleges/colleges/college7/

Spectroscopy: *cf. article 'Signature of low-dimensional diffusion in complex systems' p.66*

MODELLING AND THEORY

Modelling and theory activity at ILL is traditionally highly multi-disciplinary, and plays a key role in complementing and supporting experimental work, as well as animating the scientific community here. The properties of materials depend on the way in which the constituent elements (atoms, electrons) combine and interact with each other. Because of the enormous complexity of materials and their properties, one is very often far from a thorough theoretical understanding and rather seeks for the main mechanisms that govern the experimentally observed behaviour. Much of the best science often happens when theory is combined with detailed numerical modelling. This year we present two highlights to illustrate this.

Civelli has shown how repulsive electron interactions could cause high-T_c superconductivity, a phenomenon that continues to provide the focus for much experimental work at ILL. Using a numerical method called 'cellular-dynamic mean field theory' the time-dependence of the superconducting gap n the under-doped regime, is shown to be extremely similar to conventional BCS-superconductivity, despite the fact that many experimental properties in this regime do not reflect such a character. He shows that these differences are due to the appearance of a Mott gap (the onset of interaction-induced insulating behaviour) in addition to the superconducting gap.

Whitney *et al.* have discovered a simple yet remarkable interference effect in quantum mechanics (or any other wave mechanics). Interference can enormously reduce the opacity of a tunnel-barrier. For this to occur, one must enclose the barrier in a mirror-symmetric box, with an opening on either side through which the waves can enter and leave. They propose applying this to electrons in quantum dots or to make magnetic-field detectors of similar sensitivity to SQUIDS. Such a striking interference effect may also interest people working in all fields of wave-mechanics, from acoustics to neutron-optics.

http://www.ill.eu/science-technology/science-at-ill/theory/

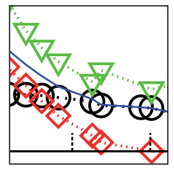

Modelling: *cf. article 'Evolution of the dynamical pairing across the phase diagram of a strongly correlated high-temperature superconductor' p.72*

Cold neutron three-axis spectrometer IN12
Thermal neutron three-axis spectrometer IN22

AUTHORS

W. Knafo (CEA-Grenoble, INAC, SPSMS and LNCMI, Toulouse, France)
S. Raymond and **J. Flouquet** (CEA-Grenoble, INAC, SPSMS, France)
P. Lejay (Institut Néel, Grenoble, France)

Antiferromagnetic criticality at a heavy-fermion quantum phase transition

Heavy fermion compounds provide a unique playground for the study of quantum criticality in strongly correlated electron systems. In recent years, a central question has concerned the microscopic nature of the magnetic quantum critical fluctuations in these systems. Are they antiferromagnetic or of local origin? Using inelastic neutron scattering experiments we have shown that the quantum phase transition in the heavy-fermion material $Ce_{1-x}La_xRu_2Si_2$ is controlled by fluctuations of the antiferromagnetic order parameter.

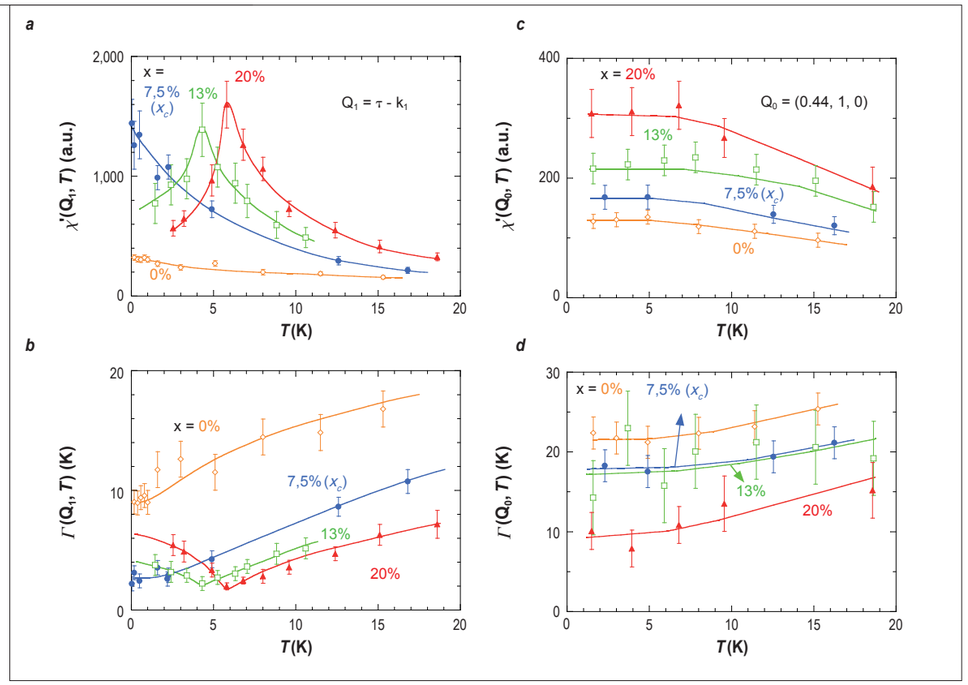

Figure 1: *Temperature variations* ***(a)*** *of the static susceptibility $\chi'(Q_1,T)$;* ***(b)*** *of the relaxation rate $\Gamma(Q_1,T)$, at the antiferromagnetic momentum transfer Q_1, for the lanthanum contents $x = 0$, 7.5 (x_c), 13 and 20 %;* ***(c)*** *of the static susceptibility $\chi'(Q_0,T)$;* ***(d)*** *of the relaxation rate $\Gamma(Q_0,T)$, at the local momentum transfer Q_0, for $x = 0$, 7.5 (x_c), 13 and 20 %. The lines are guides to the eye.*

Heavy-fermion systems are f-electron-based intermetallic compounds in which strong electronic correlations lead to a highly-renormalised Fermi liquid ground state. Huge effective masses, corresponding to 100 - 1000 times the bare electron mass, are associated with the quasi-particles of the Fermi liquid regime [1]. The low value of the related Fermi temperature enables the ground state of the system to be fine tuned as a function of pressure, chemical doping or magnetic field, and to study the physics of quantum phase transitions, which occur at zero temperature. Such transitions are generally driven by quantum fluctuations, as opposed to finite-temperature phase transitions, which are governed by thermal fluctuations. In heavy-fermion systems, the transition occurs between a magnetically ordered phase (often an antiferromagnetic one) and the Fermi-liquid paramagnetic phase. Non-Fermi-liquid behaviour and unconventional superconductivity often emerge in the vicinity of heavy-fermion quantum critical points. These are currently the subject of active theoretical and experimental work.

In the Hertz-Millis-Moriya spin fluctuation theory [2], fluctuations of the antiferromagnetic moment, i.e. of the order parameter, control the quantum phase transition. In this theory, critical antiferromagnetic fluctuations govern the paramagnetic Fermi-liquid regime and their magnitude diverges at the quantum critical point. The non-Fermi-liquid behavior observed in the vicinity of most heavy-fermion quantum critical points is believed to result from the effects of temperature on the critical fluctuations. However, standard spin fluctuation theory fails to describe quantitatively the anomalous properties of this non-Fermi liquid regime. A new theoretical approach has been proposed, based on the concept of local critical magnetic fluctuations [3].

In the present work [4], a complete microscopic study of the spin fluctuation spectrum has been made in the whole quantum critical phase diagram of the archetypal heavy-fermion system $Ce_{1-x}La_xRu_2Si_2$ that orders magnetically for $x \geq x_c = 7.5\%$. Systematic measurements were performed on the three-axis spectrometers IN12 and IN22 on the compounds of concentrations $x = 0$, 7.5, 13, and 20 % at two momentum transfers Q_1 and Q_0. Q_1 = (0.69,1,0) corresponds to the wavevector characteristic of the fluctuations of the magnetic order parameter, and Q_0 = (0.44,1,0) is characteristic of uncorrelated magnetic fluctuations. The spectra measured at Q_0 can be considered as the signature of the local magnetic fluctuations controlled by the Kondo effect, that is the single-site relaxation of a *f* electron by the conduction electrons. Energy spectra were analysed using a quasielastic Lorentzian lineshape, which permitted the static susceptibility $\chi'(Q,T)$ to be extracted, together with the relaxation rate $\Gamma(Q,T)$ plotted in **figure 1**. Maxima of $\chi'(Q_1,T)$ and minima of $\Gamma(Q_1,T)$ are observed at x_c and $T \to 0$, and also at T_N for $x = 13$ and 20 %. This confirms that fluctuations of the magnetic order parameter are maximal at both the quantum ($x_c, T \to 0$) and the classical ($x > x_c, T_N$) phase transitions. No singularity was observed in the local magnetic fluctuations at the transition to the antiferromagnetic phase both across the quantum phase transition ($x_c, T \to 0$) and across the classical phase transition ($x > x_c, T_N$). This indicates that local Kondo-type fluctuations persist in the antiferromagnetic phase, which means that the *f*-electrons still have a strong itinerant character in this regime.

The *x*-*T* phase diagram in **figure 2** summarises the magnetic energy scales and the magnitude of the real part of the static susceptibility $\chi'(Q_1,T)$ determined by neutron scattering for $Ce_{1-x}La_xRu_2Si_2$. The variation with La-doping *x* of the magnetic order parameter M_0 is also shown at the top of the figure. The temperatures $T_1 \underset{T \to 0}{=} \Gamma(Q_1,T)/k_B$ and $T_0 \underset{T \to 0}{=} \Gamma(Q_0,T)/k_B$ are the characteristic energy scales of the antiferromagnetic fluctuations and of the local magnetic fluctuations, respectively. The minimum of T_1 indicates that the low-energy antiferromagnetic fluctuations are maximum at the quantum phase transition at x_c. The absence of a minimum in the x-variation of T_0 signifies that the local fluctuations are not enhanced at the quantum phase transition.

Our data support the scenario where antiferromagnetic fluctuations are responsible for the quantum phase transition of $Ce_{1-x}La_xRu_2Si_2$, since their intensity is maximal at ($x_c, T \to 0$). On the contrary, local magnetic fluctuations are not the driving force, since their intensity varies monotonically across the quantum phase transition.

In conclusion, this study provided experimental confirmation of the pertinence of order parameter fluctuations for the quantum phase transition of the heavy-fermion system $Ce_{1-x}La_xRu_2Si_2$. We propose that similar extensive surveys of the quantum critical phase diagram might also be performed for other quantum magnetic systems, in order to pinpoint the nature of the driving fluctuations at their quantum phase transition.

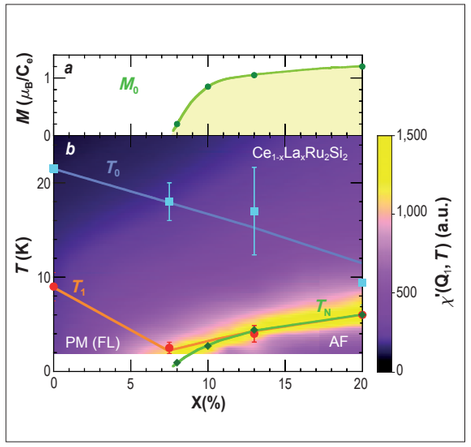

Figure 2: (a) *Variation with La-content x of the low-temperature order parameter M_0 of the antiferromagnetic phase.* ***(b)*** *x-T magnetic phase diagram of $Ce_{1-x}La_xRu_2Si_2$ extracted from neutron scattering experiments (AF = antiferromagnetic order, PM = paramagnetic regime and FL = Fermi liquid). The lines are guides to the eyes, and the intensity of the colour plot corresponds to an extrapolation, in the window $0 \leq x \leq 20$ %, of the staggered static susceptibility $\chi'(Q_1,T)$ measured here for $x = 0$, 7.5, 13, and 20 %.*

REFERENCES

J. Flouquet, Prog. Low Temp. Phys. 15 (2005) Chapter 2 **[1]**
T. Moriya and T. Takimoto, J. Phys. Soc. Jpn. 64 (1995) 960–969 **[2]**
P. Coleman, C. Pépin, Q. Si and R. Ramazashvili, J. Phys. Condens. Matt. 13 (2001) R723–R738 **[3]**
W. Knafo, S. Raymond, P. Lejay and J. Flouquet, Nature Physics, Vol. 5 (2009) 753 **[4]**

AUTHORS

N. Tsyrulin (LSSP ETH Zurich and LNS PSI Villigen, Switzerland)
T. Pardini and **R.R.P. Singh** (University of California, Davis, USA)
F. Xiao and **C.P. Landee** (Clark University, Worcester, Mass., USA)
P. Link (FRM II, Garching, Germany)
A. Schneidewind (FRM II, Garching and TU Dresden, Germany)
A. Hiess (ILL)
M. M. Turnbull (Clark University, Worcester, Mass., USA)
M. Kenzelmann (LSSP ETH Zurich and LDM PSI Villigen, Switzerland)

Quantum effects in a weakly-frustrated S=1/2 two-dimensional square-lattice antiferromagnet in zero and applied magnetic field

Low-dimensional magnets can have unusual ground states and spin correlations, especially for small spin values such as S=1/2. A prime historical example is the class of the high-temperature superconducting cuprates whose undoped phases consist of two-dimensional antiferromagnetic planes of spins S=1/2. We have studied the two-dimensional S=1/2 square-lattice antiferromagnet $Cu(pz)_2(ClO4)_2$ using neutron inelastic scattering and series expansion calculations. The presence of antiferromagnetic next-nearest neighbour interactions enhances quantum fluctuations associated with resonating valence bonds. Intermediate magnetic fields lead to a selective tuning of resonating valence bonds and a spectacular inversion of the zone-boundary dispersion, providing a novel insight into two-dimensional antiferromagnetism in the quantum limit.

The organo-metallic material $Cu(pz)_2(ClO_4)_2$ crystallises in the monoclinic crystal structure and contains perfect square lattices of Cu^{2+} ions in the crystallographic bc-plane. Tetrahedra of ClO_4- located between copper layers provide a good spatial isolation of copper square-lattice planes (**figure1**). The material represents an ideal model system for the two-dimensional XY antiferromagnet with a small nearest-neighbour interaction equal to $J_1 = 1.53$ meV [1], which corresponds to a relatively low saturation field $\mu_0 H \sim 45$ T.

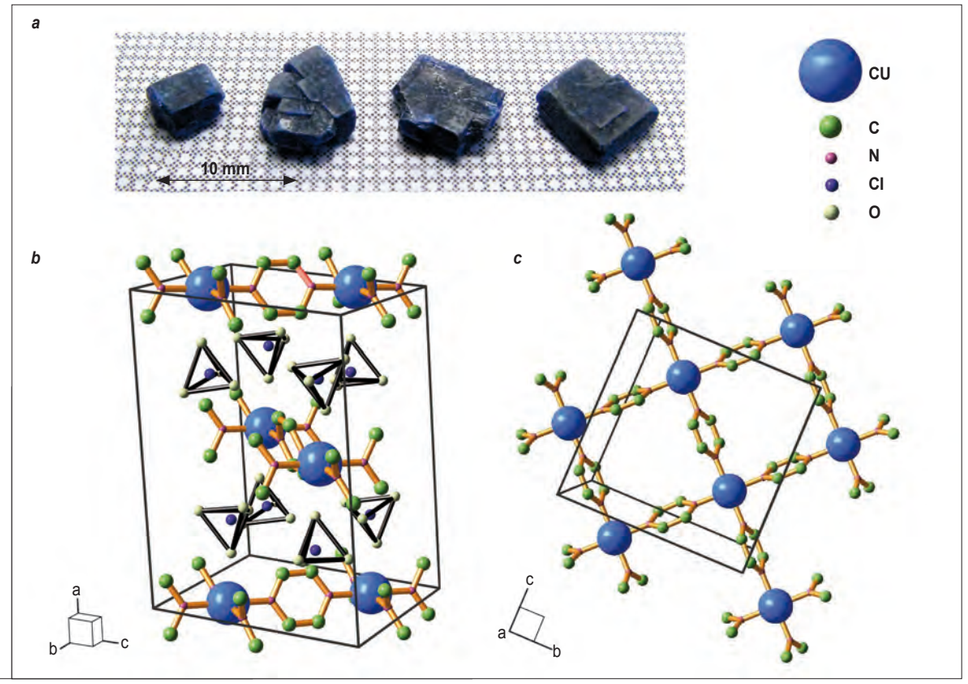

Figure 1:
(a) *Single crystals of $Cu(pz)_2(ClO_4)_2$.*
(b) *Three-dimensional view of the crystal structure of $Cu(pz)_2(ClO_4)_2$.*
(c) *The projection of the crystal structure on the bc-plane shows the Cu^{2+} square-lattice structure.*

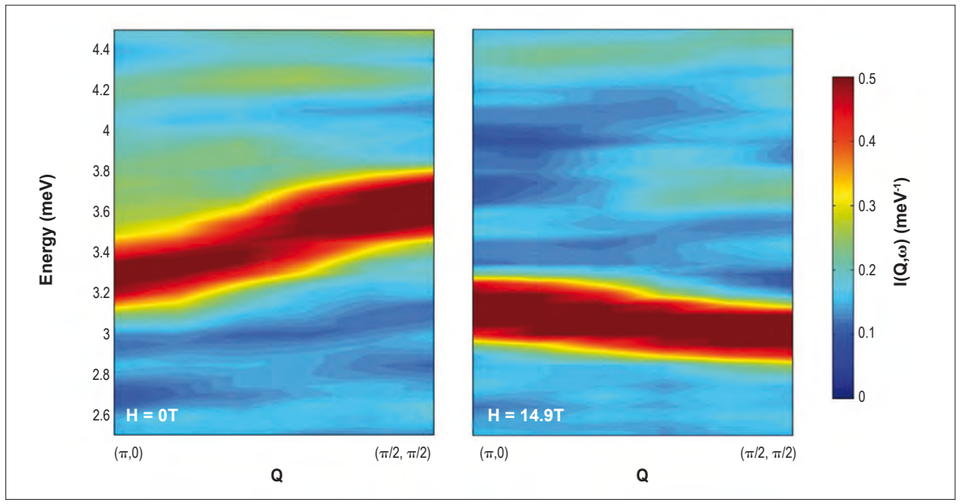

Figure 2: *Zone boundary spin dispersion at zero field and H ~ J. Colour plot of the normalised scattering intensity $I(Q,\omega)$ at T = 80 mK, showing the dispersion from $(\pi,0)$ to $(\pi/2, \pi/2)$ at zero field and $\mu_0 H = 14.9$ T under otherwise identical conditions. Both panels present smoothed data obtained by performing six constant Q-scans from $(\pi/2,\pi/2)$ to (π,π) with a 0.05 meV energy step.*

This makes the compound attractive for an experimental investigation of quantum effects in the S = 1/2 square-lattice antiferromagnet in magnetic fields. We probed the spin dynamics in a sample of single crystals of $Cu(pz)_2(ClO_4)_2$ as a function of magnetic field at millikelvin temperatures using cold neutron three-axis spectrometer IN14.

The normalised neutron scattering spectra at the antiferromagnetic zone boundary is shown in **figure 2** for zero applied field and $\mu_0 H \sim 14.9$ T. Contrary to conventional spin-wave theory, the onset of the excitation at the reciprocal wave-vector $(\pi,0)$ is diminished by 11.5(7)% in energy compared to $(\pi/2,\pi/2)$ at zero field. This zone-boundary dispersion is also larger than expected from numerical calculations for the square-lattice antiferromagnet with nearest-neighbour interactions [2]. Series expansion calculations for the J_1-J_2 model, where J_2 is the next-nearest neighbour interaction in a square-lattice plane, revealed that the observed enhancement of the zone boundary dispersion in $Cu(pz)_2(ClO_4)_2$ arises from a small antiferromagnetic next-nearest neighbour interaction $J_2 \sim 0.02$-$0.05\ J_1$. Another fascinating feature detected in our zero field experiment is the presence of a magnetic continuum near $(\pi,0)$. Being a purely quantum effect, the observed magnetic continuum arises from a local zero-temperature fluctuations between neighbour spins referred to as resonating valence-bond fluctuations [3]. These are also precisely the fluctuations that lead to the dispersion of the magnetic excitation along the antiferromagnetic zone boundary (**figure 2a**).

Figure 2b shows that a magnetic field leads to an inverted zone boundary dispersion which was measured at $\mu_0 H \sim 14.9$ T, indicating a strong coupling between magnetic fields with local quantum fluctuations. The field-induced dispersion demonstrates a field tuning of valence bond fluctuations in the two-dimensional antiferromagnet, and the presence of local quantum fluctuations in the two-dimensional S = 1/2 square-lattice antiferromagnet even for fields of the order of H ~ J.

In summary, we show that the presence of a small antiferromagnetic next-nearest neighbour interaction enhances quantum fluctuations related to resonating valence bonds in the square-lattice S = 1/2 antiferromagnet. Field tuning of resonating valence bonds brings a novel insight into two-dimensional antiferromagnetism in the quantum limit.

REFERENCES

F. Xiao *et al*, Phys. Rev. B 79 (2009) 134412 **[1]**
R. R. P. Singh, M. P. Gelfand, Phys. Rev. B 52, R15695 (1995) **[2]**
S. Sachdev, Nature Physics 4 (2008) 173 - 185 **[3]**

AUTHORS

H. Nojiri, **S. Yoshii** and **K. Ohoyama** (IMR Tohoku University, Japan)
M. Matsuda (JAEA, Tokai, Japan)
S. Michimura and **F. Iga** (Hiroshima University, Japan)
P. Frings, **F. Duc**, **B. Vignolle** and **G.L.J.A. Rikken** (LNCMI, Toulouse, France)
L.-P. Regnault (INAC-SPSMS-MDN, CEA-Grenoble, France)

Neutron diffraction in 30 Tesla pulsed magnetic fields: application to the frustrated antiferromagnet TbB_4

A magnetic field often induces an unexpected magnetic structure when various interactions are competing. By using a portable miniature pulsed magnet, we have succeeded in performing neutron diffraction in very strong magnetic fields up to 30 Tesla. We have applied the technique to determine the magnetic structure of the frustrated antiferromagnet TbB_4, which shows unusual multiple magnetisation plateau behaviour. This investigation demonstrates the great potential of this technique to perform neutron diffraction measurements in pulsed magnetic fields .

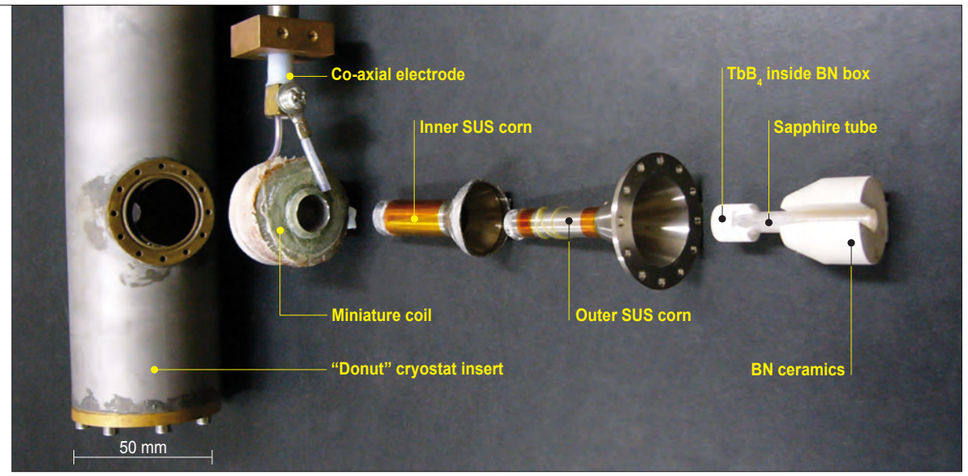

Figure 1: *Photograph of the mobile miniature pulsed magnet system. The tube on the left is the bottom of the cryostat insert. The magnet is cooled by liquid nitrogen and is separated from the sample space by the insulation vacuum between the two SUS corn pipes. The sample is attached to the sample rod made of sapphire and BN ceramics.*

A magnetic field is a powerful and precise tuning parameter for interactions in magnetic systems. It may induce various new states with unexpected magnetic structures in so-called frustrated antiferromagnets. When only one interaction is dominant, a simple ground state is realised. This is the case for the well-known ferromagnetic or antiferromagnetic systems, where magnetic moments align parallel or anti-parallel to satisfy the interactions. When several interactions are competing and/or magnetic moments are sitting geometrically frustrated lattices such as the triangular, Kagome or Shastry-Sutherland cases, it is impossible to satisfy simultaneously all interactions. In such situations, many arrangements of magnetic moments have almost identical energy and thus the system cannot find a unique ground state. When a magnetic field is applied, the degeneracy between the various arrangements may be lifted, selecting a sub-set of states, some of which may be non-trivial.

It is very difficult to predict *a priori* what kind of state will be selected. Hence, it is essential to perform neutron diffraction, which is the most direct method to determine the magnetic structure. By applying a high magnetic field to strongly frustrated antiferromagnets whilst performing neutron diffraction experiments, 'magnetists' can hope to mine a rich seam of exotic magnetic systems.

Obviously, depending on the type of magnet under investigation, this task can be more or less difficult to achieve. Neutron diffraction has so far only been combined with moderate dc magnetic fields, with a current limit of 17 Tesla. Recently, we made a breakthrough by combining a 30 Tesla portable miniature pulsed magnet and the world brightest neutron source at the ILL. In a pulsed magnet, a current as large as several kA is supplied by a large capacitor bank, generating a magnetic field of several tens of Tesla for several milliseconds. It is impossible to install a large conventional capacitor bank into the limited space of a neutron spectrometer. However, the compact design of our miniature magnet, coupled with a very compact mobile capacitor bank, provided through the High Magnetic Field Laboratory in Toulouse, enables us to use it for neutron diffraction without any modification of the spectrometer.

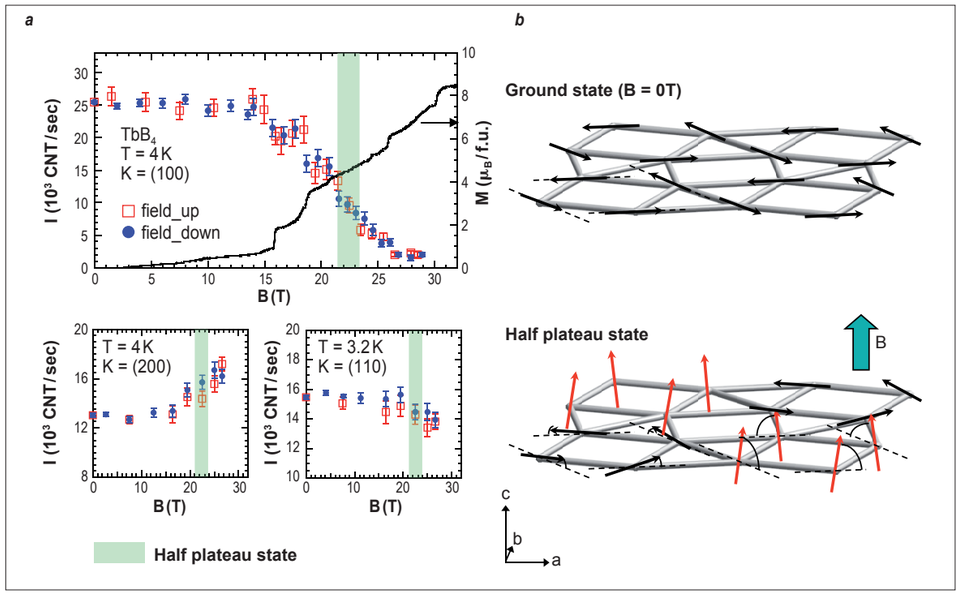

Figure 2: (a) *Magnetisation curve and the magnetic field dependence of (100), (200), (110) Bragg peaks. The coloured area is the half-plateau phase. The magnetic field is applied perpendicular to the ab-plane.* ***(b)*** *Magnetic structure of TbB_4 at zero magnetic field and in half-plateau state. The half plateau state is made of two types of magnetic blocks. It is stabilized presumably by the biquadratic interaction.*

The magnet itself, together with the compact insert system designed to fit into a standard ILL cryostat (**figure 1**) was actually carried in the pocket of a member of the experimental team when they flew from Japan .

We examined the magnetic structure on the multiple magnetisation plateaus in the frustrated antiferromagnet TbB_4 [1]. As shown in **figure 2**, the crystal forms a Shastry-Sutherland lattice, where rectangles and triangles align alternatively in a two dimensional layer. Tb moments lie within the layer due to the presence of strong planar magnetic anisotropy. When a magnetic field is applied, several steps appear in the magnetisation process. This contradicts the well-known fact that the magnetisation of a planar antiferromagnet increases linearly with magnetic field intensity when a magnetic field is applied perpendicular to the plane.

We measured the time dependence of the [100] magnetic-peak intensity in a sinusoidal shaped pulsed magnetic field of 7 milliseconds duration [2]. The data was accumulated over 100-200 shots at the rate of 10 shots/hour. It was then converted into the magnetic field dependence of the intensity as shown in **figure 2(a)**. The intensity exhibits multiple steps corresponding to the magnetization steps. By repeating measurements at several Bragg peaks, the magnetic structure model in **figure 2(b)** could be determined for the half-plateau state where the magnetization is half that of the saturation. Surprisingly enough, the structure consists of a stacking of ferromagnetic and planar antiferromagnetic blocks. This shows the large contribution of the biquadratic exchange interaction causing the orthogonal arrangement between the magnetic moments. We stress here that such a non-trivial structure could be resolved only by neutron diffraction experiments in 30 Tesla fields.

This experiment demonstrates the power of miniature pulsed magnets for neutron diffraction. It also emphasises the importance of developing a high steady magnetic-field installation, which in future may enable inelastic scattering to be combined with very high magnetic fields.

REFERENCES

S. Yoshii, T. Yamamoto, M. Hagiwara, S. Michimura, A. Shigekawa, F. Iga, T. Takabatake and K. Kindo, Phys. Rev. Lett. 101 (2008) 087202 **[1]**

S. Yoshii, K. Ohoyama, K. Kurosawa, H. Nojiri, M. Matsuda, P. Frings, F. Duc, B. Vignolle, G. L. J. A. Rikken, L.-P. Regnault, S. Michimura and F. Iga, Phys. Rev. Lett. 103 (2009) 077203 **[2]**

AUTHORS

C. Pappas (University of Delft, The Netherlands and Helmholtz-Zentrum Berlin, Germany)
E. Lelièvre-Berna, **P. Falus**, **P. M. Bentley**, **P. Fouquet** and **B. Farago** (ILL)
E. Moskvin (Helmholtz-Zentrum Berlin, Germany and PNPI, Gatchina, Russia)
S. Grigoriev (PNPI, Gatchina, Russia)

Spin-echo spectrometer IN11
Spin-echo spectrometer IN15

A skyrmion spin liquid phase in MnSi

Chirality, the breaking of symmetry between right and left, manifests itself in parity violation at the sub-atomic level, governs biology and is also an important parameter in magnetism. Moreover, chirality is an essential ingredient for the appearance of a very special type of quasiparticle called a skyrmion, which bridges the gap between waves and particles in the particle-wave duality description and was introduced by Skyrme in the early 1960's [1]. Using neutron spin-echo spectroscopy and spherical polarimetry we have proven the existence of this evasive quasiparticle in MnSi at zero magnetic field.

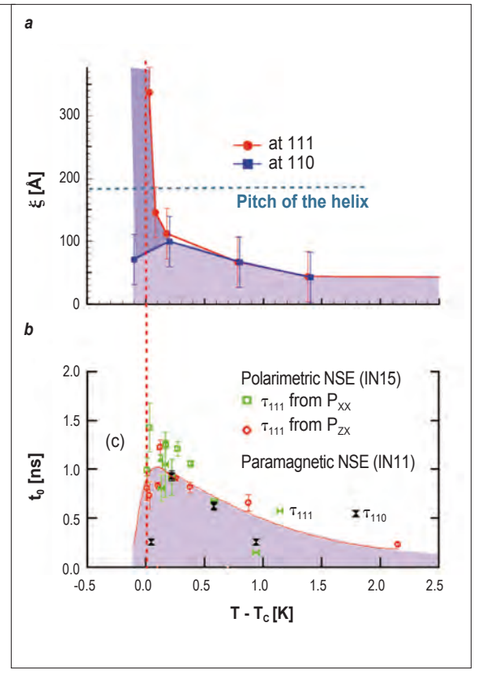

Figure 1: *Correlation lengths deduced from the Ornstein-Zernike analysis of the Q- dependent intensity* ***(a)*** *and characteristic times of the fluctuations* ***(b)*** *around τ_{111} and τ_{110}. Both at τ_{111} and at τ_{110} the fluctuations scale with the correlations at τ_{110} (light purple areas). The helical Bragg peak (dark purple area) coexists with the fluctuating skyrmion-like chiral spin liquid phase at T_C.*

Skyrmionic, vortex-like, states and lattices may occur in magnetism, when the underlying atomic structures lack inversion symmetry and the anti-symmetric Dzyaloshinskii-Moriya interactions introduce a parity-breaking term in the Hamiltonian. In the chiral itinerant-electron magnet MnSi, a skyrmion lattice was recently identified on the application of external magnetic fields [2]. Moreover, this system is a candidate for observing a spontaneous skyrmion-like short range order, similar to the partial order in liquid crystals, even at zero magnetic field [3].

The spins in MnSi order into a single-domain left-handed helix below T_C~29 K. The helix propagates along the <111> crystallographic directions with a period of ~175 Å, which leads to well defined Bragg peaks at $000+\tau_{111}$ and $|\tau|$~0.036 Å^{-1}. Immediately above T_C the Bragg peaks are replaced by diffuse magnetic scattering, which concentrates on the surface of a sphere with radius $|\tau|$ and shows up as a ring on the two-dimensional small angle neutron scattering patterns [4]. When the neutron beam is polarised, the rings reduce to half-moons due to the chiral nature of the correlations.

Our recent neutron spin-echo (NSE) and spherical polarimetry measurements on IN15 in conjunction with 'conventional' NSE on IN11 reached the high resolution required to show that this unconventional short range order is the magnetic equivalent of a liquid crystal and may be qualified as a 'skyrmionic spin liquid' [5]. NSE measures the intermediate scattering function I(Q,t) and allows for a quantitative analysis of the magnetic correlations with very high resolution both in space and time. **Figure 1a** shows the deduced characteristic helical correlation lengths ξ: at the Bragg peaks, i.e. at τ_{111}, the correlations diverge (ξ_{111} and dark purple area on **figure 1a**) whereas away from the peaks (e.g. ξ_{110} at τ_{110}) correlations stay finite and are significantly smaller than the pitch of the helix. The correlated volumes fluctuate with characteristic times t_0, which, however, do not reflect the anisotropy of the correlations. All the times t_0 scale with ξ_{110} (light purple areas on **figures 1a** and **1b**) without any critical slowing down at τ_{111}. Consequently ξ_{110} measures the fluctuating volumes even at τ_{111} and **figure 1** is a paradigm for a first order phase transition: the Bragg peaks are not borne out of the spin-liquid phase but two phases coexist at T_C. The helical first-order transition is marked by the sudden increase by more than one order of magnitude of the neutron intensity at τ_{111} (**figure 2a**). On the other hand, the perfect left-handed single-domain chirality of the helical phase is not affected by the first order transition and persists up to T_C'~T_C+1 K (**figure 2b**). Above T_C the fluctuating volumes are relatively small and an unpinned helical order, as assumed in [4], would give the dotted green line on **figure 2b**. The discrepancy between the calculated and measured curves illustrates the non-conventional character of the phase between T_C and T_C'. This phase combines dynamical disorder with a perfect left-handed single-domain chirality and is perfectly described by the theoretically predicted skyrmionic ground state for MnSi [3]: skyrmionic textures are indeed energetically stable at short distances, robust against thermal fluctuations, account for the inherent topology of this single-domain spin-liquid phase and drive the helical transition to first order.

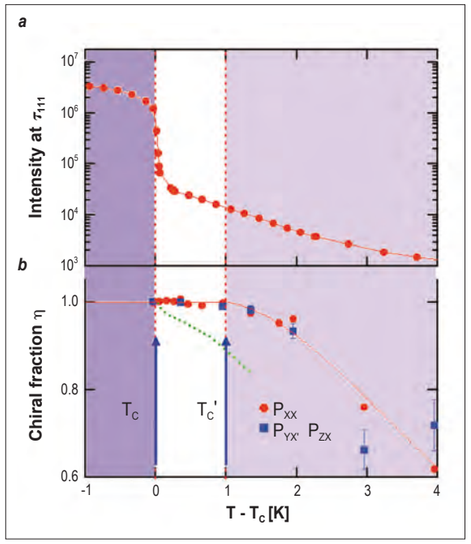

Figure 2: *Intensity at τ_{111} the position of the helical peak* ***(a)*** *and chiral fraction of the dominant left handed domain determined from spherical polarimetry* ***(b)***. *The helical phase is shown by the dark purple area, whereas the disordered fluctuating phase is indicated by the light purple area. The white area between T_C and $T_C' = T_C$ +1 K is a single domain chiral but fluctuating skyrmionic spin liquid phase.*

In summary, our high resolution neutron spin-echo spectroscopy and polarimetry measurements give evidence for the existence of a disordered skyrmion phase and provide the missing link in getting a consistent picture of the spin-liquid phase of MnSi above T_C. This phase is a completely chiral single-domain and strongly fluctuating new state of matter and occurs only in a very narrow temperature range of ~ 1 K above the helical phase of MnSi.

REFERENCES

T. Skyrme, Proc. R. Soc. Lond. Ser. A 260 (1961) 127 **[1]**
S. Mühlbauer *et al*, Science 323 (2009) 915 **[2]**
U. K. Rössler, A. N. Bogdanov and C. Pfleiderer, Nature 442 (2006) 797 **[3]**
S. V. Grigoriev *et al*, Phys. Rev. B 72 (2005) 134420 **[4]**
C. Pappas *et al*, Phys. Rev. Lett. 102 (2009) 197202 **[5]**

T. Fennell, **P.P. Deen** and **A.R. Wildes** (ILL)
K. Schmalzl (IFF, FZ Jülich, Germany - JCNS at ILL)
D. Prabhakaran and **A.T. Boothroyd** (Clarendon Laboratory, Oxford, UK)
R.J. Aldus, **D.F. McMorrow** and **S.T. Bramwell** (London Centre for Nanotechnology and University College London, UK)

Coulomb phase in the spin ice $Ho_2Ti_2O_7$

Magnetic monopoles are free particles carrying magnetic charge, whose interactions obey a magnetic Coulomb law. Their existence was postulated by Dirac in order to explain the quantisation of electric charge. Despite extensive searches no such particles have been (reproducibly!) detected. In condensed matter, many body effects are increasingly understood by appealing to emergent analogues of high energy phenomena. In this case, the quasi-particle excitations of a spin ice are a type of magnetic monopole [1]-[5].

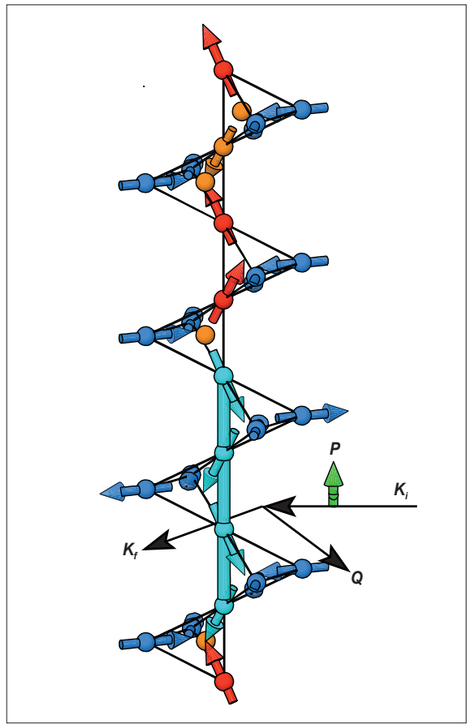

Figure 1: *Monopole phenomena in spin ice: ice rule obeying tetrahedra have two spins in and two spins out, and non-divergent magnetisation; defects are formed by spin flips leading to one in and three out (or vice versa) configurations and a pair of monopoles (top two tetrahedra). Subsequent spin flips can separate the monopoles, leaving a ferromagnetic string (e.g. in cyan, spanning the lower tetrahedra). The scattering geometry means that the scattering vector (**Q**) lies in the horizontal plane with the incident polarisation (**P**) vertical (indicated in green), such that all four spins of each tetrahedron contribute to the spin flip scattering, but only two can contribute to the non-spin flip scattering (the blue spins lie in the scattering plane so provide no component perpendicular to **Q** and parallel to **P**).*

A spin ice is a material in which the spin configurations map to the arrangement of hydrogen atoms in a crystal of water ice. In both cases, many degenerate ground states can be constructed by ensuring that the local degrees of freedom (in spin ice, the spins; in water ice, the configuration of hydrogen bonds about an oxygen atom) satisfy a simple constraint, or ice rule. In a spin ice, the rare earth ions, which are the magnetic species, lie on a lattice of corner sharing tetrahedra. Each magnetic moment can point only along the body axes of their tetrahedra and the groundstate of a single tetrahedron is obtained by ensuring that two spins point in and two point out (**figure 1**). The ground states of a spin ice are the spin configurations which satisfy the constraint on all tetrahedra. Despite the apparent simplicity of the ice rule, and the absence of long range order, it produces long range correlations. Detailed theoretical treatments show that the spin correlations decay as $1/r^3$, and have the spatial dependence of the dipolar interaction. Coarse graining the spin configurations produces a non-divergent field with properties directly analogous to an electric field, such that materials in which an ice rule constraint operates are known as Coulomb phases. A single spin flip produces a pair of topological defects in adjacent tetrahedra, where the ice rules and the divergence-free condition are broken. Ice rule defects in spin ices such as $Ho_2Ti_2O_7$ were predicted to behave as emergent magnetic monopoles, as the degenerate spin ice states allow them to unbind, but the underlying Hamiltonian is dominated by the dipolar interaction, which gives the defects a Coulomb-law interaction. Once created, the monopoles unbind because further spin flips separate the defects, without further breaking of the ice rules. The monopoles diffuse away from one another, trailing a line of head to tail spins behind them. This is a classical analogue of the string joining Dirac monopoles and the spin ice states form a network of these strings whose relaxation rapidly renders the original string unobservable, leading to unbound diffusive monopole dynamics.

The essential signature of the Coulomb phase, which can be regarded as the vacuum in which the monopole quasi-particles appear, is the existence of pinch points in the diffuse scattering. These are a direct consequence of the divergence-free condition and dipolar correlations. In many frustrated magnets, the correlations are entirely short ranged and decay exponentially with distance, leading to broad diffuse scattering. In frustrated magnets with dipolar correlations, some broad features are visible,

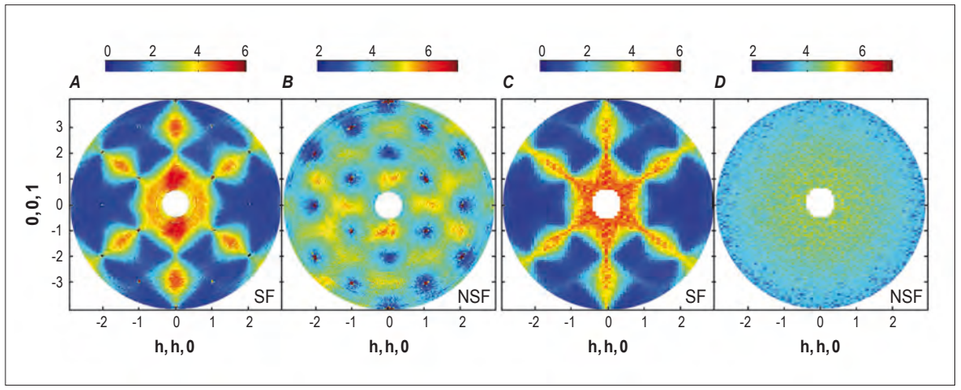

Figure 2: *Diffuse neutron scattering from $Ho_2Ti_2O_7$ at 1.7 K. The experimental scattering in the spin flip and non-spin flip channels (**A** and **B**) are compared with Monte Carlo simulations for a near neighbor spin ice model (**C** and **D**). The clear existence of the pinch points at (0,0,2), (1,1,1) and (2,2,2) in the spin flip channel indicates that $Ho_2Ti_2O_7$ is a Coulomb phase, as required for the existence of magnetic monopoles. Previous experiments have measured the total of **A** and **B**, in which the pinch points are effectively invisible.*

but also very sharp nodes, indicating that long range correlations are present. Different model Hamiltonians of spin ice are expected to produce identical dipolar correlations and pinch point scattering, irrespective of the interaction which establishes the ice rules (many ice models employ near neighbor interactions, but models based on dipolar interactions are much more realistic for $Ho_2Ti_2O_7$ and pinch points are a requirement of both for the existence of the Coulomb phase). However, the pinch points have never been clearly observed in previous experiments.

The crystal was mounted with the (*h,-h,0*) axis vertical, giving an (*h,h,l*) scattering plane. The incident polarisation was vertical (*z*) and we measured the non-spin flip (NSF) and spin flip (SF) cross sections. In this geometry two spins on each tetrahedron lie in the scattering plane and do not contribute to the NSF scattering (**figure 1**). We therefore separate the total magnetic diffuse scattering into two contributions: one due to the correlations amongst spins on all four sublattices and characteristic of the ice rules; and one not expected to show any structure on the basis of ice rule correlations alone. The upgraded instrument D7 [6] allowed unprecedented coverage of the scattering plane, enabling detailed comparison with simulation. In a Monte Carlo simulation of a simple model of spin ice, which captures the ice rule correlations, we clearly see the pinch points which are also present in the experimental SF scattering, showing that the spin ice materials do indeed enter a Coulomb phase. However, the NSF channel is quite different to the calculation, indicating that the postulated equivalence of different spin ice Hamiltonians requires further attention (**figure 2**).

The agreement between the experimental data and simulations allow one to isolate the scattering contribution from ice rule defects as the temperature is increased. For example in **figure 2** the SF channel contains a contribution which depends only on $|q|$ and increases in intensity as the temperature rises. This is due to the formation of bound pairs of monopoles, which are uncorrelated defects in the ice rules. Their concentration can be well fitted by an expression characterising the creation of single and double defects by thermal fluctuations. The intensity at the pinch point (which is at the zone centre) is due to long wavelength ferromagnetic fluctuations of the magnetisation which we identify with the longest length scale in the string network. Using IN12, we were able to extract the width of the pinch point as a function of temperature and show that as the bound pairs are suppressed at low temperature, the length scale of the string network diverges exponentially, pointing to a small population of unbound monopoles at low temperature.

REFERENCES

C. Castelnovo *et al.*, Nature 451 (2008) 42 **[1]**
T. Fennell *et al.*, Science 326 (2009) 415 **[2]**
D.J.P. Morris *et al.*, Science 326 (2009) 411 **[3]**
H. Kadowaki *et al.*, J. Phys. Soc. Japan 78 (2009) 103706 **[4]**
S.T. Bramwell *et al.*, Nature 461 (2009) 956 **[5]**
J.R. Stewart *et al.*, J. Appl. Cryst. 42 (2009) 69 **[6]**

L. Malavasi and **C. Tealdi** (University of Pavia, INSTM and IENI-CNR, Italy)
C. Ritter (ILL)

In situ time-resolved neutron diffraction investigation during oxygen exchange in layered cobaltite cathode material

The development of *in situ* methods for the characterisation of condensed matter is becoming one of the major issues in current research on materials.
Thanks to the high intensity characteristics of the D20 diffractometer at the ILL we were able to follow *in situ*, as a function of time, the structural evolution during oxygen exchange of the $HoBaCo_2O_{5+\delta}$ layered cobaltite which is a promising cathode material for clean energy applications.

Neutron diffraction (ND) is a valuable tool in order to investigate oxides due to the sensitivity of neutrons to light atoms such as oxygen and to the possibility of revealing superstructure peaks. Highly studied materials which benefit from the investigation through ND are solid state ionic materials (SSI - mainly electrolytes and mixed ionic-electronic materials) where, for example, the study of oxygen exchange processes are of great importance in order to test their performance and define the temperature range for their potential application.

We report here on *time-resolved in situ* ND measurements carried out under isothermal conditions (at temperatures where oxygen gas-solid equilibration is relatively fast) while varying the oxygen partial pressure, $p(O_2)$, inside the measurement apparatus [1]. By recording neutron diffraction patterns at proper time intervals it is possible, through the refinement of oxygen occupancies, to determine the concentration profile during oxygen exchange and, at the same time, have a clear insight into the structural changes occurring in the sample when oxygen is introduced or removed from it. This experiment has been carried out on the D20 instrument on the $HoBaCo_2O_{5+\delta}$ layered cobaltite which is a promising cathode material for solid oxide fuel cells (SOFC).
In detail, the neutron powder diffraction measurements were carried out on a sample put into a sealed quartz sample holder equipped with a gas inlet system connected to certified gas cylinders. The sample was first annealed under argon atmosphere, $p(O_2)=10^{-6}$ atm, at 573 K and left under these conditions until the equilibrium oxygen content had been achieved (followed by the evolution of selected diffraction peaks). Once equilibrium had been reached, the gas flux was suddenly changed from pure argon to pure oxygen, $p(O_2)=1$ atm, and the diffraction patterns were collected every 120 seconds at a wavelength of 1.30 Å in the angular range from 5 to 130° using the high resolution mode. After equilibration to the new oxygen content the gas flux was switched back to argon. The same procedure was then repeated at 673 and 773 K.

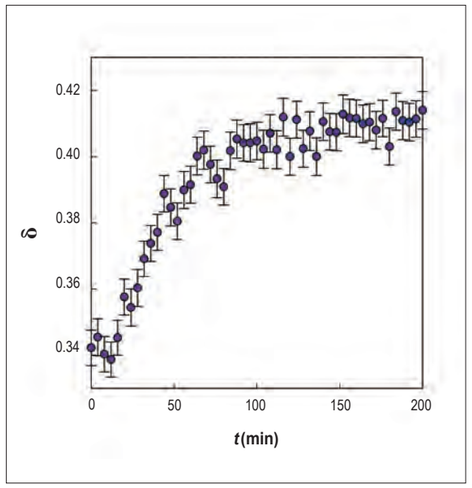

Figure 1: *δ variation of $HoBaCo_2O_{5+\delta}$ at 573 K when switching from Ar to O_2.*

From the Rietveld refinement, based on the neutron data, it was determined that for all the temperatures investigated, both under argon and oxygen atmospheres, the $HoBaCo_2O_{5+\delta}$ patterns are properly described by considering the tetragonal *P*4/mmm crystal structure with $a=b=a_p$ and $c\sim 2a_p$, in agreement with previous work in which $0<\delta<0.50$. In the tetragonal structure there are three distinct oxygen sites: O1 located at (0,0,0), O2 at (0,0,0.5) and O3 at (0,0.5,~0.301). The oxygen vacancies are located in the Ho layers and along with the increase in the population of the HoO_δ layer the coordination of the Co ions changes from pyramidal ($CoO5$) to octahedral (CoO_6) with the coexistence of both coordinations for $0<\delta<1$.

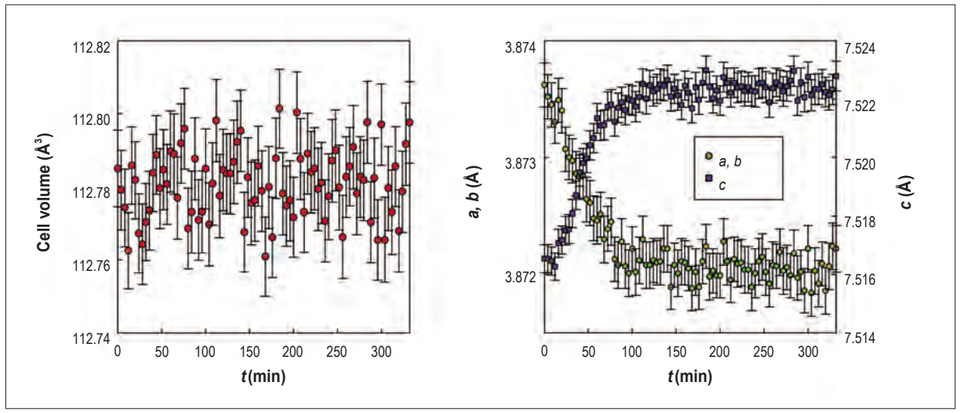

Figure 2: *Cell volume (panel A) and lattice parameters (panel B) variation as a function of time during oxygen insertion at 573 K.*

Figure 1 shows the increase of the oxygen content for the $HoBaCo_2O_{5+\delta}$ cobaltite as a function of time at 573 K when switching the gas flux from Ar to O_2. The δ-value has been determined from the refined occupancies of the O2 site while keeping the O1 and O3 sites fully occupied. In an analogous way to the data shown in **figure 1** (at 573 K), we collected and refined the data at 673 and 773 K.
Figure 2 shows the variation of the lattice parameters and cell volume as a function of time for the oxygen insertion at 573 K, selected as a representative example. It can be seen that the cell volume remains substantially unchanged upon oxygen content exchange while the *a*(*b*) and *c* lattice parameters show opposite behaviour. The *a*(*b*) parameter linearly decreases as the δ-value inccreases during oxygen exchange whereas the *c* parameter expands. Similar behaviour of the cell parameters is also found at 673 and 773 K.

Finally, **figure 3** presents the overall change of the lattice parameters of the $HoBaCo_2O_{5+\delta}$ cobaltite as a function of oxygen content (calculated by refinement of O occupancies as a function of time) determined *in situ* at the three selected temperatures. The data have been normalised for the structure expansion due to the temperature variation. Overall, the cell volume is essentially constant over the oxygen content range explored in this work.

In conclusion, we have presented here the first *time-resolved in situ* neutron diffraction experiment aimed at determining the changes occurring in the structure of an oxide material during oxygen exchange. The experimental approach presented in this work can be extended to an extremely wide class of materials and opens the possibility to precisely study the structural rearrangements involved in any gas/solid exchange process where species sensitive to neutrons are involved.

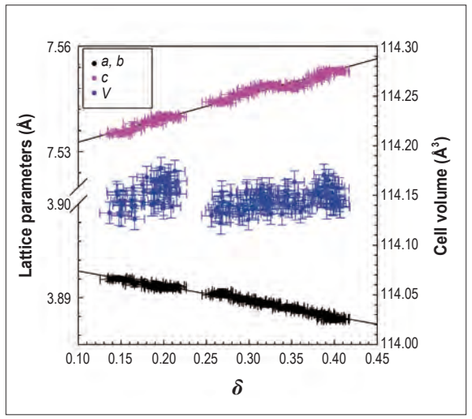

Figure 3: *Lattice parameters and cell volume variation as a function of δ for $HoBaCo_2O_{5+\delta}$.*

REFERENCES

L. Malavasi, C.Tealdi and C. Ritter, Angew. Chem. Int. Ed. 48 (2009) 8539-8542 **[1]**

AUTHORS

M. Bahout, **F. Tonus** and **T. Roisnel** (Université de Rennes 1, CNRS, France)
S.E. Dutton and **P.D. Battle** (University of Oxford, UK)
P.F. Henry (ILL and Helmholtz-Zentrum Berlin, Germany)
T. Hansen (ILL)

Use of *in situ* neutron diffraction to monitor the reaction between a complex oxide and H_2 gas at high temperature

It is important for materials chemists to be able to know the details of how compounds react at high temperatures and in aggressive atmospheres. We have demonstrated that this information can now be collected *in situ* using neutron diffraction techniques: it is no longer necessary to rely on a comparison of 'before and after' data. We show that the reaction between H_2 gas and $Pr_2Sr_2CrNiO_8$ occurs between 325 and 400°C and involves selective removal of oxygen from only one of the two crystallographic sites corresponding to a reduction of Ni(III) to Ni(II).

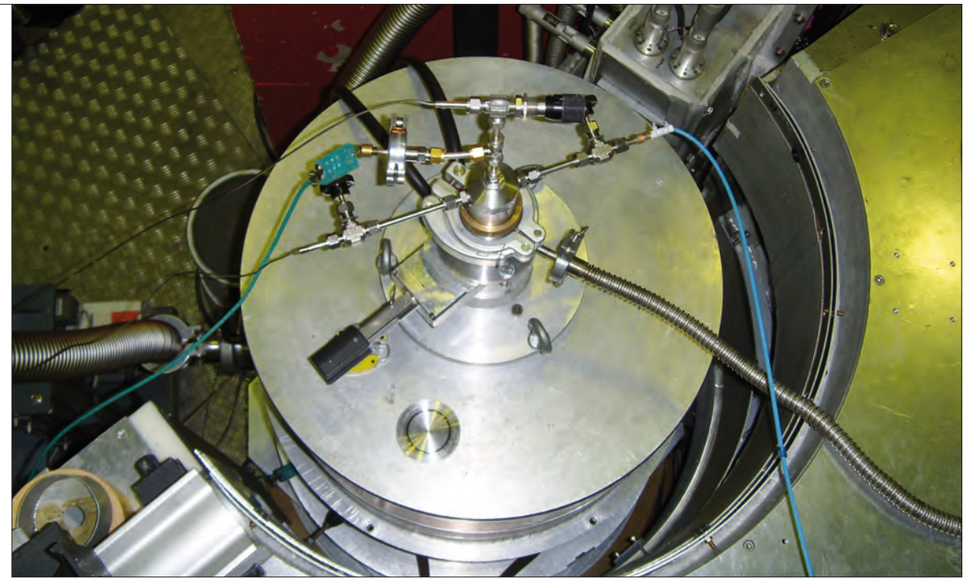

Photo: *The sample environment developed to monitor the reduction in situ on D20. (Photo credit: Mona Bahout)*

Many materials must be able to function over a wide range of temperatures and in a variety of atmospheres. In order to do so they must be chemically stable, in terms of both their composition and their structure.

Neutron diffraction has long been used in order to establish this stability. It is, for example, relatively straightforward to monitor the structure of a material as a function of temperature. However, some materials must withstand working environments that are relatively difficult to mimic on a neutron powder diffractometer within the shell of a nuclear reactor. In the past it has been usual to study these compounds in their pristine state, then to take them to a chemistry laboratory and run them through a working cycle before returning them to the diffractometer to see how well they have withstood the process.
This is not wholly satisfactory because although it gives information about the material at the beginning and the end, it does not reveal at what temperature and in what manner any changes occurred during the course of the process.

Reactions involving hydrogen gas at high temperatures have always fallen into this category. This is unfortunate given the need to develop new materials that can be used as electrodes in solid-oxide fuel cells wherein the reduction of mixed-metal oxides by hot hydrogen gas is an important process.
We have therefore adapted the sample environment equipment on the high-flux diffractometer D20 (**photo**) to enable us to monitor the reduction *in situ* [1].

The compound chosen for our initial study was the Ruddlesden-Popper (K_2NiF_4) phase $Pr_2Sr_2CrNiO_8$. The sample (about 0.5 g) was loaded in a quartz tube between two pieces of quartz wool and mounted in the D20 furnace. This arrangement allowed the reducing gas (5% H_2 in He) to flow through the powder as it was heated to 700 °C. The temperature was raised at a rate of 1 °C/min and subsequently cooled at 25 °C/min. Diffraction patterns were collected throughout the heating and cooling cycle; a pattern took about 1 min to collect, giving a maximum temperature resolution of 1 °C. In order to establish whether any changes that occurred under the reducing conditions were reversible, the sample was subsequently heated in air at 5 °C/min to 500 °C. The quality of the data collected in this way was good enough to allow full-pattern Rietveld analysis at every temperature step.

The oxygen atoms within the crystal structure of $Pr_2Sr_2CrNiO_8$ occupy two distinct sites, O1(axial) and O2 (equatorial). Analysis of the data collected using the protocol described above showed clearly that the basic crystal structure is unchanged during the heating cycle. However, as is shown in **figure 1**, when the temperature reaches about 325 °C oxygen is removed from the O2 site, but not from the O1 site. The oxygen loss is complete by about 400 °C and no further compositional change occurs between 400 and 700 °C. The composition of the reduced material was found to be $Pr_2Sr_2CrNiO_{7.5}$, which corresponds to a reduction from Ni(III) in the starting material to Ni(II) in the product. The oxygen-deficient structure undergoes no change when the material is cooled to room temperature. The data collected on heating in air showed that the reaction was reversible, albeit with some hysteresis; the reoxidation was essentially complete at 500 °C.

These experiments demonstrate that the current generation of high-flux, medium-to-high resolution powder diffractometers can play a significant role in the *in situ* investigation of many high-temperature processes in solid-state and materials chemistry, provided that the appropriate sample environment can be engineered.

Acknowledgement
This work was partially funded by the *Région Bretagne*.

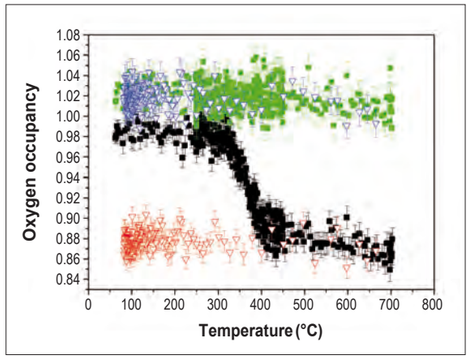

Figure 1: *Occupancy factor of oxygen sites as a function of temperature under reducing conditions. Green and black squares represent the occupancy of the sites O1 and O2 during heating; blue and red triangles represent O1 and O2 on cooling.*

REFERENCES

F. Tonus, M. Bahout, P. F. Henry, S. E. Dutton, T. Roisnel and P. D. Battle, Chem. Commun. (2009) 2556 **[1]**

High-resolution thermal neutron two-axis diffractometer D2B
LLB instrument 3T2

AUTHORS

L. Desgranges (CEA-Cadarache, France)
G. Rousseau (CEA-Cadarache and SUBATECH, Nantes, France)
G. Baldinozzi (SPMS CNRS-Ecole Centrale Paris, Châtenay-Malabry, France)
T. Hansen (ILL)

Oxidation mechanisms of nuclear fuels elucidated by neutron diffraction

The development of advanced nuclear energy systems requires scientific data in order to ensure their safe behaviour throughout the fuel life-cycle from fabrication to end of life storage. Neutron diffraction is a very valuable tool for the characterisation of UO_2 ceramic nuclear fuel, because neutrons can probe bulk samples and provide reliable information relative to the oxygen sublattice, overcoming the severe limitations of X-ray diffraction experiments. In this *in situ* neutron diffraction experiment we have demonstrated the influence of complex oxygen defects and clusters on the oxidation mechanism in UO_2.

Nuclear fuel assembly to be used in power reactor.

The engineering of future advanced nuclear energy systems will require new materials and chemical processing techniques that provide structural integrity, phase stability and process efficiency under extreme conditions of radiation, temperature and corrosive environments for timeframes that in some cases span several thousands of years. Fuel development and qualification takes decades, the process is costly and has to face specific difficulties linked to its nuclear character. Historically, the basis for fuel development has long been empirical. The fundamental properties of materials even for conventional unirradiated fuel materials are difficult to obtain not only because the materials are radioactive, but also because the properties of these systems can change sharply with composition, they have high vapour pressures, are highly reactive, and may experience internal heating due to radioactive decay. Moreover, reliable fundamental thermochemical and thermophysical information cannot yet be predicted using computational techniques due to the lack of an adequate underlying theory of the electronic structure of actinides. The problem of understanding and developing a predictive capability for the evolution of fuels is challenging, even for phenomena that appear simple. In this study, we show how this problem was solved in the case of oxidation of uranium dioxide.

Oxidation is the major risk that has to be taken into account for dry storage of nuclear fuel. During oxidation at temperatures below 600 K, UO_2 undergoes three morphotropic phase transitions, leading to the progressive formation of β-U_4O_9, β-U_3O_7 and finally U_3O_8 [1]. Only the crystal structures of UO_2, U_4O_9 and U_3O_8 have already been determined. We performed high-resolution *in situ* neutron diffraction experiments [2] to determine the changes in the UO_2 structure during oxidation; more specifically, the structure of β-U_3O_7 was determined and refined.

The isothermal oxidation experiment (483 K) was performed on the D2B instrument at ILL. The sample was put into a cylindrical vanadium sample holder and dry air was forced to flow through it to ensure a stable oxidizing atmosphere during the experiment. Since a dense sample would prevent achieving the optimum conditions for the uniform oxidation of the sample, UO_2 powder was dispersed in the cylindrical sample holder using fused silica fibres to ensure a dry air flow throughout the sample. UO_2 and U_4O_9 phases cannot be easily distinguished in our experiment because of a severe overlap of the basic fluorite peaks. A U_3O_7 single-phase is observed after about 10 hours. U_3O_8 formation occurs after about 17 hours **(figure 1**).

We used the crystal structures obtained by Rietveld analysis of the diffraction patterns to establish a mechanistic description of oxidation on an atomic level.

At the very beginning of oxidation, incorporating oxygen into UO_2 results in the formation oxygen interstitial clusters named cuboctahedra in U_4O_9 whose unit cell contains 12 isolated cuboctahedra (**figure 2a**) [3]. The formation of U_3O_7 is associated with the increase of the number and the spatial redistribution of these cuboctahedra in the crystal structure. The main difference between U_4O_9 and U_3O_7 is that the insertion of 16 cuboctahedra in the large cell cannot be done without sharing some oxygen atoms between the deformed square antiprisms surrounding each cuboctahedron (**figure 2b**). These contacts involve significant distortions of the square antiprisms. Finally, the formation of U_3O_8 possibly takes place when the topological frustration imposed on the (111) dense planes by the cuboctahedra is no longer sufficient to prevent the rearrangement from the ABC stacking of U_3O_7 into the AAA stacking of U_3O_8. From a phenomenological viewpoint, this is very similar to a martensitic phase transition.

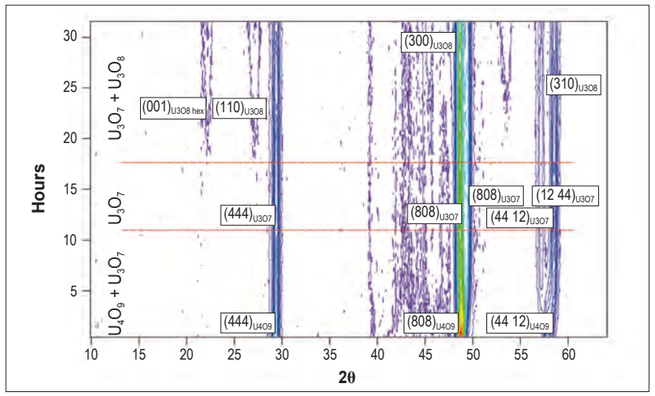

Figure 1: *Map of the diffracted intensity as a function of 2θ angle and time during the in situ experiment at 483 K.*

This description of oxidation on an atomic level provides valuable information that was included in a new model for the oxidation kinetics. Two different oxygen diffusion coefficients for U_4O_9 and U_3O_7 are necessary to describe the oxygen diffusion in U_4O_9 and the cuboctahedra reorganization in U_3O_7. The formation of U_3O_8 starts at a threshold level depending on the oxygen concentration and the initial stress in the sample. This new model successfully describes the oxidation kinetics of spent fuel samples and it enables a reliable criterion for the safe handling of oxidised defective fuel rods [4].

Acknowledgement

The authors would like to acknowledge the financial support from 'Electricité de France'.

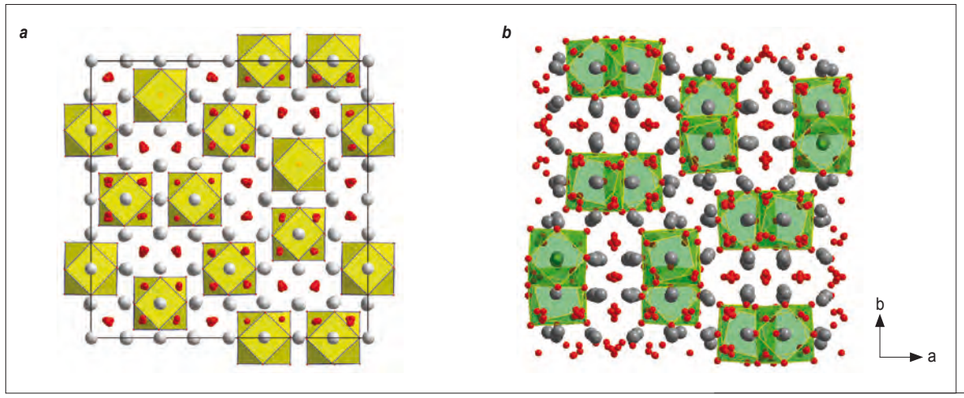

Figure 2: *Crystalline structures of U_4O_9* ***(a)*** *and U_3O_7* ***(b)*** *projected in the (a,b) plane.*

REFERENCES

R.J. McEachern and P. Taylor, J. Nucl. Mat. 254 (1998) 87-121 **[1]**
L. Desgranges, G. Baldinozzi, G. Rousseau, J.C. Nièpce and G. Calvarin, Inorg. Chem., 48 (2009) 7585-7592 **[2]**
R. I. Cooper and B. T. M. Willis, Acta Crystallogr., A60 (2004) 322-325 **[3]**
J. Rouyer, A. Poulesquen and L. Desgranges, C. Ferry, Journal of Nuclear Materials 395 (2009) 89-98 **[4]**

AUTHORS

J.-G. Cheng, **J.B. Goodenough** and **J.-S. Zhou** (University of Texas at Austin, USA)
J.A. Alonso (University of Texas at Austin, USA, and CSIC, Madrid, Spain)
E. Suard (ILL)

A new perovskite polytype in the high-pressure sequence of $BaIrO_3$

The magnetic and electronic properties of transition-metal oxides have been extensively studied in recent decades, and the correlation between the crystal structure and the properties of interest has been recognised to be a cornerstone of solid-state chemistry design. Neutron diffraction can be very useful to accurately characterise the structural peculiarities of metal oxides, especially when they contain very heavy metals. A beautiful example is the resolution of the crystal structure of a new 5H-polytype of the $BaIrO_3$ perovskite, in the narrow pressure range 3<P<5 GPa, and its correlation with the observed metallic properties of this phase, in comparison with the ambient-pressure polymorph, which is semiconducting.

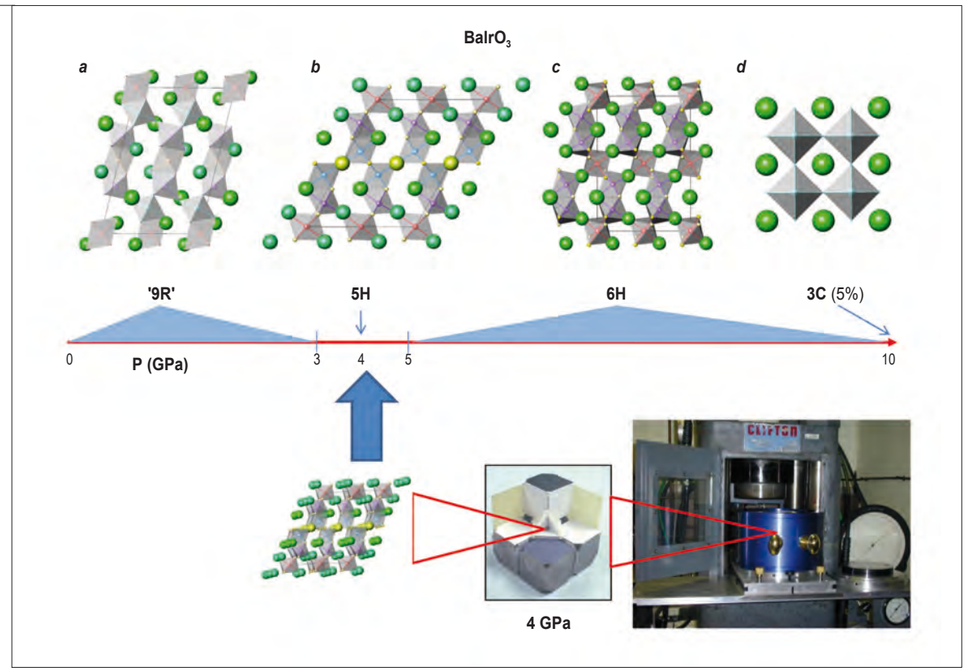

Figure 1: *High pressure preparation of the different polytypes of $BaIrO_3$:* ***(a)*** *'9R'* ***(b)*** *5H* ***(c)*** *6H* ***(d)*** *3C.*

Within the wide family of metal oxides, materials adopting the ABO_3 perovskite structure have constituted a central theme given the well-recognised flexibility of this structural type to incorporate a wide range of cations at both the 12-coordinate A position and the 6-coordinate B site. The crystal structures can be considered to be built up from the close packing of AO_3 layers with B atoms placed at the all-oxygen octahedral voids. If all of the stacking of AO_3 layers is cubic (*c*) or hexagonal (*h*), the structure is referred to as 3C or 2H, which corresponds to the corner- or face-sharing arrangement of BO_6 octahedra, respectively.

From the early work of Goodenough *et al* [1] it was established that perovskite oxides undergo a high-pressure evolution from polymorphs containing a higher proportion of hexagonal stacking to phases with predominant cubic stackings, typically along the sequence 2H-9R-4H-6H-3C, with an increasing crystallographic density.

In this work we have investigated the high-pressure sequence of the perovskite polytypes of $BaIrO_3$ at pressures up to 10 GPa, as illustrated in **figure 1**. At ambient pressure the so-called '9R' polytype has been prepared by solid state reaction and slow cooling in air to yield an almost fully oxygen-stoichiometric $BaIrO_{2.96(1)}$ composition, exhibiting a monoclinic structure (C2/m space group); it contains trimers of face-sharing octahedra (or Ir_3O_{12} trioctahedra) that are linked by their vertices to form columns parallel to the c-axis with a stacking of layers of corner sharing (*c*) and face sharing (*h*) IrO_6 octahedra along the sequence *hhchhc*, as shown in **figure 1a**. This structure is stable up to 3 GPa.

At 4 GPa the new 5H polytype was stabilised as a pure phase. The crystal structure was solved by *ab initio* procedures from powder XRD data. It is also monoclinic (C2/m space group). Given the strong scattering of Ba and especially Ir, the oxygen locations had been only approximately determined. Good quality NPD data were collected at RT in the D2B diffractometer, with 500 mg of sample gathered from 10 high-pressure syntheses. A measurement with such a small sample was only possible because of the D2B upgrade. This 5H polytype can be described as a stacking of IrO_6 octahedra along the sequence *hchcc*, as shown in **figure 2**. The structure contains chains of double dimer units of face-sharing octahedra; the twin dimers are connected to single layers of vertex-sharing octahedra, forming infinite chains along c. This is a unique stacking that, with this repetition length, has never been described before for the hexagonal polytypes of ABO_3 perovskites. The 5H polytype is stable in a narrow pressure range; at 5 GPa the 6H structure is formed (**figure 1c**), stable up to 10 GPa. At this pressure the cubic 3C perovskite structure could be identified as a minority phase, defined in the Pm-3m space group (**figure 1d**) [2].

The novel 5H polytype is intermediate between the ambient pressure '9R' structure and the high pressure (P>5 GPa) 6H structure for $BaIrO_3$, and it presents interesting physical properties which have been correlated with the crystal structure [3]. In particular, the '9R' polytype is semiconducting whereas the 5H phase is metallic. In '9R'-$BaIrO_3$, the Ir-Ir distances within the trimers take values even smaller than the separation of 2.72 Å found in Ir metal, which indicates strong interactions between iridium cations across the shared faces of the octahedra. The antibonding states of the strong Ir-Ir bonding apparently capture the hole of the low-spin Ir(IV) π-bond configuration in localized molecular orbitals, precluding an electron itinerancy across the solid. In the 5H structure, the Ir-Ir distance within the Ir_2O_9 dimers is conspicuously larger than that found in Ir metal, indicating a weaker metal-metal bond between iridium cations across the shared faces of adjacent octahedra, which makes possible an overlap of the π* band of the corner-shared $IrO_{6/2}$ layers with the Ir-Ir antibonding states of the dimers, thus freeing holes to itinerant-electron states.

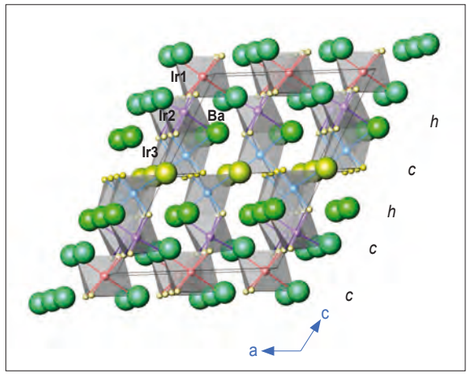

Figure 2: *View of the crystal structure of the 5H polytype approximately along [0 1 0], highlighting the stacking of hexagonal (h) and cubic (c) layers corresponding to face-sharing or vertex-sharing IrO_6 octahedra.*

Another structural feature that is worth highlighting is the different arrangement of the chains of face-sharing octahedra for 9R and 5H phases (**figure 1**). Although both crystal structures exhibit a monoclinic symmetry, the '9R' polytype exhibits a monoclinic β angle close to 90° [2], implying that the chains of face-sharing octahedra are almost perpendicular to the *ab* plane, whereas the 5H polytype presents a β angle close to 120°, with the chains of octahedra tilted strongly with respect to the *ab* plane. This particular arrangement for the 5H polytype involves a reduced rotation of the IrO_6 octahedra in the space, giving 180° angles for Ir-O-Ir bonds that promote a full overlap between Ir-5d and O-2p orbitals. Why the 5H polytype should be stabilised relative to the 4H *hchc* polytype in which holes are localised in Ir-Ir dimer bonds remains an interesting theoretical question.

REFERENCES

J.B. Goodenough, J.A. Kafalas, J. A. and J. M. Longo, High-Pressure Synthesis, Academic Press, Inc., New York and London (1972) **[1]**
J.-G. Cheng, J.A. Alonso, E. Suard, J.-S. Zhou, J.B. Goodenough. Journal of the American Chemical Society, 131 (2009) 7461-7469 **[2]**
J.-G. Cheng, J.-S. Zhou, J.A. Alonso, J.B. Goodenough, Y. Sui, K. Matsubayashi, Y. Uwatoko, Phys. Rev. B 80 (2009) 104430 **[3]**

AUTHORS

A. D. Fortes and **C. J. Pickard** (University College London, UK)
R. J. Needs (University of Cambridge, UK)
E. Suard and **M.-H. Lemée-Cailleau** (ILL)

The crystal structure of ammonia monohydrate phase II – a new semi-clathrate

Ammonia hydrates are likely to be important 'rock'-forming minerals in the outer solar system, and determination of their behaviour at high-pressure is necessary for accurate modelling of the interiors of icy satellites. The crystal structure of ammonia monohydrate (AMH) phase II at 500 MPa has been determined from data collected on D2B using the algorithm implemented in the FOX code, and found to agree closely with a structural model obtained from density functional theory (DFT) predictions. The AMH II crystal structure is a semi-clathrate, characterised by sheets of edge-sharing pentagonal rings.

The ammonia hydrates are the simplest solids to contain the mixture of homo-nuclear O–H···O and hetero-nuclear O–H···N and N–H···O hydrogen bonds typically found in biomolecules, including DNA. Experimental and computational studies of these systems as a function of the thermodynamic variables, P and T, therefore provide an insight into the parameters involved in interatomic potential functions in hydrogen bonded molecular crystals.
Ammonia hydrates are also likely to be 'rock'-forming minerals on the solid bodies of the outer solar system, giant icy moons such as Ganymede, Callisto and Titan. The high-pressure behaviour of these materials must be known in order to model the internal structure and geodynamics of these planetary bodies.

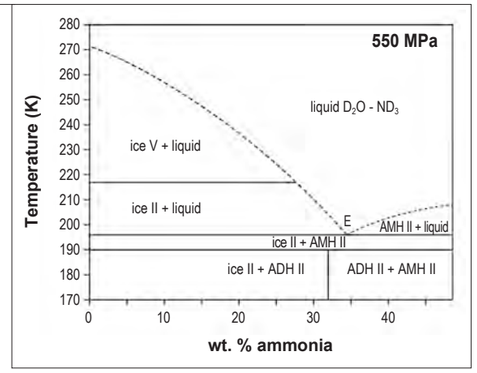

Figure 1: *Phase boundaries at the water-rich end of the system D_2O-ND_3 at 550 MPa [1]. Note that ADH II breaks down to a mixture of ice II + AMH II above 190 K, and then melts at a binary eutectic ($E = 34 \pm 1$ wt % ND_3) at 196 K.*

In earlier work, it was found that a high-pressure polymorph of ammonia dihydrate, ADH II, dissociates upon warming at 550 MPa to a mixture of the $R\bar{3}$ phase ice II, and a phase identified only as AMH II (**figure 1**). Whilst the latter was indexed with an orthorhombic unit-cell, attempts to solve the structure using the mixed-phase powder data were not successful, and the correct space-group was not determined unambiguously [1].

An *ab initio* structure prediction technique based on DFT, constrained only by the known unit-cell dimensions, cell contents, and the likely set of space-groups, was used to find the crystal structure of AMH II with the lowest free energy [2]. Neutron powder diffraction data

Ammonia monohydrate sample loading in the high-pressure cell directly at 77 K.

were subsequently collected from a specimen of single-phase AMH II using a TiZr gas pressure vessel mounted on the D2B high-resolution diffractometer [3]. The objective of the experiment was to collect high-quality single-phase powder data extending to large d-spacings which would allow us to test the results of the structure prediction exercise, and to determine independently the crystal structure from the powder data alone.

AMH I was crystallised in the pressure vessel and subsequently compressed to 350 MPa, where AMH II formed. At 502 MPa, two long integrations were made using the $\lambda = 1.6$ Å and $\lambda = 2.4$ Å wavelength options (**figure 2**).

The new powder data allowed an unambiguous determination of the space-group Pbca to be made; the structure was solved in this space-group using FOX and subsequently refined by the Rietveld method [4]. The AMH II crystal structure is characterised by sheets of edge-sharing pentagons, formed of both symmetry independent water molecules, and one of the symmetry independent ammonia molecules (**figure 3a**). The hydrogen bonds along the *c*-axis water-water chains in the sheet are ordered in one particular orientation. It is possible to adopt an alternate ordered orientation, which was found by the DFT prediction, or to combine them to form a disordered crystal. The data clearly favour the first ordered orientation. The pentagonal sheets in AMH II are very similar to those found in the tetragonal argon clathrate structure [5] and to those found in the semi-clathrate structures such as pinacol hexahydrate [6]. The sheets in AMH II differ from each of these by virtue of the ammonia bonded into the rings, which gives the sheets a distinct 'upper' and 'lower' surface (**figure 3b**). As a result, the sheets can bond directly to one another 'face to face' or 'back to back' via the second symmetry independent ammonia molecule (**figure 3c**).

In summary, this is the first of the complex high-pressure molecular ammonia hydrate structures to be solved so far. The structure obtained from the powder data collected on D2B is a novel variation of the archetypal semi-clathrate structure observed in several alcohol hydrates, and provides an important validation of modern DFT structure prediction algorithms.

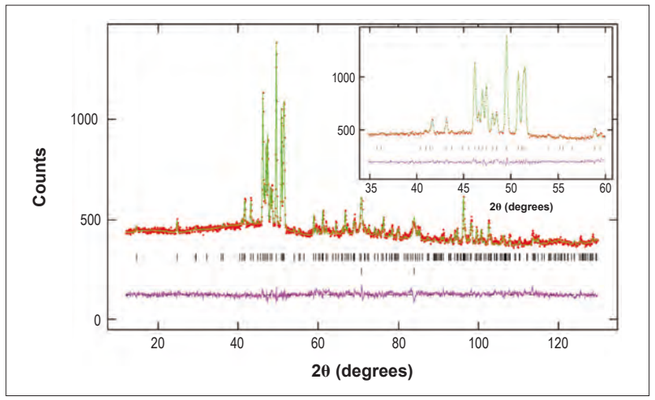

Figure 2: *Diffraction data acquired at 502 MPa, 180 K with $\lambda = 2.4$ Å radiation. The expected positions of Bragg reflections are shown by vertical black tick marks; the upper set are for AMH II, and the lower set are for copper, the latter being a component in the Bridgman seal of the pressure vessel.*

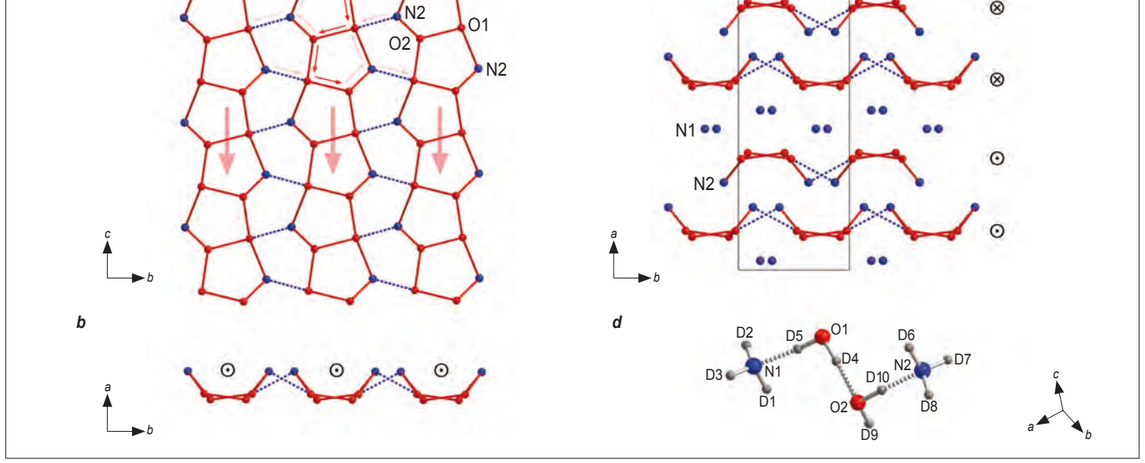

Figure 3: *Molecular connectivity and packing in the AMH II structure. Oxygen atoms are shown in red, nitrogen in blue, and deuterium in grey.* ***(a)*** *shows a view of the pentagonal sheets down the a-axis; the direction of the O–D···O H-bonds is shown by the red arrows (the return bonding across the pentagonal apex is indicted by small pink arrows), resulting in a net-directionality indicated by the large pink arrows. A view of this sheet along the c-axis is shown in* ***(b)****; note the symbol (⊙) indicating the direction of hydrogen bonds in the water-water chain is coming out of the plane of the illustration. The packing of these sheets is depicted in* ***(c)****.*

REFERENCES

A.D. Fortes *et al.* (2009) J. Appl. Cryst., 42(5) 846-866 **[1]**
C.J. Pickard and R.J. Needs (2006) Phys. Rev. Lett. 97, 045504, 1-4 **[2]**
A.D. Fortes *et al.* (2009) J. Am. Chem. Soc., 131 (37) 13508-13515 **[3]**
V. Favre-Nicolin and R. Cemy (2004) Z. Krist. 219, 847-856 **[4]**
A.Yu. Manakov *et al.* (2004) J. Incl. Phenom. Macrocycl. Chem. 48, 11-18 **[5]**
H.S. Kim and G.A. Jeffrey (1970) J. Chem. Phys. 53(9) 3610-3615 **[6]**

AUTHORS

H. N. Bordallo (Helmholtz-Zentrum Berlin, Germany)
L. P. Aldridge (ANSTO, Lucas Heights, Australia)
P. Fouquet (ILL)

Can neutrons show whether water flows through pores in concrete?

Concrete, the most frequently used building material in modern times, can be used to produce beautiful and elegant structures, such as the one shown in **figure 1**. However, since the cement industry produces 5-7% of global CO_2 emissions, which in turn is linked to climate change, increasing the service life of concrete is desirable. This can be achieved by significantly improving concrete's ability to limit the flow of water through pores of the finished material. Although water dynamics can be investigated by many techniques, the largely unknown pore structure of concrete makes its study challenging. Using the neutron spin-echo (NSE) technique, we have established that physically bound water is constrained in the small gel pores, whereas free water occupies the larger capillary pores.

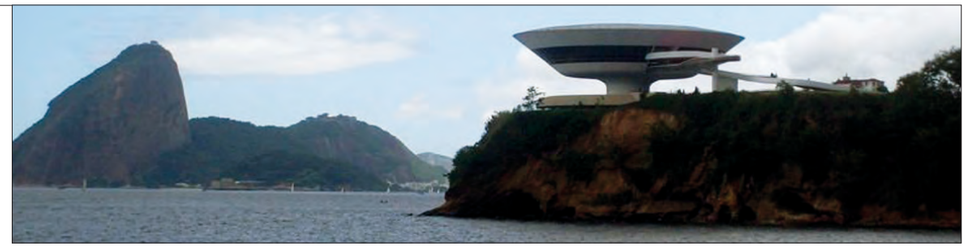

Figure 1: *Oscar Niemeyer's Contemporary Art Museum - Niteroi (Brazil). Courtesy of M.C.B. Lowen.*

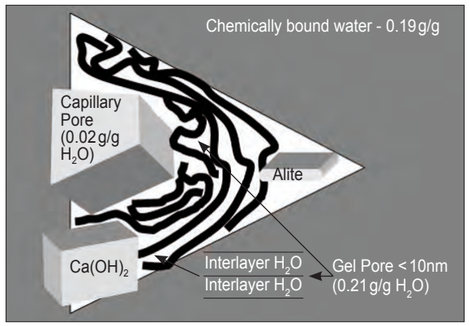

Figure 2: *Water and its relationship to the microstructure of hydrated OPC, calculated from the Powers Brownyard model [2] assuming that 95% of a w/c = 0.42 paste had been hydrated. The water is split between bound (0.19 g), gel (0.21 g), and capillary water (0.02 g). C-S-H is represented by thick irregular lines with interlayer water confined between the layers. The gel water is considered to exist in both fine pores and as interlayer water.*

The hydrated cement in the concrete matrix is the key component of concrete structures and the pore volume in this matrix affects the strength of the finished concrete. The larger pores (>10 nm in diameter), not always present in finished concrete, are defined as capillary pores whereas the smaller or gel pores (<10 nm in diameter) are always present in high quality concrete and control the rate of water transmission through that matrix. The amount of water in the pores depends both on the age of the paste and the amount of water in the original wet slurry defined by the water to dry cement ratio (w/c). The relative pore abundance can be computed as a function of w/c and the extent of cement hydration. **Figure 2** illustrates hydrated ordinary Portland cement (OPC) made at w/c 0.42 after 95% hydration (about 1 year). Note that hydrated cement made with w/c = 0.6 has capillary pore water which can be removed at 55% relative humidity (RH).

Quantifying water motion in the different cement pores is a great challenge but crucial for understanding the interaction between the water and the cement matrix. Such interactions control some of the most important macro properties of concrete. The advantage of using neutron scattering is that it probes the dynamics and geometric aspects of proton motions at very short time scales [1] giving information that both supplements and complements information supplied by NMR.
By using NSE, together with well-chosen w/c ratios, we obtained a unique insight into the transport of water in the cement matrix. Moreover, and most importantly, we verified the hypothesis that the physically bound water is constrained in the gel pores while the free water remains in the capillary pores [2].

The distinct behaviour of selected samples, (i) w/c = 0.42, (ii) w/c = 0.6 (as is), and (iii) w/c = 0.6 dried at 55% RH, is clearly illustrated in **figure 3**. What causes such differences? It is the presence of water in the capillary pores in (ii) but not in (i) and (iii). Considering that the vibrational, rotational and translational water motions are decoupled, the intermediate scattering function I(Q, t) can be expressed as: $I_{inc}(Q, t) = I_{vib}(Q, t) I_{rot}(Q, t) I_{trans}(Q, t)$. The vibrational contribution ($I_{vib}(Q, t)$) can be neglected simply because the corresponding energy transfers are beyond the cut-off energy of the NSE spectrometer. Moreover, in the case of bulk and confined water for $Q < 1.0$ Å^{-1} the contribution of the rotation of the H-atoms around their centre of mass ($I_{rot}(Q, t)$) can also be neglected. Therefore the Q resolved I(Q,t) will give information mostly on the translational motion. The ratio of I(Q,t)/I(Q,0) is accurately described by the function $I(Q,t)/I(Q,0) = [1-A]\exp(-t/\tau)^{\beta} + A$ where τ is the typical relaxation time, β a stretching parameter, A is the value of I(Q,t) at long times.

The data analysis indicates diffusive motion, with diffusion constants ranging from 0.6 to 1.1×10^{-9} m^{2}s^{-1} that are directly related to differences between water motions in the capillary or the gel pores.

In summary, we were able to quantify water motion in gel pores enabling a better understanding of the water-cement interaction at the molecular level in cured concrete. In well-made concrete these pores control water transport, and from the perspective of the construction industry this work has the potential to set understandable limits in water transport resulting in better infrastructure and service life. We conclude that NSE can tell how fast water moves through both capillary and gel pores.

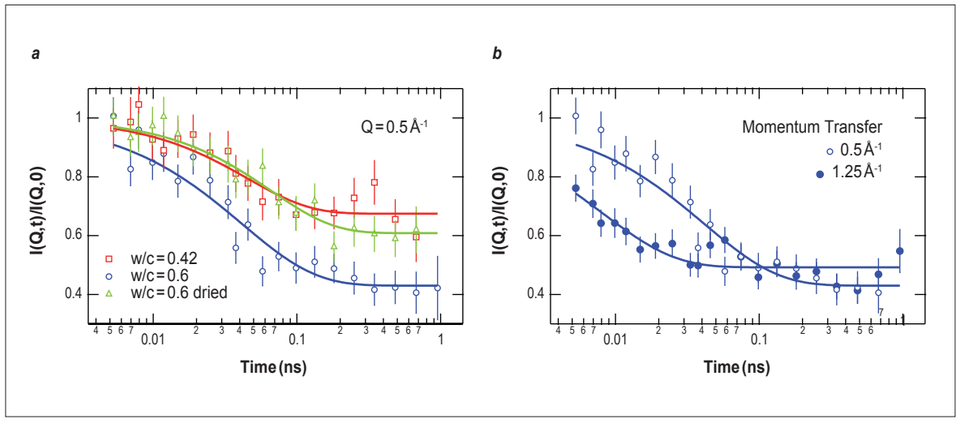

Figure 3: (a) *Dynamic structure factors at 300 K for OPC pastes with (i) w/c = 0.42, (ii) w/c = 0.6 and (iii) w/c = 0.6 dried at 55% RH for Q = 0.5 Å^{-1}.* ***(b)*** *I(Q,t) scans of OPC with w/c = 0.6 for different Q values. The lines are fits to stretched exponentials.*

REFERENCES

N. L. Ross, E. C. Spencer, A. A. Levchenko, A. I. Kolesnikov, D. J. Wesolowski, D. R. Cole, E. Mamontov and L. Vlcek, In Neutron Scattering Applications and Techniques Neutron Applications in Earth, Energy and Environmental Sciences Eds. L. Liang, R. Rinaldi and H. Schober, Springer US (2009) **[1]**

H. N. Bordallo, L. P. Aldridge, P. Fouquet, L. C. Pardo, T. Unruh, J. Wuttke and F. Yokaichiya, ACS Applied Materials & Interfaces 1 (2009) 2154 **[2]**

AUTHORS

A. Fernández-Martínez, L. Charlet and L. Murias-Fernández
(LGIT, UJF Grenoble and CNRS, Grenoble, France)
G. J. Cuello, M. R. Johnson and **H. E. Fischer** (ILL)
L. J. Michot and **M. Pelletier** (LEM, CNRS, Nancy, France)
O. Poncelet (CEA Grenoble, France)

J. Brendle and **L. Vidal**
(ISM, CNRS and Université de Haute-Alsace, Mulhouse, France)
I. C. Bourg and **G. Sposito**
(Lawrence Berkeley National Laboratory, Berkeley, USA)

Water structure on the surface of imogolite, a natural nanotube found in volcanic soils

Imogolite, $Al_2(OH)_3SiO_3OH$, is an aluminosilicate mineral of nanotubular geometry commonly found in soil environments. The internal faces of these nanotubes are dominated by silanol ($>SiOH^0$) functional groups while the external faces are made up of curved gibbsite ($Al(OH)_3$), populated by aluminol functional groups ($>Al_2OH^0$). The presence of these amphoteric surfaces and its large specific surface area (up to 600 m^2/g) gives imogolite a variable surface charge which is dependent on the pH of the soil solution, resulting in very special adsorption properties such as its high affinity for soil organic matter and for important agricultural nutriants such as phosphate anions. For these reasons, imogolite nanotubes are a very important component of the soils where they occur, controlling the mobility and the bioavailability of elements of importance for public health. In addition, the highly hydrophilic and narrow internal pores of imogolite (1 nm diameter) provide an excellent environment for the study of the structural properties of confined water.

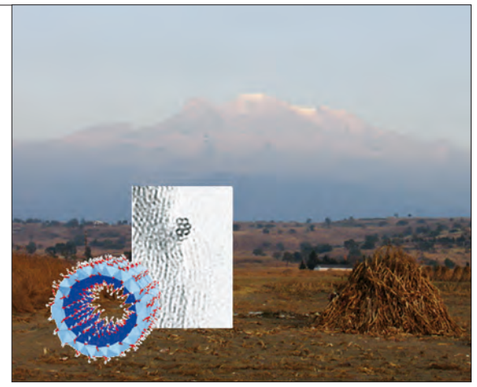

Figure 1:
View of a volcanic soil (Andosol) near the 'Iztaccihualt' volcano (Mexico). Volcanic soils in this region are rich in imogolite, a nanotubular aluminosilicate. A transmission electron microscopy image and a sketch of the imogolite structure are shown.

This study focuses on the adsorption properties of imogolite, on the molecular mechanisms that lead to the retention of high amounts of organic matter in volcanic soils, and on the impact of them on properties such as water retention or expected reduced diffusion of ions along the nanotube. For these purposes, a combination of molecular modelling and high-energy neutron diffraction experiments using H/D isotopic substitution were used, helping to describe the characteristics of water adsorbed at the surfaces of imogolite. In recent decades the development of sol-gel techniques have enabled the synthesis of pure imogolite and of derivatives such as aluminogermanate nanotubes, making possible the tailoring of the nanotube diameter and of electronic properties like the band gap [1], and opening new opportunities for industrial applications such as the solubilisation of catalytic nanoparticles [2] or its use to shield conducting nanowires [3]. Pure synthetic imogolite was used in all the thermogravimetric and neutron scattering experiments presented in this study.

Prior to the experiments, Controlled-Rate Thermal Analyses (CRTA) were performed in order to quantify the amount of water present in the structure of the nanotube.

Following the CRTA measurements, two imogolite samples with H_2O and D_2O were treated under dynamical vacuum conditions at 200°C in order to remove water adsorbed in the structural mesopores, leaving a stoichiometry of $Al_2SiO_7H_4 \cdot 5H_2O$ in the samples. The thermal treatment thus allowed us to selectively study the water confined in the internal pore of the nanotubes (which has been reported to have a strongly ordered structure [4]), as well as the first water shell adsorbed at the external surface. Application of the first difference method (D-H) yielded a partial pair correlation function for the structure surrounding an adsorbed-water hydrogen atom, considered to be at the origin, $r = 0$ (**figure 2**).

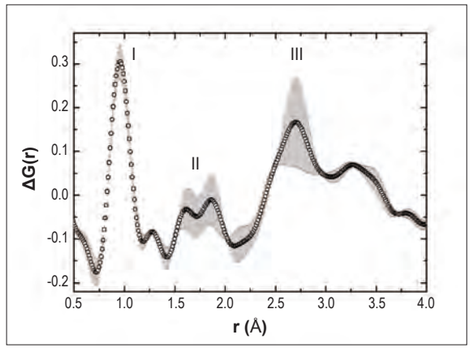

Figure 2: *Real space difference function ΔG(r) obtained from the neutron diffraction with isotopic H/D substitution at the diffractometer D4 of the ILL. Error bars have been estimated performing different Fourier transforms.*

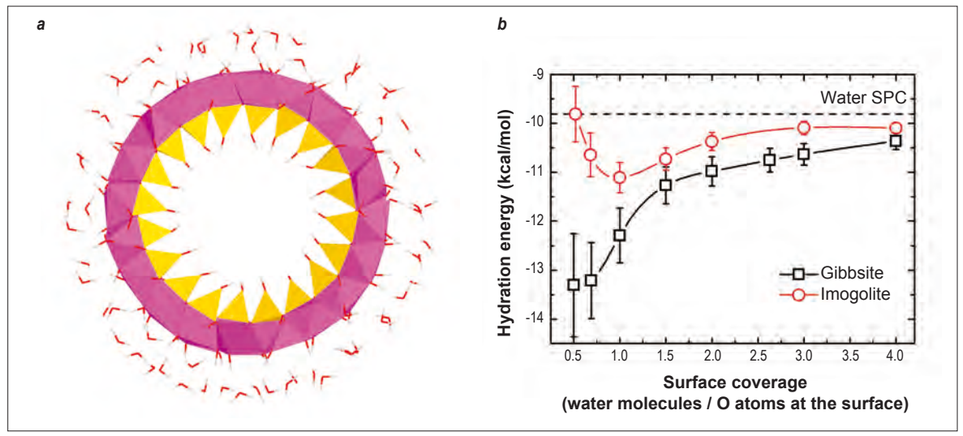

Figure 3: (a) *Model of imogolite used in the MD simulations, with the external surface hydrated with one shell of water. Aluminum octahedral are in pink, silicon tetrahedra in yellow, oxygen atoms are red and hydrogen atoms are grey.* ***(b)*** *Hydration energies as a function of surface water coverage of the gibbsite (001) and imogolite external surfaces. The dotted line corresponds to the potential energy of a water molecule in bulk water.*

This confined water shows three features that match with different distances present in the structures of liquid water: the first peak (I) corresponds to the H-O distance of water molecules; the second feature (II) represents H-H and H-O intermolecular distances including correlations with the imogolite surface oxygen atoms, and the third broad peak (III) includes, among others, H-O distances between water molecules adsorbed at different adsorption sites on the surface.

Molecular Dynamics (MD) simulations have revealed a site for water adsorption at the external surface with water molecules forming hydrogen bonds with surface oxygen atoms at a H_{water}-$O_{surface}$ distance ranging from 1.7 and 1.9 Å, explaining peak II. A similar adsorption site has been observed on the internal surface.

MD simulations are underway to interpret the distances in terms of a structural model of confined water and to separate the water contributions to the pair correlation function from the inner and outer parts of the tube.

Molecular modelling has been applied to study separately the adsorption properties of the external imogolite surface, which is considered its more relevant surface governing geochemical processes (**figure 3a**). The structure and energetics of water adsorbed on this surface were compared to those of the (001) gibbsite surface, which is the planar equivalent to the external imogolite surface. Water adsorption enthalpies as a function of the hydration degree are shown in **figure 3b**. The external imogolite surface presents a less hydrophilic character than the (001) gibbsite surface, with values for the adsorption enthalpy closer to that of bulk water, $\Delta H_{bulk} = -9.81$ kcal/mol. Entropic effects are expected to play a small role in the energetics of adsorption. Structural analyses of adsorbed water have revealed similar adsorption geometries for water molecules on both surfaces. A detailed analysis of the MD trajectories has revealed a different arrangement of the hydroxyl groups on the two minerals, inducing steric effects that result in the different adsorption enthalpies for water molecules.

This relative hydrophobicity of imogolite may be responsible for the formation of organo-mineral complexes, favouring the accumulation of organic matter in the clay fraction of volcanic soils and thus acting as an important sink for carbon in these environments. The retention of organic matter in volcanic soils, and the redox properties it confers to the volcanic soils, are thought to be responsible for the low bioavailability of elements of importance for public health such as selenium [5].

REFERENCES

F. Álvarez-Ramírez, Journal of Computational and Theoretical Nanoscience (2009) 6 (5) 1120-1124 **[1]**
L. M. Lizmarzan and A. P. Philipse, Journal of Physical Chemistry (1995) 99 (41) 15120-15128 **[2]**
A. Kuc and T. Heine, Advanced Materials 21 (2009) 1-4 **[3]**
B. Creton, D. Bougeard, K.S. Smirnov, J. Guilment, O. Poncelet, Physical Chemistry Chemical Physics 10, (32) (2008) 4879-4888 **[4]**
A. Fernández-Martínez and L. Charlet, Reviews in Environmental Science and Biotechnology 8 (2009) 81-110 **[5]**

AUTHORS

M. Zucali (University of Milan, Italy)
V. Barberini (University of Milan-Bicocca, Italy)
B. Ouladdiaf (ILL)
D. Chateigner (ENSICAEN, IUT-Caen, France)
L. Lutterotti (University of Trento, Italy)

Deformation behaviour and elastic properties of gypsum polycrystals: implications for lithosphere-scale geological processes

Gypsum plays an important role in many lithosphere-scale geological processes. We used neutron diffraction to perform quantitative texture analysis on a set of gypsum samples deformed over a range of well-characterised conditions. The resulting pole figures provide a better understanding of the deformation behaviour of gypsum and enable it to be defined in terms of active deformation mechanisms. Moreover they allow the calculation of elastic properties to be made, which helps with the geophysical interpretation of seismological investigations on a lithosphere-scale.

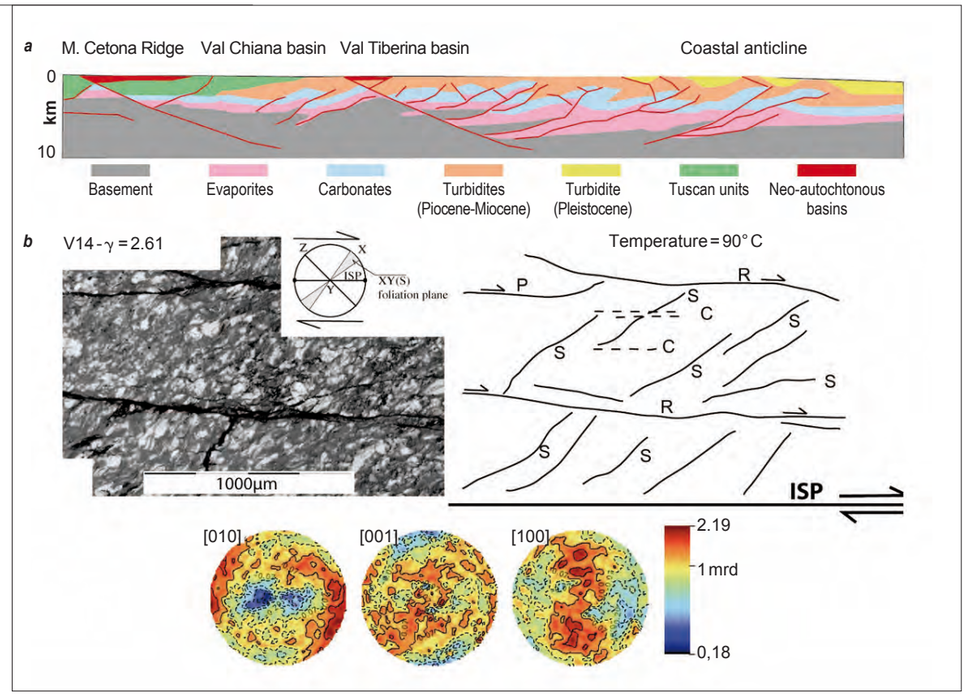

Figure 1: ***(a)*** *An example of the occurrence of evaporites within sedimentary sequences involved in tectonic processes. Geological interpretation of the seismic reflection line CROP-03, from Mount Cetona to the Adriatic Sea [2]. Evaporites are in pink.* ***(b)*** *Microphotograph image of the sample V14, experimentally deformed at strain rate (γ) = 2.61; X, Y, Z represent principal orientations of the rock samples, defined by the maximum (X), intermediate and minimum (Z) direction of alignment of gypsum grains, where the S (foliation) plane corresponds to the plane containing the X and Y directions. Schematic representation of microstructures developed during torsion deformation with the Imposed Shear Plane (ISP), where P-R-S-C planes are shear planes marked by micro-fractures or by shape preferred orientation of gypsum grains. Main axes pole figures obtained from the analysis of D20 neutron data performed with MAUD are shown at the bottom.*

Gypsum, together with halite and anhydrite, is the main rock-forming mineral of evaporitic rocks. Evaporites, interlayered within sedimentary sequences (**figure 1**), play an important role in localising deformation: evaporitic levels have often been found in horizontal layers where the deformation of rocks localises and permit lower strata to be thrust over those above [1].

A good knowledge of the mechanical behaviour and elastic properties of evaporites is of great importance in several fields: in the oil industry, because evaporites often form the cap of oil and gas reservoirs; in environmental management, where rock salt formations are being considered for nuclear waste disposal and depleted hydrocarbon reservoirs for gas storage (e.g. CO_2, H_2S). Once the mechanical properties have been rationalised, numerical modelling may be used to explore geological systems in which they play a role – for example the Northern Apennines extensional system (**figure 1a**) where deformation within evaporitic layers is accompanied by seismic activity [2].

One way to study deformation behaviour and elastic properties of rocks within the Earth's lithosphere is to perform laboratory experiments in which known conditions of, for example, confining pressure, temperature, differential stress, pore pressure are imposed on a rock sample and measurements are made of its deformation and the velocity of seismic waves, both P ('primary' or compressional) and S ('secondary' or shear). Such experiments, carried out over the last few decades, have widely demonstrated that texture is one of the most important intrinsic rock properties (together with mineralogical composition) controlling deformation behaviour and elastic properties; it is also important in understanding many other properties of rocks, including magnetic and electrical. Here we report quantitative texture analysis of experimentally deformed gypsum rock by neutron scattering and show that the elastic properties differ between single-crystal and polycrystalline aggregate samples.

The gypsum samples studied are cores about 9 mm thick and 7-15 mm long obtained from natural gypsum (gypsum > 99%) deformed in torsion experiments up to high shear strain values (up to $\gamma = 5$), at confining pressure of 300 MPa and at various temperatures (from 70°C to 90°C) and strain rates (between 10^{-3} and $10^{-5}s^{-1}$).
A complete texture characterisation could be completed in 4 hours for a 1 cm^3 volume of rock. Although this is relatively small, it is still much larger than the volume that could be analysed with any other analytical technique. The measurements were made with the D20 instrument whose detector spans a 2θ range of 153.6° with a resolution of 0.1°, and the neutron wavelength was 2.41 Å. An Eulerian cradle allows rotation about the χ and φ angles. Scans were operated from $\chi = 0$ to 90° (with a 5° step) using a fixed incidence angle ω of 10° (corresponding to the (020) Bragg position of gypsum) and from $\varphi = 0$ to 355° (also with a 5° step). Each diffraction pattern was collected for 4 seconds and quantitative texture analysis was performed using the Rietveld based programme MAUD [3].

Figure 1b shows an example of a pole figure obtained in this manner for gypsum. Pole figures are very useful in their own right, as they help to relate the deformation mechanisms that are active or dominant under specific conditions (e.g. pressure, temperature, deviatoric stress) to the evolution of the preferred orientations of grains or crystallites in the sample. But that is not all. The full set of information obtained from quantitative texture analysis i.e. the Orientation Distribution Function (ODF), derived from the pole figure, can be used as input data to calculate many properties, such as elastic macroscopic tensors (from which derive the P and S wave velocity and anisotropy), provided we know the single crystal tensor of the property we want to investigate and the abundance of different minerals (if we are dealing with polymineralic rocks). We investigated the relations between our quantitative texture analysis and seismic velocities.
Figure 2 shows the wave velocity distribution for the P (compressional) mode (Vp) and the two S (shear) modes S1 and D2 (velocities S1 and S2 respectively) within one of the samples studied, calculated with the software BEARTEX [4] using the ODF, refined from the pole figures of **figure 1** using MAUD [3].

In a single crystal of gypsum (**Table 1**), the largest diagonal components of the elastic stiffness tensor are c_{11} and c_{33}. Consequently, the velocities of the P waves are higher in the 100 and 001 crystallographic directions, and lower in the 010 direction

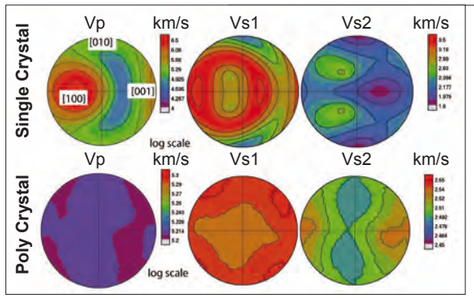

Figure 2: *Distribution of P and S wave velocities obtained from the calculation with BEARTEX. Respectively, Vp, Vs_1 and Vs_2. Input data for this calculation are the elastic stiffness tensor for gypsum single crystal and the ODF obtained from* ***figure 1****.*

(**figure 2**); however, the Vp anisotropy is small since the 3 diagonal components of the tensor are similar.
In our polycrystals, since the crystallographic preferred orientation (i.e. texture) is not very strong (**figure 1b**), a further smoothing of the seismic anisotropy is produced. This is what is shown in the values for calculated velocities of P waves in the region of 5.2-5.3 km/s, whatever the direction of the pole figure. For S waves a slightly larger anisotropy is shown, because the off diagonal values and the diagonal components c_{44}-c_{66} are more different from each other, compared to c_{11}, c_{22} and c_{33} (**Table 1**).

Textured polycrystalline gypsum aggregates show seismic anisotropy that is different from that predicted from the properties of the single-crystal model, and which is widely used for the interpretation of deep seismic data. The elastic tensor produced by quantitative texture analysis may correct this error and improve our knowledge of lithosphere-scale geological processes.

Single Crystal					
78.60	41.00	26.80	0.00	-7.00	0.00
41.00	62.70	24.20	0.00	3.10	0.00
26.80	24.20	72.60	0.00	-17.40	0.00
0.00	0.00	0.00	9.10	0.00	-1.60
-7.00	3.10	-17.40	0.00	26.40	0.00
0.00	0.00	0.00	-1.60	0.00	10.40
Poly Crystal					
62.91	32.79	33.16	-0.03	0.00	-0.02
32.79	62.93	34.11	0.00	-0.22	0.01
33.16	34.11	62.97	0.01	-0.02	0.11
-0.03	0.00	0.01	14.50	0.00	0.10
0.00	-0.22	-0.02	0.00	14.85	0.01
-0.02	0.01	0.11	0.10	0.01	15.01

Table 1: *Elastic stiffness tensor for a single crystal of gypsum and the corresponding geometric homogenized tensor for polycrystalline gypsum; polycrystalline gypsum tensor components were calculated using the ODF obtained from quantitative texture analysis. The values correspond to the elements of the tensors C_{ij}, where i and j are from 1 to 6, and are in GPa.*

REFERENCES

H.P. Laubscher, Tectonophysics, 27 (1975) 239-254 **[1]**
M. Barchi, G. Minelli and G. Pialli. Mem. Soc. Geol. It., 52 (1998) 383-400 **[2]**
L. Lutterotti, S. Matthies and H.-R. Wenk, ICOTOM-12, 1 (1999) 1599 **[3]**
H.-R. Wenk, S. Matthies, J. Donovan and D. Chateigner, J. Appl. Cryst. 31 (1998) 262-269 **[4]**

C. Rivard, I. Bihannic, M. Pelletier and F. Villiéras, (LEM, CNRS-INPL, ENSG, Vandoeuvre, France)
B. Demé (ILL)
N. Michau (ANDRA, Châtenay-Malabry, France)

Four-circle neutron diffraction of oriented clay mineral phases

The evaluation of the long-term behaviour of sedimentary rocks used in underground radioactive waste disposal is of primary importance. It requires quantitative information on mineral orientation and swelling mechanisms in the presence of water and at very small - nanometric - scale. Neutron diffraction studies on D16 show that for each phase studied, the evolution of the associated Bragg peak areas provides quantitative information on the distribution of the orientation of the clay particles. Moreover, hydration does not significantly affect the orientation distribution.

In France, the candidate host rock selected by the French national radioactive waste management agency (ANDRA) is the Callovo-Oxfordian argillite, a rock made of about 50% of clay minerals and 50% of quartz and calcite. In conditions where high-activity radioactive wastes are stored, the clay material component is expected to be changed significantly due to the high temperature generated by the waste itself and significant variations in water activity. This latter parameter plays a crucial role as the expansion of clay minerals, such as smectites, strongly depends on the water content: water molecules penetrate the interlayer spaces inducing anisotropic swelling in the direction perpendicular to the clay layers [1] (**figure 1**). The evaluation of the mechanical and chemical properties of the host rock in storage conditions requires a knowledge of the detailed nature of water uptake (known as the swelling mechanism) by clay phases in natural samples and under constant volume.

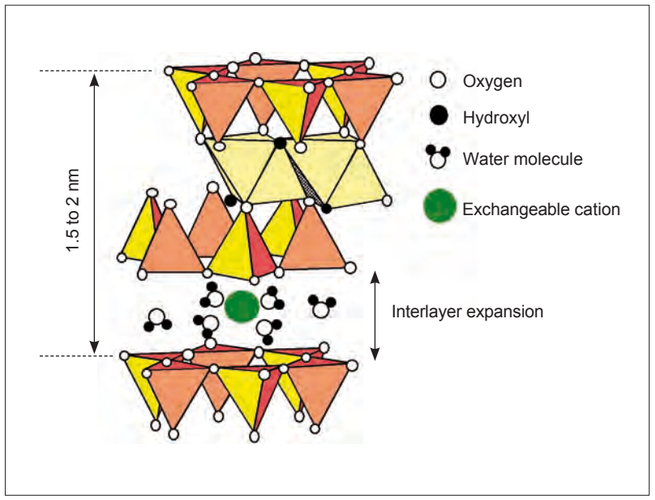

Figure 1:
The structure of smectite, a swelling clay.

Moreover, at a macroscopic scale, the sedimentary rock displays successive strata; such a feature is referred to as bedding. It is still unclear whether the organisation of clay particles and other minerals really follows a similar preferential orientation or not. Consequently, it is of prime importance to characterise how crystallites are organised relative to the rock bedding to assess the macroscopic evolution of the rock.

In order to identify the underlying swelling mechanism at very small scales in the presence of water, and to derive quantitative information on the orientation of clay particles, experiments were carried out on D16 on test pieces extracted from the host rock. Due to their large penetration depth, neutrons are particularly suited to study such thick and massive samples. 4-circle geometry was used to orient the samples along different crystallographic directions. Slices of rock were cut parallel or perpendicular to the macroscopic rock bedding and mounted in cells designed to keep the sample volume constant and allowing hydration [1].

Figure 2 displays the scattering and diffraction patterns recorded on dry samples cut either perpendicularly or parallel to the rock bedding. Depending on the orientation of the sample, the pattern observed for low diffraction angles (for q= 0 in **figure 2**) is either isotropic (parallel sample) or anisotropic (perpendicular samples), which reveals the anisotropic arrangement of the whole rock matrix. At larger angles, diffraction lines corresponding to each individual mineral are observed. The seven curves plotted on **figure 3** are obtained after an integration of the intensity of the 2D patterns of the set of data acquired at seven orientations relative to the macroscopic rock bedding. An angle of 0° corresponds to the sample orientation illustrated at the top left of **figure 2**, 90° to the sample orientation at the middle left, and intermediate angles to intermediate orientations.

For each phase, the evolution of the Bragg peak areas provides quantitative information on the orientation distribution. The intensity of the (00l) peaks corresponding to the clay basal planes is a maximum

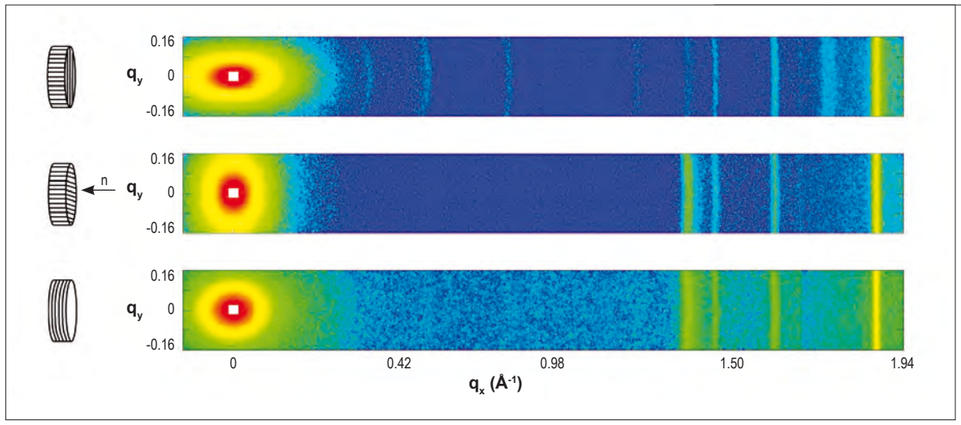

Figure 2:
2D diffraction patterns obtained on D16 with the Callovo-Oxfordian rock (dry sample) for different orientations of the bedding relative to the diffraction plane. Top and middle: perpendicular samples, Bottom: parallel sample, where the orientations refer to the cut of the sample slide in relation to the rock bedding, illustrated on the left.

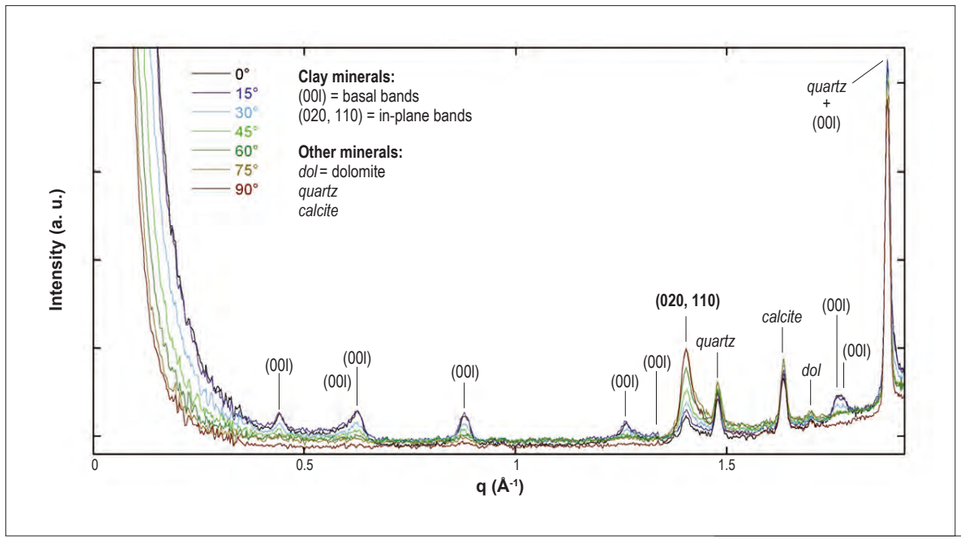

Figure 3:
Diffraction patterns obtained on a dry sample for each measured orientation where the angles are defined in the text.

for the position referred to as 0° in **figure 3**, indicating that clay particles are strongly oriented. On the curve recorded at 90°, the 00l lines have disappeared whereas the (020,110) bands corresponding to in-plane reflections are enhanced. Trends are similar for the different clay species. By contrast quartz and calcite do not display significant preferential orientations. Under hydration, the evolution of the different diffraction peaks remains the same as for dry samples indicating that there is no modification of orientation upon hydration.

In conclusion, the neutron diffraction experiments demonstrated that hydration does not significantly modify the orientation of clay particles in the Callovo-Oxfordian rock.

REFERENCES

K. Devineau, I. Bihannic, L. Michot, F. Villiéras, F. Masrouri, O. Cuisinier, G. Fragneto and N. Michau, Applied Clay Science 31 (2006) 76-84 **[1]**

K. J. Mutch, J. S. van Duijneveldt and **J. Eastoe** (University of Bristol, UK)
I. Grillo (ILL)
R. K. Heenan (ISIS, Didcot, UK)

Towards optimised crystallisation agents for proteins

Producing protein crystals which can be fully characterised remains a significant challenge in biochemistry. One approach is to add certain large polymers to a polypeptide solution; under specific conditions this triggers crystallisation of the smaller proteins. Contrast-variation small-angle neutron scattering has been employed to study the relative effects of size and concentration of model protein mimics on the system structure. Unexpected universality in behaviour was observed, showing that scaling arguments can be helpful for selecting optimised polymers as protein crystallisation agents.

The effect of adding a non-adsorbing polymer to a colloidal solution has been known for many years [1]. The so-called 'depletion effect', which arises from the exclusion of polymer from between the colloidal particles, ultimately leads to macroscopic phase separation of the two dissimilar components. The practice of adding large water soluble polymers to solutions of small protein molecules to aid crystallisation of the protein is one area where this effect is particularly useful [2].

One issue of importance in this field is the dependence of the depletion interaction on the concentrations of the two species. The promotion of crystallisation is very often a hit or miss affair, achieved without any systematic criteria for the optimum polymer size and/or concentration. However, it is known that crystallisation is only favoured under very specific conditions [3]. Hence, an ability to predict the depletion interactions for a specific system could help improve the crystallisation process.

It has been shown from scaling arguments that the demixing boundaries for such systems collapse onto a 'master curve' when plotting the colloid concentration (φ_c) against the relative polymer concentration (φ_p) multiplied by $q^{1.3}$, with q the ratio of the polymer radius of gyration to the colloid radius [4]. Contrast variation small-angle neutron scattering, as performed on D22, provides the ideal technique to study the interactions in these systems by allowing the partial structure factors to be deduced from the scattering profiles.

As a model colloidal system, microemulsions have been used, consisting of small pools of water of radius about 2-3 nm stabilised in cyclohexane by a thin layer of the di-chain anionic surfactant AOT (shown in the inset of **figure 1**), of thickness about 0.8 nm. Hydrogenated polyisoprene of radius of gyration 30 nm was used for all experiments and could be either studied or rendered "invisible" through selective deuteration of the other three system components, as shown by the contrast cartoons in the side-bars of **figure 1**. Following the regular swelling of the microemulsion droplets, different radii and hence values of q could be chosen by changing the ratio of water to surfactant.

Systems with size ratios of q=10, 12.2 and 15.8 were studied at fixed compositions of φ_c=0.09, $\varphi_p q^{1.3}$=0.23 i.e. occupying the same point in scaled phase space. The partial structure factors $S_{cc}(Q)$, $S_{pp}(Q)$ and $S_{cp}(Q)$ could be determined by studying four distinct system contrasts (**figure 1**). $S_{cc}(Q)$ represents the interaction between the colloidal particles, $S_{pp}(Q)$ between the polymer segments and $S_{cp}(Q)$ between the colloids and polymer segments .

By plotting the deduced $S_{cc}(Q)$ against $Q\sigma$, where σ is the hard sphere diameter of the microemulsion droplets, the structure factors are seen to coincide (**figure 2**). This scaling also applies to $S_{pp}(Q)$ and $S_{cp}(Q)$ when the structure factors are normalised by σ^2 and σ respectively.

The scaling of the polymer-polymer structure factors suggests that the characteristic size of the polymer mesh, which can be directly determined from $S_{pp}(Q)$, must be closely linked to σ. Indeed, the ratio of these two values is always close to 1, suggesting that the size of the polymer mesh plays a crucial role in determining the system behaviour.

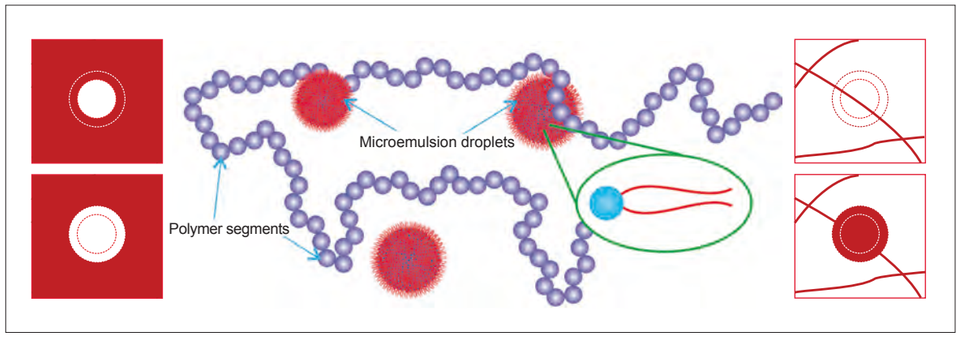

Figure 1: *Schematic of the microemulsion-polymer mixture with the polymer represented as 'segments' and the water droplets surrounded by a layer of surfactant – the two-tailed AOT molecule as depicted. The contrast cartoons depict the studied scattering contrasts, with red denoting hydrogenated regions, white deuterated and dashed lines showing invisible interfaces.*

In mixtures of large colloidal particles and small polymers, the polymer size sets the range of the depletion attraction and the concentration sets the strength. In the limit of large polymers and small colloids (as investigated here) the polymer concentrations are now above the overlap concentration and the polymer mesh size presents a convenient parameter to encompass both the range and strength of the depletion interactions.

Whilst other scattering techniques would allow the determination of (approximate) colloid structure factors, only through contrast variation SANS measurements could the full complement of individual and cross-term partial structure factors be determined.

The observed scaling properties could have implications in determining the depletion interactions for specific sample compositions, and could hence allow the enhancement of protein crystallisation processes.

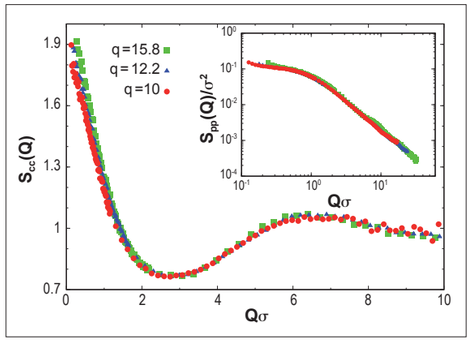

Figure 2: *The scaled colloid-colloid structure factors for mixtures of fixed φ_c=0.09 and $\varphi_p q^{1.3}$=0.23 and inset – scaled polymer-polymer structure factors.*

REFERENCES

J. Traube, Gummi Ztg. 39 (1925) 434 **[1]**
K. J. Mutch, J. S. van Duijneveldt, J. Eastoe, Soft Matter 3 (2007) 155 **[2]**
P. R. ten Wolde, D. Frenkel, Science 277 (1997) 1975 **[3]**
G. J. Fleer, R. Tuinier, Phys. Rev. E 76 (2007) 041802 **[4]**

AUTHORS

S. Rosenfeldt (University of Bayreuth, Germany)
M. Ballauff (Helmholtz-Zentrum Berlin, Germany)
P. Lindner (ILL)
L. Harnau (MPI and University of Stuttgart, Germany)

Structure and interaction of flexible dendrimers in concentrated solution

The study of the shape of flexible molecules in concentrated solutions and the influence of mutual interaction on their conformation is difficult. Using mixtures of flexible dendrimers with protonated and deuterated end groups we investigated the mutual interaction given by the partial structure factors in detail. An analysis of the small-angle scattering data obtained with the instrument D11 reveals that the shape of the flexible dendrimers is practically independent of the concentration. This is in sharp contrast to the pronounced conformational changes of flexible linear polymers.

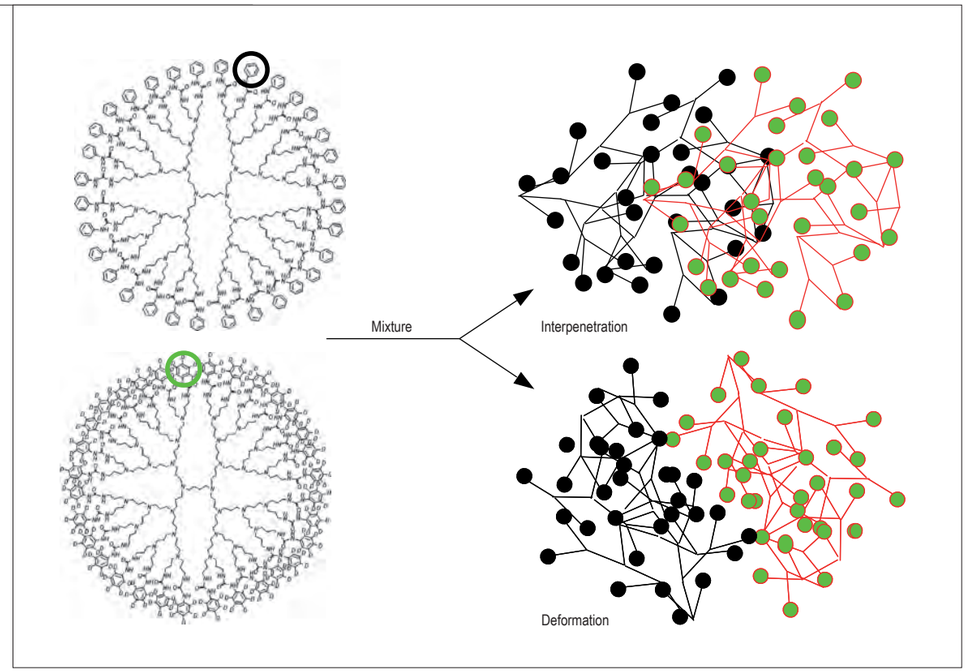

Figure 1: *Schematic illustration of a mixture of flexible dendrimers with and without deuterated end groups in concentrated solution. The particles may only penetrate each other or they may deform significantly due to mutual interaction.*

Dendrimers are macromolecules with a tree-like architecture combining properties of polymers and colloids. Depending on the morphology they may find applications such as contrast agents, light-harvesting and drug-delivery systems. Up to now, the spatial structure of dendrimers is fully understood in the limit of infinite dilution. Flexible dendrimers possess a large number of conformational degrees of freedom which follows from rotations about various chemical bonds (**figure 1**). Thus, the end groups can fold back to the centre of the molecule [1].

Much less is known about the structure in concentrated solution. If the particles only penetrate each other, the shape of the single particles can still be described by the form factor obtained in the limit of infinite dilution. Normally one expects a distortion of the shape due to mutual interaction when approaching the overlap concentration of the molecules (**figure 1**). Hence, the form factors of small and high concentration differ from each other.
Many soft materials, such as flexible polymers or semi-flexible polyelectrolytes are known to change their shape due to various interactions. Before this study, an analysis of possible shape distortions of flexible dendrimers in the concentrated regime had not been made.

Using the contrast variation technique we were able to study the conformation of the dendrimers in detail up to high concentrations. Hydrogen/deuterium (H/D) labeling does not change the conformation and interaction of the investigated dendrimer in the solvent dimethylacetamide [1,2,3] used in this study. Experimentally, we mixed a dendrimer with and without deuterated end groups at different volume fractions. The experiment was carried out at the instrument D11. The mixtures were measured at the match point of the more concentrated dendrimer. Hence, the scattering intensity was mainly determined by the excess scattering of the less concentrated dendrimer. The intensity of a mixture is compared with the intensity of the pure dendrimer with the same overall concentration at highest contrast. In this way partial scattering intensities allowed us to investigate both the structure and the interaction of dendrimers in concentrated solutions. In particular, such a study reveals whether the conformation will be distorted by mutual interactions. The method and the results are illustrated in **figure 2**.

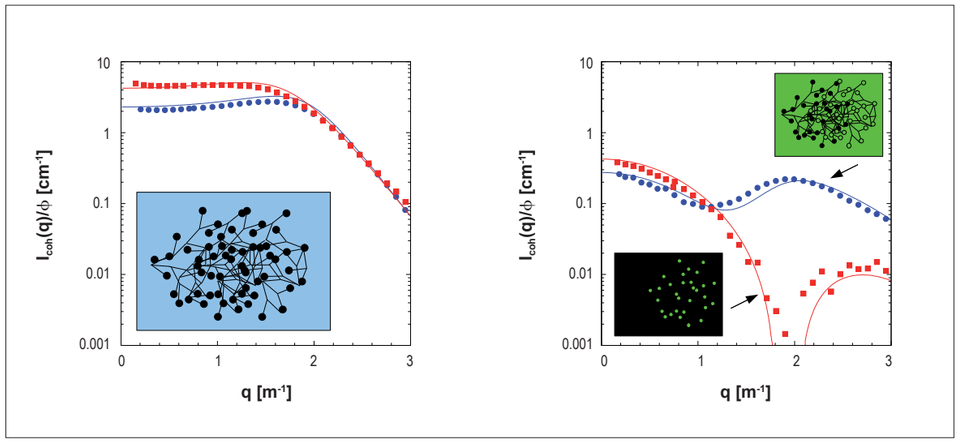

Figure 2: *Experimentally determined coherent scattering intensities $I_{coh}(q)$ normalised to the volume fraction ϕ (= ϕ_H + ϕ_D) as function of the magnitude of the scattering vector. The solid lines represent the scattering intensities calculated for a solution of interacting dendrimers, which shows only interpenetration between different molecules. The volume fractions of the protonated and partially deuterated dendrimer were denoted as ϕ_H and ϕ_D (left: squares: $\phi_H = 0.15$, points: $\phi_H = 0.23$; right: squares: $\phi_H = 0.12 + \phi_D = 0.03$, points: $\phi_H = 0.03 + \phi_D = 0.20$). The results are obtained using the instrument D11.*
Insets*: Schematic illustration of the contrast situation. Depending on the contrast different details are detectable.*

The examples correspond to an overall volume fraction slightly below the overlap concentration (ϕ=0.15) and in the range of the overlap concentration (ϕ=0.23). The solid lines represent the scattering intensity calculated for mutual interaction. For the calculation the shape of the undisturbed dendrimer was used. A detailed evaluation of the data reveals that the interactions between the dendrimers are characterised by an ultra-soft Gaussian interaction potential, as in the limit of infinite dilution. The good agreement between theory and experiment reveals the shape of the dendrimers to be practically independent of the volume fraction.

This result is in sharp contrast to the pronounced conformal changes of flexible and semi-flexible linear macromolecules in semi-dilute solution. For those systems the contributions of the intermolecular interactions to the total free energy increases with increasing concentration. In order to reduce this contribution these particles show a softening of the stiffness resulting in a variation of the size and shape of the molecules. The small deviation in case of the volume fraction 0.23 is only in the range of 2 %. However, possible deformations are negligible compared to the aforementioned changes for linear macromolecules.

We conclude that even in the range of the overlap concentration, flexible dendrimers are rather shape-persistent. This result is corroborated further by a recent computer simulation study that reveals that the overall size of those dendrimers decreases by less than 2% upon increasing the volume fraction from infinite dilution to the overlap volume fraction. [4]

REFERENCES

F. Vögtle, G. Richardt and N. Werner, Dendrimer Chemistry (2009) Wiley-VCH, Weinheim **[1]**
S. Rosenfeldt, N. Dingenouts, M. Ballauff, N. Werner, F. Vögtle and P. Lindner, Macromolecules 35 (2002) 8098 **[2]**
S. Rosenfeldt, M. Ballauff, P. Lindner and L. Harnau, J. Chem. Phys. 130 (2009) 244901 **[3]**
I.O. Götze and C.N. Likos, J. Phys. Condens. Matter 17 (2005) S1777 **[4]**

AUTHORS

D. Lugo and **G.H. Findenegg** (TU Berlin, Germany)
J. Oberdisse (Université de Montpellier, France)
R. Schweins (ILL)

Curvature-induced structure of surfactant aggregates on silica nanoparticles

Surfactants play an important role in industrial processes involving colloidal dispersions. Adsorption of surfactants on the colloidal particles often leads to enhanced stability against flocculation, but exceptions to this general observation exist. Characterisation of the adsorption layers of the surfactants helps to understand their role in dispersion stability.
In this work we studied the mesoscale structure of surfactant layers adsorbed on silica nanoparticles of uniform size (about 20 nm diameter) using small-angle neutron scattering.

Adsorption isotherms of surfactants at hydrophilic surfaces exhibit a pronounced sigmoidal shape and reach a plateau (surface concentration Γ_{mx}) near the critical micelle concentration (CMC), when micelle formation in the solution commences [1]. This behaviour suggests that adsorption represents a surface aggregation process. Scanning probe microscopy (AFM) studies at planar surfaces indicated that either laterally uniform surfactant bilayers or small surface aggregates may be formed, depending on the nature of the surfactant head group and the solid surface [2]. The nature of the surfactant layers adsorbed at colloidal particles in aqueous dispersions was studied by small-angle neutron scattering (SANS). In their pioneering work Cummins *et al.* studied alkyl polyoxyethylene ether (C_mE_n) surfactants on Ludox-type silica sols [3]. The data were analysed by adopting a spherical core-shell model, which implies a laterally uniform surfactant layer.

The present work was motivated by the desire to understand how the self-assembly of surfactants at surfaces is affected by surface curvature of the substrate. For this purpose the surface aggregate structure of the surfactant $C_{12}E_5$ on colloidal silica particles of 16 nm diameter was studied by SANS on the instrument D11 at the ILL.

In supplementary studies strong aggregative adsorption of this surfactant onto the silica beads was found, with a Γ_{mx} value similar to that on planar surfaces. SANS measurements were made with dilute silica dispersions at pH = 9 to avoid agglomeration of the silica particles. A contrast-matching H_2O/D_2O mixture (having the same scattering length density as silica) was used as the solvent, so that the scattering contrast is solely due to the surfactant layer. Samples with different surface concentrations of $C_{12}E_5$ (¼ Γ_{mx}, ½ Γ_{mx}, ¾ Γ_{mx} and Γ_{mx}) were studied. The SANS profiles I(q) of all samples exhibit a local maximum at an intermediate q value which is a direct measure of the amount of adsorbed surfactant. A spherical core-shell model corresponding to a laterally uniform surfactant layer at the surface of the silica particles accounts well for the increase of the mean thickness of the surfactant layer with increasing surface concentration.

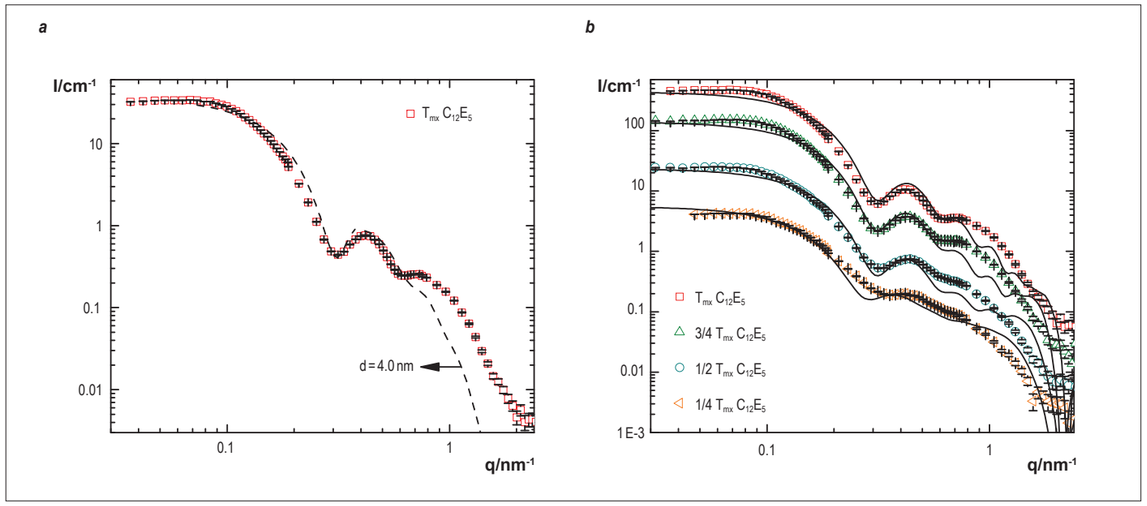

Figure 1: *SANS scattering profiles for a 1.8 wt-% silica dispersion in contrast-matching H_2O/D_2O with an adsorbed layer of $C_{12}E_5$:*
(a) *fit of the scattering data with the spherical core-shell model (surface concentration Γ_{mx});*
(b) *fit with the micelle-decorated silica model (surface concentrations ¼ Γ_{mx}, ½ Γ_{mx}, ¾ Γ_{mx} and Γ_{mx}).*

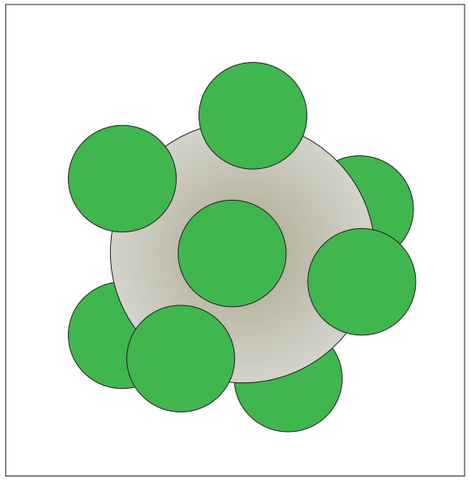

Figure 2: *Sketch of the micelle-decorated silica model.*

However, this model significantly underestimates the surface area of the surfactant layer as extracted from the high-q region of the scattering profiles (**figure 1a**). This finding implies that smaller surface aggregates (having a higher surface area for given amount of surfactant) are formed at the silica particles.

A satisfactory fit of the entire scattering profile I(q) is obtained with a model of micelle-decorated silica beads (**figure 1b**), which suggests that $C_{12}E_5$ is adsorbed in the form of individual surface aggregates of spherical geometry (**figure 2**) [4]. Some deviations from the experimental I(q) remain in the high-q Porod regime. These deviations may be due to a distribution of surface micelle sizes, which is not captured by our model in which the surface micelles have been modeled as monodisperse spheres, which induces the oscillations in the high-q region.

At low surface concentrations one further expects a distribution of the number of surface aggregates per particle. For $C_{12}E_5$ on the 16 nm silica particles the data fit yields a radius of the surface micelle of about 2 nm, nearly independent of the surface concentration. The mean number of surface micelles per silica particle increases with the surface concentration of the surfactant, almost leading to a close-packed layer of surface micelle at the highest surface concentration (**Table 1**). The diameter of the surface aggregates extracted from this model is similar to the diameter of the wormlike micelles of $C_{12}E_5$ in aqueous solutions.

The finding that $C_{12}E_5$ forms small surface micelles at the silica nanoparticles is remarkable in view of the fact that aggregates of lower mean curvature (worm-like micelles) are formed in aqueous solution, and bilayer films are formed at planar surfaces. We make the conjecture that the preference for small surface aggregates is a consequence of the high surface curvature of the silica nanoparticles.

For particles of radius 8 nm and a bilayer thickness of 4 nm the mean area per molecule in the mid-plane of the bilayer is 50 % greater than the respective area directly at the surface. Accordingly, an effective packing of the surfactant tails is not possible in a bilayer configuration. Instead, small (roughly spherical) surface aggregates are favoured as these allow the most effective packing of the tails at small colloidal particles.

Surface concentration	X	R_{sa} (nm)	N_{sa}
¼ Γ_{mx}	0.23	2.2	28
½ Γ_{mx}	0.39	2.1	52
¾ Γ_{mx}	0.55	2.1	73
Γ_{mx}	0.63	2.0	98

Table 1: *Parameters of the micelle-decorated silica model for different surfactant concentrations, of $C_{12}E_5$ on silica nanoparticles (radius 8.2 nm): X, effective volume fraction of surfactant in the adsorbed layer, Rsa, radius of the surface aggregates; Nsa, number of surface aggregates per silica particle.*

REFERENCES

F. Tiberg, J. Brinck and L.M. Grant, Current Opin. Colloid Interface Sci. 4 (1999) 411 **[1]**
S. Manne and H.E. Gaub, Science 270 (1995) 1480 **[2]**
J. Penfold, E. Staples, I. Tucker and P. Cummins, J. Phys. Chem. 100 (1996) 18133 **[3]**
G. Despert and J. Oberdisse, Langmuir 19 (2003) 7604; D. Lugo, J. Oberdisse, M. Karg, R. Schweins and G.H. Findenegg, Soft Matter 5 (2009) 2928 **[4]**

S. Klotz, **L.E. Bove** and **A.M. Saitta** (IMPMC, Université Pierre et Marie Curie, Paris, France)
T. Strässle (ETH Zurich and PSI Villigen, Switzerland)
T. Hansen (ILL)

Salty ice VII under pressure

When saltwater freezes, the ice expels almost completely the salt into the brine and the grain boundaries. It was therefore assumed that ice is unable to incorporate significant amounts of salt into its structure, and that none of the many salt hydrates in nature is structurally related to any of the known ice phases. Hovever, recent experiments on the diffractometer D20 demonstrated that this is not an intrinsic physico-chemical property of ice phases and revealed the existence of 'salty ice VII', a salt hydrate based on a high pressure ice phase.

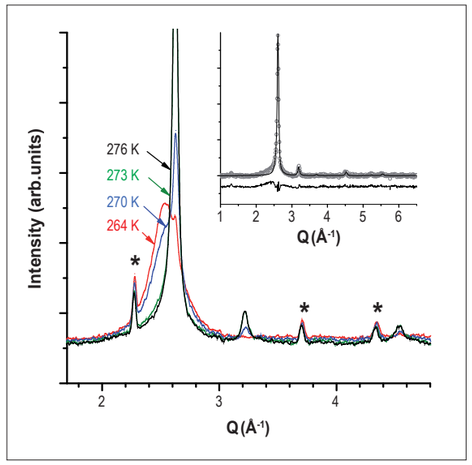

Figure 1: *Recrystallisation of a LiC·6D_2O glass at about 270 K and 4 GPa into salty ice VII. Asterisks (*) correspond to peaks from lead which served as pressure markers.*

Inset: *Rietveld fit to a sample without lead. Diffraction data were obtained with a sample of about 80 mm^3 on D20.*

Ice VII is a high-pressure ice phase stable beyond 2 GPa (20 kbar) which can incorporate substantial amounts of dissolved LiCl by building the salt homogeneously into its structure [1]. Such 'alloyed' ice VII has significantly different structural and dynamical properties compared to 'non-salty' ices.

The trick in these experiments was to start with a solid solution of LiCl in its glassy state. In fact it is known that aqueous LiCl solutions of molar concentrations of about 1 : 6, i.e. LiCl·6D_2O, can be deeply undercooled and transformed below about 130 K directly into a glass [2].
The ILL Paris-Edinburgh high-pressure cell was used to compress a 80 mm^3 sample of such a glass at 80 K to 4 GPa. Upon heating under pressure crystallisation of the glass is observed at about 270 K into a structure which corresponds to ice VII, the stable phase under these conditions. However, the refinements show an 8% larger unit cell volume than expected for pure ice VII at this pressure, unusually large displacement factors, and diffuse scattering, as shown in **figure1**. Also, when cooled, such samples do not convert to hydrogen-ordered ice VIII, as would be expected for ordinary ice VII.

All these features are fingerprints for the incorporation of Li and Cl ions into the ice VII structure, i.e. the formation of an 'alloyed' high pressure ice form. It turns out that the bcc like structure of ice VII

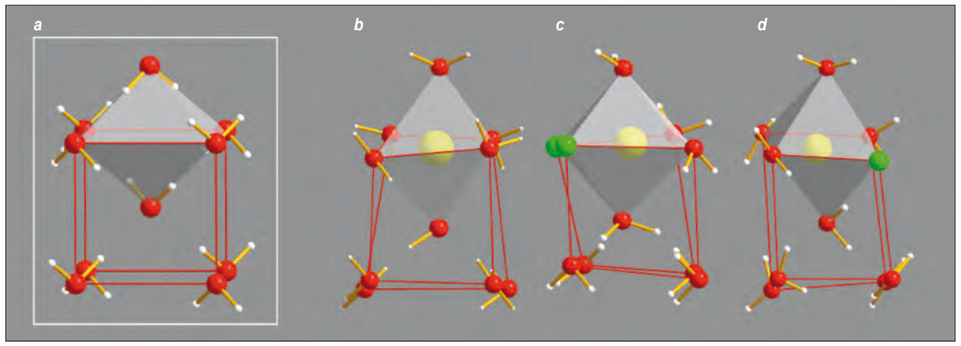

Figure 2: *Local structural configurations in salty ice VII* ***(b-d)*** *compared to pure ice VII* ***(a)****, obtained by computer simulations. Red: oxygen, yellow: Li^+, green: Cl-.*

[3] is ideally suited for incorporation of Li^+ and Cl^- since it provides Li-O and Li-Cl distances which coincide to within ±0.3 Å to typical distances found in other LiCl-hydrates (see for example lithium chloride monohydrate LiCl·H_2O [4]).
The evidence is that Li^+ ions occupy the octahedral interstitial sites of the ice VII structure, whereas the Cl- ions randomly occupy oxygen sites. Computer simulations carried out within the same experimental team support the structural model and give a detailed insight into the local topology (**figure 2**), and its dynamics.

Apart from the local distortions, the presence of ions leads to the reorientation of H_2O molecules in their immediate vicinity and the breaking of hydrogen bonds. At 300 K, the orientational dynamics of the H_2O molecules seems to be governed by the diffusion of the Li^+ ions between the interstitial sites, which freezes in upon cooling to below about 180 K.

The data suggest that other salty high pressure ice forms exist in nature which would make incorporation easier, since their densities are much lower than ice VII. Latest unpublished results from experiments at D20 seem to confirm this.

Salty ices are expected to show ionic conductivity, similar to other LiCl hydrates which exist at ambient pressure. If salty ices exist in nature in sizable quantities, they should be relevant to the modelling of satellites in the outer solar system, of which ice is a major constituent.

REFERENCES

S. Klotz, L.E. Bove, Th. Strässle, Th. Hansen and A.M. Saitta, Nature Materials 8 (2009) 405 **[1]**
B. Prevel, J. Dupuy-Philon, J.F. Jal, J.F. Legrand and P. Chieux, J. Phys.: Condens. Matter 6 (1994) 1279 **[2]**
W.F. Kuhs, J.L. Finney, C. Vettier and D.V. Bliss, J. Chem. Phys. 81 (1984) 3612 **[3]**
A. Hönnerscheid, J. Nuss, C. Mühle and M. Jansen, Z. Anorg. Allg; Chem. 629 (2003) 312 **[4]**

AUTHORS

J. W. E. Drewitt and **P. S. Salmon** (University of Bath, UK)
A. C. Barnes (H.H. Wills Physics Laboratory, Bristol, UK)
S. Klotz (IMPMC, Université Pierre et Marie Curie, Paris, France)
H. E. Fischer (ILL)
W. A. Crichton (ESRF, Grenoble, France)

Hot neutron liquids and amorphous diffractometer D4
X-ray beamlimes: ID11 and BM29 (ESRF, Grenoble); XAS (LURE, Orsay); 11-ID-C (APS, Argonne)

Structure of GeO_2 glass at pressures up to 8 GPa

Many liquid and glassy materials are thought to undergo polyamorphic phase transitions in which there is an abrupt change in their structure and physical properties with change of temperature and/or pressure. Silicates, for example, are the most abundant compounds present within the crust and upper mantle of the Earth and terrestrial planets.

The transformations associated with silicate minerals and melts govern some major geophysical principles including deep-earthquake faulting, the differentiation and evolution of the composition of planetary interiors, and the response of the Earth's crust and mantle to meteorite impacts. This article reports on the development of *in situ* neutron diffraction methods to accurately measure the structure of glasses up to about 8 GPa. The focus is on the network glass GeO_2, an analogue of silica for which the transformations in structure occur at lower pressures that are more amenable to experiment. The results show the operation of two densification mechanisms for the network structure but we find no evidence in support of an abrupt transformation over the investigated pressure range.

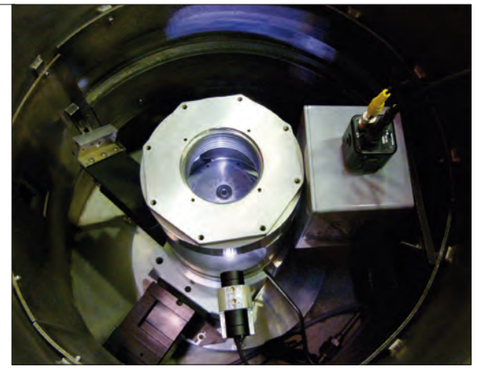

Figure 1: *The Paris-Edinburgh press mounted in the vacuum bell jar of D4. The picture shows several of the developments (z-axis motor and optical camera) associated with an ILL long-term proposal. A neutron (Hewat) camera is mounted to the right-hand side of the bell jar and is used for the initial alignment of the incident beam relative to the press.*

Structural investigations of liquid and glassy materials require an accurate evaluation of the intensity measured in a diffraction experiment so that bond distances and coordination numbers can be reliably obtained. This task is difficult to achieve in the case of high pressure experiments because the sample volume is typically small and there is much extraneous scattering from the gasket material in which the sample is contained and from the anvils of the high pressure press. Also, the scattering geometry changes with pressure as, for example, the sample compresses when the anvils of the press close. We have therefore initiated a programme of research, supported through the recently introduced long-term proposal scheme, to develop high pressure techniques for the liquid and amorphous materials diffractometer D4 at the ILL. The work makes use of the Paris-Edinburgh press and the latest experimental configuration is shown in **figure 1**. An optical camera is used to observe the sample position and a z-axis drive enables vertical movement of the press so that the sample can be centred in the incident neutron beam for each pressure point. **Figure 2** shows part of the team that has supported these developments.

Figure 2: *Removal of the Paris-Edinburgh press from the D4 bell jar at the end of a successful neutron diffraction experiment.*

The fully corrected total structure factors, $S_N(k)$, which have been extracted from the diffraction patterns measured *in situ* for GeO_2 glass at pressures up to 8 GPa, are shown in **figure 3** [1]. The increase in position and decrease in height of the first peak, which appears at a scattering vector $k = 1.53(2)$ Å^{-1} at ambient pressure, indicate a gradual change of the intermediate range order of the glass network with increasing density. The diffraction patterns observed for pressures > 5 GPa are rather different to those measured for samples that have been compacted under pressure, heat treated and recovered to ambient conditions, thus emphasizing the importance of making *in situ* structural measurements [1,2].

The real space information corresponding to each $S_N(k)$ function is obtained by Fourier transformation. The nearest neighbour Ge-O bond distances and associated coordination numbers are shown

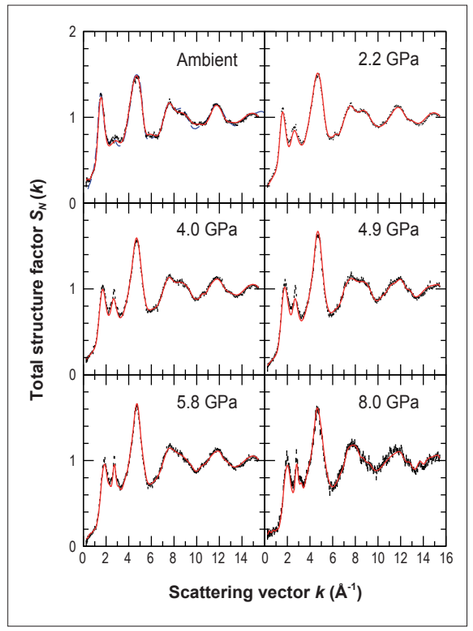

Figure 3: *The total structure factors $S_N(k)$ measured for GeO_2 glass by in situ neutron diffraction experiments. The data are given by the points with error bars and the solid (red) curves are Fourier back-transforms of the corresponding real space functions after the unphysical features at small distances have been removed.*

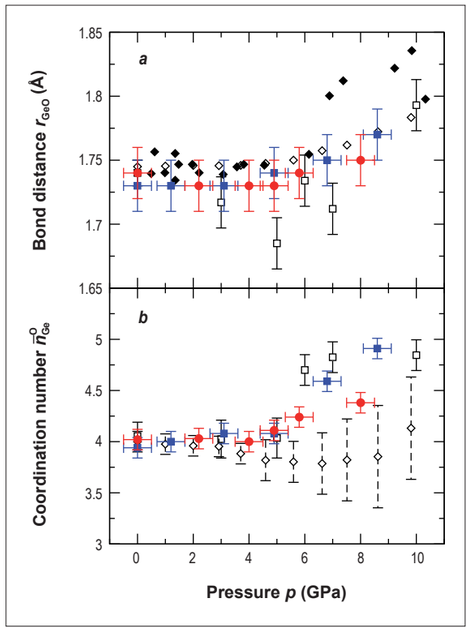

Figure 4: *The pressure dependence of **(a)** the Ge-O nearest-neighbour distance r_{GeO} and **(b)** the mean Ge-O coordination number $\bar{n}^O_{Ge}$ for GeO_2 glass. The blue and red symbols show the results obtained in two separate neutron diffraction studies, the red symbols corresponding to the data presented in figure 3. Also shown are the results obtained from the X-ray diffraction study of Guthrie et al. [2] (open squares), the EXAFS study of Vaccari et al. [3] (open diamonds), and the EXAFS study of Itié et al. [4] (closed diamonds in **(a)**). According to Ref. [3], the discrepancy between the coordination numbers obtained from diffraction and EXAFS may arise from the difficulty in treating the amplitude of the EXAFS signal measured in high pressured experiments.*

in **figure 4** where a comparison is made with the results obtained from previous *in situ* X-ray diffraction and extended X-ray absorption fine structure (EXAFS) spectroscopy experiments. The results show that Ge remains tetrahedrally coordinated to oxygen as the pressure is increased from ambient to about 5 GPa. As the pressure is increased further to about 8.5 GPa, however, a steady increase from 4.0(1) to 4.9(1) is observed in the Ge-O coordination number as the corresponding distance expands from 1.73(2) to 1.77(2) Å in order to accommodate the increased number of nearest neighbours. The results are consistent with the operation of two densification mechanisms, the low pressure one associated with squeezing the open network of corner linked tetrahedral motifs and the high pressure one associated with a transformation of those motifs.

In summary, we have developed methods to make accurate neutron diffraction experiments on glasses at pressures up to about 8 GPa. It may therefore be possible to use the method of isotope substitution in neutron diffraction to gain information at the partial structure factor level on the ordering in materials like glassy GeO_2 under high pressure conditions. This would provide a breakthrough in understanding the mechanisms of pressure induced transformations.

REFERENCES

J. W. E. Drewitt, P. S. Salmon, A. C. Barnes, S. Klotz, H. E. Fischer and W. A. Crichton, Phys. Rev. B 81 (2010) 014202 **[1]**
M. Guthrie, C. A. Tulk, C. J. Benmore, J. Xu, J. L. Yarger, D. D. Klug, J. S. Tse, H.-K. Mao and R. J. Hemley, Phys. Rev. Lett. 93 (2004) 115502 **[2]**
M. Vaccari, G. Aquilanti, S. Pascarelli and O. Mathon, J. Phys.: Condens. Matter 21 (2009) 145403 **[3]**
J. P. Itié, A. Polian, G. Calas, J. Petiau, A. Fontaine and H. Tolentino, Phys. Rev. Lett. 63 (1989) 398 **[4]**

F. Gabel, **M. Ringkjøbing Jensen** and **M. Blackledge** (IBS, Grenoble, France)
G. Zaccai (ILL)

Protein denaturation studied by a combination of small-angle neutron and X-ray scattering

Characterisation of the conformational properties of denatured proteins is essential to our understanding of the molecular basis of protein folding and stability. We combined small-angle neutron and X-ray scattering to study the interaction of urea with ubiquitin, an 8.6 kDa protein which assumes a number of important functions in biological cells, in particular the preparation of proteins for proteasomal degradation. Comparing the intensity of coherent scattering at zero angle we determined quantitatively the number of urea molecules preferentially bound during the unfolding of ubiquitin. We find that a pH change from 6.5 to 2.5 triggers the recruitment of about 20 urea molecules per ubiquitin molecule, from the bulk solvent.

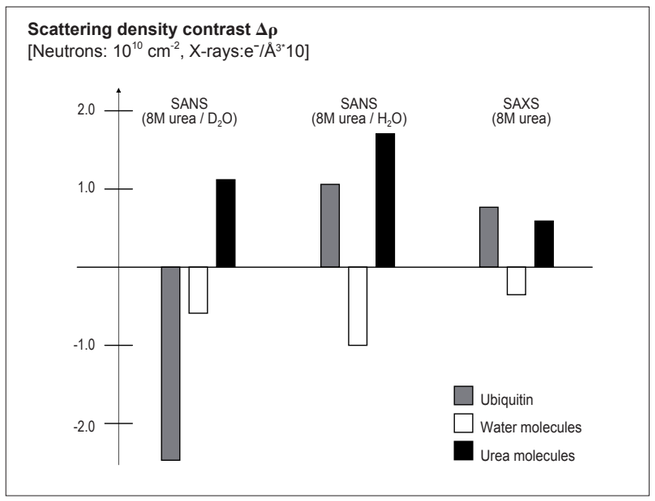

Figure 1: *Scattering contrast for ubiquitin, water and urea molecules for neutrons in 8M urea/(D_2O and H_2O) and for X-rays in 8M urea (identical values in H_2O and D_2O). Opposite signs in contrast of two components associated in solution induce an apparent diminution of the molecular weight while identical signs lead to an increase.*

Despite the abundance of biophysical and biochemical data from unfolded proteins in the presence of a denaturant, the molecular origins of solvent-induced protein denaturation remain unclear. An accurate description of the unfolded state is also important for the investigation of protein misfolding (as occurs in certain neurodegenerative diseases), as well as to describe the relationship between flexibility and function in physiologically intrinsically disordered proteins. Whereas one model invokes the disruptive effects on water structure, such that urea acts as a better solvent for hydrophobic protein groups [1], an alternative model proposes that urea binds directly to multiple sites on the protein backbone, thereby destabilising the native fold relative to the unfolded state [2].

In this study we applied a powerful combination of small-angle neutron (SANS) and X-ray (SAXS) scattering on ubiquitin in 8M urea solution (H_2O and D_2O at pH 2.5 and 6.5) in order to study the interaction of urea with ubiquitin in the native and denatured states [3]. We exploited the fact that ubiquitin, urea, H_2O and D_2O molecules, respectively, have different, specific scattering length densities for neutrons and X-rays. They scatter each radiation differently, in terms of both amplitude and phase (**figure 1**). In the forward scattering direction, the scattered signal of a particle in solution is $I(0)=A^2$, where the scattered amplitude A corresponds to the sum of the scattering lengths of the nuclei (SANS) or electrons (SAXS) minus the sum of scattering lengths in an equivalent volume of solvent.

The scattering curve as a function of the scattering vector Q, I(Q), yields information on the overall shape of the particle in solution (e.g. globular, elongated, …).

By comparing the scattered signal from ubiquitin in H_2O and D_2O urea solutions by SANS (ILL instrument D22) and SAXS (ESRF beamline ID02), we observed that at pH 6.5 the experimental scattering curve matches the one predicted for folded ubiquitin over the entire Q-range, indicating that the protein is in its native conformation even when dissolved in high concentrations of denaturant. Lowering the pH to 2.5 resulted in a change in overall shape of the scattering curve along with a significant increase in radius of gyration, suggesting that under these conditions the protein unfolds into a disordered conformation (**figure 2**).

A remarkable feature, observed by both SAXS and SANS is the change in I(0) on lowering the pH: an increase is observed by SAXS upon denaturation, while SANS in D_2O shows a significant decrease. The situation for SANS in H_2O is ambiguous due to large errors (**figure 2**). Both the extent and the sign of the intensity change can be explained quantitatively by assuming that about 20 urea molecules are recruited by each ubiquitin molecule upon unfolding. The number was calculated by considering the different scattering densities of ubiquitin, water and urea molecules for X-rays and neutrons (**figure 1**): for SANS in D_2O, for example, the scattering length densities of ubiquitin and urea molecules are of opposite sign, leading to a partial extinction of the signal scattered by ubiquitin after recruitment of urea. In the case of SAXS, urea and ubiquitin have scattering length densities of the same sign, leading to constructive interference and an increase in I(0) upon preferential binding of urea during unfolding.

It is very important to stress here that our results rely strongly on the complementarity of neutrons and X-rays and could not have been unambiguously obtained by either technique alone. For example, the SAXS data could have been interpreted in terms of a hydration shell of different density than the bulk solvent [4]

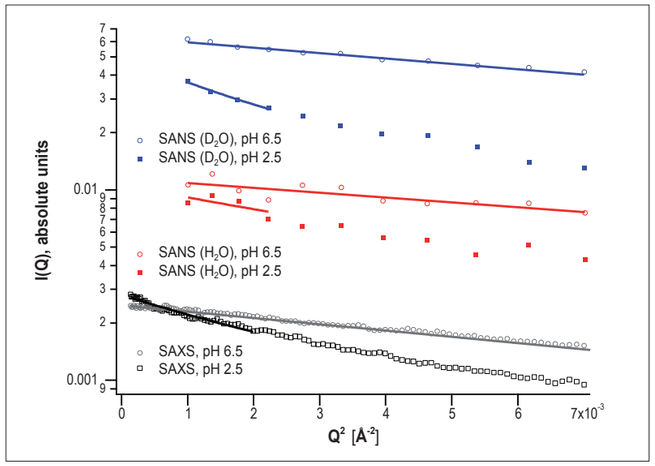

Figure 2: *Guinier plots (ln(I) vs. Q^2) of SAXS and SANS data. The (long) lines denote Guinier-fits of the pH 6.5 data, the (short) lines denote Debye-fits of the pH 2.5 data, used for the determination of I(0).*

that increases its volume upon unfolding. However, this interpretation is inconsistent with the SANS results. Our combined data analysis rather suggests that the hydration shell of unfolded ubiquitin does not have the same thickness as that of the folded protein and/or it must have a different density.

In conclusion, the complementary scattering properties of H_2O, D_2O, ubiquitin and urea for SANS and SAXS enabled a quantitative and model-free analysis of the interaction of urea with the protein ubiquitin under denaturing conditions. Our results contribute to a more detailed understanding of the molecular mechanisms of protein denaturation, by supporting the model of direct binding of urea to the protein.

REFERENCES

C. Tanford, J. Am. Chem. Soc. 86 (1964) 2050 **[1]**
J. A. Schellman, J. Phys. Chem. 62 (1958) 1485 **[2]**
F. Gabel *et al.* J. Am. Chem. Soc. 131 (2009) 8769 **[3]**
D. I. Svergun *et al.* Proc. Natl. Acad. Sci. USA 95 (1998) 2267 **[4]**

M.C. Rheinstädter (McMaster University, Canada)
K. Wood (Bragg Institute, ANSTO, Australia)
K. Schmalzl (IFF, Jülich, Germany)
D. Strauch (University of Regensburg, Germany)

Protein-protein interactions in a biological membrane

Understanding how proteins – life's worker molecules – interact with each other is a major goal of biological sciences and one of its greatest challenges. Inelastic neutron scattering has proven to be a powerful tool for studying dynamics in bio-molecular materials because it can access the relevant length and time scales. We report experimental evidence for a protein-protein interaction in a biological membrane, the purple membrane.

Purple membrane (PM) is a well-characterised native membrane system and one of the simplest bio-energetic devices. Due to its simple organisation, and easy spectroscopic access to its functional state, PM is one of the best suited model systems for the experimental study of biological function. A possible interaction between membrane embedded proteins may lead to dynamic coupling between proteins, i.e., concerted protein dynamics. One way for proteins to communicate is to use the membrane as a signal transmitting medium.

Collective molecular motions are attracting increasing attention because of their potential impact on membrane and protein function and our understanding of biological systems in general. However, very few approaches and techniques are capable of accessing collective molecular motions. Theoretically, coupled molecular motions can be modeled using molecular dynamics computer simulations, and inter-protein motions in a carboxymyoglobin protein crystal were recently found in simulations [1]. On the experimental side, only inelastic X-ray and neutron scattering experiments can directly access collective dynamics in membranes and proteins. Phonon-like excitations of proteins in hydrated protein powder were reported from X-ray scattering experiments using synchrotron X-ray radiation [2]. Through neutron scattering experiments, we have recently presented experimental evidence of protein-protein interaction in a biological membrane under physiological conditions.

PM occurs naturally in the form of a two-dimensional crystal, consisting of 75% (wt/wt) of a single protein, bacteriorhodopsin (BR), that functions as a light-activated proton pump, and 25% various lipid species (mostly phospho- and glycolipids). BR is a proton transporting membrane protein, formed of seven transmembrane alpha helices arranged around the photosensitive retinal molecule. The protein in the lipid matrix is organised into trimers that form a highly ordered 2D hexagonal lattice with lattice parameter a = 62 Å.

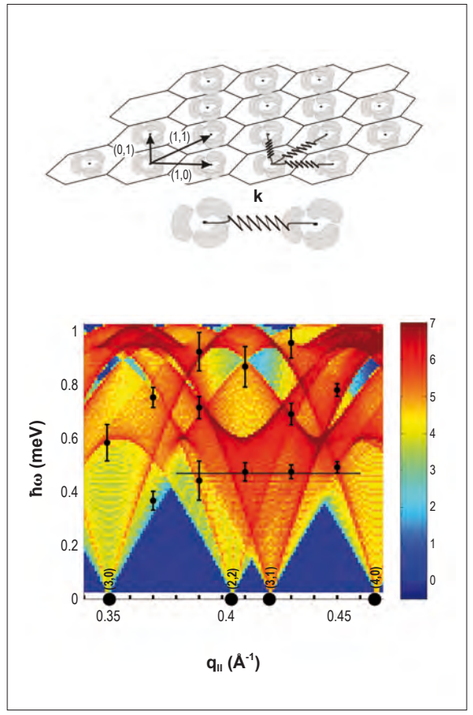

Figure 1: (a) *BR trimers are arranged on a hexagonal lattice of lattice constant a = 62 Å. The interaction between the protein trimers is depicted as springs with effective spring constant k.* ***(b)*** *Calculated excitation spectrum $C_l(q,\omega)$ in the range of the experimental data. Data points mark the positions of excitations. The horizontal line at $\hbar\omega = 0.45$ meV marks the position of a possible optical phonon mode, not included in the calculations.*

Deuterated PM was produced and hydrated with H_2O. The experiments were performed on the IN12 cold three-axis spectrometer. The excitation spectrum of the 2D protein lattice was modeled analytically. The protein trimers were taken as the centres of a primitive hexagonal lattice, and the spectrum of the acoustic phonons was calculated. The model is depicted in **figure 1 (a)**. The calculated longitudinal spectrum $C_l(q,\omega)$, defined by $C_l(q,\omega)=\omega^2/q^2\ S(q,\omega)$, is shown in **figure 1 (b)**. The statistical average in the plane of the membrane leads to a superposition of the different phonon branches. The positions of experimentally determined excitations are marked by the data points. The effective protein-protein spring constant k was calculated as k = 53 N/m. Using the same approach, the spring constant for graphite for comparison is calculated to be 27 000 N/m for the in-plane interaction, and 3.5 N/m for out-of-plane interactions.
The force constant that we measure in PM is therefore 1–2 orders of magnitude larger than the effective van der Waals force constant in graphite, but 2–3 orders of magnitude weaker than a C-C bond.

The protein coupling reported here may be relevant for the photo cycle in PM. The BR proteins undergo structural changes during the photo cycle, involving displacements of up to 1.7 Å [3]. Because of the elastic coupling of the BR proteins, those distortions can propagate to neighbouring proteins. On the microscopic level, displacing or distorting a BR trimer by 1.7 Å yields a force between neighbouring trimers of 9 nN (using the model presented here). It can therefore be speculated that there is a protein-protein communication during the photocycle in PM.

Protein communication may be important for understanding macromolecular function in a cellular context. It is common sense that biological systems act as coherent entities. But the degree of cooperation and more importantly, the level of biological organisation where this cooperation occurs, are completely unknown. Our previous results suggest that already the basic building blocks, such as lipids and proteins interact and show a concerted dynamics [4]. Besides the interest in fundamental science, the study of biological membranes is motivated by applications in nano-technology and bio-inspired materials science, as shown in **figure 2**.

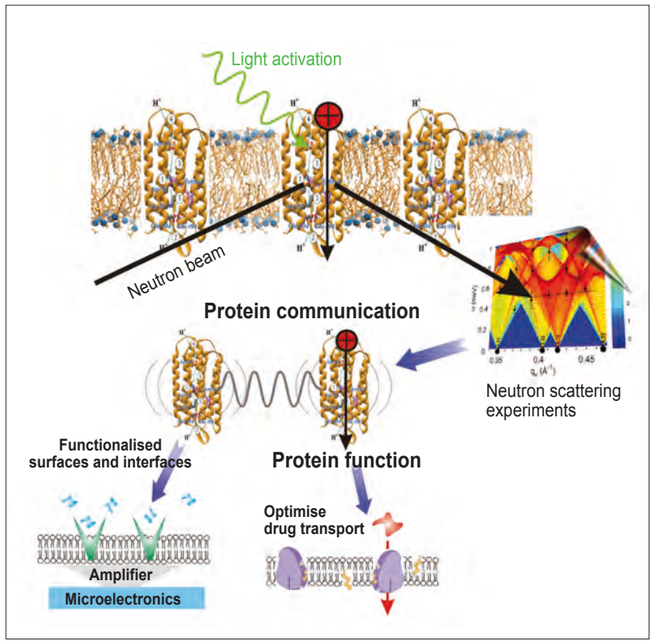

Figure 2: *Neutron scattering is a powerful tool to investigate protein function and protein communication in biological membranes. The outcome may eventually be used for the development of highly efficient biosensors and to optimise drug transport.*

Trans-membrane proteins and membrane-associated proteins are for instance the first to be attacked in many infectious diseases. To establish a clear relationship with protein function, protein dynamics of activated proteins, i.e., the collective dynamics of proteins undergoing the photo cycle, will be studied using recently developed laser-neutron pump-probe experiments [5]. While the protein concentration in PM is very high and the proteins are very close to a 2D crystal, it can be speculated that there is also protein coupling in less dense membrane systems

REFERENCES

L. Meinhold, J. C. Smith, A. Kitao, and A. H. Zewail, Proceedings of the National Academy of Science U.S.A. 104 (2007) 17 261 **[1]**
D. Liu, X. Chu, M. Lagi, Y. Zhang, E. Fratini, P. Baglioni, A. Alatas, A. Said, E. Alp, S. Chen, Physical Review Letters 101 (2008) 135501 **[2]**
N. Dencher, D. Dresselhaus, G. Zaccai, G. Büldt, Proceedings of the National Academy Science U.S.A. 86 (1989) 7876–7879 **[3]**
M. C. Rheinstädter, J. Das, E. J. Flenner, B. Brüning, T. Seydel, I. Kosztin, Physical Review Letters 101 (2008) 248106 **[4]**
J. Pieper, A. Buchsteiner, N.t A. Dencher, R. E. Lechner, T. Hauß, Physical Review Letters 100 (2008) 228103 **[5]**
Reference for this paper: M. C. Rheinstädter, K. Schmalzl, K. Wood, D. Strauch, Physical Review Letters 103 (2009) 128104

F. Roosen-Runge, **F. Zhang**, **S. Zorn** and **F. Schreibe**r (University of Tübingen, Germany)
M. Hennig (University of Tübingen, Germany and ILL)
T. Seydel, **M. Maccarini** and **P. Fouquet** (ILL)
M.W.A. Skoda (ISIS, UK)
R.M.J. Jacobs (University of Oxford, UK)

Protein diffusion in crowded electrolyte solutions

Proteins in the intracellular environment occur in highly concentrated "crowded" aqueous solutions of different macromolecules and salts. Both the molecular crowding and the presence of different salts affect the mobility and in particular the diffusion of the proteins.
Salts also affect protein aggregation and induce complex phenomena such as reentrant condensation, i.e. a solubility which is not monotonously related to the ionic strength.
We investigate these issues on simplified model systems, by applying neutron spectroscopy and complementary techniques to study globular proteins and salts with different valency in aqueous solution.

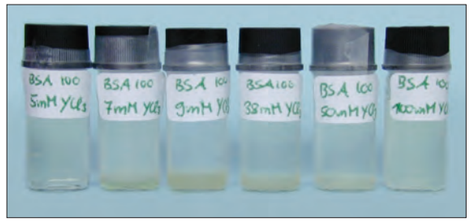

Figure 1: *Photograph of solutions of BSA proteins (concentration 100mg/ml, i.e. volume fraction 6.9%) in water (D_2O) with rising YCl_3 salt concentration C (from left to right).*
The proteins are fully dissolved at C<C (left, see text), precipitate at C*<C<C** (precipitate visible at the bottom of the vials), and re-enter into a fully dissolved regime at C>C** (turbid solution without precipitate on the right). On the depicted concentration series, C* is at approximately 7mM YCl_3 and C** is slightly above 50mM.*

Proteins in solution form monodisperse colloidal suspensions. In addition to their biological role, proteins in solution are therefore of fundamental interest in the context of soft matter science.
Proteins, however, differ in one important aspect from many simple colloidal systems: the distribution of charges on the surface of a protein is in general inhomogeneous. This inhomogeneous surface charge distribution can in turn be assumed to have a fundamental biological relevance in controlling for instance aggregation phenomena and biological activity such as docking processes.
Living cells contain proteins at high concentrations. A characteristic of proteins in their native environment is therefore the *macromolecular crowding* – i.e. relatively large volume fractions being occupied by proteins – *and the aqueous solvent containing salt ions*. These salt ions are crucial for the understanding of the effective interactions of proteins and the resulting structures as well as indeed the dynamics.

While mean-field based concepts for the description of charge effects in colloidal suspensions have been known for some time, there are surprisingly few quantitative studies of the effective interactions of proteins depending on their charge. Recently, new effects have been found, most notably the reentrant condensation induced by the addition of higher-valent salts such as YCl_3 [1]. This reentrant condensation is characterised by different regimes defined by the protein volume fraction φ and salt concentration C: for low salt concentrations C<C* with a characteristic concentration C*(φ), the proteins are in solution, whilst for C*<C<C** with a second characteristic concentration C**(φ), a phase separation regime occurs, which re-enters into a solution regime for C>C** **(figure 1**).
Reentrant condensation has previously been observed for DNA or polyelectrolytes and a charge inversion theory has been proposed to explain the observations [2]. However, this phenomenon has never been directly observed in a protein system before. Monitoring the effect of the salt type and concentration on protein dynamics therefore promises a deeper understanding of both the salt-protein and protein-protein interactions, including phenomena such as the binding of salts, protein aggregation and re-dissolution. Protein aggregation is by itself a phenomenon which should to be explored for its dynamic aspects. Controlled aggregation, namely crystallisation, is still one of the 'holy grails' of protein science.

Here we review our first steps in this investigation of the static and dynamic aspects of proteins in aqueous solutions containing salts. These address the issues of crowding and of the effects of monovalent salts for the model protein Bovine Serum Albumin (BSA) [3], using a combination of small-angle X-ray scattering (SAXS), and the quasi-elastic neutron scattering (QENS) techniques backscattering (BS), and spin-echo (NSE). SAXS thereby accesses the static structure on protein-protein nearest neighbour distances, whereas BS and NSE provide information on different regimes of the protein diffusion on nanosecond time scales.

From SAXS data we find a qualitative change with rising protein concentration from an uncorrelated to a strongly correlated solution. For weaker charge screening (i.e. less salt) this correlation is found already for lower protein concentrations. We conclude that below a volume fraction of approximately 10% crowding is induced by unscreened charges. In this case the SAXS correlation peak disappears with the addition of NaCl due to the salt screening

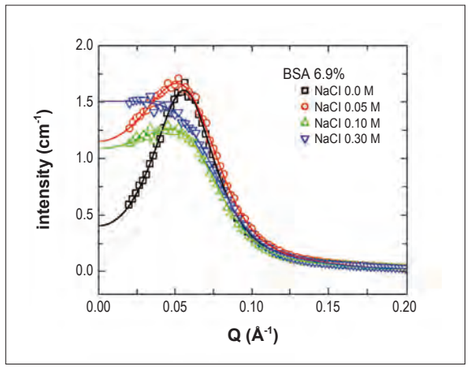

Figure 2: *Intensity data from SAXS measurements on aqueous BSA solutions (volume fraction 6.9%) for increasing NaCl concentrations.*

effect (**figure 2**), i.e. with increasing ionic strength the surface potential decays faster as a function of distance and reduces the long-ranged repulsion between protein molecules. By contrast, above that volume fraction, crowding is dominated by the excluded-volume contribution, and the SAXS correlation peak is conserved upon salt addition (data not shown). The conservation of the correlation peak also for higher salt concentrations implies the absence of aggregation in this highly concentrated protein solution.

Neutron backscattering and spin-echo probe different regimes of diffusion due to the different scattering vector ranges accessed by these techniques and different sensitivity to coherent and incoherent scattering. The scattering vectors accessed by spin-echo are approximately commensurate with those accessed by SAXS, whilst backscattering measures at larger vectors corresponding to intramolecular length scales. From the backscattering and spin-echo data we find a continuously changing behaviour of the self-diffusion of the proteins due to the excluded-volume effect.
The addition of salt has little or no effect on the apparent diffusion coefficients observed in backscattering (**figure 3a**), although charge screening is assumed to change both interaction time and coupling strength.
In contrast to backscattering data, we see an increase of diffusion upon addition of salt in neutron spin-echo data (**figure 3b**), whereas the dependence on protein concentration remains qualitatively the same, i.e., a decrease of apparent diffusion upon increasing protein concentration. In the protein concentration range thus far covered by our experiments, i.e. from approximately 4% to 27% volume fraction, our data are in agreement with a continuous decrease of the apparent diffusion constants with the protein concentration. In contrast to the static data, our dynamic data show no distinct value where crowding due to the excluded-volume contribution sets in.

Macromolecular crowding, caused by a variety of hydrodynamic and direct interactions, is an important feature of cellular environments and has to be studied in further detail. With our study we prepare the ground for future experiments using multivalent salts and the extension to other protein systems. In order to clarify the physical picture of protein solutions, the combination of different experimental techniques recording both static and dynamical information is required.

The X-ray and neutron data will be complemented by techniques such as dynamic light scattering provided by the ILL/ESRF through its newly established Partnership for Soft Condensed Matter (see p100).

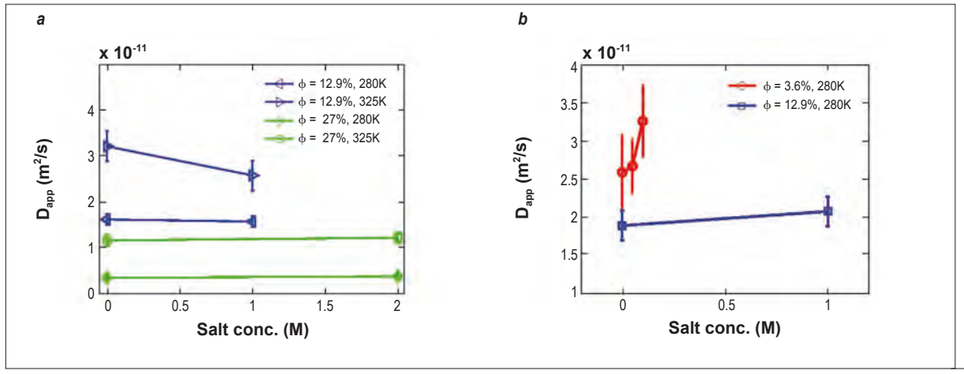

Figure 3: *Apparent diffusion constants versus molar NaCl concentration for different BSA volume fractions and temperatures.* ***(a)*** *Results from neutron backscattering.* ***(b)*** *Results from neutron spin-echo.*

REFERENCES

F. Zhang, M. Skoda, R. Jacobs, *et al.*, Physical Review Letters 101 (2008) 14 **[1]**
A. Y.Grosberg, T. T. Nguyen, B. I. Shklovskii, Rev. Modern Phys. 74 (2002) 329 **[2]**
F. Roosen-Runge, M. Hennig, T. Seydel, F. Zhang, *et al.*, BBA – Proteins and Proteomics 1804 (2010) 68 **[3]**

M.G. Ortore, **F. Spinozzi** and **P. Mariani**
(Università Politecnica delle Marche and CNISM, Ancona, Italy)
A. Paciaroni (University of Perugia and CNISM, Perugia, Italy)
L. R. S. Barbosa (University of Sao Paulo, Brazil)
J. Ollivier (ILL)
H. Amenitsch
(Institute of Biophysics and Nanosystems Research, Graz, Austria)
M. Steinhart
(Institute of Macromolecular Chemistry, Prague, Czech Republic)
D. Russo (CNR-INFM and CRS-SOFT, c/o ILL)

High pressure simultaneously modifies structural and dynamical properties of the lysozyme hydration shell

High pressure is a powerful, if still exotic parameter that can be used to elucidate the singular properties of proteins in solution, especially when non-denaturing conditions are achieved. Here, elastic and quasi-elastic neutron scattering results have been combined with a small-angle X-ray scattering (SAXS) study, to emphasize the pressure-induced changes on particle-particle interactions, low-resolution structure as well as overall and local dynamics of lysozyme in solution. Quite strikingly, significant structural and dynamical changes occur in the same pressure range, thus suggesting a strong correlation between hydration properties and protein mobility.

The pressure cell: *The high-pressure sample holder is made of an inox capillary enrolled into an anular. It has been tested to work up to 7 kbar; it was manufactured by Top Industry and designed by D. Russo.*

High-pressure effects on protein structure and dynamics are of major interest in biology, not only to account for the adaptation of living organisms to extreme environments, but also to understand how macromolecules behave under normal conditions [1]. Moderate pressures are particularly relevant since it is well known that proteins in solution are marginally stable under high temperature and pressure, and their catalytic efficiency may be reduced even at non-denaturing pressures. Owing to the present view of proteins as dynamic objects, the study of the pressure effects on the internal dynamics of proteins appears crucial [2].

Indeed for proteins in solution, several conformational states, which may differ in terms of partial molar volume and accommodate various internal motions to fulfil specific functions, may be present in dynamic equilibrium.

The solvent arrangement around a protein can greatly modify its stability. As unfolding processes for proteins in solution are induced by pressures larger than 2000 bar, non-denaturing pressures may modify the shape of the protein energy landscape, by altering the local curvature of the potential well minima or the height of the energy barriers between substates, they may also affect the properties of water at the protein surface. On the other hand, changes of dissipative forces of the solvent, induced by pressure, can strongly modify the fast structural fluctuations of proteins. One might therefore expect new insights into the relationship between the protein dynamics and the properties of the hydration shell to be obtained by perturbing the system with moderate pressures, and following the protein and solvent structural alterations together with protein thermal fluctuations [3]. In this study, small-angle X-ray and neutron scattering experiments have been combined to investigate the high-pressure-induced changes on particle-particle interactions, low-resolution structure and overall and local dynamics of lysozyme in deuterated aqueous solutions. In particular, the lysozyme concentration was 10 wt% and the pD of the solutions was adjusted to 7.5; pressures up to 2000 bar were applied.

High-pressure SAXS experiments, performed at the Elettra Synchrotron (Trieste, Italy), were analysed using SASMOL [3], an algorithm for calculation of hydrated protein form factors using atomic coordinates and solvation molecules as dummy atoms, whose positions are defined by burying the protein in a tetrahedral close-packed assembly of Gaussian spheres (**figure 1**). The results indicate that lysozyme maintains its globular structure up to 1500 bar, while the density of the hydration shell slightly increases as pressure increases, with a discontinuity between 600 and 1000 bar. In the same pressure range, the height and

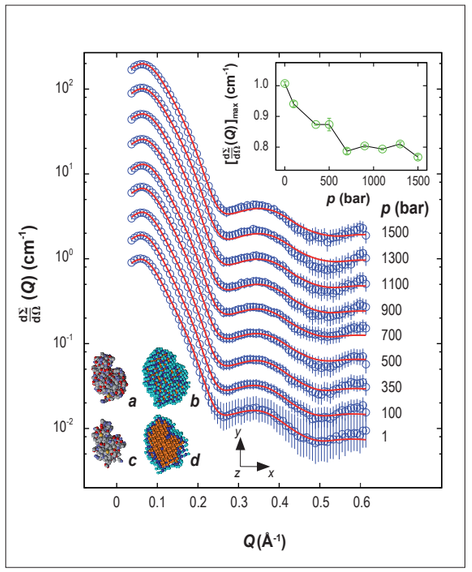

Figure 1: *Experimental SAXS curves obtained for lysozyme solution at increasing pressures at 20°C. Continuous lines represent the fitting curves. The inserted graph shows the pressure dependence of the intensity of the interaction peaks. The lysozyme atomic structure with the solvation dummy spheres found by SASMOL is also reported.* ***(a)*** *and* ***(c)****: Spacefill representation of the protein atoms.* ***(b)*** *and* ***(d)****: View of tetrahedral close-packed spheres assigned to the protein (orange), to the first (blue) and second (cyan) solvation shells. In (c) and (d) only spheres and atoms with coordinates z<0 are shown.*

position of the interference peak at small Q also show a discontinuity (**figure 1**). The fitting parameters indeed confirm that the interaction potential strongly changes at intermediate pressures.

The neutron scattering experiments were performed at ILL. Elastic incoherent neutron scattering experiments performed at the IN13 spectrometer show that the mean square displacement of the protons decreases as pressure increases even at 300 bar, and suggest a loss in protein mobility that may follow a change in the local energy landscape. A less-marked change in protein mobility is also observed between 700 and 1500 bar. Quasi-elastic neutron scattering experiments, performed at the IN5 spectrometer, show that the dynamic structure factor does not vary up to 1000 bar (**figure 2**), but above this value, the quasi-elastic signal progressively tails off, indicating a change in the diffusive properties of lysozyme. The complete reversibility of the pressure application/release procedure was checked by testing that the dynamic structure factor is the same before and after the high-pressure measurement.

The pressure dependence of the half-widths at half-maximum of the Lorentzian curves, which are related to internal diffusive and re-orientational motions, shows that above 1000 bar there is a modification of the side-chain dynamics at the surface of the protein. This change could be a consequence of new structural packing and dynamical properties of the first hydration layer, which can be related to a higher density of water clusters around the protein surface. This result is in full agreement with SAXS observations. Therefore, both global and local lysozyme dynamics change at the same threshold pressure, and a clear evolution of the internal protein dynamics from diffusing to more localised motions is proved. According to SAXS results, the new configuration of water in the first hydration layer induced by pressure may be at the origin of the observed local mobility changes.

The determination of a simultaneous structural and dynamical model of the changes occurring on a protein in solution under compression, but before unfolding, is the main result of this work. However, we want to emphasize that such a description was possible thanks to the high signal to noise ratio of the experimental data, due to the benefits of the large-scale facilities used.

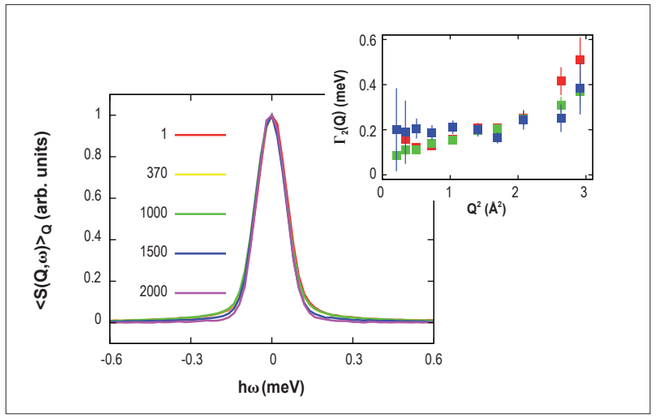

Figure 2: *Incoherent dynamic scattering functions averaged over all the investigated Q values and normalised to the peak height, plotted as a function of pressure at 20°C. The inserted graph shows the half-width at half-maximum for the Lorentzian functions related to lysozyme intrinsic dynamics, plotted for three pressure values according to the colour legend.*

REFERENCES

C. Balny, Biochimica et Biophysica Acta 1764 (2006) 632 **[1]**
W. Doster, R. Gebhardt, Chemical Physics 292 (2003) 383 **[2]**
M. G. Ortore, A. Paciaroni, F. Spinozzi, P. Mariani, H. Amenitsch, J. Ollivier, L. R. S. Barbosa, M. Steinhart and D. Russo, Journal of the Royal Society Interface 6 (2009) S619 **[3]**

AUTHORS

A. Fomin, S. Ivanov, E. Kolomensky, I. Krasnoshekova, A. Pirozhkov, A. Vasiliev and **A. Serebrov** (PNPI Gatchina, Russia)
N. Dovator and **S. Dmitriev** (IPTI St. Petersburg)
P. Geltenbort and **O. Zimmer** (ILL)

The ALPs in the focus of ultra-cold neutrons: search for a new fundamental force

Axion-like particles (ALPs) may induce a new fundamental force, which would affect the behaviour of particles with spin in the vicinity of non-magnetic bulk matter.
Depolarisation of trapped ultra-cold neutrons and Ramsey's resonance technique improve by several orders of magnitude previous constraints on the coupling strength of ALPs to ordinary matter.

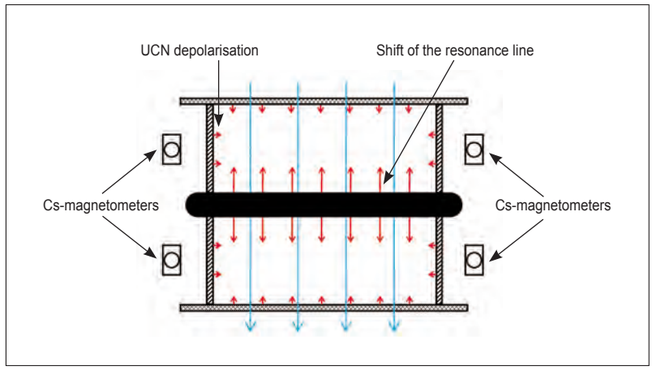

Figure 1: *Sketch of the double UCN storage chamber, equipped with a central heavy mirror to induce the sought effect due to ALPs. Blue arrows indicate a weak magnetic field applied to the chambers, red arrows show the direction of the pseudo-magnetic fields due to ALP exchange between the trap walls and the trapped neutrons.*

Axion-like particles are hypothetic light pseudo-scalar bosons, which would mediate a parity and time reversal violating interaction between massive fermions over a macroscopic distance. Still very little is known about such forces if their range λ lies within a so-called 'axion window' $2\,\mathrm{cm} \gtrsim \lambda \gtrsim 20\,\mu\mathrm{m}$, corresponding to masses $10\,\mu\mathrm{eV} \lesssim m_A \lesssim 10\,\mathrm{meV}$ of the exchanged boson.

For ranges outside this window, tight limits on the force strength were already derived from astrophysical and cosmological arguments, based on the observed neutrino signal from the supernova SN1987A and the possible role of ALPs as a dark matter component. It is therefore of high current interest to search for ALPs in laboratory experiments.

Provided the coupling of ALPs to ordinary matter is sufficiently strong, they would induce neutron spin-precession in the vicinity of non-magnetic matter. One can therefore say that a piece of matter creates a kind of 'pseudo-magnetic field' for a neutron acting as a probe. As is well known, one can detect tiny spin precessions with extreme sensitivity using Ramsey's resonance method for trapped ultra-cold neutrons (UCNs). Ongoing searches for a neutron electric dipole moment (EDM) and also a recent test of Lorentz invariance, described in another highlight in this annual report, employ this technique. In the search for ALPs we try to detect a precession effect induced by a neutron mirror made of a heavy material [1]. A more simple, and in the present stage, fully competitive method investigates depolarisation of trapped UCNs [2].

We have employed both methods in the present study, using an existing apparatus to search for the neutron EDM [3]. As shown in **figure 1** it comprises a double chamber for UCN storage. A heavy plate made from copper forms the central trap wall. It would induce a shift of the magnetic resonance [1], whereas the pseudo-magnetic fields of the (cylindrical) side walls of the traps would lead to UCN depolarisation [2]. The apparatus is presently installed at ILL's UCN facility PF2 and is pictured in **figure 2**.

We found a depolarisation of 13% during 100 s of UCN storage in the traps of the spectrometer. The corresponding probability of spin-flip per sidewall collision is 4.5×10^{-5}. Assuming magnetic impurities on the surface as most likely reason for depolarisation one can interpret the observed effect as a sensitivity limit on the coupling strength $g_S g_P$ of the hypothetic ALP-induced force (with g_S and g_P denoting scalar and pseudoscalar coupling constants of the ALP vertices to the nucleons between which it is exchanged). **Figure 3** shows as a function of λ a corresponding line, excluding with 95% confidence forces with stronger coupling strength.

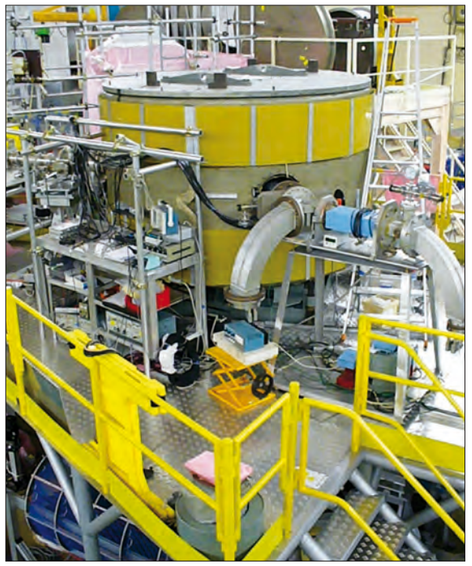

Figure 2: *Double-chamber EDM spectrometer installed at ILL's UCN facility PF2.*

In the search for the shift of magnetic resonance due to the pseudo-magnetic field of the central heavy mirror we changed the direction of the magnetic field applied to both chambers (blue arrows in **figure 1**), and measured for both field directions the neutron resonance frequency in each chamber. We also performed a test for systematic effects with a light central mirror made of aluminium instead of the heavy one made of copper. The strength of the magnetic field around the storage traps were controlled by means of 8 Cs-magnetometers. The difference of resonance shifts was (4.36 ± 5.14) rad, with the uncertainty being dominated by hysteresis effects of the magnetic screen of the spectrometer upon magnetic field reversal. The obtained limits are about the same as those from the depolarisation study and are also shown in **figure 3**.

Previous limits on $g_S g_P$ between nucleons within the axion window were obtained from an analysis of an experiment on gravitational quantum states of the neutron above a plane mirror [4].

This experiment was also performed at ILL's UCN facility PF2. Compared to those limits the present study has led to a considerable improvement, ranging up to 4 to 5 orders of magnitude for forces with $1\,\mathrm{cm} \gtrsim \lambda \gtrsim 1\,\mathrm{mm}$. Having however evaded detection so far, the ALPs still wait to be discovered in future experimental searches.

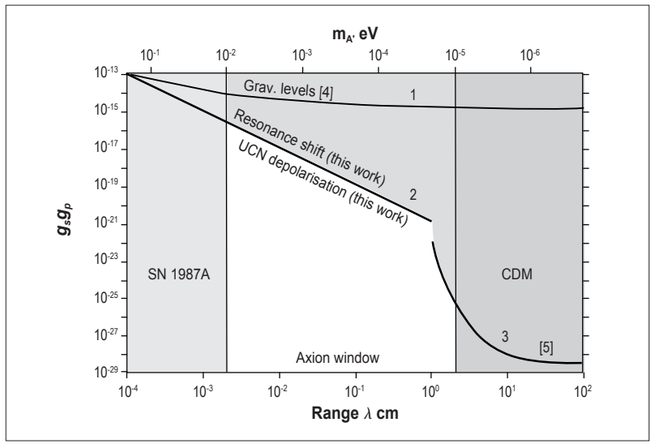

Figure 3: *Constraints on the product $g_S g_P$ of coupling constants of axion-like particles to nucleons, as a function of the range λ of the macroscopic force. The shaded areas to the left and the right are excluded due to astronomical observations, and limits due to laboratory experiments are shown as: line 1 - gravitational levels [4], lines 2 – this work, line 3 – ^{199}Hg/Cs precession frequency comparison [5].*

REFERENCES

O. Zimmer, arXiv:0810.3215v1, accepted for Phys. Lett. B **[1]**
A. Serebrov, Phys. Lett. B 680 (2009) 423 **[2]**
I.S. Altarev, Yu. Borisov, N.V. Borikova *et al*., Phys. At. Nucl. 59 (1996) 1152 **[3]**
S. Baeßler, V.V. Nesvizhevsky, K.V. Protasov, A. Yu. Voronin, Phys. Rev. D 75 (2007) 075006 **[4]**
A.N. Youdin, D. Krause Jr, K. Jagannathan *et al*., Phys. Rev. Lett. 77 (1996) 2170 **[5]**

G. Pignol, D. Rebreyend and **S. Roccia** (LPSC, UJF Grenoble 1, CNRS/IN2P3, INPG, Grenoble, France), on behalf of the experimental team

Is our world really isotropic?

Physics at the Planck scale could be revealed by looking for tiny violations of fundamental symmetries in low-energy experiments. A sensitive test of the isotropy of the Universe has been performed using stored Ultra Cold Neutrons to obtain the first limit on the coupling of a free neutron with a hypothetical cosmic axial field.

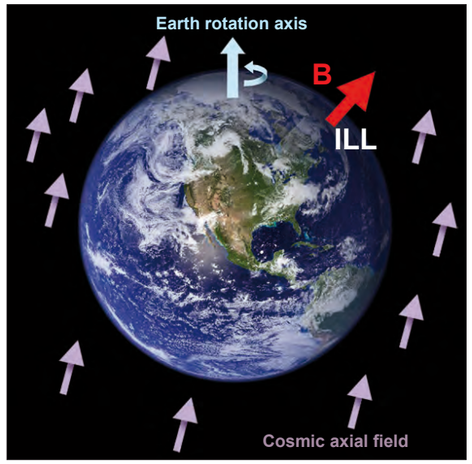

Figure 1: *The hypothetical cosmic axial field, defining a privileged direction in the Universe, is searched for in daily modulation of precision observables.*

The Standard Model (SM) of particle physics on one hand and the General Relativity theory of Einstein on the other are the two cornerstones on which our current understanding of the Universe relies. Although of seemingly irreconcilable natures, these two models are based on the common basic assumption that the laws of physics depend neither on the orientation nor on the velocity of the observer, i.e. are Lorentz invariant. Unification of the two models in a more general theory, bringing together the four known interactions in a consistent way, is one of the main challenges of contemporary physics.

Such a theory would certainly be less symmetric than the SM and, among the many directions that are being explored one of the most radical is to abandon Lorentz symmetry. Kostelecky has recently proposed a general framework to study such Lorentz violating (LV) effects [1], based on the idea that symmetry breaking at extremely high energies – far beyond the range experimentally accessible in the foreseeable future – could be tested via high precision low-energy experiments sensitive to tiny residual traces of symmetry breaking at high energy. One of those possible effects would be the existence of a constant cosmic axial field, filling the whole Universe and therefore defining a privileged direction (**figure 1**). The resulting anisotropy is, by definition, forbidden by Lorentz invariance.

Such a cosmic field would act as a magnetic field on particle spins. In the absence of any other field, spins would therefore precess at a rate proportional to its amplitude times a coupling constant, equivalent to the gyromagnetic factor. Measuring in a weak magnetic field the ratio of Larmor frequencies of two cohabiting species while the earth is rotating – the so-called clock comparison experiments – provides a very sensitive way to test the existence of this hypothetical cosmic field. First, due to the earth's rotation, a constant field would induce a field oscillating at the sidereal period in a terrestrial experiment. Looking for a daily modulation in the ratio of frequencies increases enormously the sensitivity of the measurement as compared to looking for a constant shift. Second, the use of two species can be applied to disentangle the modulation due to the cosmic field from the unavoidable fluctuations of the magnetic field itself.

Clock comparison experiments using two atomic species have already put severe constraints on the existence of such a cosmic axial field. In the present work, we have performed the first measurement using the combination free neutrons/mercury atoms.

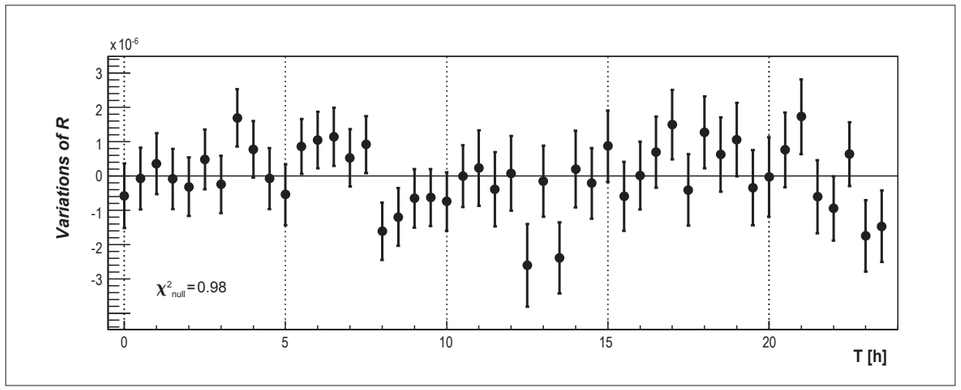

Figure 2: *Variation of the ratio R around its average after the data have been folded modulo 24 hours and binned every half hour. No daily modulation is observed.*

We used the high sensitivity RAL/Sussex/ILL spectrometer, originally designed to search for the neutron electric dipole moment [2]. As a unique feature of this apparatus, a mercury comagnetometer is used to measure the magnetic field. Based on a four-layer mu-metal shield and a set of current-stabilised coils, a constant and homogeneous magnetic field permeates a storage chamber of about 20 litres. The neutron precession frequency is extracted using the well-known Ramsey method of separated oscillating fields while the mercury precession frequency is optically analysed.

Using data collected over a dedicated week at the ILL PF2 Ultra Cold Neutron source, an upper limit of 0.8×10^{-6} on the amplitude of a daily modulation of the neutron/mercury frequency ratio R has been obtained (**figure 2**). Knowing that the coupling of the mercury with a cosmic field has already been constrained to a higher precision, this upper bound directly translates into a limit on the coupling with the free neutron [3]. In terms of energy, this implies that the daily oscillation of the Zeeman splitting – if any – must be less than 2×10^{-20} eV. Equivalently, if the neutron would only see a cosmic field at this level, it would take three full days – assuming it forgets to decay – to make one turn.

This result is the first limit obtained on the coupling of a free neutron with a hypothetical cosmic field. Moreover, it improves by more than one order of magnitude the limit for a free proton. Combined with other existing limits, this puts stringent constraints on the possible existence of such a field. More generally, despite the impressive precision of a wide range of experiments aiming at observing LV processes, not the faintest evidence has been obtained so far.

Our Universe certainly dislikes anisotropy!

REFERENCES

http://nedm.web.psi.ch/

http://www.neutronedm.org/

D. Colladay and V. A. Kostelecky, Phys. Rev. D 55 (1997) 6760 **[1]**

C. A. Baker *et al.*, Phys. Rev. Lett. 97 (2006) 131801 **[2]**

I. Altarev *et al.*, Phys. Rev. Lett. 103 (2009) 081602 **[3]**

AUTHORS

N. Malikova, **S. Longeville** and **J.-M. Zanotti** (LLB, UMR CEA-CNRS 12, CEA Saclay, France)
E. Dubois, **V. Marry** and **P. Turq** (UMR-UPMC-CNRS-ESPCI 7195, Université Pierre et Marie Curie, Paris, France)
J. Ollivier (ILL)

Signature of low-dimensional diffusion in complex systems

Dimensionality is an essential characteristic of diffusion under confinement, resulting from the local geometry of the confining matrix and the diffusion mechanism. We present a novel analysis of neutron scattering signals, which enables the determination of the diffusion dimensionality for the difficult case of powder matrices (encountered in many areas, from catalysis to hydrogen storage materials). Our analysis relies on data at several experimental resolutions and focuses on the detection of a divergence in the measured signal.

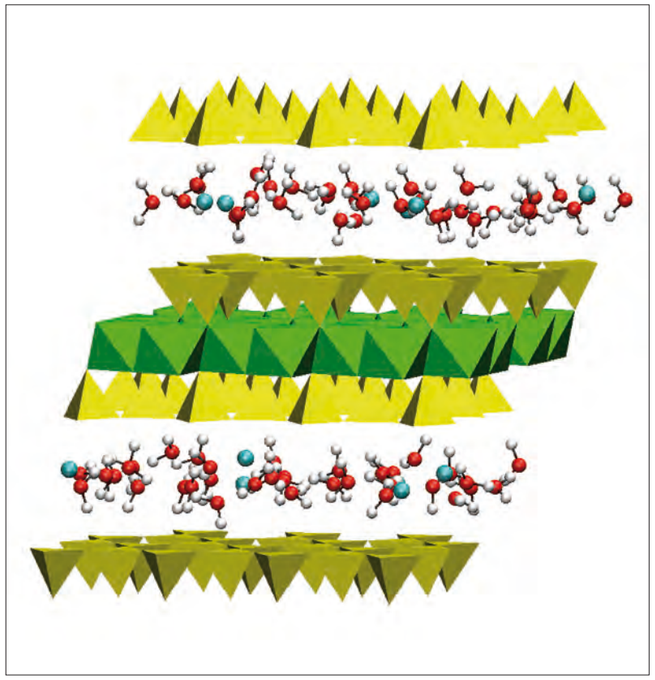

Figure 1: *Planar confinement in a clay. Regular stacks of negatively charged alumino-silicate layers (each formed of octahedral (green) and tetrahedral (yellow) sheets) accommodate mobile compensating cations (blue) and water molecules (red and white) in between.*

Studying the diffusion of guest atoms or molecules inside porous networks within solid matrices is crucial for a number of areas such as catalysis, the development of hydrogen storage materials or electrolytes for fuel cells, and in environmental science (for example soil permeability). Our work focuses on lifting the limitations of 'powder-averaging' of the signal detected from diffusing atoms, which blurs the signature of low-dimensional diffusion. This is highly relevant as matrices usually come as a powder to increase the surface area accessible for guest incorporation.

Neutron scattering has contributed greatly to the study of diffusion in many systems due to its exceptional sensitivity to the H atom, in comparison to all the commonly encountered heavier elements. In the above systems, H atoms are part of the diffusing guest molecules (water or small organic species) and at the same time are absent (or almost) in the structure of the host matrices (carbon, oxides of aluminium or silicon). The sensitivity of neutrons to H atoms concerns the incoherent part of the scattering which tells us about the individual atomic motion.

The scattering function, $S(Q,\omega)$, measured at a wave-vector Q (defining a spatial scale and a direction along which motion is probed) is simply the number of neutrons detected as a function of the energy transfer ω they have undergone while interacting with the atoms in the sample. For an atom diffusing along the direction of Q with a diffusion coefficient D, $S(Q,\omega)$ is centred on $\omega=0$ with a finite broadening in ω (a Lorentzian broadening of DQ^2, with $Q=|Q|$). How do we detect the difference between diffusion in one, two or three dimensions (1D, 2D, 3D respectively)? Contrary to 3D, for diffusion in lower dimensions we can detect one or more directions, or orientations of the Q vector, for which the diffusing atom is seen to be immobile. In this case the scattering leads to no energy transfer and $S(Q,\omega)$ is a delta function at $\omega=0$ (zero energy transfer).

In other words, a divergence of the signal at $\omega=0$ occurs and it is a good indication of low-dimensional diffusion, as it is not present in the 3D case. However, both the presence of a powder matrix and a finite experimental resolution mask this divergence. As we show later on, it is nevertheless possible to detect it.

Consider two experimental systems with H atoms diffusing in 3D (bulk water) and in 2D inside a powder matrix. For the latter we use water confined in a powder of synthetic hectorite clay. Each grain of the clay powder is a highly regular stack of crystalline aluminosilicate layers, between which water molecules are confined to a planar geometry (**figure 1**) [1]. The theoretical scattering function for such a system, measured along any direction, contains a broadened component due to some mobile water molecules (the broadening is no longer a simple function of D and Q due to the powder averaging of 2D diffusion) but it also retains the divergence of the signal at $\omega=0$, as for any direction there are some grains with layers oriented at 90 degrees. The experimental scattering function does not feature the divergence itself, while it is smeared out by the resolution function. We detect only a finite increase in scattered intensity at $\omega=0$. However, as we improve the resolution, we can slowly approach this divergence [2]. In **figure 2** we plot a quantity, $S^M(Q,0)$, characterising the shape of the measured scattering function (a product of its broadening and its maximum value) versus a parameter representing an increasing experimental resolution, α [3]. For poor (low) experimental resolution, the difference between the shapes of the scattering functions for a powder-averaged 2D motion and 3D motion is indistinguishable. For good (high) resolution, $S^M(Q,0)$ for 3D motion reaches an asymptotic limit of 1, while for a powder-averaged 2D motion, we see the approach to the divergence, which would be reached for an infinitesimally narrow resolution, i.e. $\alpha=1$. Due to the dimensionless nature of both $S^M(Q,0)$ and α, the curves in **figure 2** represent master curves for 3D and powder averaged 2D motion. In other words, they are independent of the actual diffusion coefficient, D, of water molecules in either system used, as well as independent of the value of Q at which the scattering functions were measured. Their shapes depend solely on the dimensionality of the motion in the system and the shape of the resolution broadening.

This simultaneous test at multiple experimental resolutions provides an unambiguous piece of evidence for low-dimensional diffusion even inside a powder matrix.

The test was made possible due to the high flexibility of the disk-chopper spectrometer IN5, which gives access to a wide range of energy resolutions, from a few to several hundreds of μeV.

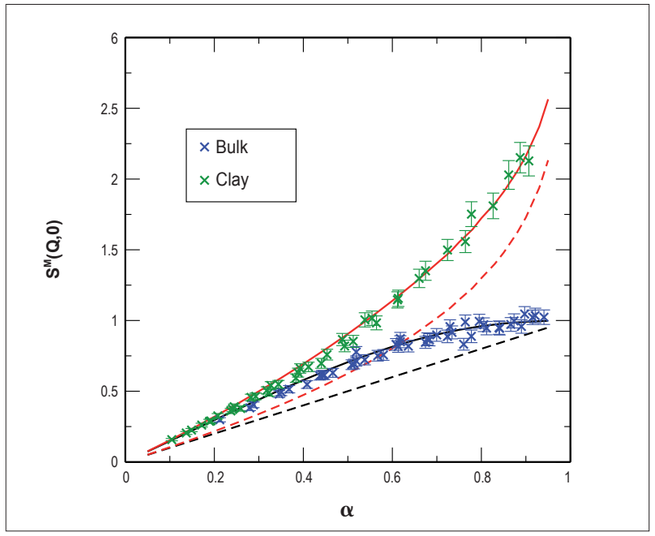

Figure 2: *Signature of 2D diffusion inside a powder matrix. $S^M(Q,0)$, a parameter reflecting the shape of the scattering function ($=S(Q,0)\pi DQ^2$) versus a measure of increasing experimental resolution, α ($=DQ^2/(DQ^2+H)$, with H the resolution broadening). Curves: master curves for powder-averaged 2D motion (red) and 3D motion (black). Full curves correspond to Gaussian resolution broadening, dashed curves to Lorentzian resolution broadening. Data points: experimental data for water confined in a hectorite clay (green) and for bulk water (blue).*

REFERENCES

N. Malikova, A. Cadène, E. Dubois, S. Durand-Vidal, V. Marry, P. Turq, J. Breu, S. Longeville and J.-M. Zanotti, J. Phys. Chem C 111 (2007) 17603-17611 **[1]**
R. E. Lechner, Solid State Ionics 77 (1995) 280 **[2]**
N. Malikova, S. Longeville, J.-M. Zanotti, E. Dubois, V. Marry, P. Turq and J. Ollivier, Phys. Rev. Lett. 101 (2008) 265901 **[3]**

AUTHORS

A.J. Horsewill and **K. Panesar** (University of Nottingham, UK)
S. Rols and **M.R. Johnson** (ILL)
M.H. Levitt, **M. Carravetta**, **A. Danquigny**, **M.C. Grossel** and **S. Maltsev** (University of Southampton, UK)

The quantum dynamics of H_2 molecules trapped inside fullerene cages

The wave-like nature of the hydrogen molecule is revealed in neutron scattering experiments on the quantum dynamics of endofullerenes. These are remarkable novel complexes in which a hydrogen molecule is permanently trapped inside the cage of a fullerene molecule. The system is strongly quantum mechanical: spectra recorded on the IN4 time-of-flight spectrometer reveal that all degrees of freedom of the hydrogen molecule are quantised. Furthermore, the Pauli Exclusion Principle is pivotal in determining the distinctive thermodynamic properties of the system.

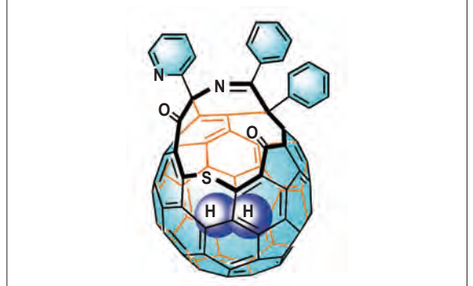

Figure 1: *Azacyclic-thiacyclic open cage fullerene (ATOCF) contains a 13-membered opening through which H_2 has been introduced resulting in the endohedral 1:1 complex H_2@ATOCF.*

At the heart of quantum mechanics is the concept of a particle confined to a small region of space by a steep potential energy surface. A practical realisation of an entrapped hydrogen molecule has become possible using 'molecular surgery', a novel technique in synthetic chemistry. Using a series of reactions an orifice in a C60 molecule is opened and chemically stabilised, whereupon under high temperature and pressure a hydrogen molecule is inserted through the orifice into the fullerene cage. Further reactions subsequently close the opening, permanently trapping the hydrogen molecule inside [1,2]. The fullerene host can be functionalised by design, enabling the quantum dynamical properties of the hydrogen molecule to be investigated as a function of the potential energy surface defined by the interactions with the cage walls. Investigations – using the time-of-flight spectrometer IN4 - have been conducted on hydrogen inside C60, (H_2@C60), the isotopomer HD@C60 and H_2@ATOCF. The latter is an open cage fullerene (**figure 1**) and the spectra were recorded on a 495 mg sample containing just 0.46 mmol H_2 [3].

A strong quantum mechanical signature of the H_2 molecule arises from the Pauli Exclusion Principle. Spatial and nuclear spin degrees of freedom are entangled since the molecular wavefunction must be antisymmetric under exchange of identical fermions. Consequently, two nuclear spin-symmetry species are identified: orthohydrogen has total nuclear spin $I = 1$ and odd rotational quantum numbers, J; parahydrogen has total nuclear spin zero and even J. To interconvert orthohydrogen and parahydrogen requires a nuclear spin flip; this means a transition between the two species is strongly forbidden unless a magnetic interaction with a third party is involved. Since the interaction that mediates the scattering event involves spin, inelastic neutron scattering (INS) can directly drive orthohydrogen-parahydrogen transitions, revealing peaks that are totally absent in photon spectroscopy.

IN4 spectra of H_2@ATOCF are shown in **figure 2** [3]. The two spin-symmetry species are completely decoupled and orthohydrogen is metastable at low temperature. Only upon arrival of a neutron with spin ½ is orthohydrogen converted to the energetically more stable parahydrogen. This is the origin of the single peak in neutron energy gain at 2.5 K which is the lowest energy component of a rotational triplet ($J = 1$: $m_J = 0, \pm 1$). The triplet splitting arises from the anisotropy of the fullerene cage potential. All members of this triplet are observed in the neutron energy loss spectrum centred on $\Delta E = 14.7$ meV, depicting the reverse process converting parahydrogen into orthohydrogen. With increasing temperature, **figure 2**, all three members of the triplet are revealed in neutron energy gain as the components of orthohydrogen's rotational manifold become thermally populated.

As a result of the close confinement, translational energy of H_2 is also quantised; this motion is sometimes referred to as 'quantum rattling'. In H_2@ATOCF, due to the cage anisotropy, translational energy is different in each of three dimensions and there are three members of the translational manifold. Two of these are revealed in a doublet centred on 17.5 meV in neutron energy loss (**figure 2**); the third is observed at 30 meV. An analysis of the momentum transfer dependence of the INS spectra also provides information on the physical dimension of the entrapped molecule and its spatial confinement. Therefore INS spectra recorded as a function of energy and momentum provide quantitative insight into the dynamical wavefunctions of H_2.

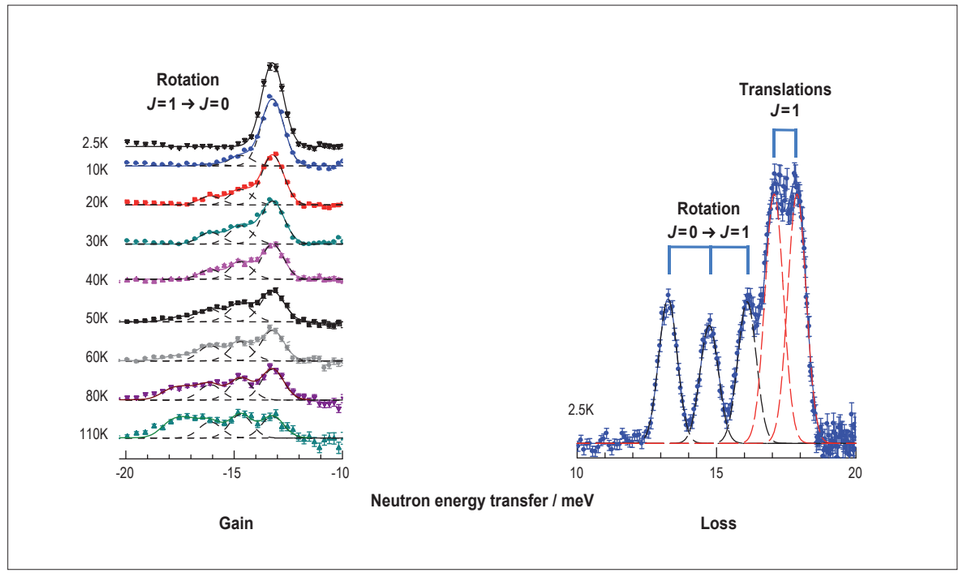

Figure 2: *: INS spectrum of H_2@ATOCF showing rotational transitions converting parahydrogen ($J = 0$) and orthohydrogen ($J = 1$). In neutron energy gain the spectrum is of orthohydrogen which is metastable because of the inefficiency of orthohydrogen-parahydrogen conversion. However, the sub-states of orthohydrogen are in equilibrium internally, as revealed in the temperature dependence of the amplitudes of the rotational triplet in neutron energy gain. Two of the three translational modes are also identified in this spectrum.*

Endohedral H_2-fullerene complexes are superb model systems for understanding quantum molecular dynamics. The IN4 spectra have enabled a full determination of the low-lying energy states of the entrapped H_2 molecule and provide quantitative insight into the potential energy surface that is determined by the non-bonding interactions with the cage. A complete picture is emerging, including the role of the potential in coupling translation and rotation.

This INS investigation complements and informs NMR experiments where the nuclear magnetic properties of endofullerenes are exploited as 'cryorelaxors' and in realising protocols for nuclear polarisation enhancement.

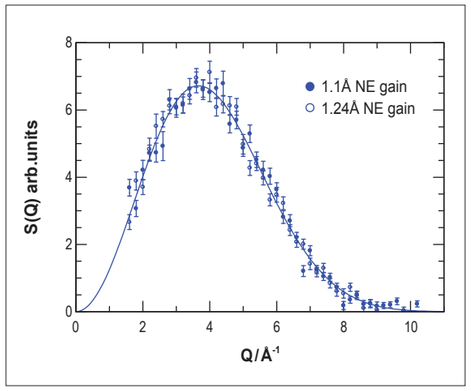

Figure 3: *H_2@ATOCF: The momentum dependence S(Q) provides quantitative insight into the molecular wavefunctions of H_2.*

REFERENCES

Y. Rubin *et al*, Angew. Chem. Int. Ed 40 (2001) 1543 **[1]**
K. Komatsu, M. Murata and Y. Murata, Science 307 (2005) 238 **[2]**
A.J. Horsewill *et al*, Phys. Rev. Lett 102 (2009) 013001 **[3]**

AUTHORS

R. S. Whitney (ILL)
P. Marconcini and **M. Macucci** (University of Pisa, Italy)

Quantum interference pierces opacity

Interference is one of the fundamental differences between quantum mechanics and Newtonian mechanics. All waves interfere if their coherence is maintained, and this leads to a huge variety of quantum effects which have no analogue in Newton's laws. Here we show theoretically that constructive interference can enable a wave to pass easily through a highly opaque barrier. It simply requires enclosing the barrier in a box with two openings. The box can be of any shape so long as it is mirror-symmetric about the axis of the barrier.

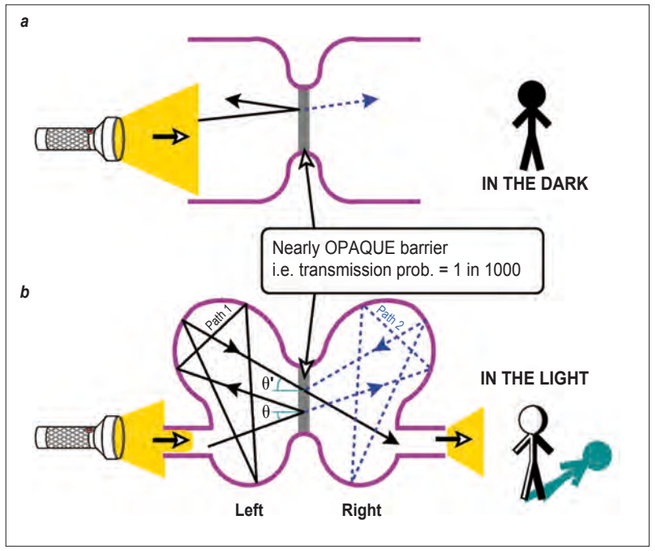

Figure 1: *A sketch of how constructive interference helps a wave pass through a highly opaque barrier inside a box which has left-right mirror-symmetry.*
In ***(a)*** *there is no constructive interference; the light hits the barrier once. Then only 0.1% of the light passes through the barrier to illuminate the object (indicated by the 'man').*
In ***(b)*** *we place a box around the barrier, then only a part of the light enters the box. However quantum interference means that as much as 25% of the light entering the box ends up illuminating the object. The effect should work with any wave, be it light (as sketched here), electrons (as considered in Ref. [1]) or perhaps neutrons.*

We have recently shown how interference can hugely enhance quantum tunnelling through a highly opaque barrier [1]. We consider a barrier placed in the centre of a box. The box can be almost any shape, so long as it is mirror-symmetric (for example the butterfly-shaped box in **figure 1** or the stadium-shaped box in **figure 2**). We ask if a beam of particles entering through the hole on the left, will result in particles exiting through the hole on the right. If the barrier is highly opaque then one would say that almost none of the particles injected into the box would pass though the barrier to exit through the hole on the right. Thus we were shocked to discover that a *quarter* of the particles can actually exit through the hole on the right, independent of how opaque the barrier is (so long as it is not completely opaque).

This remarkable fact can be understood by using a ray-optics argument. If the box is much bigger than the wavelength, λ, then rays (wave-packets) follow straight-lines and reflect specularly at the boundaries of the box. However as they travel through the box they acquire a phase $\Phi = kl$ where l is the length of the path, and $k=2\pi/\lambda$ is the wavenumber.

For simplicity let us assume that there are only two paths for wave-packets through the box (instead of an infinite number of different paths) and that they are those shown in **figure 1b**. Path 1 does not tunnel the first time it hits the barrier, but does tunnel the second time it hits it.
Path 2 tunnels the first time it hits the barrier, but not the second time. Quantum mechanics gives the probability to go from the left lead to the right lead as $|r(\theta)\ t(\theta')\exp[ikl_1] + t(\theta)\ r(\theta')\exp[ikl_2]|^2$, where the scattering matrix of the tunnel barrier has amplitudes $r(\theta)$ and $t(\theta)$ for reflection and transmission at angle θ. If there is no correlation between the lengths of the two paths (l_1 and l_2), then the cross-term cancels upon averaging over energy (averaging over small variations in k), leaving the probability as $|r(\theta)\ t(\theta')|^2 + |t(\theta)\ r(\theta')|^2$. In contrast, if there is a perfect mirror symmetry, then one has $l_1=l_2$ and the probability is $|r(\theta)\ t(\theta')+ t(\theta)\ r(\theta')|^2$, which is significantly larger. Indeed, if we could drop the θ-dependence of $r(\theta)$and $t(\theta)$, the probability would be doubled by the constructive interference induced by the mirror symmetry.

Now consider a path that hits the barrier n+1 times, it will have 2^n partners with exactly the same phase (each path segment that begins and ends on the barrier can be reflected with respect to the barrier axis). Thus one might guess that the probability to exit on the right is enhanced by 2^n. This is a little too naive; we must include the phase acquired by transmitting or reflecting at the barrier. Then we see that not all path-pairs interfere constructively and the enhancement of tunnelling is much less than 2^n. None the less, the enhancement is such that under the right circumstances, as much as a quarter of the particles can exit to the right even if the transmission through the barrier is tiny (say 1 in 1000).

This effect is a cousin of a number of known interference effects; resonant tunnelling, Fabry-Perot interference, or reflectionless tunnelling into a superconductor. However in all cases there are significant differences which make our effect unique [1,2]. It is also remarkable that new interference effects are being discovered despite so many years of work on quantum mechanics, and other wave mechanics (such as optics).

One possible application of this effect would involve the transmission of electrons through a double quantum-dot (a dot divided in two by a barrier across the middle). There the big experimental challenge is to make two quantum dots which are the mirror image of each other. The huge enhancement of tunnelling through a barrier only occurs when the mirror-symmetry is respected up to the scale of about 1/10 of a wavelength, i.e. about 5nm in dots made using GaAs 2DEGs. **Figure 2** shows numerical simulation of conductance (proportional to the transmission probability). Conductances up to 25% of full transmission are observed. The horizontal dashed blue line indicates the transmission of the barrier itself, G_{tb}. For large asymmetries (**figure 2a**) the transmission is less than that of the barrier alone. However, for perfect symmetry the interference enhances tunnelling by more than an order of magnitude larger. For charged-particles (like electrons), this enhancement is destroyed by a tiny magnetic flux. This means that the conductance of the double quantum-dot could change by a huge factor with application of less than a quantum of flux (**figure 2b**). This should enable one to make a magnetic field detector with a similar sensitivity to a SQUID.

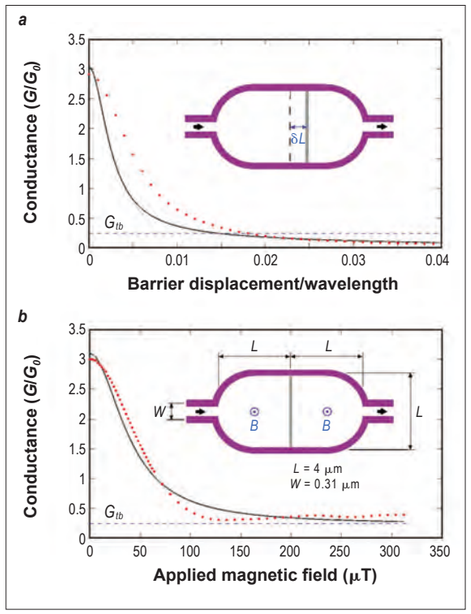

Figure 2: *Average conductance as* ***(a)*** *a function of the barrier position, and as* ***(b)*** *a function of applied B-field. In the former the mirror-symmetry is broken because the barrier is no longer central, in the latter it is broken by the B-field. The curves comes from the semiclassical theory, the data points come from numerical simulations performed for each structure. The conductance of the tunnel barrier alone is G_{tb}. In this geometry full transmission corresponds to G/G_0=12. Data taken from Ref. [1].*

REFERENCES

R. S. Whitney, P. Marconcini, M. Macucci, Phys. Rev. Lett. 102 (2009) 186802 **[1]**
R. S. Whitney, P. Marconcini, M. Macucci, *in preparation* **[2]**

M. Civelli (ILL)

Evolution of the dynamical pairing across the phase diagram of a strongly correlated high-temperature superconductor

According to most experimental results and theories on cuprate-based high-temperature superconductors, the physical properties of these materials (**figure 1**) are strongly unconventional at low doping (in the pseudogap phase) and more conventional at high doping (in the Fermi liquid phase).
Our study shows that this general rule is not respected by the Cooper pairing mechanism, which is at the root of the superconducting state.

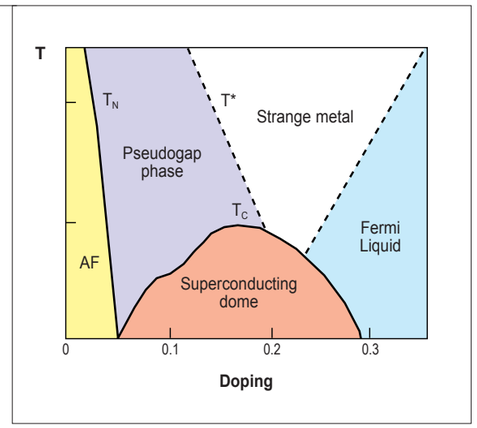

Figure 1: *High-temperature cuprate superconductors phase diagram.*

Over twenty years have passed since the discovery of superconductivity at unprecedented temperatures in layered cuprates, yet a full understanding of the mechanism of the effect remains elusive. Neutron scattering plays a key role in exploring the significance of magnetic correlations in the coupling mechanism for the Copper pairs. However, complementary experimental methods and theory are required for a complete examination of the underlying physics. Here we study the mechanism of superconductivity in the Hubbard model [1], employing Cellular Dynamical Mean Field theory [2] to extract the frequency-dependent Cooper pairing function. Our results show that the pairing function is unconventional at high doping, while it assumes a more standard form at low doping. The crossover between these two different regimes takes place at optimal doping, where the critical temperature is maximal. We relate these findings to the appearance of a pseudo-gap in the one-particle spectral function. Finally we show how these properties can be measured by scanning tunnelling spectroscopy experiments (STM).

Before presenting our results, it is useful to recall that in the standard theory of superconductivity [3] the Cooper pairing function Δ is time-dependent with real and imaginary parts. Its form is better described in Fourier frequency space, where $\Delta(\omega)$ has a characteristic shape, which in the following we describe in detail.

In a conventional superconductor the electron pairing is mediated by the lattice vibrations, which are described as phonons, i.e. bosonic particles. The boson exchange between pairing electrons resonates as $\omega \to \omega_0$, which is a characteristic frequency of the phonon energy-distribution. This fact is made evident by a hump in $\mathrm{Re}\Delta(\omega)$ (black line in **figure 2a**). For $\omega > \omega_0$ (the characteristic boson frequency) however a real boson can be emitted; this is marked by $\mathrm{Re}\Delta(\omega)$ changing sign and by $\mathrm{Im}\Delta(\omega)$ acquiring a peak (red line in **figure 2a**). This peak occurs at a frequency $\Omega \sim \omega_0 + \Delta(\omega=0)$, $\Delta(\omega=0)$ being the superconducting gap.

In the over-doped (OD) region (**figure 2b**), $\mathrm{Im}\Delta(\omega)$ for our high-temperature superconductor shows a long positive tail extending to $\omega \sim 2t$, of the order of the bandwidth reduced by the strong interaction (the bare bandwidth is 8t in our model, where t is the orbital hopping integral). In the standard theory, $\mathrm{Im}\Delta(\omega)$ typically shows only one or a few peaks, corresponding to well defined characteristic boson-frequencies. Therefore the superconducting pairing we find in the OD region is rather unconventional. Around optimal doping δ_{opt} (**figure 2c**) the long tail of $\mathrm{Im}\Delta(\omega)$ reduces strongly. In the under-doped (UD) region (figure 2d), the tail disappears, and $\Delta(\omega)$ assumes a more standard form.

We now link the doping-dependent evolution of $\Delta(\omega)$ with the relevant energy-scales of the system. In the standard theory of superconductivity there is only one such scale, the superconducting gap Δ_{sc}, proportional to ω_0.

In our results, however, there are two relevant energy-scales. The first is also directly related to Δ_{sc} and represents the superconducting gap which can be measured close to 'nodal' points of momentum space $k_{nod} \sim (\pi/2, \pi/2)$ (for example by photo-emission).

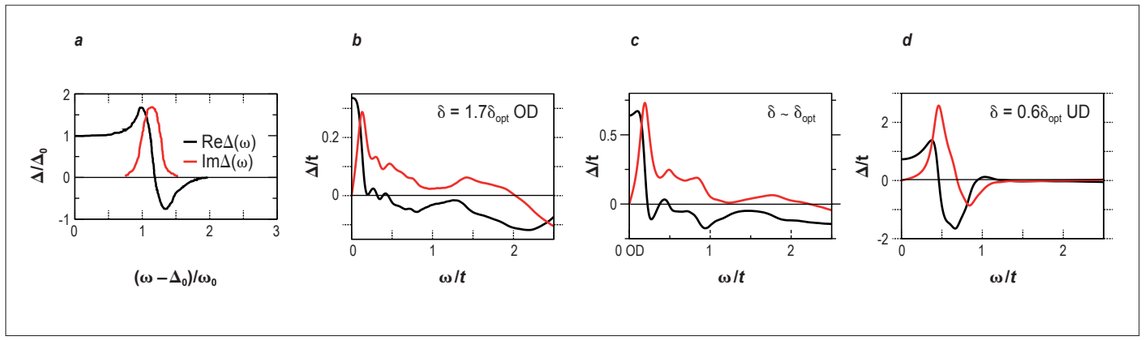

Figure 2: *The frequency-dependence of the pairing function in a standard superconductor **(a)**. The pairing function of our unconventional superconductor in the over-doped side **(b)**, at optimal doping **(c)** and in the under-doped side **(d)** of the phase diagram.*

Its behaviour is non-monotonic with doping δ (**figure 3a**). The second energy scale is connected with the pseudo-gap Δ_{pg} observed in the normal state, and it is monotonic with δ (**figure 3a**).

We also plot the total gap $\Delta_{tot} = (\Delta^2_{sc} + \Delta^2_{pg})^{1/2}$, which is measured close to the 'anti-nodal' points $k_{anod} \sim (\pi, 0)$ and $(0, \pi)$. To clarify whether $\Delta(\omega)$ can be related to any of these gaps, we estimate its characteristic frequency $\omega_0 \sim \Omega - \Delta_{tot}(k_{anod})$ (at $\omega = \Omega$ we locate the first maximum of $\mathrm{Im}\Delta(\omega)$ in **figures 2b**,**c**,**d**) and plot it as a function of doping. We find that ω_0 follows the behaviour of the pseudo-gap Δ_{pg} rather than the superconducting gap Δ_{sc}. Coming from the OD region, ω_0 is roughly constant, just as $\Delta_{pg} = 0$, while Δ_{sc} increases. In the UD region, ω_0 monotonically increases as doping reduces; it follows the rise of Δ_{pg} rather than the fall of Δ_{sc}, in spite of the more standard form of $\Delta(\omega)$.

Finally we show that these findings can be observed in experiments. In a standard superconductor it is possible to relate the behaviour of $\Delta(\omega)$ to STM measurements [4] of the ratio N_T, between the superconducting and normal-state tunnelling conductances $dI(\omega)/dV$, obtained under the same conditions:

$$N_T(\omega) = \frac{dI(\omega)/dV|_{sc}}{dI(\omega)/dV|_{nor}} = \frac{N_{sc}(\omega)}{N_{nor}(\omega)} \approx$$

$$N_T^{simp.}(\omega) = 1 + \frac{1}{4\omega^2}\left[\mathrm{Re}\Delta(\omega)^2 - \mathrm{Im}\Delta(\omega)^2\right]$$

where $N_{sc[nor]}(\omega) = (1/\pi)\Sigma_k \, \mathrm{Im}G(k,\omega)$ is the superconducting [normal-state] local density of states. $N_T^{simp.}$ is the simplest approximate form of N_T for a d-wave superconductor, which is an explicit function of $\Delta(\omega)$. Its behaviour is shown in **figure 3b**. The sharp drop below unity (due to the fact that $\mathrm{Re}\Delta(\omega) \to 0$ and $\mathrm{Im}\Delta(\omega)$ acquires a maximum (**figure 2**)) marks the presence of the boson (at $\omega = \Omega$, vertical-up and horizontal arrows in **figure 3b**).

We can clearly observe the sudden increase of Ω in passing from the OD region to the UD region, mainly due to the increase of ω_0, as portrayed in **figure 3a**. The approximations used to extract $N_T^{simp.}$ no longer hold in the real-case situation, where the momentum dependence of the band cannot be neglected and $N_{sc[nor]}(\omega)$ is strongly ω-dependent. We have however performed a full momentum-energy-dependent calculation in Ref. [1] and we have found that the features of $N_T^{simp.}$ are still present, showing that it should be possible to observe them in experiments.

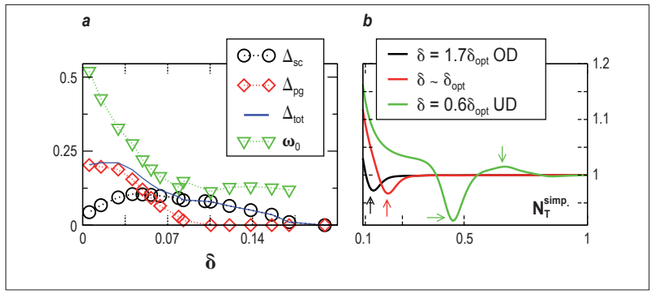

Figure 3: *Doping-dependence of the relevant energy scales **(a)**. Predicted tunnelling-conductance-ratio in STM experiments **(b)**.*

REFERENCES

M. Civelli, Phys. Rev. Lett. 103 (2009) 136402 **[1]**
See e.g.: G. Kotliar, S. Y. Savrasov, K. Haule, V. S. Oudovenko, O. Parcollet and C. A. Marianetti, Rev. Mod. Phys. 78 (2006) 865 **[2]**
J. Bardeen, L.N. Cooper and J.R. Schrieffer, Phys. Rev. 106 (1957) 162 **[3]**
See e.g.: D.J. Scalapino, in *Superconductivity*, edited by R.D. Parks (Marcel Dekker) (1969) 449 **[4]**

J. Ollivier and **H. Mutka** (ILL)

One year of experiments for the rejuvenated time-of-flight spectrometer IN5

Since the commissioning of the fully rebuilt IN5, this highly efficient time-of-flight spectrometer has now been producing data for more than one year. We highlight in this article some of the first remarkable experiments that have been made possible thanks to the large position sensitive detectors (PSDs) in the vacuum time-of-flight chamber of the secondary spectrometer.

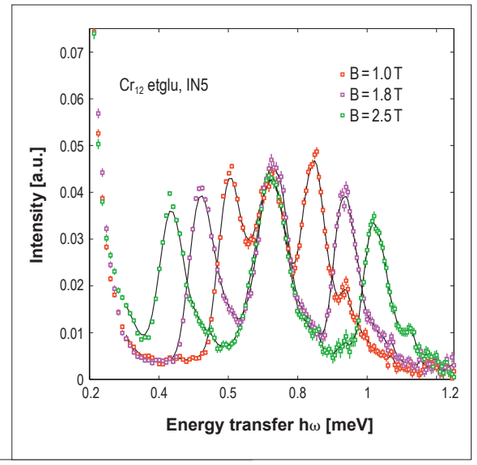

Figure 1: *Lifting of the degeneracy of the Cr_{12}-etglu molecular magnet triplet under a magnetic field (image courtesy of M. Baker, ILL).*

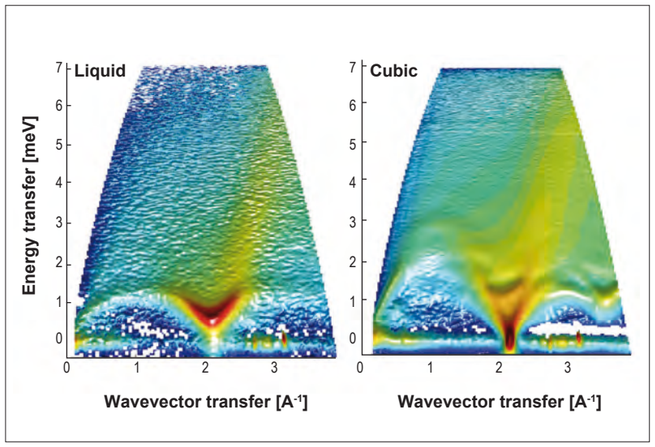

Figure 2: *Spectrum of helium in the liquid (left) and cubic (right) phase at T = 1.67K. In the cubic phase the spectrum is an average over all directions. The Bragg peak corresponds to the (110) diffraction peak. The newly accessible low Q-transfer enables the full acoustic branch to be measured down to Q = 0.09 A^{-1} and up to 3.9 A^{-1} (incident wavelength λ = 3 Å, images courtesy of J. Bossy, CNRS Grenoble).*

The commissioning period of IN5 started in September 2008 and the first users were on the instrument by the beginning of November of the same year [1]. Despite some minor problems with both the hardware and the data acquisition and analysis software that were fixed over this period, users were able to obtain analysable data in all the scheduled experiments. For most of these experiments the allocated beamtime was more than adequate because of the fast data acquisition that is now possible.

Improved signal-to-noise ratio and extended Q-range

Another important improvement is the low signal to noise ratio. In normal operating conditions the measured background is now 77 neutrons per hour and per metre of detector tube. This reduces further the acquisition time required for high quality data. A typical run for a 0.1 mm thick sample of light water does not exceed a few minutes counting time. It also enables users to measure the dynamics of very small amounts of scatterers, such as hydrogen adsorbed on different substrates, a field of surface-science that is benefiting from high counting rates on cold neutron time-of-flight instruments. Among other fields, studies of molecular magnets have also gained from the high flux. The facility to choose a wide range of instrument configurations helps to resolve the fine details of transition peaks, whereas high quality data can be collected in very reasonable time even with sample environments that impose further constraints such as magnetic fields (see the error bars in **figure 1**).

Measurements on bulk liquid and solid helium have highlighted one aspect of the importance of the vacuum chamber for the secondary spectrometer: the enlarged Q-range toward small wave vectors. It was possible in this case, to reveal for the first time the full dispersion curve down to the low-Q acoustic branch in a single spectrum (**figure 2**).

As a consequence of the improved performance, the time now spent on changing samples and making temperature changes has become a much more significant fraction of the total experimental time – and is now often the most significant bottleneck in efficient use of time. Owing to the ageing sample environment, a replacement of the cryostat is under study. It will also provide the opportunity to improve the standard tails for sample environment equipment in the beam to eliminate any spurious scattering that appears for wavelengths below the aluminium cut-off (incident wavelengths below 4.8 Å).

Direct view of the reciprocal lattice of single crystals

The possibility of carrying out single crystal experiments on the new IN5 equipped with PSDs was a major challenge and a justification for the new type of detectors.

Several single-crystal experiments have been performed since the upgrade was completed, all on magnetic systems. The size of the samples examined was similar to that used on triple-axis spectrometers at the ILL (1 cm^3 or less). Reconstruction of the scattering in the crystal reciprocal space requires the assembly of several spectra (up to hundreds) for different crystal orientations. Depending on the instrument setup, the size and scattering power of the crystal, counting times of 10 mn to 1 hour are needed to obtain reasonable statistics for each spectrum. This amounts to between one to two full days (24 h to 48 h) of counting time for a complete survey of the reciprocal space for a high symmetry case (1/4 of the reciprocal space visited, ~ 90 spectra). A test experiment on a copper germanate ($CuGeO_3$) single crystal, extensively studied in relation to spin Peierls behaviour, compared favourably to IN12 results, demonstrating that IN5 is now complementary to cold neutron triple-axis spectrometers.

For single crystal experiments, the spectra need to be processed in a specific way. The basic transformations are made within the ILL data manipulation and analysis package LAMP with specially adapted routines. Each processed spectrum is exported into the Horace suite from ISIS [2], enabling $S(Q_x,Q_y,Q_z,\omega)$ to be calculated and cuts to be made in three, two or one dimension(s).

The example in **figure 3** shows the magnetic excitations in a single crystal of the geometrically frustrated antiferromagnet iron langasite BNFS ($Ba_3NbFe_3SiO_{14}$) in the (b^*, c^*) reciprocal space plane at low temperature [3]. The good signal-to-noise ratio enables an unambiguous determination of the dispersion branches. The magnetic dispersion curves emanating from the satellites (0 k l+/- δ) with δ = 1/7 are clearly visible (additional rules apply for the intensities) either along high symmetry directions as in **figure 3a** or as iso-energy cuts in the (b^*,c^*) reciprocal plane (**figure 3b**).

Now that the performance of the instrument is well established, it is time to focus on the standard sample environment and the analysis software. A dedicated high magnetic field coil is scheduled and a XYZ polarisation analysis option (PASTIS-like) will be proposed within the framework of the next phase of the ILL Millennium Programme.

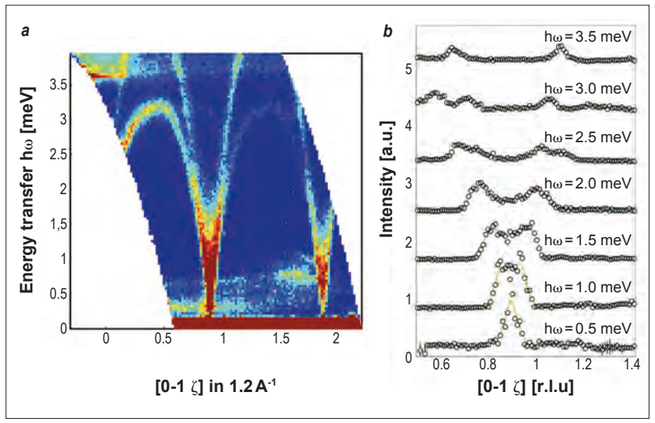

Figure 3a: ***(a)*** *Spectrum of $Ba_3NbFe_3SiO_{14}$ (BNFS) iron langasite taken at 1.6K along the c* direction around the [0 -1 ζ] position.* ***(b)*** *one dimensional iso-energy cuts in the c* direction. (images courtesy of R. Ballou, CNRS, Grenoble).*

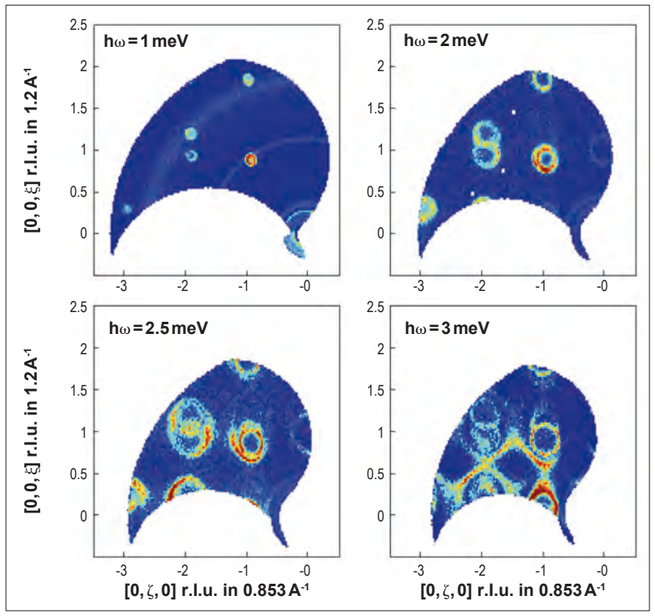

Figure 3b: *Iso-energy cuts in the (b*, c*) reciprocal lattice plane (width of the energy integration is = 0.1 meV).*

REFERENCES

J. Ollivier, L. Didier and H. Mutka, ILL Annual Report 2008 **[1]**

Horace and Libisis suites at http://horace.isis.rl.ac.uk/ **[2]**

See, e.g., K. Marty Phys. Rev. Letter 101(2008) 247201. Presented IN5 results unpublished: R. Ballou *et al.* (CNRS, Grenoble) **[3]**

AUTHORS

R. A. Campbell, **H. P. Wacklin**, **G. Fragneto** and **R. Cubitt** (ILL)
A. P. Dabkowska and **M. J. Lawrence** (King's College London, UK)
J. Holdaway and **K. Edler** (University of Bath, UK)

First science on the new horizontal reflectometer FIGARO

The ILL's new horizontal neutron reflectometer FIGARO was launched on 15 April 2009 and throughout the year has delivered a packed schedule of 34 user experiments. FIGARO is a versatile instrument with features including a choice of six chopper pairs to balance resolution and flux, deflector mirrors that direct the beam upwards or downwards towards the reflecting surface and a 2D detector to image off-specular scattering. A range of sample environments exists on the instrument including a Langmuir trough for studying compressed surface films at the air/liquid interface, adsorption troughs for studying molecules at the air/liquid interface, and a number of sample cells for studying phenomena at the solid/liquid and liquid/liquid interfaces. Two of the first experiments on the instrument using a range of these configurations are described in this report.

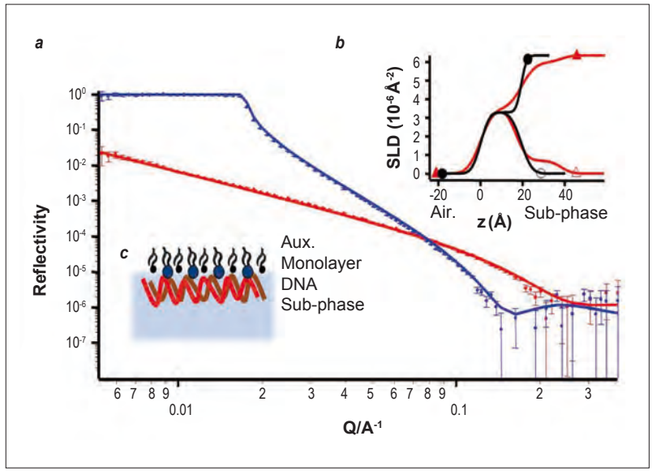

Figure 1: (a) *NR profiles of DDAB:DOPE (1:1 molar ratio) monolayers at the air/water interface at a surface pressure of 30 mN/m. The markers indicate experimental data while the lines are the fitted models for d_{74}DDAB:DOPE on D_2O containing 0.067 mg/mL of DNA [blue], d_{74}DDAB:DOPE on acmw containing 0.067 mg/mL of DNA [red].* ***(b)*** *The scattering length density (SLD) profile in the z-direction. The SLD was obtained from the fitting for all the contrasts: d_{74}DDAB:DOPE on D_2O [●], d_{74}DDAB:DOPE on null reflecting water (NRW) [○], d_{74}DDAB:DOPE on D_2O containing 0.067 mg/mL of DNA [▲], d_{74}DDAB:DOPE on NRW containing 0.067 mg/mL of DNA [Δ].* ***(c)*** *A depiction of the modelled structure at the surface when DNA was present in the sub-phase.*

Understanding the relationship between the molecular structure of a gene vector and its ability to elicit a therapeutic response is critical for effective gene therapy. Prof. Jayne Lawrence's group (King's College London) used FIGARO to study the interaction of a lipid mixture known to effect gene delivery, composed of a cationic lipid, dimethyldioctadecylammonium bromide (DDAB) and a neutral 'helper' lipid, dioleoylphosphatidylethanolamine (DOPE) with DNA. A neutron reflectivity (NR) study of the monolayers formed by this mixture has proven almost impossible due to the differential solubilities of the lipids in the water sub-phase, which results in unstable monolayers in the presence of vibrations. The careful design of FIGARO's sample table enables the formation of stable mixed lipid monolayers. **Figure 1** shows experimental and fitted NR profiles of DDAB:DOPE monolayers with and without DNA. The results revealed that although DNA formed a layer 19 Å thick, directly below the lipid monolayer, it did not alter the packing of the mixed lipid film. This study shows the potential of FIGARO for the study of complex monolayers, hitherto impossible to perform.

Dr. Karen Edler's group (University of Bath) is currently researching the formation and mesostructure of surfactant-templated polymer films at the air/water interface. These films are promising materials for structurally controlled sensors as they form spontaneously upon mixing of polymer and surfactant solutions and exhibit three-dimensionally ordered phases. The group used the adsorption troughs to control the surfactant imparted mesostructure on the films through surfactant/polymer interactions using glucose responsive polymers containing phenylboronic acids. FIGARO was chosen for this experiment primarily for the horizontal sample configuration, time-of-flight data collection and 2D detector. The troughs were ideal as they have an automated optical alignment system directed through tilted quartz windows that saves valuable beam time. The group found it gratifying to gain high statistics in the data whilst recording sub-minute NR scans for the first time, an example of which is shown in **figure 2**. They have previously not achieved such time-resolution on these systems when using neutrons or X-rays, and the data collected will assist greatly in understanding the mechanism for the formation of the films.

Other experiments during 2009 have included a climate change investigation by Dr. Christian Pfrang (Reading University) into the destruction of organic monolayers at the air/liquid interface by nitrous oxide gases, a structural study of surfactants at the oil/water interface by Prof. Ali Zarbakhsh (University of London), and measurements of the conformation of modified cyclodextrins in mixed membranes formed on solid supports by Prof. Jean Daillant (Saclay).

As 2009 draws to a close, all the essential features of FIGARO have been commissioned by the instrument team (**figure 3**). During the long shutdown in 2010, FIGARO will undergo a number of important upgrades, including the installation of an *in situ* Brewster angle microscope, a kinetic data-acquisition mode for automatic data histogramming, and a stopped-flow system and an HPLC pump for remote sample injections.

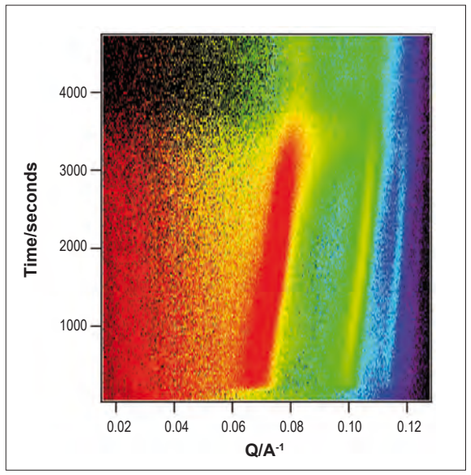

Figure 2: *2D image showing film formation data on a solution of molar ratio 7CTAB:3SDS, 0.05 M total surfactant concentration with 0.1wt% polyacrylamide contining phenylboronic acid, showing a Pn3m (double diamond) cubic phase film structure collected at 30 s time resolution. The 110, 211 and 222 reflections (left to right) show that the cubic phase is fully visible at 390 s with a unit cell size of 330 Å which decreases at a rate of 0.07 Ås^{-1} to 140 Å before the film macroscopically roughens.*

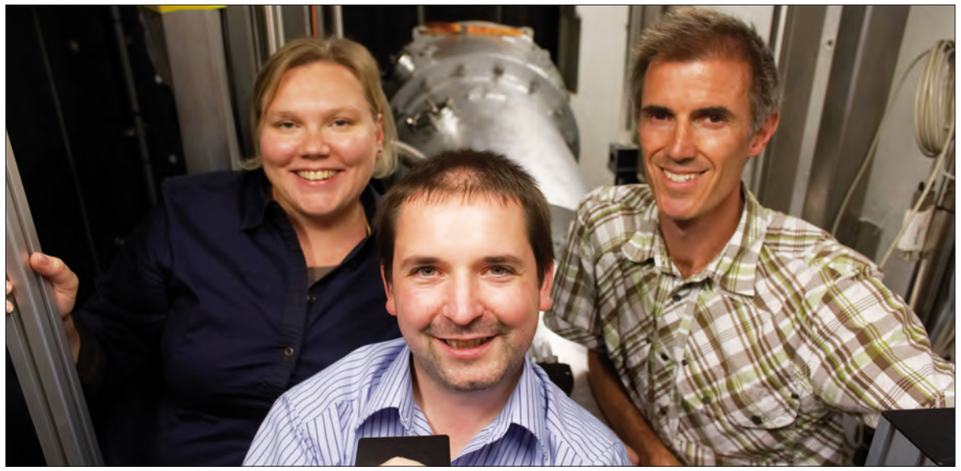

Figure 3: *Photo of the instrument running team, Hanna Wacklin (left), Richard Campbell (centre) and Simon Wood (right), taken in the FIGARO sample area with a view of the detector flight tube.*

P. Lindner and **R. Schweins** (ILL)

D11 – a new benchmark for SANS at ILL

From 26 March 2009 D11 was fully available for routine user operation. This was preceded by a short commissioning period. Since its restart, after the 15-month shutdown in 2008/2009, the new instrument has been running extremely reliably [1]. 160 days of beamtime were used at D11 in 2009 for 71 different experiments. Comments for instrument performance from our user satisfaction forms gave the overwhelming evaluation 'excellent'.

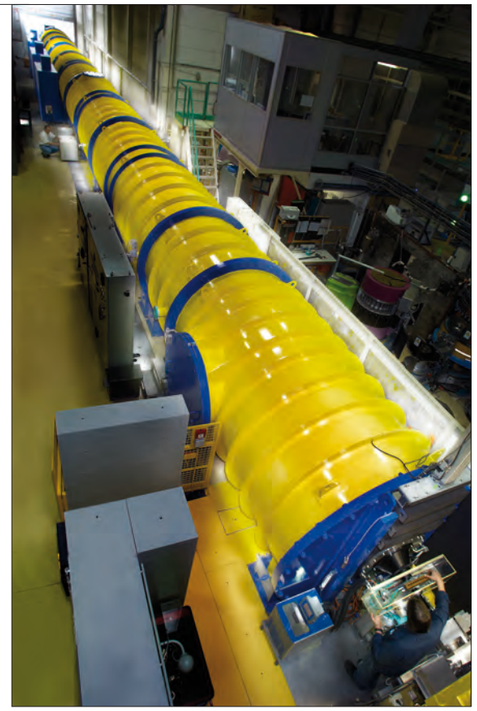

The new D11 sample zone and detector tube.

With its new detector [2], D11 provides a broader dynamic range due to the larger (1m x 1m) detector, better detector resolution, and shorter dead time. Furthermore, the neutron flux at the sample position is significantly increased due the new collimation guides, based on an innovative design change [3]. Thus, D11 allows now for better quality small-angle neutron scattering (SANS) data and new science in the field of soft matter and biology: the higher neutron flux and the increased dynamic range allow for faster experiments, favouring time-resolved and kinetic studies. With the larger detector, the range of length scales to be explored is considerably broadened, both for the lowest as well as for the highest values of momentum transfer. A very recent study in the field of biology concerns haemoglobin, a blood protein [4].

A recent D11 study of haemoglobin

The concentration of proteins in cells under physiological conditions is around 300 mg/ml. There exists much controversy over whether proteins at such a high concentration associate into larger assemblies. For this experiment haemoglobin was extracted from red blood cells and prepared at the concentrations of 290, 227 and 137 mg/ml. With the new, larger detector at D11, SANS experiments were, for the first time ever, possible at a wavelength of $\lambda = 20$ Å and with 3 sample-to-detector settings in a range of momentum transfer from $q \approx 0.17$ Å^{-1} down to $q \approx 3 \times 10^{-4}$ Å^{-1} (**figure 1**).

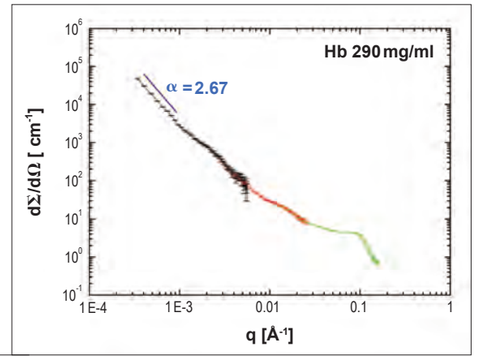

Figure 1: *SANS data of a concentrated haemoglobin solution, measured at D11 with wavelength $\lambda = 20$ Å and detector distance 39 m, 8 m and 1.2 m.*

The peak at ~0.1 Å^{-1} corresponds to the closest packing distance of haemoglobin proteins. The appearance of the shoulders in the scattering curve at ~ 2 x 10^{-3} Å^{-1} and ~1.5 x 10^{-2} Å^{1} at the highest concentration might be indicative of a large-scale superstructure in the protein solution. At small q-values the scattering curve shows power-law scattering behaviour with $I(q) \sim q^{\alpha}$ and $\alpha = 2.67$, which would indicate a mass fractal distribution of the superstructure. Data evaluation is currently being finalised.

News from sample environment at D11

After the successful restart of D11 in March 2009 and resuming routine user operation, new technical developments at D11 concern sample environment.

Simultaneous SANS and Dynamic Light Scattering at D11

In collaboration with Thomas Nawroth (University of Mainz) we succeeded in mounting a combined set-up at D11, implementing a stopped-flow mixing technique with an *in situ* combination of Dynamic Light Scattering (DLS) and SANS (**figure 2**). The laser is mounted at 45° with respect to the neutron beam. The scattered light intensity is recorded at 170° in backscattering. Time-resolved studies of the processing of nanoparticles for biomedical applications in cancer therapy could be followed up at different length scales with the dual-beam instrumentation [5]. DLS looks at wide distributions of up to 20 µm particle sizes at 20 % precision, but cannot distinguish between particle components. This is where SANS comes into the game by using contrast variation of solvents or single particle components. The structure and shape is elucidated precisely in the range of 1 and 300 nm. SANS is also the faster method, where time slices of 1 s are feasible. DLS needs at least a measurement time of 10 s.

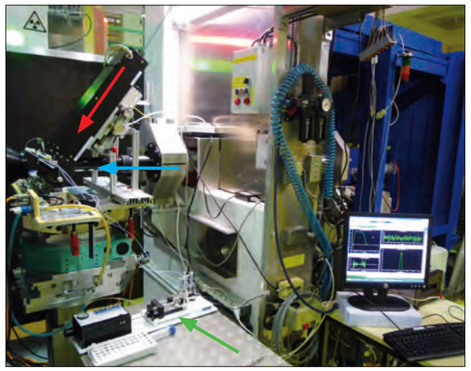

Figure 2: *DLS-SANS set-up at D11 (courtesy of Th. Nawroth, U Mainz). The red arrow marks the incident laser light direction, the blue arrow the incident neutron beam direction and the green arrow highlights the stopped-flow mixing device.*

The 'tumbling rack' sample changer for SANS

A frequently encountered problem in SANS studies is the instability of liquid suspensions. For solutions containing large particles, the particles may settle down during the time of the scattering experiment. Thus, concentration changes inside the scattering volume make it often difficult to interpret SANS data quantitatively. Therefore a 6-position changer rack for liquid samples in standard quartz cells has been developed, with the quartz cells rotating at variable speed around an axis parallel to the neutron beam (**figures 3a** and **3b**). The prototype works with 404 QS Hellma cells but adapters for other cell types are foreseen. The copper block holding the cell adapters can be connected to a thermostated bath and allows for temperature control.

Both devices - the DLS setup as well as the tumbling rack changer - are also compatible with the sample position of D22.

Outlook

Our next project is the development of a multi-beam USANS option for D11 [6], following successful tests performed on D11 in 2007 before the instrument reconstruction. The technique is based on 2 two-dimensional multi-hole apertures, which are to be installed inside the diaphragm changers at the 20.5 m collimation exit of D11 and at the sample position. At a distance of 20 m away from the sample position a CCD camera with enhanced spatial resolution is mounted inside the detector tank and will collect the superimposed individual SANS pattern of every hole.

Acknowledgement

We gratefully acknowledge the commitment and the enthusiasm of the whole D11 project team.

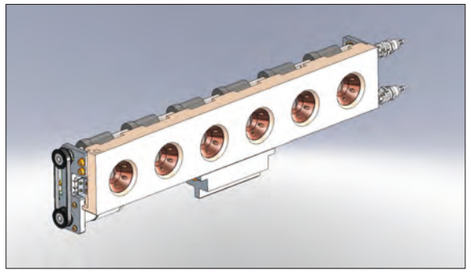

Figure 3a: *Schematical view of the 'tumbling rack', seen from the detector side.*

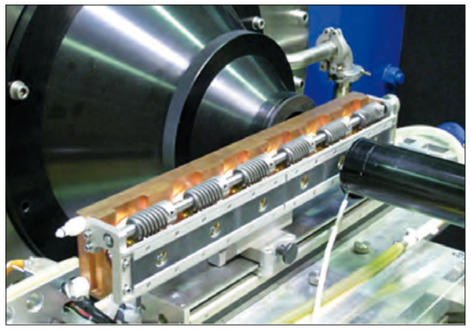

Figure 3b: *Photo of the 'tumbling rack' at D11.*

REFERENCES

A. Harrison and J.L. Martinez, Neutron News, 20 Vol. 3 (2009) 25 **[1]**
P. Lindner and R. Schweins 'A new D11 detector and tank: the scientific case', ILL Technical Report ILL06LI02T (2006) **[2]**
K. Lieutenant, P. Lindner and R. Gähler, J. Appl. Cryst. 40 (2007) 1056 **[3]**
A. M. Stadler, R. Schweins, G. Zaccai, G. Büldt and P. Lindner (2010) to be published **[4]**
T. Nawroth and R. Schweins (2009) to be published **[5]**
C. Grünzweig, T. Hils, S. Mühbauer, M. Ay, K. Lorenz, R. Georgii, R. Gähler and P. Böni, Applied Physics Letters 91 (2007) 203504 **[6]**

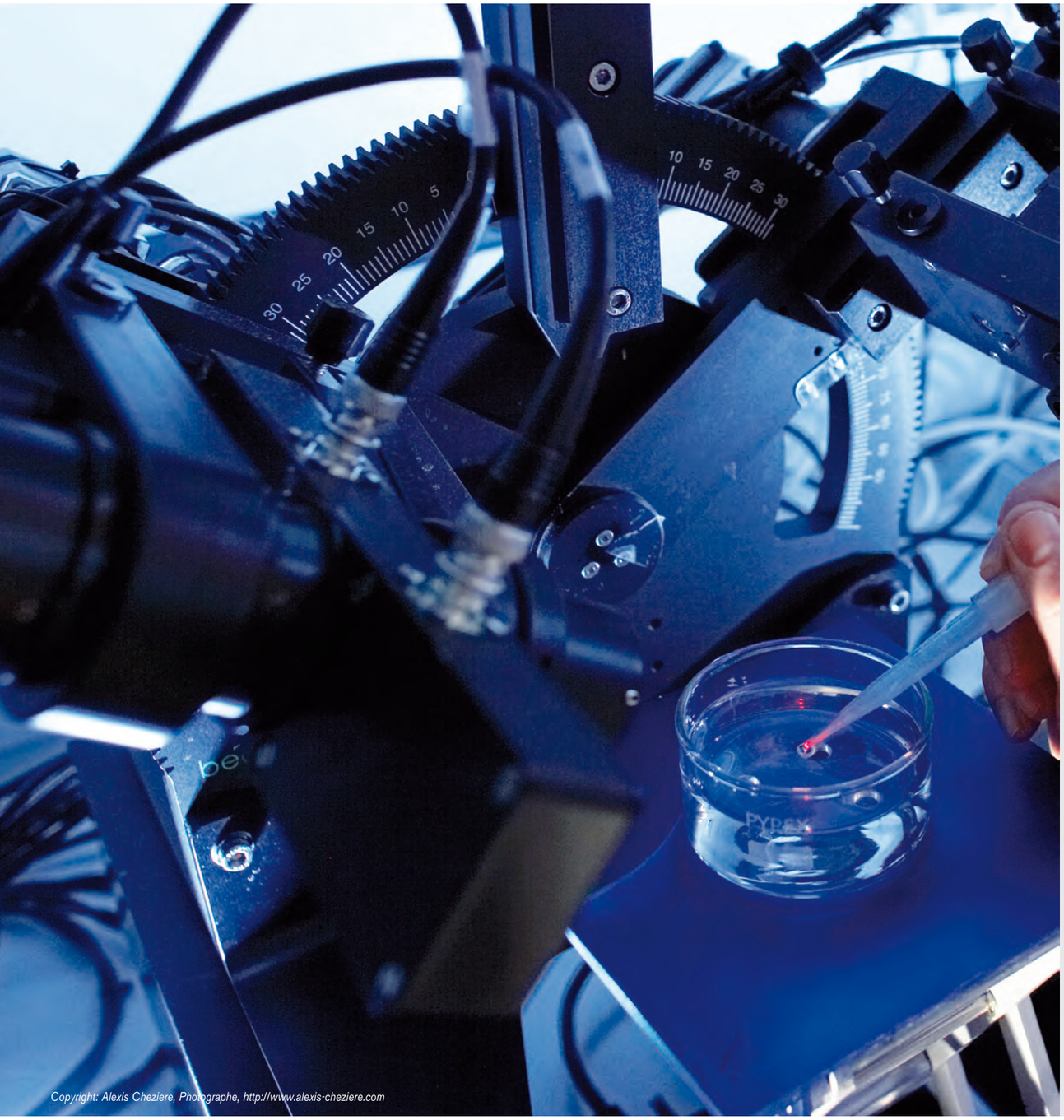

Copyright: Alexis Cheziere, Photographe, http://www.alexis-cheziere.com

MILLENNIUM PROGRAMME
NEW EXPERIMENTAL TECHNIQUES
TECHNICAL AND COMPUTING DEVELOPMENTS

In 2009, most of our efforts within the framework of the Millennium Programme were focused on finalising the design and initiating the procurement of the new instruments to be housed in the neutron guide hall ILL 7, and the associated infrastructure and neutron delivery systems. These efforts were rewarded by the fact that we were able to utilise more than 95% of the budget earmarked for 2009, with the remaining 5% already committed and due to be spent in early 2010. To achieve such figures required not only a very high level of commitment on the part of all the scientific and technical project leaders involved, but also a significant amount of coordination and planning with the various ILL services, both within the 'Projects and Techniques Division' (DPT) and throughout the Institute (including in the Reactor and Administration Divisions). We are proud to congratulate everyone involved who helped to make these achievements possible.

We have faced up to our problems with determination, 2009 represents a crucial step forward for the future of the ILL

One important achievement in 2009 was the delivery of a new asymmetric split-pair cryomagnet with a 10 Tesla vertical magnetic field. The magnet was designed by the ILL in collaboration with Oxford Instruments and is optimised to reduce helium consumption and overall cooling time (sample and coil) and to minimise neutron absorption and background, while maintaining a very wide opening access of 130 degrees. A second magnet with similar performances and a maximum field of 7 Tesla, optimised for reflectometers and time-of-flight instruments, is due to be delivered in March 2010. The corresponding dilution refrigerators will also be provided for both magnets. These new devices will satisfy a long-standing demand from our users to improve our high magnetic field and very low temperature facilities.

Another important step forward was the completion in 2009 of a comprehensive numerical model of our neutron source, the High-Flux Reactor (HFR). The model, which is described in detail later in this section, was validated using different codes and cross-checked by international experts within the framework of an external collaboration. It is able to reproduce the neutron flux and spectral distribution on ILL's various beam tubes, as well as the duration of the reactor cycle. The new model will be a very important tool when designing not only future modifications to reactor components, but also new instruments and experiments, which depend so heavily on the fine details of our neutron source.

In an excellent example of collaboration between ILL's Science, Reactor and Projects and Techniques divisions, preliminary tests were also carried out during the year for the production of radioisotopes for medical applications. Initial results indicate that our neutron source is a unique tool for producing some very specific and highly demanded radioisotopes. The success of these preliminary tests opens up an opportunity for the ILL to make a significant contribution to society and could place the Institute at the forefront of the production of highly specific radioisotopes.

Of course, maintaining our current strengths is as important as acquiring new ones. Three clear examples of this from the field of neutron optics are presented in this section. The successful production of intercalated graphite crystals for cold neutron monochromators, in the 4 Å to 15 Å range, is a unique achievement and much in demand from laboratories around the world. Similarly, progress made with the development of sophisticated, highly specialised polarising supermirrors and with neutron guide optimisation has dramatically improved the performance of certain instruments which have severe geometrical constraints, allowing the Instrument Responsibles to make more efficient use of these instruments.

To conclude, although 2009 will be remembered by historians as a difficult year, characterised by economic failure, social problems and the financial crisis, at the ILL we have faced up to our problems with determination, by creating an even greater sense of team spirit, taking up new goals and challenges, maintaining our leadership in neutron technologies, providing a better and more user-oriented service, encouraging cross-service collaboration, making more efficient use of our limited resources, and focusing even more closely on meeting the needs of society. In fact, 2009 represents a crucial step forward for the future of the ILL.

José Luis Martínez
Associate Director

AUTHOR
J.L. Martínez (ILL)

Millennium programme 2009

The on-going programme for the upgrade of ILL's instrumentation and infrastructures progressed as planned in 2009. The phase of the programme covering the period 2007-2014 involves the upgrade of four instruments (IN4C, IN1-LAGRANGE, D11 and D17) and the construction of four new instruments (ThALES, WASP, IN16B and D33). This phase also includes the installation of almost 600 metres of new neutron guides, the associated improvements to the neutron guide shielding, the extension of the two neutron guide halls (ILL7 and ILL22), and the replacement and upgrade of the sample environment equipment.

The upgrade programme is technically very ambitious and very demanding from a workload point of view. This article is a brief summary review of the current status of the different projects.

D11 (small-angle neutron scattering diffractometer) was successfully completed at the end of 2008. The **IN1-LAGRANGE (hot neutron triple-axis spectrometer)** design phase has been completed and the various components of the secondary spectrometer are in the manufacturing stage. Delivery of these components and final assembly at the IN1 position are scheduled for the end of 2010.

The IN16B project progressed as planned in 2009 and procurement of the massive vacuum chamber, neutron velocity selector and background chopper and Phase Space Transformer (PST) mechanics was done during the year. The corresponding neutron guide H112 (122.5 metres) is currently being manufactured. A large portion of this guide has already been delivered in two stages, at the end of 2009 and early in 2010.

The final design of the main components of the third small-angle neutron diffractometer D33 has also been completed. The new design for a high-resolution MAM detector for D33 has been validated with the construction and testing of a small-size prototype. The final design of the corresponding guide H14 has been completed.

The WASP (wide-angle spin-echo spectrometer) and ThALES (cold neutron triple-axis spectrometer) projects are both still in the feasibility phase, involving the design of the different components in parallel with the optimisation of their common guide H5.

The civil engineering works for the extension of ILL7 began in the summer of 2009. Delivery of the extended ILL7 neutron guide hall is anticipated in October 2010.

Finally, the new 10 Tesla cryomagnet for triple-axis and diffractometer instruments was delivered in 2009, and the new optimised 7 Tesla cryomagnet for reflectometers will be delivered in early 2010.

We will now review in more detail the progress made on some of the projects. Within the **IN4C (thermal neutron time-of-flight spectrometer)** project, a considerable amount of effort has been devoted to understanding the complex electronics for the Fermi Chopper. The complete overhaul of the chopper power electronics was completed in December 2009. The new double-focusing mechanics for the monochromator (4-face monochromator) is currently being mounted and aligned by the ILL's Neutron Optics Service. Within the scope of the project only three (out of the four) faces of the monochromator will be available and equipped with Highly Oriented Pyrolitic Graphite (HOPG) and two copper faces: Cu (111) and Cu (220). The fourth face will be reserved for future improvements. Finally, the very old detector electronics will be replaced in 2010 by a new set of electronics offering similar performance levels but greater reliability because each board will have new components.

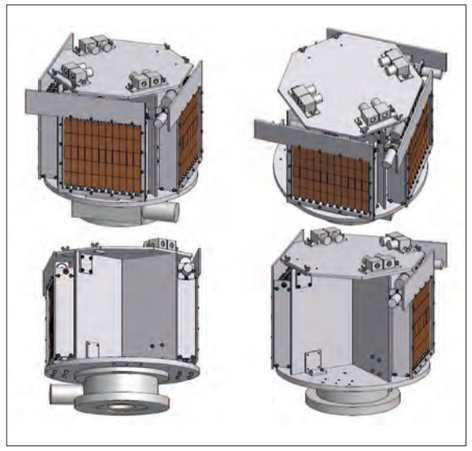

Figure 1: *Mechanical design of the 4-face monochromator for IN4C with fixed vertical focusing and variable horizontal focusing.*

The final design of **D33 (small-angle neutron diffractometer)** has been completed and procurement of the various components began in 2009 with the tendering process for the approximately 20 metre-long detector vacuum tube. The sophisticated design of the new collimation systems has also been finalised and the manufacturing process will begin in early 2010. Clearly one of the key components of D33 is the new MAM detector with its improved performances compared to D22's multitube detector. The final mechanical characteristics of the detector involve 128 tubes of 4.5 mm x 7 mm with 0.5 mm separation and 66 cm tube length. In order to test the viability of this new detector, a prototype composed of 32 tubes of 7.5 mm x 11 mm pitch and 1 metre long (in three welded pieces of 33 cm each) was constructed and tested in September 2009. The final test measurements at the neutron test position (CT2), as well as some additional tests carried out directly on D22, indicate that the performance of the new detector is 13 % more efficient than the present detector of D22. Detector manufacturing in the ILL workshop began at the end of 2009, and is expected to be completed in 2011.

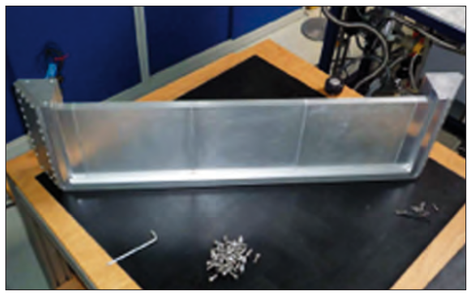

Figure 2: *Small-size prototype of the D33 multitube MAM detector.*

The corresponding **H14 guide,** which will feed with neutrons D33, IN12, IN10 and LADI, is already fully designed and the tendering process has been completed. The main suppliers for this guide are Swiss Neutronic and S-DH. The guide design is rather sophisticated with an initial split of the main guide into four separate guides, which will host the four instruments at four separate end-guide positions.

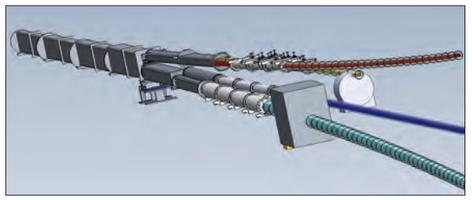

Figure 3: *Current design of the H14 guide.*

The new instrument **IN16B (high-resolution back-scattering spectrometer)** is in the manufacturing and procurement stage, in particular for the vacuum chamber, the various components of the Phase Space Transformer (PST) system (crystal cassettes and chopper), and the new velocity selector. Some of the main orders have been placed and delivery of the various components is expected in 2010. The initial commissioning phase is planned for the end of 2011. The first 60 metres of the associated guide (H112) are currently being aligned. One important element of the guides is the housing system. It might be expected that the housing element designed for the **H112 guide** will become a new standard design for guide housing. The new housing element consists of a single aluminium tube of 2.5 m in length, with the corresponding connecting flanges at either end. It houses a single optical element of 2.5 m in a fixed position for the neutron guide. The overall alignment is achieved by the positioning of the entire tube with respect to the next and previous elements. The lower price of the housing element and the simplified alignment procedure are expected to lead to significant savings in terms of budget and workload. The full length of the guide is scheduled to be installed at the end of 2010, in time for the commissioning of the complete guide during the first reactor cycle of 2011.

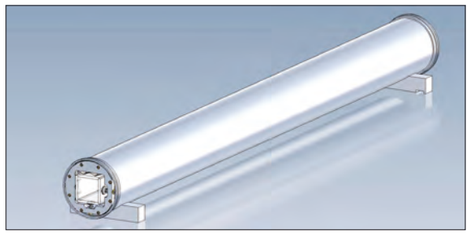

Figure 4: *New standard guide housing of 2.5 metre in length, to be implemented in the H112 guide.*

D17 (vertical reflectometer) was upgraded in 2008 and 2009. The project is almost complete, apart from the final commissioning of the new detector. The new focusing guide (m=4 made of Borofloat glass) became fully operational at the beginning of 2009, producing a significant gain in flux at the sample position. The S-bender is also almost finished, following the successful design of a similar S-bender for IN14 (cf. article on p.94). The final component of D17 is the new, high-performance detector, which is similar to the one installed on FIGARO (horizontal reflectometer). The main characteristics of the detector are: active area of 500 x 250 mm^2, vertical resolution 7.5 mm and horizontal resolution 2.5 mm, maximum counting rate 50 kHz per tube. The detector has already been manufactured and tested in the Neutron Detector Service. Final commissioning on D17 is planned for the first cycle of 2010.

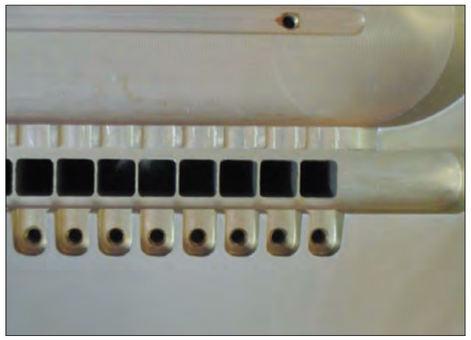

Figure 5: *Detail of the new D17 MAM detector, showing the individual tubes tailored by spark erosion in a single block of aluminium.*

AUTHORS

U. Köster, **Y. Calzavara**, **B. Desbrière**, **S. Fuard** and **M. Samuel** (ILL)
C. Barkhausen and **K. Zhernosekov** (Institute for Radiochemistry, TU Munich, Germany)
M. Harfensteller, **R. Henkelmann**, **P. Juntunen**, **S. Marx** and **T. Nikula** (Isotope Technologies Garching – ITG, Germany)
R. Baum and **R. Wortmann** (Klinik für Nuklearmedizin, Bad Berka, Germany)

Radioisotope production for nuclear medicine

There is an in-pile position known as V4 at the ILL reactor which offers a thermal neutron flux reaching 1.5×10^{15} n/cm^2/s. Although less well known than the ILL's intense extracted neutron beams and the 40 experimental instruments they serve, this is a facility unrivalled in western Europe. It is only surpassed by the neutron flux traps of the specialised high-flux irradiation reactors at Oak Ridge (USA) and Dimitrovgrad (Russia).
Until 2009 V4 was mainly used for specific cross-section measurements and the production of small quantities of special radioisotopes for scientific purposes.
In 2009, however, two test irradiations were performed to produce radioisotopes for nuclear medical applications.

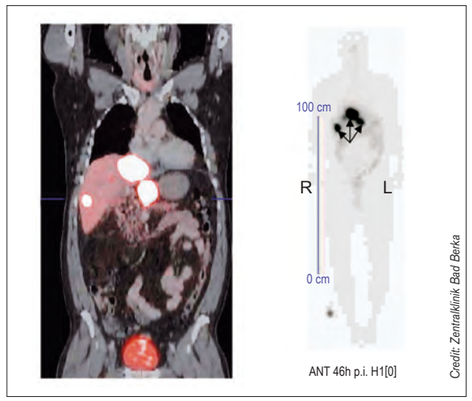

Figure 1: *The ^{68}Ga DOTA-TATE-receptor PET/CT scan (left image) was taken to localise the primary tumour and to stage the disease of a 59 year-old male patient with liver metastases (bright spots mark the tumour locations). Based on the observed strong DOTA-TATE uptake, the patient was treated with 6500 MBq of ^{177}Lu DOTA-TATE. A whole body scan of ^{177}Lu gamma rays (right image) taken 46 hours after injection revealed intense uptake of the peptide in the tumour lesions. This demonstrates the high tumour selectivity of the DOTA-TATE, so essential for the success of this type of therapy.*

High neutron fluxes guarantee high specific activity in single-neutron-capture reactions. They are particularly useful for double-neutron-capture reactions with short-lived intermediate radioisotopes. The tungsten isotope ^{188}W is produced by double-neutron-capture on enriched ^{186}W targets. The neutron flux has to be high if the intermediate ^{187}W, which has a half-life of only 1 day, is to have a chance of capturing another neutron to produce ^{188}W instead of decaying.

At ILL, irradiation tests in V4 over 49 days have shown specific activity of over 120 GBq of ^{188}W per g of ^{186}W. The ^{188}W produced was shipped to Isotope Technologies Garching (ITG, a spin-off of the Institute for Radiochemistry of TU Munich) where it was used to produce ^{188}W/^{188}Re generators for direct elution of ^{188}Re at high concentrations (>10 GBq/ml). The ^{188}Re can be used directly without further post-concentration.

The ILL could provide an almost continuous supply of up to 5 TBq of ^{188}W per year (with 4 reactor cycles). Used in combination with high-quality ITG ^{188}Re generators this would provide the isotopes required for the large-scale application of ^{188}Re in endovascular brachytherapy (to prevent blood vessels from clogging after balloon dilatation [1]) and of ^{188}Re-labelled radiopharmaceuticals (e.g. for skin cancer).

Peptide receptor radionuclide therapy uses tumour-selective peptides (e.g. octreotide or octreotate) linked physically to radionuclides with suitable half-lives (few days) and decay modes (alpha- or low-energy beta rays). After injection, the active compound is distributed in the body. The peptide, with its associated radionuclide, binds to the cancer cells. When the radionuclide decays, a good fraction of its decay radiation damages or destroys the cancer cells.

This treatment has given impressive results on inoperable neuroendocrine tumours (i.e. cancerous hormone-producing cells, e.g. pancreatic tumours). Compared to traditional treatment (chemotherapy) the results indicate higher remission rates for the patients (disappearance of the tumour), improved survival rates and quality-of-life, and fewer side effects. The best clinical results for small and medium-sized metastases have so far been obtained with the radioisotope ^{177}Lu; for larger metastases a combination of ^{177}Lu and ^{90}Y is indicated.

Isotope production
The radioisotope ^{177}Lu (half-life of 6.7 days) is usually produced by neutron-capture on enriched ^{176}Lu targets in a medium-flux reactor. The cross-section is high (2100 barn), but the reaction also unfortunately produces a long-lived ^{177m}Lu isomer with a 160-day half-life. This long-lived activity creates serious waste management problems for hospitals, since about 80% of the injected activity is released with the patient's urine during the first day of treatment. The ^{177m}Lu isomer activity released by a single patient may exceed the legal limits and poses problems for the disposal of clinical waste after the decay of the shorter-lived ^{177}Lu [2]. This is an obstacle to the widespread application of a very promising treatment. Moreover, the ^{177}Lu is not 'carrier-free', as it contains remains of stable ^{176}Lu from the irradiation target. This means that many of the sites on the cancerous cells will be blocked with peptides linked to stable ^{176}Lu; part of the therapeutic benefit is lost.

There is an alternative route. The ^{177}Lu isotope can be produced by neutron-capture on enriched ^{176}Yb targets. The resulting ^{177}Yb decays with a 1.9-hour half-life to ^{177}Lu, with no undesirable ^{177m}Lu. A chemical separation provides ^{177}Lu of 'non-carrier-added' quality, due to the quasi-absence of stable ^{176}Lu. Nearly every peptide will therefore be marked with a radioactive isotope capable of destroying cancer cells. The only drawback to the indirect method using a ^{176}Yb target is the much smaller cross-section obtained (< 3 barn); this means that a very high neutron flux is required to produce significant ^{177}Lu activity from the rare, highly enriched ^{176}Yb material.

In the V4 test, samples of ^{176}Yb were irradiated and then delivered to ITG for chemical separation of the ^{177}Lu. The final product fulfilled all the quality requirements for clinical use. Over 30 cancer patients have already benefitted from ILL-supplied ^{177}Lu in five nuclear medicine units in Germany. Regular production at ILL could provide the ^{177}Lu required to treat several thousand such patients per year. More frequent target changes would be necessary however (once or twice a week), and this implies the redesign of the irradiation shuttle (reusable instead of single-use) and a streamlining of the extraction and dispatching process.

The ^{99}Mo supply crisis
About 80% of all of today's nuclear medicine imaging operations use ^{99m}Tc for 28 million applications per year. ^{99m}Tc (half-life of 6 hours) is eluted from ^{99}Mo generators (half-life of 66 hours). Due to the radioactive decay of the mother isotope, the generators need to be replaced on a weekly basis. Until recently 95% of the world's supply of ^{99}Mo was produced by 5 of the world's reactors, by fission of highly enriched uranium (HEU) targets. The biggest producer, the NRU reactor in Chalk River (Canada), is presently undergoing repairs during a shutdown that may last many months or even years; the second-largest producer, the high-flux reactor in Petten (the Netherlands), is scheduled to shut down for an extended period starting from February 2010. With overall production down by more than 50%, a serious supply crisis is looming in the short- to mid-term [3,4]. The installation at other reactors of additional facilities for irradiating HEU targets is likely to take time due to the licensing process.

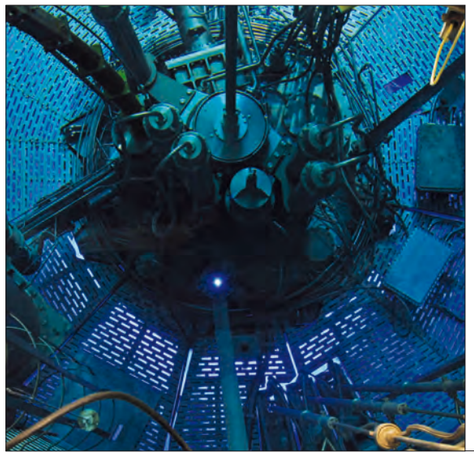

Figure 2: *The V4 vertical beam tube (bright spot below centre of image) penetrates to the position of highest flux within the ILL reactor, only 15 cm from the fuel element.*

The production of ^{99}Mo by neutron capture on enriched ^{98}Mo targets, on the other hand, involves no fissile targets and produces much less radioactive waste. The excess ^{98}Mo remaining after irradiation, however, makes the production of reliable ^{99}Mo/^{99m}Tc generators far more challenging. The specific activity required for the well-proven acid alumina column technology can only be obtained in neutron fluxes of several 10^{14} n/cm^2/s. At ITG a ^{99}Mo/^{99m}Tc generator loaded with $^{98}MoO_3$ irradiated at the ILL produced eluted ^{99m}Tc activity conforming to strict radiopharmaceutical quality requirements.

If an unused beam port on the ILL reactor was equipped with a special ^{99}Mo irradiation facility ILL could make a significant contribution, together with other medium- and high-flux reactors, to solving the ^{99}Mo supply crisis.

Conclusion
The addition of regular radioisotope production for nuclear medicine applications to the ILL's traditional fields of excellence could ensure as bright a future for the ILL as the Cherenkov light in the V4 beam tube!

REFERENCES

W.A. Wohlgemuth *et al.*, Cardiovascular and Interv. Radiology 31 (2008) 698 **[1]**
R. Henkelmann *et al.*, Eur. J. Nucl. Med. Mol. Imaging 36 (2009) S267 **[2]**
J. Raloff, ScienceNews 176 (2009) 16 **[3]**
D. Lewis, Eur. J. Nucl. Med. Mol. Imaging 36 (2009) 1371 **[4]**

Y. Calzavara and **S. Fuard** (ILL)

Modelling the high-flux reactor of the ILL (HFR)

For a number of years, the ILL's Projects and Calculations Office (*Bureau des Projets & Calculs*, BPC) has been developing an extremely detailed model describing the neutronic characteristics of our high-flux reactor (HFR). Such a comprehensive model of the reactor is a very useful tool both for ILL scientists and reactor staff. On the one hand, it can be used to estimate the neutron flux or brightness in each of the ILL beam tubes and, on the other hand, it helps to improve our understanding of reactor behaviour.

In our study, we chose to model the HFR using the well-known Monte Carlo code MCNP. We used the MCNPX 2.6f release and the cross-section library ENDF/B-VII.0. We also employed the latest available release of thermal structure factors for low energy neutrons. In this model, all in-pile components have been taken into account, including beam tubes (H,IH,V), safety rods, and cold and hot neutron sources (**figure 1** and **2**).

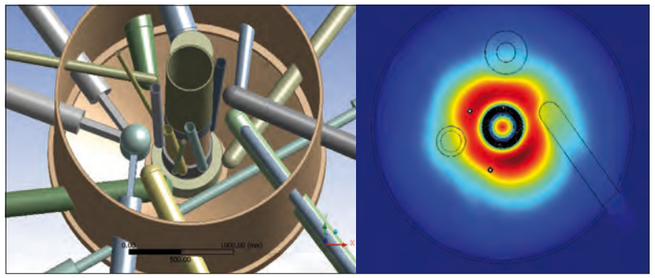

Figure 1: *3D view of the HFR model produced using the MCNP code.*

Figure 2: *Mapping of the neutron flux in the reactor median plane. The flux modifications induced by the cold and hot neutrons sources and the H10 beam tube can be clearly observed. The dark red regions correspond to a neutron flux of $1.5 \cdot 10^{15}$n/cm²/s at nominal reactor power of 57 MW.*

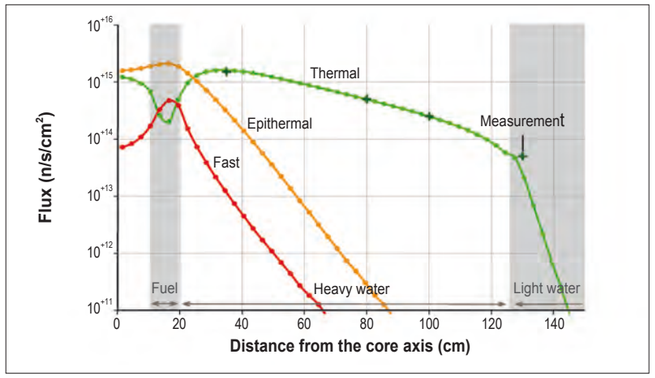

Figure 3: *: Undisturbed thermal (E≤0.625eV), epithermal (0.625eV≤ E≤1MeV) and fast (E≥1MeV) flux distribution in the reactor median plane.*

Material densities, compositions and fuel characteristics match the HFR Safety Report or have been updated if needed. The HFR fuel element has been modelled in detail with a high degree of accuracy. We have actually made as few simplifications as possible both to the geometry and to the material definitions, even though this was not necessary for a simple k_{eff} calculation. All 280 fuel plates of the fuel element have been modelled separately with the closest geometry available (involutes have been modelled by cylinder sections). Control and safety rod positions can be adjusted to match experimental conditions.

We carried out several benchmarks in order to validate our model. We considered, for example, the neutron brightness produced directly by the cold neutron sources or a MCNP/McSTAS coupling in order to match our results with measurements carried out on some instruments. In all cases, good agreement between experiment and calculation was obtained. Furthermore, we performed two international benchmarks on the k_{eff} calculation by comparing our calculations with two series of subcritical approaches performed recently by the Reactor Division. Again, agreement with the measurements was excellent.

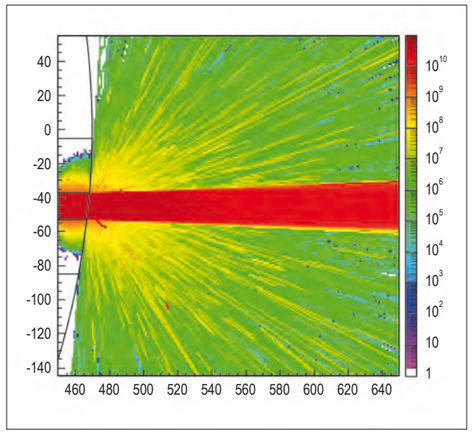

Figure 4: *Divergence of the H12 beam at the exit point of the beam tube. Distances are given in cm from the core axis. Total flux is given in n/cm²s.*

One of the first applications of this model was to determine the flux distribution for thermal, epithermal and fast neutrons in the D_2O reflector vessel under undisturbed conditions (i.e. far from in-pile components that locally modify the flux). The results match very well the measurements performed. The optimal distance from the core axis is 45 cm: at this position the thermal flux remains at its maximum while the epithermal flux falls (**figure 3**). This explains why the RHF designers chose to place the ends of the beam tubes at this distance from the core.

The spectral brightness and beam divergence at the exit point of the beam tube can also be calculated. Calculations have been carried out at a distance of 5 m from the reactor core and range from 10 meV up to 10 MeV. The results are of interest both for scientists (spectrum, influence of the control rod, etc) and for the health physics services (proportion of epithermal and fast neutrons) (**figure 4** and **5**).

Another application of this model was the simulation of the Vertical Cold Source and its optimisation. It is in fact possible to increase the brightness of this cold neutron source by changing the shape and the material composition of its re-entrant hole, originally designed by P. Ageron and usually called the 'insert'. V. Nesvizhevsky *et al.* recently measured the reflectivity of a layer (1 cm thick) of diamond nanoparticles for cold, very and ultra-cold neutrons [3].

These measurements showed that for energies below 1 meV, the reflectivity dramatically increases by up to 10^3 times the normal values for carbon atoms at the same neutron energies. Thanks to a collaboration with W. Haeck (IRSN), we were able to modify the ENDF cross-section file of natural carbon in order to take account of this specific effect of diamond nanoparticles on low-energy neutrons (**figure 6**).

We were thus able to design an improved Vertical Cold Source with a modified insert, basing our model on another design by P. Ageron. We left a volume of liquid deuterium between a nanoparticle layer and the insert. The reason for this is that the lowest energy neutrons are only extracted in the last centimetres of liquid deuterium because of their high probability of being absorbed. We recorded the neutron brightness at the entrance of the H15 beam tube and compared it to the present situation (**figure 7**). In this new configuration, neutron brightness is significantly increased for wavelengths above 7Å. It can even reach a factor of 5 at 20Å. This means that, thanks to the diamond nanoparticles, we have a promising way to optimise the vertical cold source.

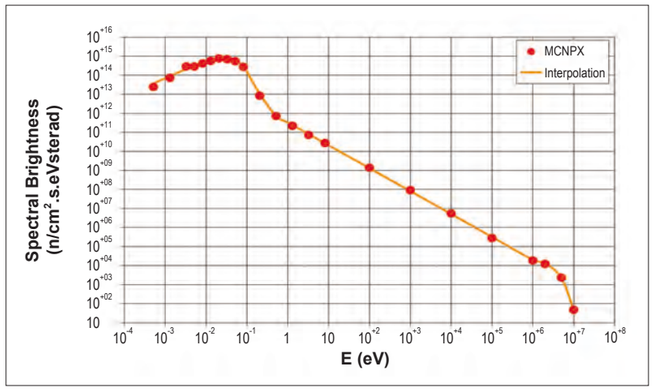

Figure 5: *Spectral brightness of the H12 beam.*

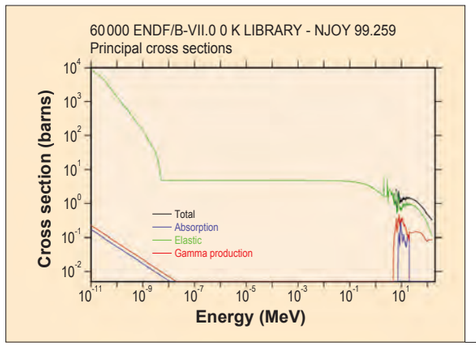

Figure 6: *Modified cross-section of diamond nanoparticles (in green).*

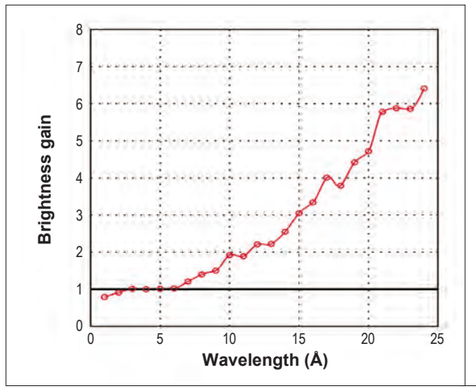

Figure 7: *Brightness gain in the H15 beam tube as a function of the wavelength.*

REFERENCES

E. Farhi, S. Fuard, *et al.*, International Workshop on Applications of Advanced Monte Carlo Simulations in Neutron Scattering, October, 2-4, 2006 at PSI, Switzerland **[1]**

Y. Calzavara and S. Fuard, International Handbook of Evaluated Reactor Physics Benchmark Experiments, HFR-HWR-RESR-001 CRIT, Nuclear Energy Agency (OECD), 2009 **[2]**

V. Nesvizhevsky, E.V. Lychagin, A.Yu. Muzychka, A.V. Strelkov, G. Pignol and K.V. Protasov, Nucl. Instr. & Meth. A, Volume 595, Issue 3 (2009) 631-636 **[3]**

P. Courtois, C. Menthonnex, R. Hehn, J. Baudin-Cavallo, E. Hetzler, B. Mestrallet and K.H. Andersen (ILL)

Intercalated graphite crystals for cold neutron monochromators

Three years ago, we started a new campaign for the production of intercalated graphite crystals (i-HOPG) in collaboration with the ILL Nuclear and Particle Physics group and the Oak Ridge National laboratory in the USA. We are now able to produce high-quality i-HOPG single crystals in large quantities, based on potassium and rubidium intercalation. These compounds offer the opportunity to build very efficient neutron monochromators for wavelengths in the 4-15 Å wavelength range, extending the wavelength above what can be achieved using pure graphite, or overlapping the presently-accessible wavelength range with a much broadened wavelength spread and hence increased beam intensity.

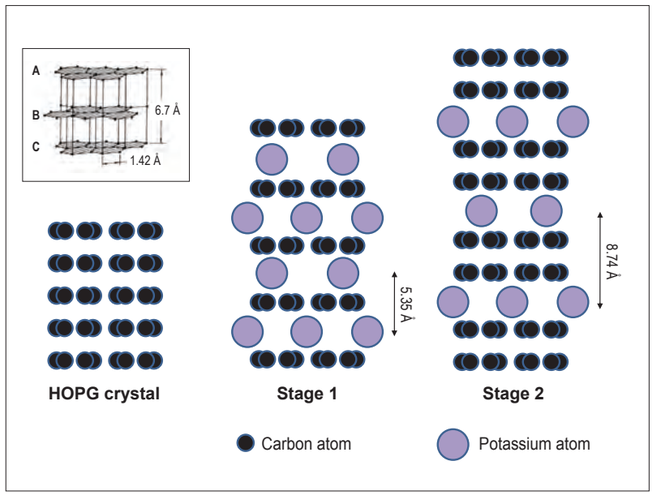

Figure 1: *Schematic diagram illustrating the layered structure of HOPG, stage 1 KC_8 and stage 2 KC_{24} intercalation compounds. The interplanar distance increases with the index of intercalation.*

An Intercalated HOPG compound (i-HOPG crystal), is a graphite crystal in which atoms or molecules are intercalated between the carbon layers (**figure 1**). Not every layer is necessarily occupied by the intercalant and the stage index denotes the number of graphite layers between intercalate layers. In so-called stage 1 compounds, graphite layers and intercalated layers alternate. In stage 2 compounds, two graphite layers alternate with an intercalated layer. Among the large number of intercalation compounds, KC_8, RbC_8 (stage 1), KC_{24}, and RbC_{24} (stage 2) are the most interesting compounds for neutron applications. These crystals are characterised by a large d-spacing of up to 8.75 Å and a theoretical neutron peak reflectivity of about 80 % at a wavelength of 9 Å [1].

Preparation

The 'two zone vapour transport' technique is well adapted for the intercalation of potassium and rubidium atoms into HOPG single crystals [2]. Because of the high reactivity of these compounds, i-HOPG crystals are prepared in quartz ampoules composed of two bulbs (**figure 2**). The first bulb contains the graphite crystal and the second one the potassium metal. The graphite is heated to a fixed temperature $T_g = 593$ K and the potassium heated to a lower temperature T_k. We control the intercalation by the temperature difference T_g-T_k. Stage 1 KC_8 is obtained when applying a small value of T_g-T_k close to 30 K, whereas a higher value of about 110 K is needed for stage 2 KC_{24} (**figure 3**). The intercalation process is very sensitive to the potassium vapour pressure inside the ampoule, which depends on T_k. Moreover, since it is a diffusion process, intercalation is also strongly time dependent: 3 days are needed for stage 1 to be produced and 7 days for stage 2. The same procedure can be applied to RbC_8 and RbC_{24} compounds.

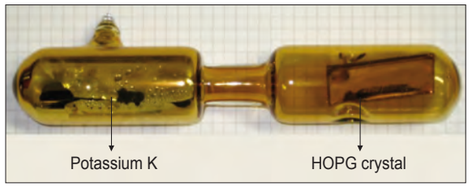

Figure 2: *The glass cell used for the intercalation of graphite crystals.*

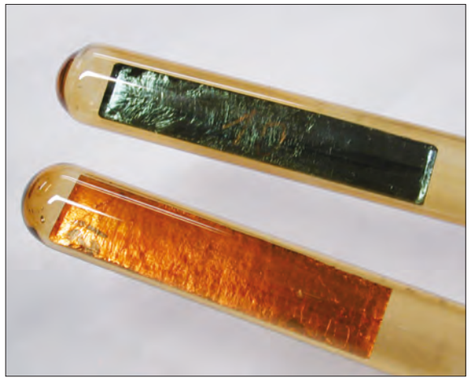

Figure 3: *Stage 1 KC_8 (gold colour) and stage 2 KC_{24} (blue colour) i-HOPG crystals.*

A neutron theta-2θ scan is used in order to reveal the stage of intercalation. Theta-2Θ scans were performed on the test instrument T13A using a perfect Ge111 monochromator (no λ/2 contamination). Following Bragg's law, the (00l) diffraction peaks from stage 1 or stage 2 can easily be identified (**figure 4**). The crystal is characterised inside its quartz ampoule to avoid degradation of the crystal from exposure to air. Afterwards, we remove the crystal from its glass cell: we break the ampoule inside a glove box, compress the crystal and immediately enclose it in a sealed aluminium box for storage. This will allow the crystal to be further characterised using neutron diffraction (**table 1**). The crystal must at all times be kept in an inert atmosphere, as it reacts strongly with oxygen and moisture in the air.

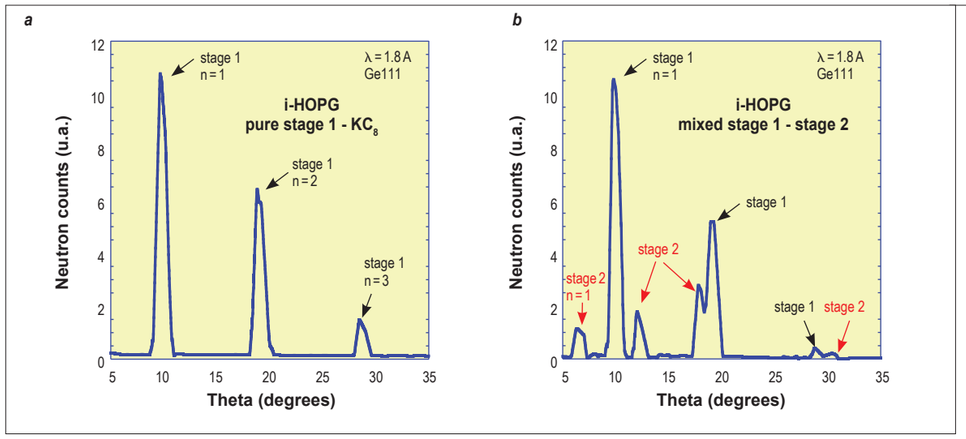

Figure 4: *Neutron θ -2θ scan from i-HOPG crystals.* ***(a)*** *(00l) diffraction patterns from pure stage 1;* ***(b)*** *(00l) diffraction patterns from a stage 1 crystal containing a small amount of stage 2.*

Neutron Mosaic and Reflectivity

The mosaic of the crystal is determined from neutron rocking curves at 1.8 Å. Because of the expansion along the c-axis (**figure 1**), the intercalation strongly increases the mosaic spread of the HOPG crystals both for stage 1 and stage 2. The effect is more pronounced for stage 1 for which a mosaic of 3° is typically obtained.

The peak reflectivity at long wavelength is measured on the instrument MIRA at FRM2 Munich. As can be seen in **table 1,** i-HOPG crystals exhibit excellent properties for cold neutron monochromator applications. Even though the mosaic is large, the peak reflectivity of the intercalated compounds is still high, about 75 % for stage 1 and 65 % for stage 2 for neutrons of 9.8 Å.

i-HOPG crystal	d-spacing	Neutron mosaic (λ = 1.8 Å)	Experimental peak reflectivity (%) (λ = 9.8 Å)
KC8	5.35 Å	4° +- 0.5°	70 - 80
KC24	8.74 Å	2° +- 0.3°	60 - 70
RbC8	5.65 Å	2.5° +- 0.5°	65 - 75
RbC24	9.05 Å	2° +- 0.5°	-

Table 1: *Neutron diffraction properties of i-HOPG compounds: d-spacing, typical mosaic spread at 1.8 Å and peak reflectivity at 9.8 Å.*

REFERENCES

A. Boeuf, A. Freund and R. Caciuffo, Synthetic Metals, 8 (1983) 307-312 **[1]**

P.R. Huffman *et al*, Physica B 344 (2004) 343-357 **[2]**

E. Lelièvre Berna, E. Bourgeat-Lami, O. Losserand, S. Turc and **X. Tonon** (ILL)

Zero-boil-off asymmetric cryomagnets

Within the framework of the Millennium Project 'Modernisation of Sample Environment', the ILL has decided to provide a better suite of cryomagnets for carrying out experiments on three-axis spectrometers, reflectometers, and small-angle and time-of-flight spectrometers.
The objectives are numerous and somewhat contradictory: reduced neutron absorption, reduced neutron scattering, no liquid nitrogen, zero liquid helium boil-off and fast sample cooling time with a base temperature of 40 mK.
The new design proposed by the ILL has been developed in collaboration with Oxford Instruments (UK).

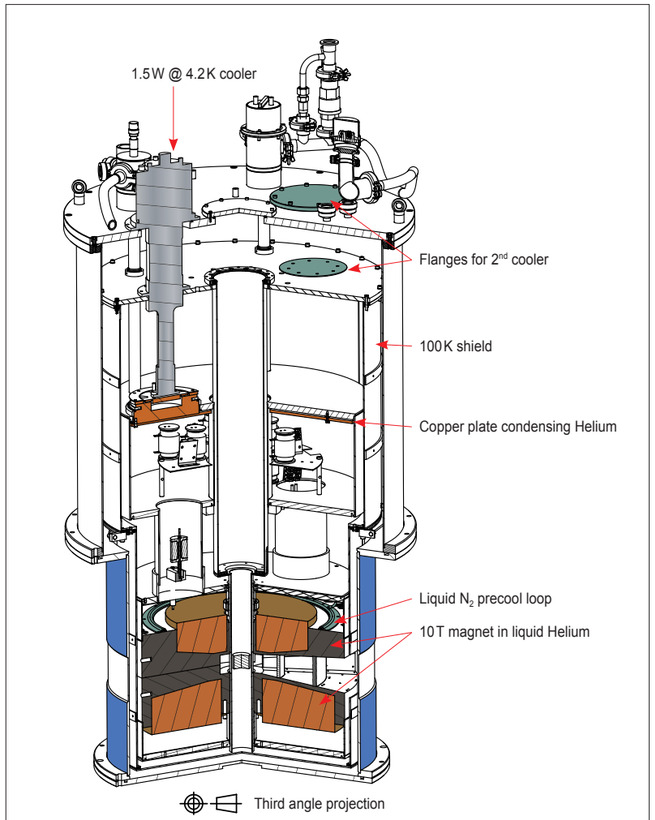

***Figure 1:** Overview of the new 10 T cryomagnet to be used primarily on the three-axis spectrometers.*

In an initial phase, two asymmetric split-pair cryomagnets were ordered: a 10 Tesla vertical field magnet to be used primarily on the three-axis spectrometers and a 7 Tesla vertical field magnet, co-financed by Bochum University, for the reflectometers and the small-angle neutron scattering instruments. The 10 T (**figure 1**) and 7 T magnets will have a horizontal opening access of ± 130° and ± 20°, respectively, and a vertical opening access of ± 5°.

For both magnets, the design has been optimised so as to minimise the amount of material in the beam and avoid unwanted neutron absorption and neutrons scattered to the detectors. The geometry of the magnet former of the 10 T (**figure 1**) consists of two diametrically opposed pillars and aluminium alloy rings. Compared with the conventional geometry, this new design means that the amount of aluminium alloy in the scattered beam is divided by a factor 2. For the 7 T magnet, sapphire or silicon windows will be mounted to reduce scattering and there will be only 2 mm of pure aluminium in the beam.

The absence of a room-temperature bore also contributes to a lower amount of material in the beam and provides a much larger sample volume compared with dry systems. An ILL variable temperature insert will be mounted inside the cryostats to control the sample temperature between 1.5 K and 300 K at any applied field. The maximum sample volumes will be respectively a Ø 38 x 30 mm and a Ø 25 x 20 mm cylinder. Rotating stages and dilution refrigerators will also be provided to orient the samples inside the cryomagnets and reach 40 mK.

The superconducting coils are reliably maintained at low temperature within a liquid helium bath cooled by a Gifford-McMahon cold-head, and the nitrogen jacket is replaced by a 50 K shield attached to the first stage of the cooler. The mechanical Gifford-McMahon cooler is capable of achieving full system boil-off re-condensation in static mode of operation and during slow field ramps. The pressure of the helium bath is controlled using either two copper interface heaters or bath-immersed heaters. The efficiency of both methods is comparable and the temperature, pressure and level inside the helium bath are kept stable. For the 10 T magnet (**figure 1**) delivered this summer, the indirect cool-down to ~ 100 K is achieved in less than 24 hours using ~ 400 litres of liquid nitrogen at a transfer pressure of 2 bar. The cool-down from 100 K to base temperature is achieved within a further 16 hours using about 70 litres of liquid helium. The spare cooling power is of the order of 500 mW in persistent mode.

The cooler can be switched off to move the magnet to another instrument while keeping the system cold. In the event of cooler failure, there is also sufficient time to perform some measurements and run the magnet down. Currently the rate of level drop does not exceed 8 % per hour. This rate could even be reduced by cooling the 50 K shield with the helium venting out of the helium bath.

Because the 10 T cryomagnet will be used for carrying out long experiments, there will be an option to re-condense the helium pumped through the variable temperature insert with a second cold-head. The gas pumped through the cold-valve will be filtered and cooled down in a capillary wound and brazed around the tubes of the cooler before being injected onto the copper plate located at the top of the helium bath. Calculations and actual tests confirm that up to 6 litres of helium gas can be re-condensed per minute. With a standard 40 m^3/h primary pump, the zero-boil-off will therefore be maintained except when the cold-valve is opened widely, i.e. during fast cooling ramps.

These two new cryomagnets are due to be commissioned during the first cycle of 2010 and the dilution inserts will be available a few months later.

Stray magnetic field issues

The effects of stray magnetic fields on system performance and the environment can often require complex finite element modelling. We therefore provide some guidelines (http://www.ill.eu/sane/safety/high-magnetic-fields) and dedicated apparatus for measuring the magnetic forces. The vertical force is measured with a standard dynanometer and the horizontal one is obtained by clamping the device shown in **figure 2** to both the cryomagnet and the sample table. This device measures 3 forces at 120° and calculates the direction and total magnitude of the force.

For safety reasons, the magnetic force measurements are compulsory after each modification to an instrument. From discussions with magnet suppliers and experts, we have established an area of horizontal and vertical forces that must be respected to ensure the safe operation of the instruments (**figure 3**). Sometimes the scattering angles covered by an instrument are limited above a given field strength. The operation conditions are summarised on the above-mentioned web page.

***Figure 2:** Device used to measure the horizontal force on the instruments.*

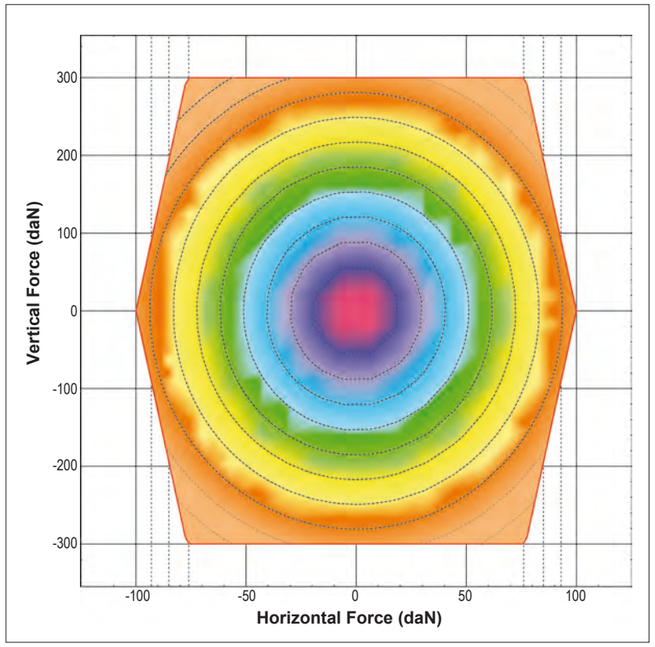

***Figure 3:** The area of horizontal (F_h) and vertical (F_v) magnetic forces accepted on an instrument is defined by: $F_h < 100$ daN, $F_v < 300$ daN and $F_v < 13\ (100 - F_h)$.*

P. M. Bentley and **K. H. Andersen** (ILL)

Simultaneous global optimisation of a neutron instrument suite

The refurbishment of the H5 guide system in ILL 22 presents a complex guide optimisation problem, with a classic game-theory solution. If neighbouring instruments could each sacrifice a small quantity of their unused phase space, perhaps a global improvement could be found in which no instrument loses useful flux. Invariably, this involves exploration of a high-dimensional search space of many coupled parameters. Such problems are ideally suited to particle swarm optimisation as we have demonstrated previously [1, 2]. In this report, we present the results of such a global optimisation of an entire neutron guide hall.

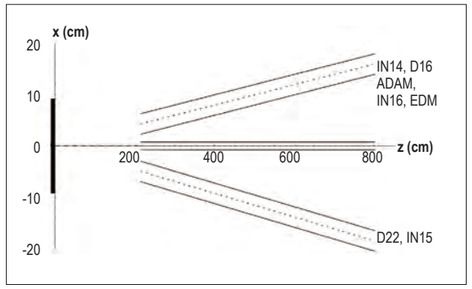

Figure 1: *Present H5 guide system, viewed from above and plotted with an exaggerated aspect ratio. The solid black region on the left is the moderator face.*

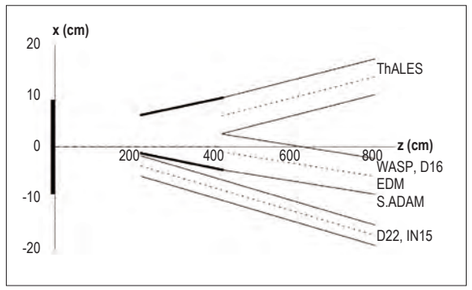

Figure 2: *Baseline separator design.*

This project concerns directly the present and future instruments in the second (ILL22) guide hall (see instrument layout, p.99), viewing the horizontal cold source via the H5 guide system. The current setup consists of three separate guides, of which the central one is unused, as shown in ***figure 1***.

Previous optimisation work has arrived at an upgraded geometry using a separator for two of the guides, as shown in ***figure 2*** [3]. The IN14 upgrade (ThALES) will have a dedicated, focusing elliptic guide on the beam port shown in the upper part of the figure. The instruments D16, Cryo-EDM and the upgrade of ADAM (SuperADAM), move onto the currently unused, central beam port. The IN11 upgrade (WASP), takes the end position of this guide, which is curved and therefore has a different initial beam axis to that of the current (unused) guide. The guide in the lower part of the figure serves D22 and IN15 with minimal changes. This is the reference geometry, against which we will compare our further optimisations.

For simplicity and engineering reasons, we assumed that the guide directions and distances to the sample positions are fixed. We allowed the geometry of the separator and the supermirror m-number to vary, as well as in-pile widths of the ThALES and WASP guides, and the WASP guide curvature. The method works by maximising a figure-of-merit, defined as the sum of the flux gains, while penalising nonsensical overlapping guides and any instrument losing more than 2% of the reference flux. We calculated the flux at the maximum and minimum wavelengths for all key instruments except D22, which was given a rarely used, worst-case configuration of longest possible wavelength and shortest possible collimation.

It is essential that the neutron beam is modelled as far through the instrument as possible, so the calculation bottleneck is instrument modelling. Our solution to this problem, neutron acceptance diagram shading (NADS), can be orders of magnitude faster than Monte-Carlo especially for low-acceptance instruments such as SANS [4, 5].

The optimised separator design is shown in ***figure 3***.

The separator wall at the top of the figure has been removed, allowing a direct view of the source, which is mainly advantageous at short wavelengths. The supermirror coating of the separator (shown as a thicker line) is increased to m=4, again to favour the shorter wavelengths.

In the vertical plane, the separator has a slight outward tapering from 11.2 cm to 12 cm. This tapering and the high m-value of the supermirror coating feature in the vast majority of the optimisation runs that were performed.

One of the advantages with this method, as for other similar artificial intelligence optimisation studies, is that the guide system can be re-optimised in only a day or so to consider new information from feasibility and engineering studies.

As such, it is likely that the final design will evolve beyond that presented in this article. Nonetheless, we have demonstrated that the tools now exist for globally optimising entire suites of instruments, from moderator to sample, with useful gains in neutron flux at minimal additional cost.

Acknowledgements

The authors would like to thank the European Commission for financial support in the framework of the ESFRI project ILL 20/20, and P. Fouquet, M. Boehm, B. Farago, P. Falus, C. Dewhurst and I. Sutton of ILL for their valuable contributions.

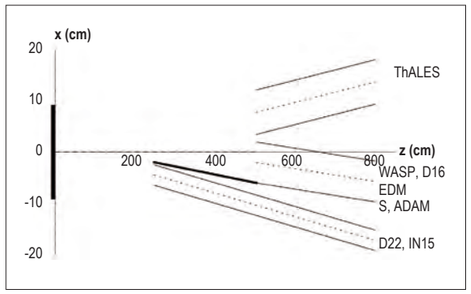

Figure 3: *Optimised guide geometry.*

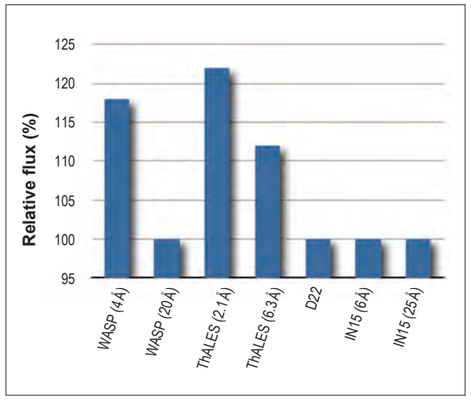

Figure 4: *Flux gains of the optimised design relative to the reference baseline design.*

REFERENCES

P. M. Bentley, K. H. Andersen, J. Appl. Cryst. 42 (2009) 217 **[1]**

P. M. Bentley, K. H. Andersen, ILL Scientific Highlights, ILL Annual Report (2007) **[2]**

M. Boehm, A. Hiess, J. Kulda, ILL internal report ILL06B006T (2006) **[3]**

P. M. Bentley, K. H. Andersen, Nuc. Inst. Meth. Phys. Res. A. 602 (2009) 564 **[4]**

P. M. Bentley, K. H. Andersen, J. Saroun, ILL Annual Report (2008) **[5]**

Hey, big S-bender!

A new polariser has been built for the IN14 cold neutron 3-axis instrument. It consists of a stack of about 250 thin Si wafers coated with polarising supermirrors and bent into an S-shape. The polarised beam thus emerges in the same direction as the beam entering the polariser, greatly facilitating the switch between the polarised and the unpolarised instrument set-ups. The neutrons are transmitted through the Si wafers and the unwanted spin-state is absorbed in a Gd coating deposited on the supermirrors. The polariser covers the full beam cross-section of 5 x 8 cm^2.

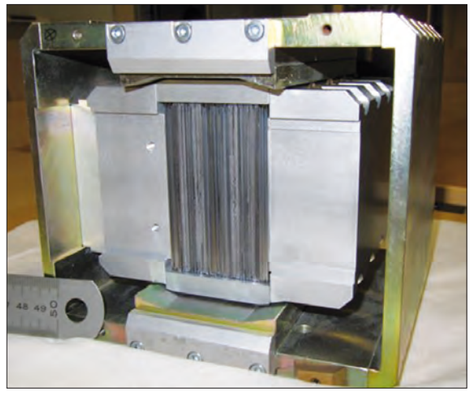

Figure 1: *S-bender with its magnetic circuit, covering a beam 5 cm wide and 8 cm high.*

The S-bender is based on a design successfully commissioned previously [1]. The main difference is the number of silicon wafers, which is now 244 instead of 32 in the prototype. This allows us to increase the accepted beam width up to about 5cm, with the same compact mechanical design including the magnetic circuit (**figure 1**). All the mirrors, coated on both sides with inverted-sequence Fe/Si supermirrors, were coated at the ILL by magnetron sputtering, with a typical coating time of 40 hours per deposition. In order to optimise the production schedule, a critical angle of m=3.2 was chosen for the supermirror, instead of m=3.6 as for the prototype. The individual Si wafers are 0.2mm thick with a length along the beam axis of 114mm.

The stack of wafers is mounted in S-shaped anvils ensuring (double) reflection of each neutron. The Fe/Si supermirrors are magnetically saturated using permanent magnets. Contrary to conventional C-bent polarising mirror stacks, the present design ensures that the beam direction remains unchanged and we did not need to realign the IN14 spectrometer when we tested the device using the last neutrons available in 2009. Using the set-up shown in **figure 2** and simply rotating the device optimises its performance. At maximum intensity with a bender rotation RB = 0.5 (dotted line in **figure 2**) the flipping ratio of the beam polarisation is R = I(up)/ I(down) ~15 only. By rotating the bender further to RB = 1.5, the flipping ratio was improved to R > 30 when tolerating a 10% reduction in intensity (dashed line in **figure 2**). This observation is consistent with some remaining direct view i.e. incomplete bending of the stack within the anvils.

We intend to optimise the curvature of the anvils to improve its performance gaining back the last 10% in intensity. Throughout all tests reported in the following, a bender rotation RB=1.5 corresponding to R >30 and an intensity reduced by 10% has been used. For reference, the maximum flipping ratio which can be achieved with the Heusler analyser is R = 35.

We measured the polarised flux at the sample position using the set-up shown in **figure 3**. The performance of the S-bender can be compared to an unpolarised set-up using a 60' Soller collimator as well as to the polarised flux obtained with the routinely-used IN14 C-bender. The flux corrected for higher-order contamination is shown in **figure 3**. Within the wavelength range from 4 Å < λ < 5 Å the S-bender has a similar performance to the C-bender, but the S-bender outperforms the latter for shorter wavelengths down to λ = 3 Å. Bragg scattering from the Si wafers produces a significant drop in transmission which reduces the useful wavelength range to 3 Å < λ < 5 Å.

The new S-bender is a powerful device to rapidly install polarised neutrons on IN14 without realigning the spectrometer. Even though the S-bender cannot be used at the longest wavelengths it shows better performance at shorter wavelength than the polarisation option routinely used until now. Improving the anvils will improve its performance further and the device will be used regularly on IN14 from the start-up in 2010 onwards.

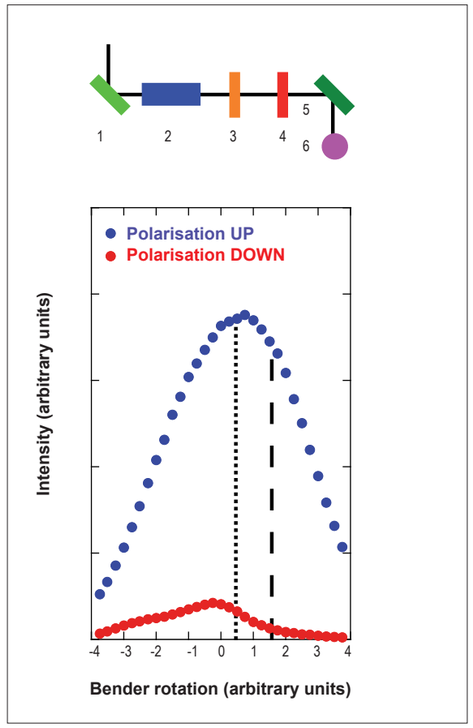

Figure 2:
(Top): Experimental set-up for polarisation measurement:
(1) PG(002) monochromator (green)
(2) S-Bender (blue)
(3) Be filter (orange)
(4) Flipper (red)
(5) Heusler(111) analyser (dark green)
(6) Detector (magenta)

(Bottom): Intensity of beam polarisation UP and DOWN vs. bender rotation. Maximum intensity (dotted line) and the position with improved flipping ratio R > 30 (dashed line) are indicated. The data were taken at a wavelength of λ = 4 Å but similar results were obtained at all other wavelengths 3 Å < λ < 5 Å.

Before operating the S-bender in user mode on IN14 we will complete our tests by exploring the transmitted beam divergence and polarisation in more detail.

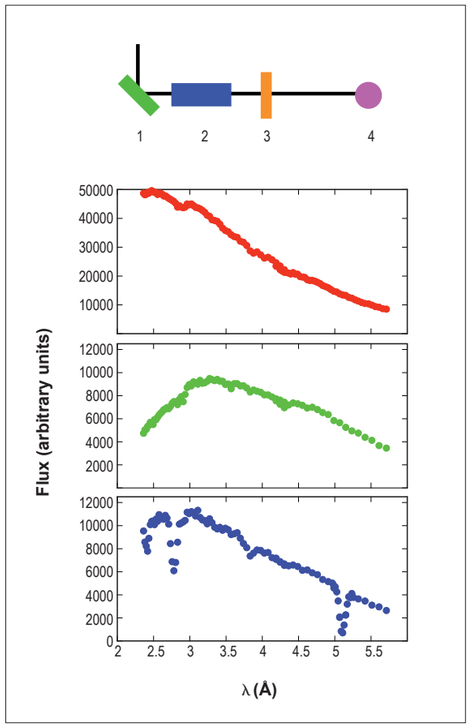

Figure 3:
(Top): Experimental set-up for flux measurements:
(1) PG(002) monochromator (green)
(2) S-bender, C-bender 20m or 60' Soller collimator (blue)
(3) Be filter (for λ > 4Å) (orange)
(4) Calibrated monitor (magenta)

(Second): Unpolarised flux vs. wavelength using a 60' Soller collimator. For wavelength λ > 4Å a Be filter was used to suppress higher orders. For wavelengths λ < 4Å the higher-order contamination was corrected for using previously determined monitor correction factors.

(Third): Polarised flux vs. incident wavelength using the IN14 C-bender with r = 20m. Same corrections as in panel above were applied.

*(Bottom): Polarised flux vs. incident wavelength using the new S-bender with a bender rotation RB = 1.5 (dashed line in **figure. 2**). Same corrections as in panel above were applied.*

REFERENCES

A. Stunault, K. H. Andersen, S. Roux, T. Bigault, K. Ben-Saïdane and H. M. Ronnow, Physica B 385-386 (2006) 1152-1154 **[1]**

ILL instruments

D1A (50%)	powder diffractometer	operational
D2B	powder diffractometer	operational
D3	single-crystal diffractometer	operational
D4 (50% with IN1)	liquids diffractometer	operational
D7	diffuse-scattering spectrometer	operational
D9	single-crystal diffractometer	operational
D10	single-crystal diffractometer	operational
D11	small-angle scattering diffractometer	operational
D16	small momentum-transfer diffractometer	operational
D17	reflectometer	operational
D19	single-crystal diffractometer	operational
D20	powder diffractometer	operational
D22	small-angle scattering diffractometer	operational
FIGARO	horizontal reflectometer	operational
IN1 (50% with D4)	three-axis spectrometer	operational
IN4	time-of-flight spectrometer	operational
IN5	time-of-flight spectrometer	operational
IN6	time-of-flight spectrometer	operational
IN8	three-axis spectrometer	operational
IN10	backscattering spectrometer	operational
IN11	spin-echo spectrometer	operational
IN14	three-axis spectrometer	operational
IN16	backscattering spectrometer	operational
IN20	three-axis spectrometer	operational
PF1	neutron beam for fundamental physics	operational
PF2	ultracold neutron source for fundamental physics	operational
PN1	fission product mass-spectrometer	operational
PN3	gamma-ray spectrometer	operational
SALSA	strain analyser for engineering application	operational
VIVALDI	thermal neutron Laue diffractometer	operational

CRG instruments

SuperADAM	reflectometer	CRG-B operational
BRISP	Brillouin spectrometer	CRG-B operational
CRYO EDM	installation for the search of the neutron electric dipole moment	CRG-C operational
D1B	powder diffractometer	CRG-A operational
D15	single-crystal diffractometer	CRG-B operational
D23	single-crystal diffractometer	CRG-B operational
GRANIT	gravitation state measurement	CRG under construction
IN12	three-axis spectrometer	CRG-B operational
IN13	backscattering spectrometer	CRG-A operational
IN22	three-axis spectrometer	CRG-B operational
S18	interferometer	CRG-B operational

Jointly funded instruments

DB21 (50%)	single-crystal diffractometer	operational with EMBL
LADI (50%)	Laue diffractometer	operational with EMBL
IN15	spin-echo spectrometer	operational with FZ Jülich and HMI Berlin

Test and characterisation beams

CT1, CT2	detector test facilities
CYCLOPS	Laue diffractometer
TOMOGRAPHY	neutrography
OrientExpress	Laue diffractometer
T3	neutron optics test facility
T13A, C	monochromator test facility
T17	cold neutron test facility

Neutron guide hall / ILL 22

Reactor operational level (D)

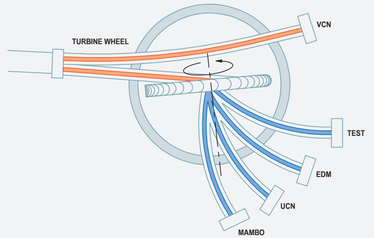

Reactor hall / Inclined guide H4

Neutron guide hall / ILL 7 - Vercors side (WEST)

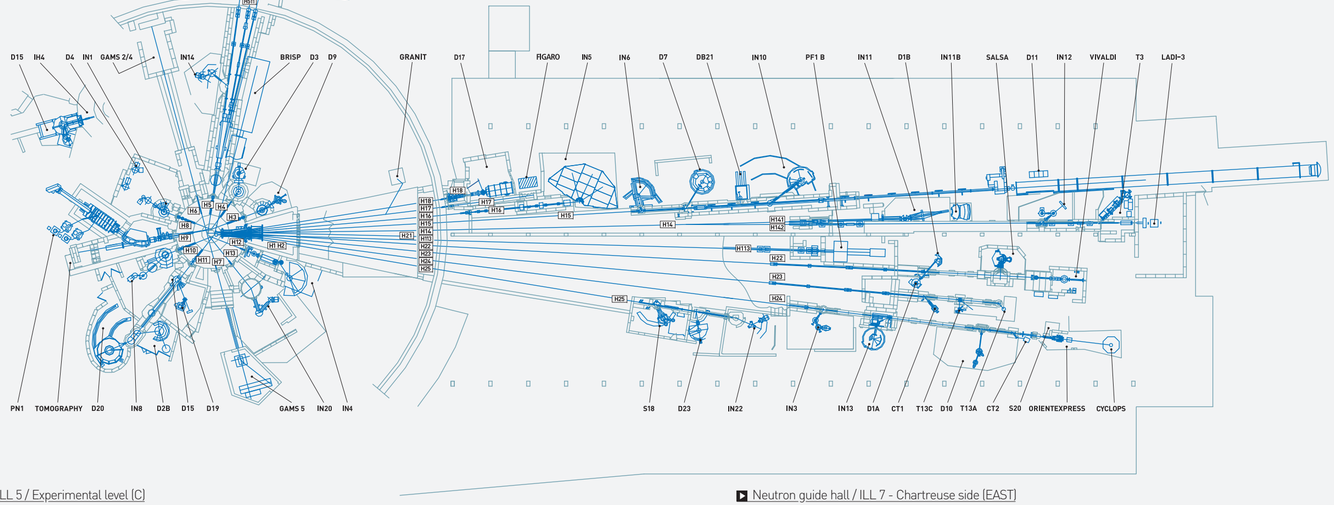

Reactor hall ILL 5 / Experimental level (C)

Neutron guide hall / ILL 7 - Chartreuse side (EAST)

MORE THAN SIMPLY NEUTRONS

SCIENTIFIC SUPPORT LABORATORIES ON THE ILL SITE

Partnership for Structural Biology
The Partnership for Structural Biology (PSB) contains a powerful set of technology platforms that are contributed by the various partner institutes (ILL, ESRF, EMBL, IBS, and the unit for host-pathogen interactions). These platforms include advanced capabilities that complement the powerful neutron scattering facilities available to ILL users: synchrotron X-rays, electron microscopy, NMR, high-throughput methods (soluble expression and crystallisation), and a range of biophysical techniques such as isothermal calorimetry and surface plasmon resonance. A joint SANS/SAXS platform is being developed and there is also an initiative to develop a joint X-ray/neutron low resolution crystallography capability. The aim of the PSB is to enhance the interdisciplinary capabilities of each of the facilities co-located on the site. Further details are provided on its website ***http://www.psb-grenoble.eu/***

Deuteration Laboratory
Of particular interest to ILL's biology users is the ILL-EMBL Deuteration Laboratory. The aim of the platform is to provide a focus for European scientists wishing to make their own deuterated materials for neutron scattering or NMR experiments. D-lab has had a decisive impact on biological neutron scattering at the ILL and it plays a key role for the user community, as the fact of having partially or totally deuterated molecules has now become essential to get beamtime. Information about the availability of this facility for external users is given at: ***http://www.ill.eu/sites/deuteration/index.htm***

Materials Science Support Laboratory
The joint ILL-ESRF Materials Science Support Laboratory provides a range of support to our users, from advice with experiment proposals to advanced sample metrology. In particular, the Laboratory works with users to optimise the experimental methodology before the start of an experiment. This takes the form of standardised specimen mounting, digitisation of samples, definition of measurement macros and liaising with the instrument responsible. It is recommended that users arrive at the ILL a day or two prior to the start of an experiment to enable these off-line preparations to be performed. The extra subsistence costs may be available from the SCO if requested beforehand. More information about this support may be found on the MSSL's website ***http://www.ill.eu/others/mssl/***

Partnership for Soft Condensed Matter
The Partnership for Soft Condensed Matter (PSCM) is an initiative first discussed back in 2004 that has seen considerable progress in the last few years. The PSCM, in the medium term, will provide a platform for promoting the complementary aspects of neutron and synchrotron techniques. The long-term mission of the PSCM is to streamline neutron and synchrotron based Soft Matter Research to address 21st century challenges in nanomaterials, biotechnology, environmental and energy sciences. New laboratories equipped for sample preparation and characterisation will be hosted in the new Science Building to be soon implemented on-site.

The ILL and ESRF have agreed on the programme for pursuing the collaboration. It involves developing together the scope and content of the partnership, demonstrating its feasibility with a well-defined scientific programme, and achieving a **Memorandum of Understanding**, which was signed on 27 November this year. The partnership demonstrates the long-term commitment of both Institutes to establishing and maintaining a SCM laboratory on their site.

A joint ILL-ESRF workshop was held on 16-18 December 2009, with the aim to gather potential Associate Partners, discuss the scientific agenda of the partnership as well as possibilities for external funding.

Further details are provided at ***http://www.ill.eu/instruments-support/labs-facilities/pscm/***

C-Lab
The Computation-Lab is offering support to ILL users for atomistic simulations using classical and ***ab initio*** methods. Typical applications for simulations are structure, magnetism and phonons in crystals and liquid/glass structure and dynamics. As samples become more complex, simulations can provide key, complementary information that will help to interpret experimental data and understand how systems behave.

Scientists and thesis students at the ILL benefit from the software, hardware and expertise of the C-Lab and users can benefit via their local contacts. In order to improve access to simulations for users, they are now able to request simulation support for their neutron scattering experiments on the official ILL proposal forms by ticking the appropriate box. For more information see ILL News N.47, June 2007 ***http://www.ill.eu/top-links/publications/ill-news/***

The ILL User Support Team is dedicated to helping all visiting researchers to make the most of ILL's facilities.
If you are coming to the ILL to carry out experiments, the User Office is here to give you the organisational and administrative support you need for the successful operation of your experiments. Neutron beams and instrument facilities are free of charge for proposers of accepted experiments.
Scientists affiliated to the Institute's member countries will also, in general, be assisted with necessary travel and daily subsistence for a limited period. The User Support Team makes all arrangements for accommodation and will process claims for expenses after you have completed your experiment.

In order to maintain their position on the international scene, European research institutes are optimising their resources and developing synergies at every level. The ILL - in collaboration with the ESRF and other institutes - is actively responding to our users' needs and new support facilities have been already set up on the site.

If you would like more information about the Institute's facilities, application for beamtime, user support and the experimental programme, please visit our web-site:
(http://www.ill.eu/users)

USER PROGRAMME

THE ILL VISITORS CLUB

All administrative tools for our scientific visitors are grouped together and directly accessible on the web, thanks to the Visitors Club. All information is presented in a user-friendly environment. After having logged in with your own personal identification[1], you will have direct access to all the available information which concerns you. Users with particular responsibilities have privileged access to other tools, according to their role. The ILL Visitors Club includes the electronic proposal and experimental reports submission procedures, and electronic peer review of proposals. Additional electronic services have also been put in place: acknowledgement of proposals, subcommittee results, invitation letters, user satisfaction forms and so on.

(1) *If you are not yet registered in the Visitors Club and you wish to join it, you can register directly at http://club.ill.eu/cv/.*

PROPOSAL SUBMISSION

There are different ways of submitting a proposal to the ILL:

- Standard submission - twice a year - via the Electronic Proposal System (EPS)
- Long-Term Proposals - once a year - via the Electronic Proposal System (EPS)
- EASY access system (EASY) throughout the year
- Director's Discretion Time (DDT) throughout the year
- Special access for proprietary research and industrial users

Submission of a standard research proposal

Applications for beamtime should be submitted electronically, via our Electronic Proposal Submission system (EPS), available on the Visitors Club web-site. Proposals can be submitted to the ILL twice a year, usually in March and in September. The web system is activated two months before each deadline.

Submitted proposals are divided amongst the different colleges (see **box below**) according to their main subject area.

The ILL scientific life is organised into 10 colleges:

College 1 - Applied Metallurgy, Instrumentation and Techniques
College 2 - Theory
College 3 - Nuclear and Particle Physics
College 4 - Magnetic Excitations
College 5A - Crystallography
College 5B - Magnetic Structures
College 6 - Structure and Dynamics of Liquids and Glasses
College 7 - Spectroscopy in Solid State Physics & Chemistry
College 8 - Structure and Dynamics of Biological Systems
College 9 - Structure and Dynamics of Soft-condensed Matter

Proposals are judged by a Peer Review Committee of the Subcommittees of the ILL Scientific Council. Subcommittee members are specialists in relevant areas of each College and they evaluate the proposals for scientific merit and recommend to the ILL Management the award of beamtime to the highest-priority proposals.

Before the meeting, the subcommittee receives a report on the technical feasibility and safety of a proposed experiment from the appropriate College at the ILL. Two proposal review rounds are held each year, approximately six weeks after the deadline for submission of applications.

There are normally 4 reactor cycles a year, each of which lasts 50 days. Accepted proposals submitted by March will receive beamtime in the second half of the year and those submitted by September, in the first half of the following year. More detailed information on application for beamtime and deadlines is given on our website at ***http://www.ill.eu/users/proposal-submission/.***

Easy Access System

The Easy Access System (EASY) grants diffraction beamtime to scientists from ILL member countries, who need a rapid structural characterisation of samples and data analysis. Access is open all year long, and it does not go through the ILL standard proposal round and consequent peer review system.

The system offers one neutron day per cycle, on five instruments (D1A, D2B, D16, VIVALDI and OrientExpress) to perform very short experiments at room temperature. The users will not be invited to the ILL, but will send their samples to one of two designated ILL scientists, who will be responsible for the measurements and sample radiological control. The ILL will ship back the sample once the measurement is finished. You can apply for EASY beamtime on the Visitors Club. More information is available at ***http://club.ill.eu/cvDocs/EASY_Guidelines.pdf.***

Long-Term Proposals

Users from ILL member countries can also apply for extended periods of beamtime, by submitting a Long-Term Proposal (LTP). The purpose of the scheme is to facilitate users to develop instrumentation, techniques or software through the award of beamtime over several cycles. Both the ILL Scientific Council and the ILL Management believe that LTPs could be beneficial to the ILL community as a whole, bringing extra resources or capabilities, so it was launched for a trial period of three years in the scheduling round of autumn 2008. The total amount of beamtime that may be allocated to LTPs on any particular instrument is capped at 10%, and beamtime is not awarded to LTPs to perform science beyond essential testing.

LTPs can be submitted once a year at the autumn proposal round using the specific LTP application form. The primary criterion for acceptance of a LTP is the excellence of the science that it will ultimately enable. The length of LTP projects is expected to be 3 years typically, with continuation approved at the end of each

year, based on an annual report; a final report is also required at the end of the project. More details are given at ***http://www.ill.eu/users/proposal-submission/.***

Submission of a proposal to the Director's Discretion Time
This option allows a researcher to obtain beamtime quickly, without going through the peer-review procedure. DDT is normally used for 'hot' topics, new ideas, feasibility tests and to encourage new users. Applications for Director's Discretion Time can be submitted to the Head of the Science Division, Prof. Andrew Harrison, at any time.

Access for proprietary research and industrial users
The ILL's mission is to provide neutrons for both public and industrial research. Our Industrial Liaison and Consultancy Group (ILC) ensures rapid access and total confidentiality for industrial companies, and provides specialised technical and scientific support. The ILC Group is composed of scientists with considerable experience and expertise in neutron techniques applied to industrial R&D, and it facilitates and coordinates all aspects of industrial R&D at the ILL: initial enquiries, contractual questions, planning, experimental operations. To apply for proprietary beamtime, please contact the ILC Group at ***industry@ill.eu*** or consult the web site under ***http://www.ill.eu/industry/.***

Experimental reports
Users are asked to complete an experimental report on the outcome of their experiments. The submission of an experimental report is compulsory for every user who is granted ILL beamtime. Failure to do so may lead to rejection in case of application for beamtime for a continuation proposal.
All ILL Experimental Reports are archived electronically and accessible via the web server as PDF files (under ***http://club.ill.eu/cv/***). You can search for a report by experimental number, instrument, college, date of experiment, title, institute, experimental team or local contact.
Experimental reports for experiments performed in 2009 are included in the CD-ROM of this year's Annual Report.

COLLABORATIVE RESEARCH GROUP INSTRUMENTS

The ILL provides a framework in which Collaborating Research Groups (CRGs) can build and manage instruments on ILL beamlines to carry out their own research programmes. CRGs represent a particularly successful form of long-term international scientific collaboration.
CRGs are composed of scientists from one or two research disciplines, and often multinational, carrying out a joint research programme centred around a specific instrument. CRGs enjoy exclusive access to these instruments for at least half of the beamtime available. The CRGs provide their own scientific and technical support and cover the general operating costs of these instruments. If there is demand from the user community and the resources are available, the beamtime reserved for ILL can be made accessible to users via the subcommittees.

USER AND BEAMTIME STATISTICS

THE ILL USER COMMUNITY

The ILL welcomed 1316 users in 2009, including 284 from France, 263 from Germany and 282 from the UK (**figure 1**). Many of our visitors were received more than once (for a totalof 2116 visits).

We value feedback from our users as an indicator of how well our facility is fulfilling their needs and to initiate actions when this is not the case. The *User Satisfaction Form* is a means of finding out what our users think of the facility. Users who have just finished an experiment at the ILL are asked to complete the questionnaire on the Visitors Club and give us their views on different topics. User comments are made available to managers for their information and actions when appropriate.

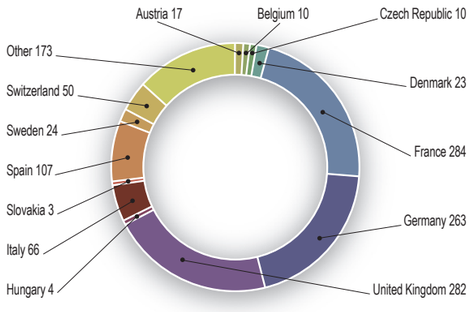

Figure 1: *National affiliation of ILL users in 2009.*

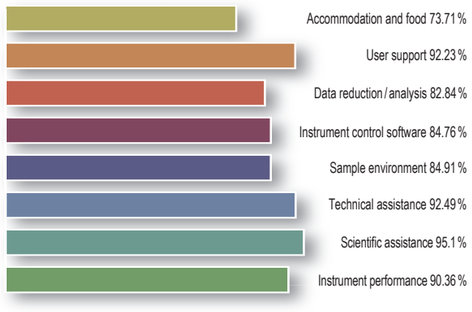

Figure 2: *User satisfaction survey results for 2009.*

INSTRUMENTS

The instrumental facilities at the ILL are shown in the schematic diagram on page 98.
Besides the 28 ILL instruments, there are 10 CRG-instruments, which are operated by external Collaborating Research Groups to carry out their own research. There are currently three different categories of CRG instruments.
- CRG-A in which the external group leases an instrument owned by the ILL. They have 50% of the beamtime at their disposal and for the remaining 50% they support ILL's scientific user programme.
- The CRG-B category owns their instrument and retains 70% of the available beamtime, supporting the ILL programme for the other 30%.
- Finally, CRG-C instruments are used full time for specific research programmes by the external group, which has exclusive use of the beam.

DB21, LADI and IN15 have a special status, since they are joint ventures of the ILL with other laboratories: in the case of DB21 and LADI with EMBL and for IN15 with FZ Jülich and HMI Berlin. Cryo-EDM is a CRG-C instrument and is not available as a 'user' instrument.
The list of instruments as of December 2009 is summarised below (CRG instruments are marked with an asterisk *):

- powder diffractometers: D1A, D1B*, D2B, D20, SALSA
- liquids diffractometer: D4
- polarised neutron diffractometers: D3, D23*
- single-crystal diffractometers: D9, D10, D15*
- large scale structures diffractometers: D19, DB21, LADI, VIVALDI
- small-angle scattering: D11, D22
- low momentum-transfer diffractometer: D16
- reflectometers: SuperADAM*, D17, FIGARO
- diffuse scattering and polarisation analysis spectrometer: D7
- three-axis spectrometers: IN1, IN3, IN8, IN12*, IN14, IN20, IN22*
- time-of-flight spectrometers: BRISP*, IN4, IN5, IN6,
- backscattering and spin-echo spectrometers: IN10, IN11, IN13*, IN15, IN16
- nuclear physics instruments: PN1, PN3
- fundamental physics instruments: PF1, PF2, S18*

Details of the instruments can be found on the web at ***http://www.ill.eu/instruments-support/instruments-groups/.***

In early 2010, the small momentum transfer cold neutron diffractometer D16 and the low resolution neutron crystallography diffractometer DB21 have merged in the ILL22 guide hall.

BEAMTIME ALLOCATION & UTILISATION FOR 2009

Overall, the Subcommittees of the Scientific Council examined 1 272 proposals requesting 8 471 days for 2009, out of which 817 proposals received beamtime, allocating 4 768 days of beamtime on the different instruments.
The distribution of beamtime requested and allocated amongst the different countries is shown in **Table 1**. In 2009, the member countries of the ILL were: France, Germany, UK, Austria, Belgium, the Czech Republic, Denmark, Hungary, Italy, Slovakia, Spain, Sweden and Switzerland. Poland was considered a member country only for the beamtime allocation of the first two cycles of the year, because its contract was not renewed.

Table 1a*: Distribution amongst the different countries of beamtime requested and allocated in 2009 during the Subcommittees of the Scientific Council.*

All countries		Before national balance			After national balance	
Country	Requested days	Requested in %	Allocated days	Allocated in %	Allocated days	Allocated in %
AE	0.29	0.00	0.29	0.01	0.29	0.01
AR	5.29	0.06	0.00	0.00	0.00	0.00
AT	**79.06**	**0.93**	**50.43**	**1.04**	**51.73**	**1.08**
AU	82.62	0.98	49.57	1.02	47.41	0.99
BE	**64.80**	**0.76**	**29.70**	**0.61**	**29.70**	**0.62**
BG	6.14	0.07	2.64	0.05	2.94	0.06
BW	2.00	0.02	0.00	0.00	0.00	0.00
BH	0.86	0.01	0.86	0.02	0.86	0.02
BR	9.62	0.11	7.40	0.15	7.40	0.16
BY	1.00	0.01	0.60	0.01	0.60	0.01
CA	23.93	0.28	13.77	0.28	13.77	0.29
CH	200.03	2.36	103.88	2.14	106.28	2.23
CN	16.67	0.20	16.50	0.34	16.50	0.35
CZ	**65.10**	**0.77**	**38.08**	**0.78**	**38.08**	**0.80**
DE	**1449.32**	**17.11**	**805.47**	**16.60**	**819.51**	**17.16**
DK	85.05	1.00	48.55	1.00	48.55	1.02
EG	4.00	0.05	0.00	0.00	0.00	0.00
ES	**357.40**	**4.22**	**204.41**	**4.21**	**207.00**	**4.33**
ESRF	**70.84**	**0.84**	**41.78**	**0.86**	**41.94**	**0.88**
FI	28.38	0.33	8.13	0.17	8.13	0.17
FR	**1223.01**	**14.44**	**785.58**	**16.19**	**786.78**	**16.47**
GB	**1588.78**	**18.75**	**1014.76**	**20.91**	**1009.97**	**21.15**
GR	7.93	0.09	4.33	0.09	4.33	0.09
HK	0.50	0.01	0.00	0.00	0.00	0.00
HU	**22.27**	**0.26**	**4.92**	**0.10**	**4.92**	**0.10**
IE	7.53	0.09	4.37	0.09	4.37	0.09
IL	3.00	0.04	0.00	0.00	0.00	0.00
ILL	**1411.89**	**16.67**	**832.88**	**17.17**	**820.88**	**17.19**
IN	70.04	0.83	26.21	0.54	26.21	0.55
IT	**473.58**	**5.59**	**215.68**	**4.45**	**215.68**	**4.52**
JP	73.86	0.87	43.09	0.89	39.19	0.82
KR	6.76	0.08	5.05	0.10	5.05	0.11
LT	0.67	0.01	0.00	0.00	0.00	0.00
MY	40.00	0.47	0.00	0.00	0.00	0.00
MX	2.00	0.02	2.00	0.04	2.00	0.04
NL	43.63	0.52	27.32	0.56	31.32	0.66
NO	6.27	0.07	3.00	0.06	3.00	0.06
NZ	0.43	0.01	0.43	0.01	0.43	0.01
PL	**92.23**	**1.09**	**31.82**	**0.66**	**31.82**	**0.67**
PT	5.93	0.07	4.77	0.10	4.77	0.10
RO	0.67	0.01	0.33	0.01	0.33	0.01
RU	183.74	2.17	100.22	2.07	59.39	1.24
SE	**123.89**	**1.46**	**49.57**	**1.02**	**49.57**	**1.04**
SG	2.60	0.03	2.60	0.05	2.60	0.05
SK	**11.00**	**0.13**	**4.33**	**0.09**	**4.33**	**0.09**
TH	8.00	0.09	8.00	0.16	8.00	0.17
UA	15.35	0.18	2.40	0.05	2.40	0.05
US	477.91	5.64	244.84	5.05	192.94	4.04
ZA	15.92	0.19	11.50	0.24	11.50	0.24
Total	*8471*	*100.00*	*4852*	*100.00*	*4768*	*100.00*

In calculating the statistics of beamtime per country, shown in ***Table 1a***, the attribution is based on the location of the laboratory of the proposers, not their individual nationality.

Only member countries		Before national balance			After national balance	
Country	Requested days	Requested in %	Allocated days	Allocated in %	Allocated days	Allocated in %
AT	135.07	1.66	76.66	1.62	77.24	1.65
BE	86.11	1.06	36.95	0.78	36.52	0.78
CH	299.51	3.68	172.65	3.64	172.66	3.69
CZ	108.41	1.33	46.13	0.97	45.74	0.98
DE	**2116.11**	**25.99**	**1164.87**	**24.55**	**1158.05**	**24.76**
ES	471.72	5.79	263.35	5.55	262.83	5.62
FR	**1911.84**	**23.48**	**1189.09**	**25.06**	**1164.02**	**24.88**
GB	**2247.55**	**27.60**	**1416.68**	**29.85**	**1386.47**	**29.64**
HU	33.90	0.42	10.29	0.22	9.90	0.21
IT	564.72	6.93	266.39	5.61	263.70	5.64
PL*	70.31	0.86	28.87	0.61	28.65	0.61
SE	244.44	3.00	69.14	1.46	67.98	1.45
SK	9.10	0.11	4.21	0.09	4.13	0.09
Total	***8143***	***100.00***	***4745***	***100.00***	***4678***	***100.00***

***Table 1b**: Distribution amongst the Associate and scientific-member countries of beamtime requested and allocated in 2009 during the Subcommittees of the Scientific Council.*

For a proposal involving laboratories from more than one member country, the total number of days is divided amongst the collaborating countries, and weighted by the number of people for each country. Local contacts are not counted as proposers except when they are members of the research team.

In **Table 1b**, the beamtime requested by and allocated to ILL, ESRF and EMBL is amongst the member countries according to their financial contributions to the Institutes. In this same table, when a proposal involves collaboration with a non-member country, the allocated time is attributed entirely to the collaborating member country (or countries), and weighted by the number of people for each member country. Proposals for which all proposers are from non-member countries therefore do not appear in this table.

***Figure 3:** Beamtime allocation in 2009: distribution amongst the different colleges.*

A more complete view about beamtime use is given in **Table 2.** Request and allocation of beamtime as well as the number of scheduled experiments refer to standard submissions to the subcommittee meetings. The effective number of days given to our users takes into account also Director's Discretion Time and CRG time for CRG instruments.

INSTRUMENT PERFORMANCE

Table 2 also gives a summary of instrument performance for 2009. For each cycle, a record is kept of any time lost from the total available beamtime and the reasons for the lost time are analysed for all the instruments. The table gives a global summary for the year.
Overall 6181 days were made available to our users in 2009 on ILL and CRG instruments, which represents about 78 % of the total days of operation. 554 days were used by ILL scientists to carry out their own scientific research. About 12 % of the total beamtime available on the ILL instruments is allowed for tests, calibrations, scheduling flexibility, minor breakdown recuperation and students training.

Beam days delivered for science in 2009 amount to 6735 (used for users and internal research).

A total of 871 experiments were scheduled. During 2009 the reactor operated for 4 cycles, representing 200 days of neutrons (see § **Reactor Operation, p.109**).

In 2009, 377 out of 7975 days were lost due to various malfunctions, which represent less than 5 % of the total available beamtime. The breakdown by reasons for beamtime losses is shown in **figure 4b**.

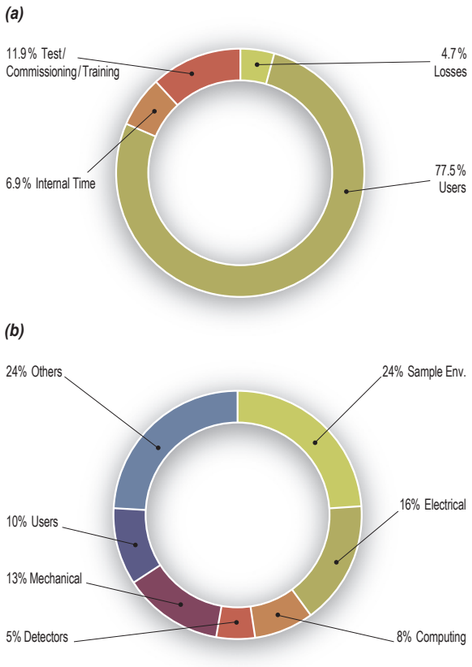

***Figure 4: (a)** Use of ILL beamtime **(b)** Reasons for beamtime losses.*

Instrument	Days requested	Days allocated*	Number of scheduled experiments	Available days	Days used for users**	Days lost	Days for commissioning /test/training	Days for internal research
SuperADAM	**23**	**7**	**2**	**100**	**7**	**0**	**93**	**0**
BRISP	**221**	**61**	**6**	**197**	**149**	**3**	**24**	**21**
D10	271	173	23	197	174	4	10	10
D11	230	94	44	197	151	2	42	2
D15	**38**	**38**	**4**	**197**	**149**	**15**	**11**	**22**
D16	145	132	20	197	137	23	37	1
D17	225	132	36	197	156	3	27	12
D19	209	156	19	196	139	0	36	21
D1A	107	100	33	197	123	0	20	54
D1B	**112**	**87**	**33**	**197**	**167**	**1**	**28**	**1**
D20	316	137	55	197	174	5	10	10
D22	525	124	51	197	145	6	32	14
D23	**121**	**56**	**8**	**197**	**160**	**9**	**16**	**12**
D2B	210	146	59	197	166	1	16	14
D3	165	115	14	197	133	11	43	10
D4	182	104	23	147	123	8	9	7
D7	233	143	22	197	174	11	13	0
D9	201	137	19	197	166	22	5	4
DB21	115	96	11	197	82	68	28	19
FIGARO	158	90	29	197	99	22	76	0
IN1	50	32	5	50	30	1	15	5
IN10	49	123	13	197	134	4	41	19
IN11	311	131	17	197	165	11	13	8
IN12	**83**	**51**	**7**	**197**	**180**	**4**	**13**	**0**
IN13	**167**	**84**	**16**	**193**	**165**	**3**	**18**	**7**
IN14	431	153	23	197	161	3	15	19
IN15	284	89	12	197	144	7	26	20
IN16	303	151	28	197	163	4	22	8
IN20	195	150	21	197	159	4	22	12
IN22	**83**	**49**	**8**	**197**	**193**	**3**	**1**	**0**
IN4	215	131	31	197	168	7	16	7
IN5	290	126	33	197	154	6	30	7
IN6	277	146	35	197	166	4	12	15
IN8	205	114	16	197	146	13	20	18
LADI	285	145	13	197	187	1	5	4
PF1B	325	190	4	197	197	0	0	0
PF2	170	125	7	197	130	3	24	31
PN1	309	157	14	197	131	36	23	7
PN3	218	163	5	197	169	23	12	89
S18	**99**	**68**	**3**	**197**	**158**	**17**	**7**	**15**
SALSA	175	137	27	197	164	7	17	9
VIVALDI	140	125	22	197	146	5	24	22
Total	***8471***	***4768***	***871***	***7975***	***6181***	***377***	***950***	***554***
Percentage of the total available beamtime					***77.5%***	***4.7%***	***11.9%***	***6.9%***

** days allocated refers to only those days reviewed by the subcommittees (i.e., excluding CRG days and DDT)*
*** days used refers to the total number of days delivered to users (i.e., including CRG days for CRGs and DDT)*
PF2 consists of 5 different set-ups where several experiments are running simultaneously. The values given are averages for these 5 positions.
D4 and IN1 share the same beam port and cannot be run simultaneously.

***Table 2**: Beamtime request/allocation (via standard subcommittees and DDT together) by instrument and instrument performance. CRG instruments are in blue.*

Detailed comments on the larger beamtime losses (above 25 days) are as follows:
- **DB21** 68 days lost, most of them because samples were not ready for a number of scheduled experiments;
- **PN1** lost 31 days because of electronics failures.

ILL 2020 VISION

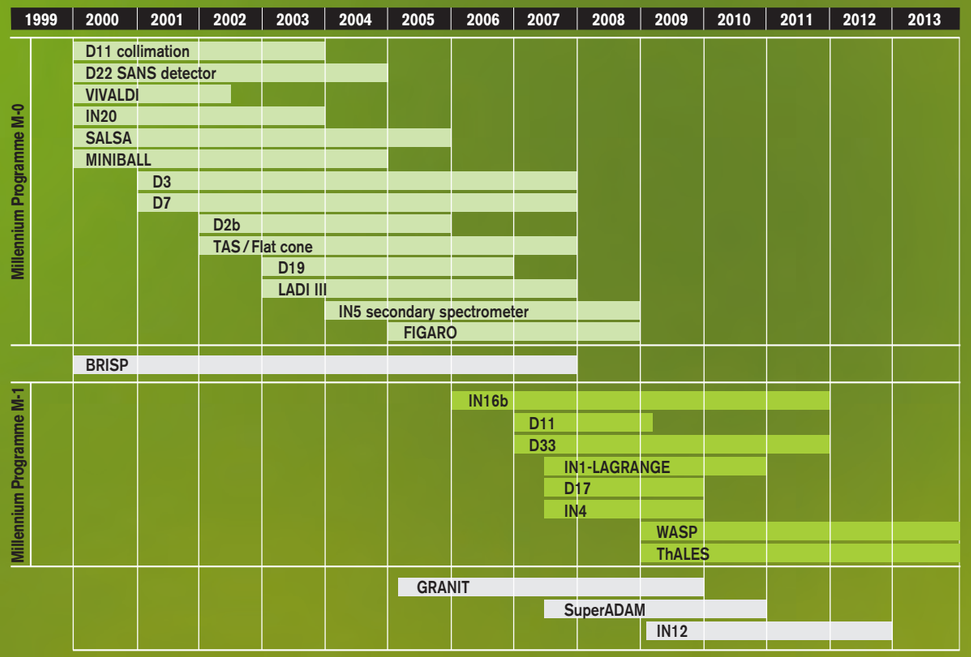

***Figure 2**: Millennium Programme time-table past, present and near-future, divided into the completed (M-0) phase and the current (M-1) phase. BRISP, IN12, SuperADAM and GRANIT are displayed slightly differently because they are largely or entirely funded through external bodies.*

The Millennium Programme has furnished our user community with 14 new or renovated instruments, replaced many guides with higher-reflectivity models, and upgraded much of the sample environment equipment, leading to an increase in the average neutron detection rate across the instrument suite by a factor of almost 20 (figure 1). Funding and planning are in place to maintain the momentum of the Programme to 2014, delivering many new or upgraded instruments (figure 2). Now is the time to ask the question 'what next ?'

Since 2007 the process of planning for the future has been supported by ESFRI - the European Strategy Forum for Research Infrastructures - through its 2006 European Roadmap programme.

ILL's project outlined a strategy largely based on new technologies. Besides the construction of new instruments it included the delivery of both hot and cold neutrons, the production of ultra-cold neutrons, and plans for a third cold neutron source. It also included a benchmarking exercise to assess the performance of instruments in our suite compared to those at long- and short-pulse spallation sources – based both on current specifications of our instruments and the limits of what is currently possible. This exercise was given a new focus in 2009 with the decision that the site for a future long-pulse European Spallation Source (ESS) would be Lund, Sweden. However, it will take a minimum of 10-15 years for such a source to build up to full operating strength and for at least that period the community will continue to need a spectrum of instruments across a broad range of incident energy. Beyond then, it could be argued, ILL should focus more on areas which are inherently better suited to reactor sources: measurements at single values of (Q,ω) – *e.g.* cryopad, triple-axis spectroscopy, single-crystal diffractometers; hot neutrons; Bragg optics, enabling large incoming solid angle with focusing devices. In addition, reactor sources inherently provide more stable flux where long, continuous exposures are crucial, for example during kinetic measurements, and when differences between data sets of long exposure time are needed.

Armed with such information, together with an analysis of current and emerging scientific and societal challenges that can be met with neutron methods, and the size and strength of the communities that would be served, we have started to draw up plans for future upgrades to the instrument suite, aiming for the period 2013 – 2017.

The user community has been invited to submit its own suggestions for new instrumentation and infrastructure, to be presented and discussed at the 'ILL 2020 Vision' User Meeting from 15 - 17 September 2010 (http://www.ill2020-vision.eu). Such a vision needs to consider every step in the path - from user access routes and proposals, to the measurement of data and its final analysis. The success of the science we support depends on much more than our hardware: building on the models used to establish the successful Partnership for Structural Biology, we have now launched a Partnership for Soft Condensed Matter and are working on plans for a new Partnership for Extreme Conditions Science.

All of these ventures are in partnership with the ESRF, and the PSB also draws on the strengths of the Grenoble outstation of the European Molecular Biology Laboratory, underlining the benefits of closer ties between these three institutes. In recognition of this, we have found a name for our common site – the European Photon and Neutron science campus - or 'EPN science campus', for short. And since the beginning of February it has also a dedicated web site http:

www.epn-campus.eu/

the first tangible result of this new union.

The aim of this new web site is to provide our visitors with the latest news on our activities and practical information for their visit. In the near future ILL and ESRF users will be able to access the two Institutes' online user portals (for proposal submissions for instance) via a single log-on.

***Figure 1:** Increase in gain factor for average integrated detection rate across the ILL instruments compared to that in 2002 (line connecting points) as well as the development in recent years of the number of submitted proposals (bars). Note that the anomaly in 2005 is due to the fact that there was just one scheduling round, and the corresponding data fall below the bottom of the scale.*

This ILL High-Flux Reactor (HFR) produces the most intense neutron flux in the world: 1.5 x 10^{15} neutrons per second per cm^2, with a thermal power of 58.3 MW.

The reactor normally operates 50-day cycles, with each cycle of operation followed by a shutdown period during which the fuel element is changed and a number of checks are carried out. Occasional longer shutdowns allow for equipment maintenance. There are normally 4 reactor cycles per year, supplying 200 days of neutron flux for scientific use.

The ILL reactor normally operates four 50-day cycles per year, producing 200 days of beamtime for the experimental programme

As part of the ILL's determination to guarantee the safety and reliability of its facilities over future years, the Reactor Division runs a 'key reactor components programme', the aim of which is to ensure the development and replacement as necessary of the essential main components of the reactor. The current plans under this programme cover the period up to 2017.

The reactor ran impeccably throughout 2009 and provided for 197 days of scientific activity. In August the fuel element was kept in position in the reactor block; this reduced our possibilities for work on the reactor, but some major operations were nevertheless performed during the longer shutdowns.

Overall, however, the shutdowns over the year were reduced to the minimum necessary for regular testing, inspections and pre-start-up procedures; this ensured that the 4 cycles could be delivered as scheduled.

Even the second cycle went ahead as planned, despite vacuum problems on the cold source cryogenic systems; no beamtime was lost, thanks to major efforts by the staff.

In a nutshell: **100% reactor availability in 2009!**

Cycle no.	Start of cycle	End of cycle	Number of days of operation	Number of days of scheduled	Number of unscheduled shutdowns
154	10.03.09	29.04.09	50	50	0
155	14.05.09	03.07.09	50	50	0
156-1	16.07.09	31.07.09	15	15	0
156-2	24.08.09	25.09.09	32.1	32	0
157	08.10.09	27.11.09	50	50	0
Total			***197.1***	***197***	***0***

The Key Reactor Components Programme continues

The ILL continues to invest in the Key Reactor Components programme, designed to ensure the long-term safety and reliability of the reactor.
The aim is to replace or upgrade a number of key components. Work on this started in 2005 and our plans now extend to 2017, the date of the next ten-yearly safety review by the nuclear authorities.

The operations so far completed include amongst others: the upgrade of the vertical cold source's out-of-pile systems and the manufacture of new safety rods.
We also procured sufficient AG3NET aluminium alloy to satisfy requirements for the manufacture of reactor parts up to the year 2030 (beamtubes, new parts), which need to be regularly replaced because of the severe neutron radiation.

The seismic reinforcement of the polar crane was also completed in 2009. We finished all the work and investigations required to ensure the crane's stability under Safe Shutdown Earthquake conditions in time for its period of intensive use, the long winter shutdown 2009-2010.
A study is now underway to further reinforce the crane for its operation under rotation (some 20 hours of use annually).

Operations foreseen during the long 2010 winter shutdown

There will be no shortage of work for the future of this programme. The long 2010 winter shutdown will be used to perform a number of important operations, such as:

- Installation of three important safety systems as part of our reactor safety plan (the emergency core reflood system, the containment depressurisation system and the gaseous decay tank).
- Replacement of the gamma-ray monitoring channels and installation of new filters for the Drac river water intake; this will maintain the high levels of performance of the cooling circuits.
- There are also plans, at a later stage, for amongst others: the manufacture of beamtubes and a spare vertical cold source (2013/2014 if possible) and the replacement of various monitoring systems.

The Reactor Division teams are working together with a great sense of team spirit, taking up new challenges and ensuring that we are ready for the next safety review in 2017!

Radioactive waste and effluents

The ILL's activities in 2009 generated waste and effluents respecting the regulatory limits applicable to our installation, as follows:

Evacuation of radioactive waste	Quantity
Decay bin (60l)*	0
5m³ pre-concreted crate (low and intermediate level waste)	0
5m³ crate (low and intermediate level waste)	9
200l drums of 'incineratable' (low-level waste)	0
HDPE drums 120l (low-level waste)	7

** Waste stocked in these decay bins is still quite active and requires several years of interim storage before meeting ANDRA's specifications for processing as intermediate-level waste.*

Gaseous effluents	Released in 2009 (TBq)
Tritium	1.2E+01
Rare gas	1.4E+00
Carbon 14	7.6E-01
Iodine	5.4E-06
Aerosols	1.8E-08

Liquid effluents	Released in 2009 (TBq)
Tritium	3.2E-02
Carbon 14	1.1E-04
Iodine	8.2E-07
Other activation products	3.3E-05

The new air-conditioning system for the ILL reactor. Copyright: Bernhard Lehn, Fotodesign, studio@bernhardlehn.de.

Copyright: Bernhard Lehn, Fotodesign, studio@bernhardlehn.de.

Workshops and schools in which the ILL was a major player in 2009

FullProf School 2009
http://www.ill.eu/news-events/events/past-events/fpschool-2009/
26 - 30 January

HERCULES
Higher European Research Course for Users of Large Experimental Systems, practicals at ILL.
1 March - 4 April

Symposium in honour of Francis Tasset
http://www.ill.eu/news-events/events/past-events/symposium-francis-tasset-march-2009
6 March

Course on Software Development for Crystallography
http://www.ill.eu/news-events/events/past-events/csdc/
15 - 19 June

Workshop on neutron delivery systems
http://www.ill.eu/news-events/events/past-events/nds/
1 - 3 July

SKIN 2009 workshop
http://www.ill.eu/news-events/events/ past-events/skin2009/
5 - 7 October

TiCN'ToF workshop
http://www.ill.eu/news-events/workshops-events/ticntof/
26 - 28 November

PSCM workshop
http://www.ill.eu/news-events/events/pscm2009/
16 - 18 December

Short reports on the ILL workshops can be found in the 'ILL News for Reactor Users' (June and December 2009 issues)
http://www.ill.eu/top-links/publications/ill-news/

ILL chronicle 2009

20 January	Visit of a group of German journalists
22 January:	Visit by the Deans of the University of Copenhagen (Denmark)
29 January:	Visit of the Swedish Research Council (Prof. Dan Holstam)
13 March & 10 April:	Visits of delegations from 'la Metro' (the Grenoble urban agglomeration)
6 April:	Visit of Christos Profilis from the European Commission DG REsearch
14 April:	ILL PhD students clip session
17 April:	Visit of John Womersley, the STFC Director of Science Programmes
20 April:	Visit of the ESS-Scandinavia team
21 - 24 April:	Meetings ILL Scientific Council and its Subcommittees
28 April:	Visit of a delegation of the China Institute of Atomic Energy (Prof. Chen, Prof. Peng, Prof. Yue)
29 - 30 April:	Meeting of the Subcommittee on Administrative Questions (SAQ)
18 June:	Heads of Service outdoor meeting
25 - 26 June:	Meeting of the Steering Committee in Munich (Germany)
1 July:	Denmark joins the ILL
9 September:	Visit of Yves Caristan, Director of CEA/Saclay and DSM
26 - 27 September:	ILL Open Day
22 - 23 October:	Meeting of the Subcommittee on Administrative Questions (SAQ)
12 November:	Visit of a delegation of the U.S. Department of Energy (Prof. W.F. Brinkman, Dr. J.S. Binkley, Ms R. Gonzalez)
17 - 20 November 2009:	Meetings of ILL Scientific Council and its Subcommittees
23 November:	Visit of a CNRS delegation (Ms G. Chambaud, M. B. Girard)
30 November:	Visit of the chair of the STFC Scientific Council (Prof. M. Sterling)
26 - 27 November:	Meeting of the Steering Committee meeting in Grenoble

Visits & events

ILL Open Days

The CNRS at the ILL: the directors of the Chemistry Institute and the Physics Institute, Mme Gilberte Chambaud and Mr Bertrand Girard, respectively, on tour at ILL during their visit to Grenoble.

Participants in the ILL PhD students clip session, held on 14 April.

Prof. John Womersley (STFC Director of Science Programmes, front right) and Jennifer Scratcher (STFC Programme manager) on a guided tour of our facilities with the ILL Directors (José Luis Martínez, Richard Wagner and Andrew Harrison).

The Deans of the University of Copenhagen are welcomed by Andrew Harrison - far left - and Sine Larsen (Directors of Science at the ILL and ESRF, respectively) during their visit on 22 January.

ILL welcomes a delegation of the U.S. Department of Energy on 12 November: Richard Wagner accompanies Dr J.S. Binkley (Director of Science, left) and Prof. W.F. Brinkman (Senior Advisor, right) on a visit of the ILL reactor.

Prof. Chen, Prof. Peng and Prof. Yue, China Institute of Atomic Energy, visit the ILL facilities on 28 April.

The ILL staff welcome the Grenoble public to the site during the Open Days, held on 26-27 September.

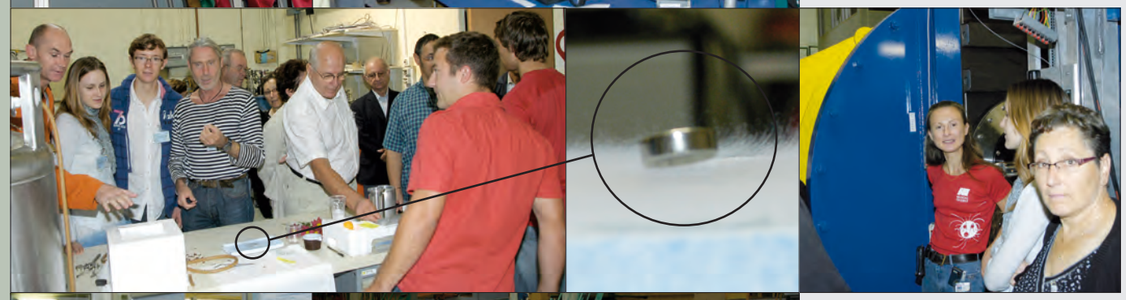

Happy scientists and users

Cristina Fernandez-Martin from Corning SAS on D22.

Marion Jasnin (MPI Martinsried, Germany) on IN6.

Marco Maccarini (second from the left) and Peter Fouquet (second from the right) on their instrument IN11 with two PhD students from Bayreuth (Germany): Yvonne Hertle, and Michael Zeiser.

Helmut Schober and Mohamed Zbiri on their way to check an exciting experiment on IN6.

Mette Schmokel from the University of Aarhus (Denmark) on D9, performing an experiment with Garry McIntyre.

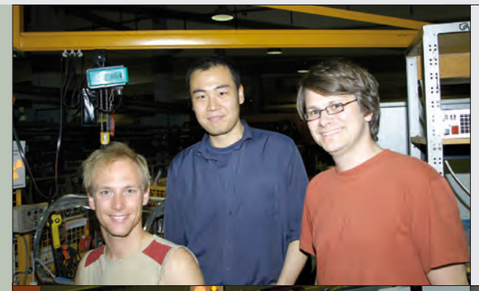

A PERKEO III user group photo (from left to right): Dominik Werder (diploma student, University of Heidelberg), Xiangzun Wang (TU Vienna), and Bastian Maerkisch (at that time University of Heidelberg).

Darren Hughes on SALSA with Sayeed Hossain and Simon Lewis (University of Bristol).

Hannu Mutka helping Michael Baker (thesis student ILL/Manchester) and Rebecca Docherty (thesis student Manchester) on their IN5 experiment.

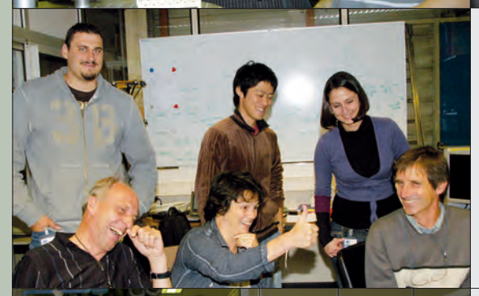

Bernhard Frick (front right) on IN16 with a team of very happy users! Back row, left to right: Linas Vilciauskas (MPI Stuttgart), Ken Akizuki (Nissan, Japan, currently at CEA Grenoble), Carla C. de Araujo (MPI Stuttgart); front from left: Klaus-Dieter Kreuer (MPI Stuttgart), Sandrine Lyonnard (CEA Grenoble).

'Beato fra le donne!' Phil Callow with some of the students of the PSB SAXS/SANS course held in April. From left: Bettina Hartlieb, Juliette Devos, Manuela Delvecchio and Marion Sevajol.

ADMINISTRATIVE MATTERS

2009 was a busy year for the Administrative Division, charged with many and varied projects essential for ILL to develop and thrive.

There is the constant but crucial need to respond to changes in legislation that will have a big impact on our future. We are now required to demonstrate to the French government that our Associates are willing and able to finance eventual decommissioning costs, and to incorporate such a statement in the Intergovernmental Convention that binds them together to support us. There were initial concerns that this would force the discussions to extend the Convention to be brought forward from 2013 to 2011. However, a dedicated ILL working group - working closely with our Associates to solve legal and technical problems - has secured agreement to retain the later date for extension.

Another change in law concerns the new right of staff to work to 70 rather than 65 if they wish. This obliged us to review and renegotiate the whole framework of agreements on retirement. It was particularly complex to find a solution for staff on shift work or who perform arduous duties and who may retire early (Cessation Anticipée d'Activité or CAA). 6 months of negotiation secured an accord both for staff already covered by the CAA scheme, and due to qualify for early retirement after 1 January 2010, the date on which the new French legislation came into effect.

Progress has also been made with the 'Jobs, skills and recognition project', which aims to improve career perspectives for ILL staff, increase internal mobility and strengthen collective performance. Extensive engagement by many staff to establish a common understanding of the nature of their jobs enabled the definition of 55 ILL job profiles and their respective responsibilities. The next phase, planned for 2010, is the definition of the skills associated with each job profile and will mark a further step in equipping ILL to meet the challenges in an increasingly competitive international research environment.

Our contracting services have been kept busy with a host of co-operation agreements with academic institutions and industry, as well as the increasing number of common projects with the ESRF such as the Partnership for Soft Condensed Matter and in the framework of the common CPER projects.

The Financial and Purchasing Service too has risen to new challenges, preparing to conform to requirements to adopt International Financial Reporting Rules, establishing an inventory for all of its assets and improving purchasing procedures – with one intended aim being an improvement of 'fair return' on investment among all our Partners.

STAFF

- 493.5 people including 67 experimentalists in the scientific sector and 29 thesis students
- 320.5 French, 53 German, 56.5 British, 38 from Scientific Member countries and 25.5 from others

Staff on 31/12/2009		%
French	320.5	64.94
German	53	10.74
British	56.5	11.45
Scientific Members	38	7.70
Others	25.5	5.17
Total	*493.5*	*100*

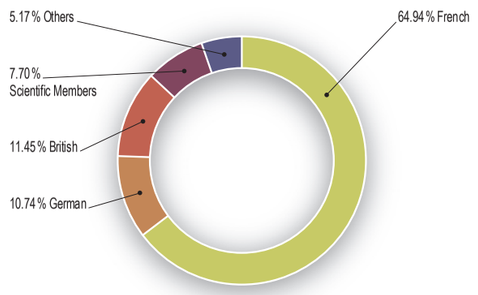

BUDGET 2009: 82 M€ (excluding taxes)

Income	M€	%
Income from Associates	61.0	74.30
Income from Scientific Members	17.6	21.44
Own income	2.9	3.53
Carry forward & reserve	0.6	0.73
Total	*82.1*	*100*

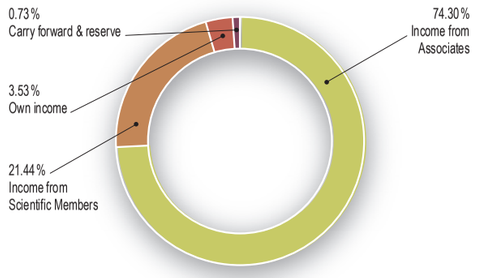

Expenditure	M€	%
Staff costs	43.0	52.38
Operating costs	15.3	18.63
Investment costs	14.4	17.54
Fuel cycle	9.4	11.45
Total	*82.1*	*100*

DISTRIBUTION OF ILL PURCHASES

(Figures at the end of Dec. 2009 - without French captive market: 10 M€)

Income	M€	%
France	17.69	62.84
Germany	4.3	15.28
United Kingdom	0.96	3.41
Scientific Members	2.69	9.56
Others	2.51	8.92
Total	*28.15*	*100*

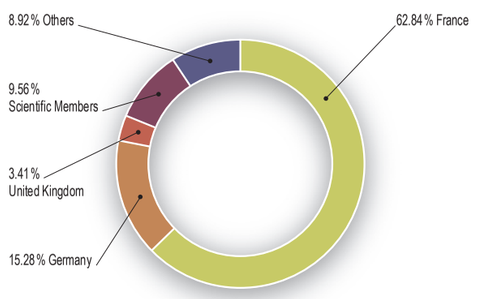

NAME

Institut Max von Laue - Paul Langevin (ILL)

FOUNDED

17 January 1967. International Convention signed until 31 December 2013.

ASSOCIATES

France
Commissariat à l'Energie Atomique (CEA)
Centre National de la Recherche Scientifique (CNRS)

Germany
Forschungszentrum Jülich (FZJ)

United Kingdom
Science & Technology Facilities Council (STFC)

COUNTRIES WITH SCIENTIFIC MEMBERSHIP

Spain
Ministerio de Ciencia e Innovación (MICINN)

Switzerland
Staatssekretariat für Bildung und Forschung (SBF)

Italy
Consiglio Nazionale delle Ricerche (CNR)

CENI (Central European Neutron Initiative)
Consortium, composed of:
- Austria: Österreichische Akademie der Wissenschaften
- Czech Republic: Charles University of Prague
- Hungary: Research Institute for Solid State Physics and Optics on behalf of the Hungarian Academy of Sciences (MTA)
- Slovak Republic: Comenius University Bratislava

BELSWENI
- Belgium: Belgian Federal Science Policy Office (BELSPO)
- Sweden: Swedish Research Council (SRC)

Denmark
Danish Agency for Science, Technology and Innovation
Interim scientific membership 01/07/2009 – 30/06/2011

SUPERVISORY AND ADVISORY BODIES

- Steering Committee, meeting twice a year
- Subcommittee on Administrative Questions, meeting twice a year
- Audit Commission, meeting once a year
- Scientific Council with 9 Subcommittees, meeting twice a year

REACTOR

- 58 MW, running 4 cycles in 2009 (with cycles of 50 days)

EXPERIMENTAL PROGRAMME

- 871 experiments (allocated by subcommittees) on 28 ILL-funded and 10 CRG instruments
- 1316 visitors coming from 38 countries
- 1272 proposals submitted and 817 accepted

Organisation chart - December 2009

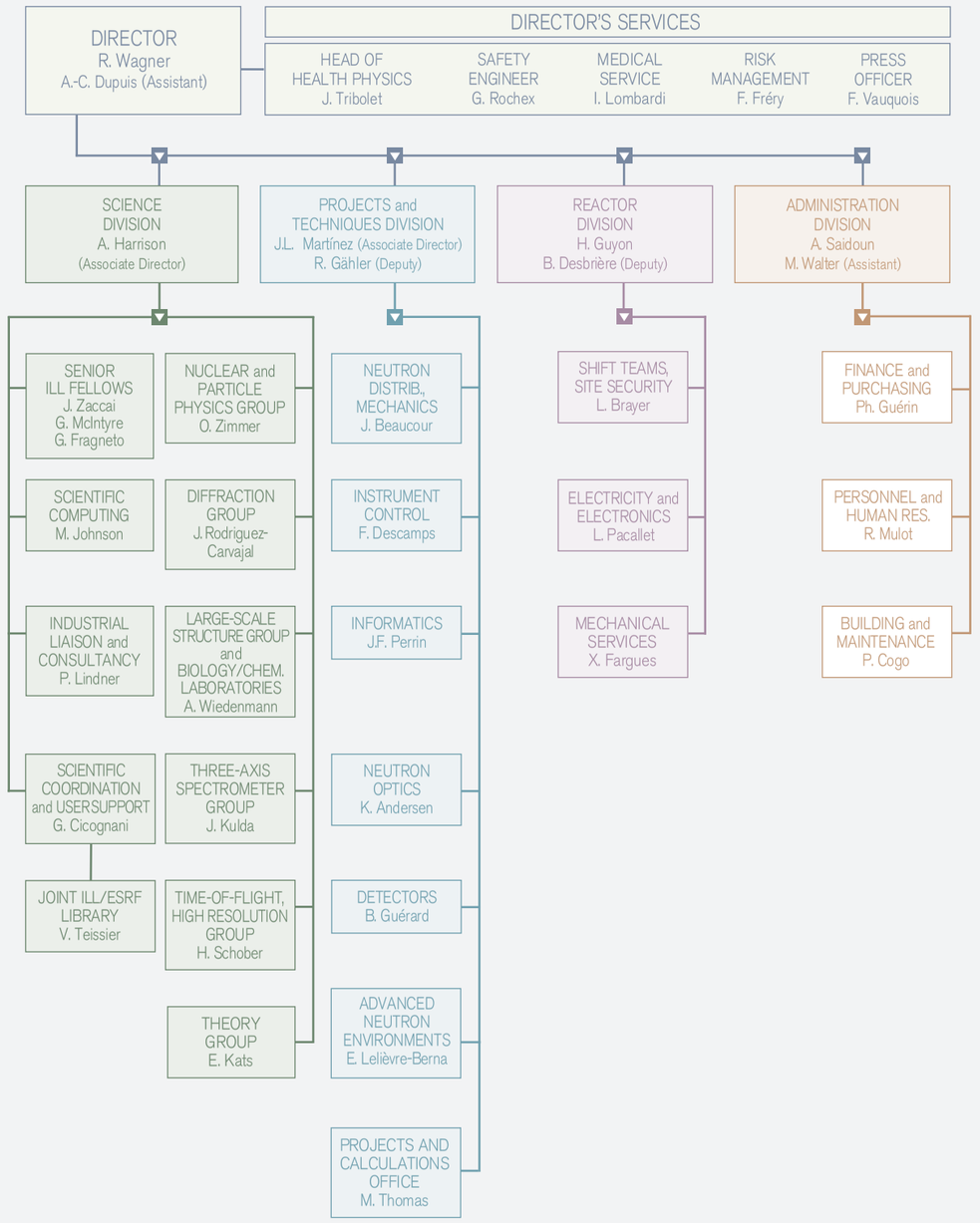

Publications

In 2009, the ILL received notice of 635 publications by ILL staff and users

The distribution by subject is as follows:

Applied physics, instrumentation and techniques	51
Materials science and engineering	59
Theory	16
Nuclear and particle physics	61
Magnetic excitations	51
Crystallography	79
Magnetic structures	114
Liquids and glasses	25
Spectroscopy in solid state physics and chemistry	51
Biology	52
Soft matter	76

ILL PhD studentships

PhD students at ILL in 2009	36
PhD theses completed in 2009	8

The EPN science campus

The joint ILL, ESRF and EMBL site now has a new name: the European Photon and Neutron science campus - or 'EPN science campus', for short. And since early February it has its own web site

http//www.epn-campus.eu/

The aim of the new web site is to provide our visitors with the latest news on our activities and practical information for their visit. In the near future ILL and ESRF users will be able to access the two Institutes' online user portals (for proposal submissions for instance) via a single log-on.